TESIS DE LA UNIVERSIDAD DE ZARAGOZA

2019

77

Andrea Calvo Echenique

Human lumbar spine biomechanics: study of pathologies and new surgical procedures

Departamento

Instituto de Investigación en Ingeniería [I3A]

Director/es

PÉREZ DEL PALOMAR ALDEA, AMAYA

ISSN 2254-7606

Prensas de la Universidad
Universidad Zaragoza

ISSN 2254-7606

Tesis Doctoral

HUMAN LUMBAR SPINE BIOMECHANICS: STUDY OF PATHOLOGIES AND NEW SURGICAL PROCEDURES

Autor

Andrea Calvo Echenique

Director/es

PÉREZ DEL PALOMAR ALDEA, AMAYA

UNIVERSIDAD DE ZARAGOZA
Instituto de Investigación en Ingeniería [I3A]

2018

Human lumbar spine biomechanics: study of pathologies and new surgical procedures

Thesis by

Andrea Calvo Echenique

Faculty Advisor

Dra. Amaya Pérez del Palomar Aldea

Doctoral Degree in *Biomedical Engineering*

Escuela de Ingeniería y Arquitectura (EINA)
Universidad de Zaragoza
Zaragoza, April 2018

A mi madre

El saber no sirve de nada si no sabes para que sirve lo que sabes.

Los ojos del Tuareg. Alberto Vázquez Figueroa

Agradecimientos

Con la sensación de cerrar una etapa de mi vida, no puedo sino pensar en agradecer a quienes con su ayuda, ilusión y compresión han estado a mi lado todo este tiempo.

En primer lugar, quiero agradecer a mi directora de tesis Amaya Pérez del Palomar, quien hace ya más de seis años confió en mi, por mostrarme el mundo de la investigación y darme la oportunidad de formar parte de el. Por guiarme a lo largo de todo el camino y ofrecerme sus consejos. Me gustaría extender este agradecimiento a toda la gente que de una forma u otra ha colaborado en la realización de esta tesis, José Cegoñino, Luciano Bances y al grupo de Laura Correa en Cáceres, gracias por haberme permitido crecer a vuestro lado.

Ahora me gustaría cambiar al ingles to acknowledge those who have welcomed me in their research groups, Prof. Daniel Kelly and Prof. Hendrik Schmidt because they kindly offered me all their valuable knowledge. I would also like to say thank you to all the people from the Trinity Biomedical Institute Science in Dublin and the Julius Wolff Institut in Berlin for their help and support.

Millones de gracias a todos los compañeros, ahora amigos, con los que he compartido infinitos momentos. A los que ya terminaron: Sara, Marina, Enrique y Raquel por compartir conmigo sus rinconcitos de llorar y sus mundos de reir. A los que han recorrido junto a mi desde el brillante principio al tortuoso final: Ismael, Jorge y Mar (L.E.S.) porque sin sus locuras estos últimos momentos no habrían sido tan maravillosos. Y a los que llegarón más tarde: Javi, Bea y tantos otros, por traer ese aire fresco tan necesario.

A mis amigos que han estado siempre ahí para conseguir que deje de pensar, Saray, Laura, Marimar, Aitor, Sandra y en especial a Nacho por escucharme durante horas sin interrumpir.

A Raúl, por no huir a pesar de que en la primera cita le hablé de “papers”. Pero sobre todo, por ser mi refugio.

Y cómo no, a mi familia, la de sangre y la de corazón. Ana y Jesús por ofrecerme asilo político y valiosos consejos, Pedro por alimentar mi estómago y mi ilusión, mis peques Eva y Raúl por regalarme sus sonrisas, Javi porque aunque parco en palabras se que siempre estarás ahí y especialmente a Conchi, que me apoyó desde el principio. Por último, aún sabiendo que jamás existirá una forma de agradecer sus constantes sacrificios y desvelos quiero transmitirle a mi madre Elena mi más profundo y sincero agradecimiento. Mi logro es el tuyo.

Andrea, 4 de Abril de 2018.

Abstract

This thesis aims to shed light on the process that undergoes the lumbar spine as a result of intervertebral disc degeneration and different lumbar surgeries, paying special attention on the main risk factors and how to overcome them.

Low back pain is the leading musculoskeletal disorder in all developed countries generating high medical related costs. Intervertebral disc degeneration is one of the most common causes of low back pain. When conservative treatments fail to relieve this pain, lumbar surgery is needed and, in this regard, lumbar fusion is the “gold standard”technique to provide stability and neural decompression.

Degenerative disc disease has been studied through two different approaches. An in-vivo animal model was reproduced and followed-up with MRI and mechanical testing to see how the water content decreased while the stiffness of the tissue increased. Then, degeneration was induced in a single disc of the human lumbar spine and the effects on the adjacent disc were investigated by the use of the finite element models.

Further on, different procedures for segmental fusion were computationally simulated. A comparison among different intersomatic cage designs, supplemented with posterior screw fixation or placed in a stand-alone fashion, showed how the supplementary fixation drastically decreased the motion in the affected segment increasing the risk of adjacent segment disease more than a single placed cage. However, one of the main concerns regarding the use of cages without additional fixation is the subsidence of the device into the vertebral bone. A parametric study of the cage features and placement pointed to the width, curvature, and position as the most influential parameters for stability and subsidence.

Finally, two different algorithms for tissue healing were implemented and applied for the first time to predict lumbar fusion in 3D models. The self-repairing ability of the bone was tested after simple nucleotomy and after instrumentation with internal fixation, anterior plate or stand-alone intersomatic cage predicting, in agreement with previous animal and clinical studies, that instrumentation may be not necessary to

promote segmental fusion. In particular, the intervertebral disc height was seen to play an important role in the bone bridge or osteophyte formation.

To summarized, this thesis has focused in the main controversial issues of intervertebral disc degeneration and lumbar fusion, such as degenerative process, adjacent segment disease, segment stability, cage subsidence or bone bridging. All the models described in this thesis could serve as a powerful tool for the pre-clinical evaluation of patient-specific surgical outcomes supporting clinician decisions.

Keywords: Biomechanics; Finite element method; Lumbar spine; Intervertebral disc; Disc degeneration; Animal model; In-vivo; Intersomatic cage; Stand-alone cage; Pedicle screw fixation; Subsidence; Stability; Lumbar fusion; Bone remodelling; Tissue healing

Contents

LIST OF FIGURES

LIST OF TABLES

List of Abbreviations

AF Annulus fibrosus

ALIF Anterior lumbar interbody fusion

ALL Anterior longitudinal ligament

ASD Adjacent segment disease

BEP Bony endplate

BMP2 Bone morphogenetic protein 2

CEP Cartilage endplate

CT Computerized tomography

EP Endplate

FC Facet capsule ligament

FDA Food and drug administration

FE Finite element

FL Flavum ligament

FSU Functional spinal unit

ISL Interspinous ligament

ITL Intertransverse ligament

IVD Intervertebral disc

MRI Magnetic resonance imaging

MSC Mesenchymal stem cell

NP Nucleus pulposus

NZ Neutral zone

ODI Oswestry disability index

PLF Posterolateral lumbar fusion

PLIF Posterior lumbar interbody fusion

PLL Posterior longitudinal ligament

PSF Pedicle screw fixation

RCT Randomized controlled trial

ROM Range of motion

SSL Supraspinous ligament

TLIF Transforaminal lumbar interbody fusion

VAS Visual analogue scale

XLIF Extreme lateral interbody fusion

Chapter 1

Introduction

A brief description of lumbar spine anatomy and function is provided in this chapter. Each of the structures which are part of the lumbar spine is defined with a particular focus on the composition and function of the different tissues involved. Besides, the most common pathologies that affect intervertebral discs are described, as well as the surgical techniques used to treat these diseases.

Finally, a wide overview of the clinical, animal and computational studies made on this topic is supplied with special emphasis on what still remains to be done. The main goals and the thesis outline followed to achieve them are presented at the end of the chapter.

1.1 The lumbar spine

The human spine is a complex anatomical structure with three main functions: protection of the spinal cord and nerves, mechanical support of the body and provision of mobility to the head and torso.

The spine consists of 24 vertebrae articulated by cartilage elements named intervertebral discs (IVD) (7 cervical (C1-C7), 12 thoracic (T1-T12) and 5 lumbar (L1-L5)), and 9 fused vertebrae at the sacrum and coccyx. As shown in Figure 1.1[1], the spine is placed in the posterior mid-longitudinal axis of the back. It houses the spinal canal formed from a central hole within each vertebra. The spinal cord travels through the spinal canal and the spinal nerves emerge adjacent to each vertebra. The shape of the spine varies with the region. The cervical spine has a convex forward curvature, known as lordotic curve, the thoracic curve, concave forward is known as kyphotic curve and finally, the lordotic curve in the lumbar region which is convex anteriorly and ends in the sacrum. This sinusoidal shape acts to dissipate the great loads during daily activities [78]. However, the lumbar spine's lowest segments L4-L5 and L5-S1 bear the most weight and are, therefore, the most prone to degeneration and injury [322].

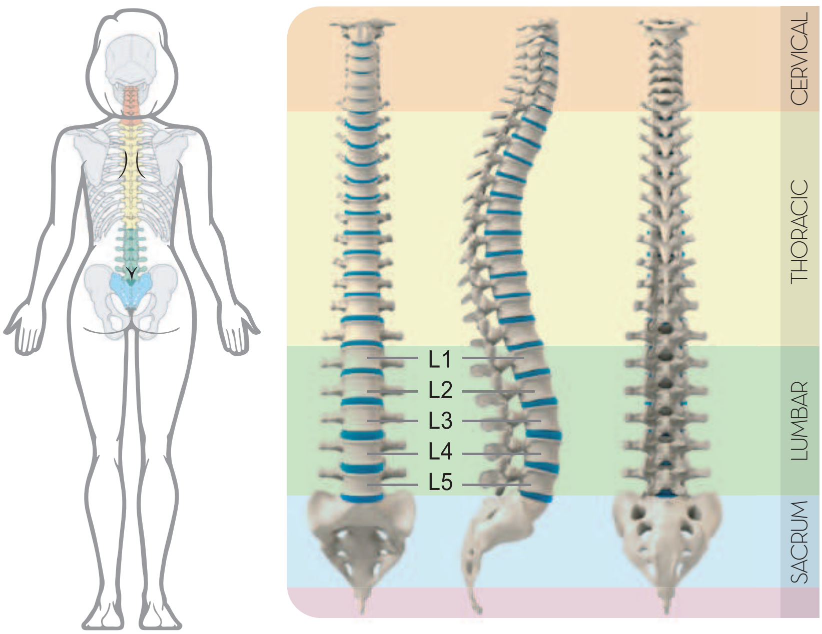

Figure 1.1: *Spine anatomy: from cervical to coccygeal region.*

A functional spinal unit (FSU) is defined as the smallest unit capable of carrying out the main functions of the spine. Each FSU is comprised of two vertebrae with an IVD between them and the group of ligaments and muscles which link the vertebral

[1] Adapted from:https://thrivewellnesscenter.com/hurley-osborne-new

bodies. The two vertebrae are connected in the back part by two small joints called facet joints which allow bending and twisting movements but control the amplitude. At the same time, the ligaments and muscles that connect the bones provide stability and flexibility to the entire trunk.

1.1.1 Lumbar vertebrae

Lumbar vertebrae, designated L1 to L5 starting at the top, are the largest bones of the spine. Each vertebra consists of two main parts: vertebral body and vertebral arch as detailed in Figure 1.2a. The vertebral body has a cylindrical shape wider from side to side than antero-posterior and is concave at the upper and lower surfaces. The size of the vertebral body increases in the inferior levels due to the fact that their main role is to withstand the upper body weight. The vertebral arch comprises: two pedicles, which join the arch to the vertebral body enclosing the spinal canal, two laminae and a number of processes (spinous, transverse and articular), which are thick structures that provide attachment to ligaments and muscles. In particular, the articular processes project up and down and host the hyaline cartilage that takes part in the facet joints with the adjacent vertebrae.

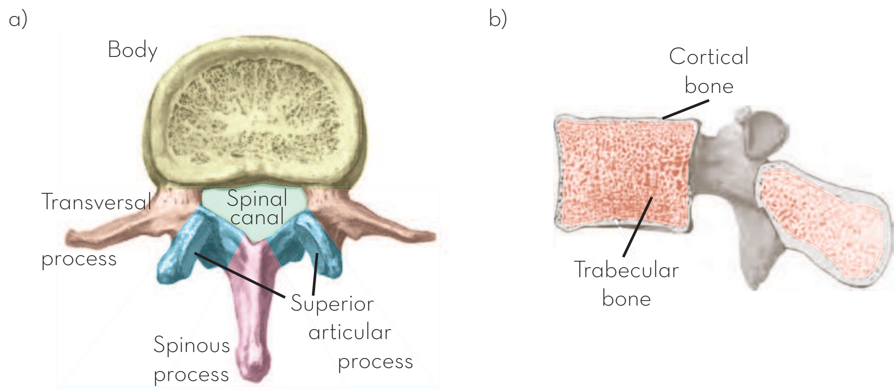

Figure 1.2: *a) Lumbar vertebra anatomy. b) Vertebral bone distribution*

The bone is composed of an outer cortical layer that covers the trabecular bone as shown in Figure 1.2b. The cranial and caudal aspects of the vertebral body, named bony endplates (BEP), are vascularized osseous layers which, together with the cartilaginous endplate (Section 1.1.2), form the endplate (EP). The main function of the BEP is to ensure the delivery of nutrients such as glucose and oxygen to the avascular tissues of the IVD [351]. Finally, regarding the strength of this thin layer, the central region seems to be weaker while the outer part is thicker and stronger [213].

1.1.2 Intervertebral disc

The IVD is an aggregate of different tissues that provides relative movement between two vertebral bodies and cushions mechanical loads. It is composed of the *nucleus pulposus* (NP) surrounded by the *annulus fibrosus* (AF) and the *cartilage endplates* (CEP), placed caudal and cranial, which are the interface with the vertebrae. All of these structures work as a whole when the disc is loaded, the AF being responsible for withstanding tensile stresses and the NP for bearing compressive stresses [215]. Figure 1.3 shows the different parts of the IVD and their main attributes which are explained in further detail below.

Due to the biochemical composition of the different tissues, the IVD is a highly hydrated tissue that presents a swelling behaviour in an unloaded condition. When an external load is applied, the hydrostatic pressure created in the NP is transmitted radially to the AF, which thanks to its fibre network is capable of bearing the tensile stresses. At the same time, the water is expelled from the disc reducing its height and, afterward, recovered because of the osmotic pressure [87]. The mechanical properties of the disc are greatly dependent on the magnitude of the applied load, while it offers low resistance to small forces, it is stiffer under larger forces. The region where the resistance is low is named the neutral zone. This concept was defined by Panjabi et al.[270] to evaluate clinical instability of the FSU.

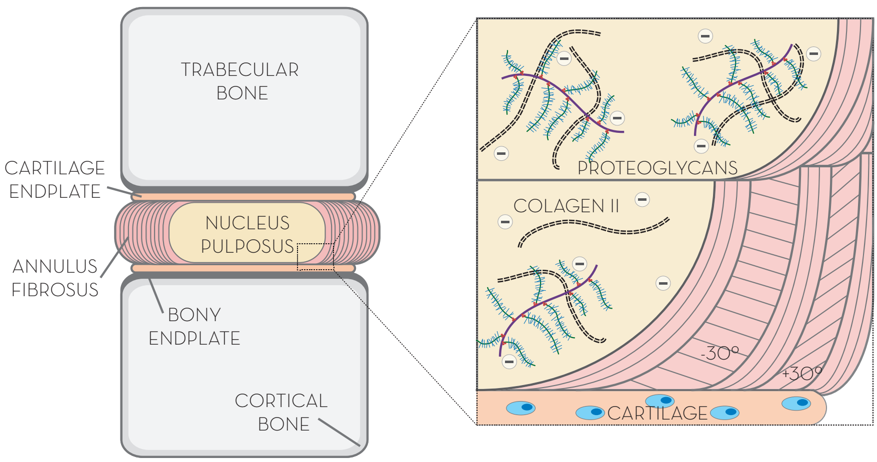

Figure 1.3: *Intervertebral disc anatomy and composition: nucleus pulposus, annulus fibrosus and cartilage endplate*

- **Nucleus pulposus:** The NP is a gel-like material placed in the core of the IVD which is mainly made of water, proteoglycans and a loose network of collagen and elastin fibers suspended in a mucoprotein gel. Proteoglycans are the most abundant macromolecules in the NP accounting for as much as 65% of the dry weight [156]. These molecules make it a tissue with a high swelling capacity as they allow for tissue hydration [353]. As a result, the NP acts as a shock absorber cushioning the impact of daily activities by the pressure transmission to the AF.

- **Annulus fibrosus:** The AF is a highly organized structure composed of concentric layers of collagen Type I and II [6] fibres oriented ±30 degrees to the disc mid-height plane [221]. These layers are arranged in a criss-cross pattern among adjacent lamellae which, in turn, are linked together by elastin fibres [379] and embedded in an extracellular matrix. Such organization provides the anisotropy to the AF and makes it biomechanically adapted to withstand any type of shear deformation. Therefore, in healthy conditions, the AF fibres resist the pressure transmitted by the NP preventing it from leaking out of the core of the IVD.

- **Cartilage endplates:** The CEP is a thin layer of hyaline cartilage with a heterogeneous composition similar to that of the articular cartilage [300]. The fibres from the AF are strongly attached to the CEP creating a capsule around the NP. As mentioned above, the CEP, along with the BEP constitutes the EP, which is the interface between vertebra and IVD that allows nutrients diffusion from the vascularized bone into the avascular tissues. Changes in the composition of the EP, such as those occurring with degeneration and ageing can result in nutrient transport alterations [301].

1.1.3 Lumbar ligaments

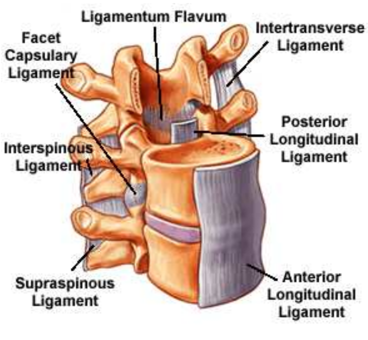

Figure 1.4: *Lumbar ligaments*

The spinal range of motion is passively restricted by a group of ligaments which are fibrous bands of connective tissue attached to the bone as shown in Figure 1.4. The ligaments bear tensile stresses to avoid excessive motion and to prevent the failure of the IVD.

The anterior (ALL) and posterior (PLL) longitudinal ligaments run along the spine covering the vertebral bodies and IVDs and are the primary stabilizers under extension and flexion movements, respectively. The strongest ligament is the ligamentum flavum (FL) which connects the laminae and protects the spinal cord and nerves. Moreover, the facet capsular ligament (FC) provides stability to the facet joints. Finally, a group of ligaments connects the processes of adjacent vertebrae: the interspinous (ISL) and supraspinous (SSL) ligaments link the spinous processes and the intertransverse ligament (ITL) links the transverse processes.

1.1.4 Lumbar spine biomechanics

One of the main functions of the spine, as mentioned above, is to provide flexibility to the trunk. As such, the IVDs are constantly under mechanical loads exerted by the musculature. External loads such as inertial effects and muscular forces are related to body weight. In a standing position, the centre of gravity lies in front of the spine creating a flexion moment. To balance it the posterior spinal muscles exert a force that results in high compressive loads acting on the IVD [137]. Keeping and changing postures increases the spinal loads and introduces more stress components [253]. Since spinal loads cannot be easily measured in vivo, some studies investigated the intradiscal pressure in different positions [371] reporting pressures of $0.1-0.2$MPa in supine rest that increases to 0.5MPa in standing position or 1.1MPa during flexion reaching a peak value of 2.3MPa while carrying a weight in flexed position.

The state of hydration of the IVD and its intradiscal pressure are important determinants of mechanical behaviour [17]. When subjected to compression force, the pressure within the NP rises exerting pressure on the EPs and the AF. As a result of this pressure, the fibres of the AF tighten and resist the applied force. In turn, a radial IVD bulge may be observed. This bulge will be more pronounced in the areas where the compression is more concentrated as shown schematically in Figure 1.5. For instance, during flexion, the NP is pushed backwards and the bulging is more obvious in the posterior part of the disc while, during extension, the NP is pushed towards and the bulging is greater in the anterior part. In torsion, the excessive motion is prevented by the zygapophysal or facet joints which bear 65% of the loads while the IVD contributes the remainder [215]. Although difficult to measure, it is believed that the behaviour of

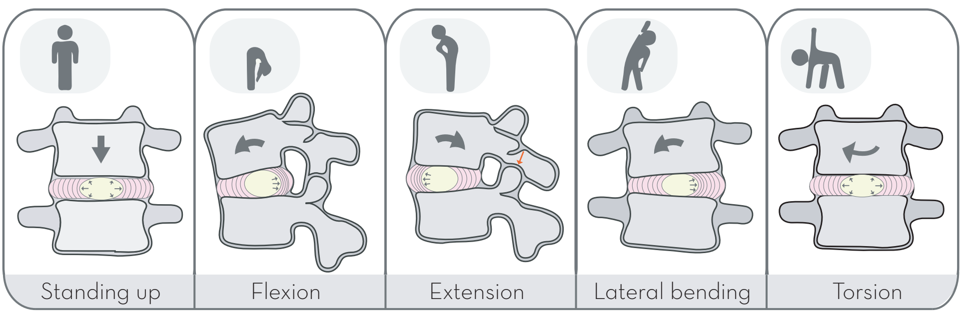

Figure 1.5: *Main movements of the functional spinal unit.*

the AF during bending moments is different from that in compression. It has been proposed that the collagen fibres change their orientation allowing the adjacent vertebrae for a wider separation. The facet joints also play an important role in providing resistance and stability under bending movements [5].

1.2 Intervertebral disc diseases

During life, the IVD is subjected to a physiological process of growth along which the mechanical and biological characteristics of the disc undergo strong changes. Proteoglycan fragmentation in the NP starts during childhood, and with age, proteoglycan and water content in the disc decreases. However, due to the entrapment of the AF fibres, the loss of proteoglycan fragments is slow as they develop a similar function while they are entrapped [352]. At the same time, in the AF the collagen type II turns into type I in the inner part while, in the outer, a thickening of type I collagen occurs. With increasing age the NP becomes smaller and loses hydrostatic pressure, hence more load should be borne by the AF which, in turn, becomes stiffer and weaker [87]. Nonetheless, the disc does not show a major decrease in height with ageing [102].

The difference between the normal aging process and the degeneration disease progression remains unclear, but some authors agree on the understanding of the degeneration as a cascade event that magnifies and accelerates structural failures and biochemical changes related with age [6]. Disc degeneration and herniation are the most common pathologies affecting IVD and the major source of back pain due to nerve pinching or excessive load at the facet joints.

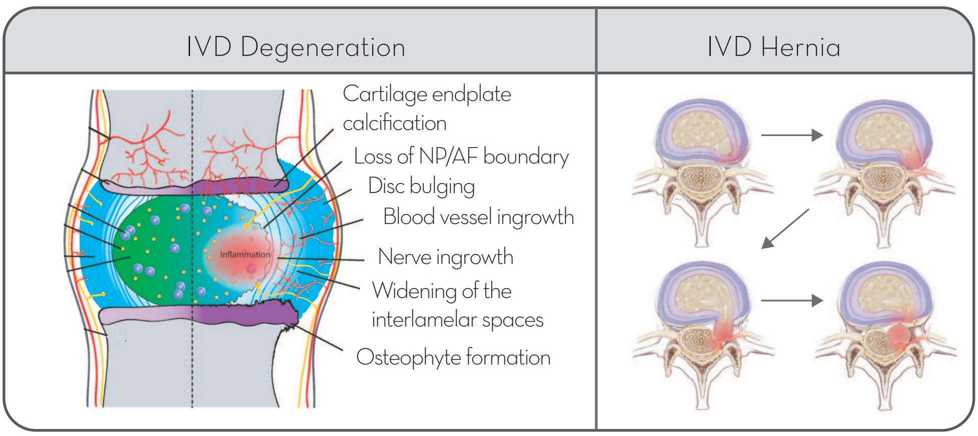

Figure 1.6: *Intervertebral disc degeneration and hernia. Adapted from [231] [368]*

1.2.1 Degenerative disc disease (DDD)

As defined by Adams and Roughley the IVD degeneration is *an aberrant cell-mediated response to progressive structural failure* [6]. The degenerative process is thought to be initiated at the NP [334] with a loss of proteoglycan content. This loss is responsible for a fall in the osmotic pressure and, therefore, a loss of hydration that has a major effect on the load-bearing behaviour of the tissue [352]. Meanwhile, the collagen fibres of the AF change, as explained above, and become disorganized making the NP/AF boundary unclear.

When a load is applied, the NP is unable to distribute compressive forces between the vertebral bodies and, consequently, the forces are transmitted non-uniformly to the AF. The AF is subjected to a progressive structural deterioration with alterations in mechanical properties [259] that can lead to radial and circumferential tear formation [135]. These tears are often followed by radial bulges or herniations of the NP.

In the healthy tissue the swelling pressure in the NP helps to maintain disc height, but with degeneration, the biomechanics of the IVD is altered and the disc height is reduced. Such changes have a strong influence on other spinal structures. For instance, the facet joints in the degenerated FSU may be subjected to abnormal loads and, as a result, they may develop osteoarthritic changes [103]. Furthermore, the tensional forces on the ligament flavum are reduced and could cause remodelling and thickening, and eventually could lead to spinal stenosis [284]. To summarize, the macroscopic changes seen during DDD are shown in Figure 1.6. Considering the appearance and severity of the changes previously explained, grading scales for IVD degeneration have been established. In 1990, Thompson and co-workers classified the degeneration grades from I to V regarding morphologic changes such as fibrous tissue formation in the NP, focal disruptions of the AF or bone osteophytes appearance at vertebral body margins [344]. Later on, a classification system based on routine magnetic resonance imaging (MRI) was codified by Pfirrmann et al. [277]. This system accounts for aspects like signal brightness, a clear distinction between NP and AF or disc height.

Although the aetiology of IVD degeneration is not fully understood yet, some factors are known to influence the initiation and progression of the disease [305]. The cells are sensitive to compressive stress so abnormal mechanical loads may trigger disc degeneration as has been highlighted in experimental animal studies [211] [193]. On the other hand, endplate calcification seems to play a crucial role in disc degeneration as long as solute transport through the cartilage is important for physiologic and metabolic processes. Movement of solutes depends on solute size, shape or charges but also on cartilage matrix composition, hence changes in CEP composition may affect transport and reduce nutrition of the tissues [301]. Finally, hereditary and genetic factors could also predispose to disc degeneration [333] and are in continuous study as a promising tool for treatment of early DDD [334][231].

1.2.2 Lumbar hernia

When radial fissures in the AF allow the gel of the NP to migrate out of the IVD core, the disc is said to be herniated [6] (Fig 1.6). Depending on the extent of nucleus migration, the herniation could be classified as: disc protrusion, when the AF fibres and the posterior longitudinal ligament are intact; extrusion, if these elements are disrupted but there is an intact tail of nucleus material extending into disc space; and sequestration, when the material from the nucleus is completely unconnected to the IVD [368]. Because of the AF geometry, which is thinner in the posterior part of the IVD, the herniation is more prone to appear in the posterior or postero-lateral portions of the disc [135], thus invading the spinal canal or pinching the nerve roots [294]. Although degeneration is one of the most probable causes of disc herniation, an overloading of the disc, as the caused by weight lifting, can also lead to IVD hernia. The NP hydrostatic pressure greatly increase when the spine is overloaded, pushing the gel-like material to the annulus and causing the leaking of the nucleus material. Another risk factors observed are obesity, posture or repetitive work [283][84]

1.3 Surgical procedures

In most of the cases, IVD diseases are treated with conservative therapies like analgesia for inflammation and pain relief or physical therapy. When no successful results are reached with these treatments, the surgical option may be considered. Operative management includes minimally invasive discectomy or open procedures for removal of herniated tissue, disc height recovery and spinal stabilization [366] (Fig. 1.7). In the last years, the research efforts have been focused on the regenerative therapies to stop the degeneration progression and restore the physiological function of the disc [260].

1.3.1 Nucleus discectomy

A discectomy or nucleotomy is the surgical removal of herniated disc material that presses on a nerve root or the spinal cord relieving pain. The procedure involves removing a portion of the NP which is invading the neural space. The first discectomy was described by Love in 1939 [212] and, although the procedure has been refined, it is still in use. In fact, discectomy is the most common surgery for the treatment of IVD hernia. Later on, in 1977, Caspar [57] described a surgical microdiscectomy technique which reduced the size of the incision, and, with the development of technology, a minimally invasive technique was used for microendoscopic discectomy. This evolution achieved a reduction in hospital stay and the time to return to work [37].

1.3.2 Segment fusion

One of the major concerns in degenerated discs is the loss of intervertebral space which could lead to segment instability and osteoarthritis at the facet joints. To restore disc height and stabilize the FSU, fusion has proven to be a successful surgical solution. The goal of spinal fusion is to immovilize the segment, restore the foraminal height and promote bone growth until achieving a complete fusion between the two adjacent vertebrae [264].

The first case of spinal fusion reported dates from 1911, when Hibbs [141] and later Albee [11] described a process where the lamina and facet were decorticated and fused with autologous bone graft. Unfortunately, these processes required months of bed rest and immobilization for fusion to occur. Efforts to reduce the long post-operative periods of immobilization prompted the development of internal fixation devices. Multiple screws designs and placement were tested prior to reach the pedicle screw system, which has become a common procedure over the past three decades [43].

To improve the fusion rate and achieve a biomechanically superior fusion, considerable attention has been directed towards interbody fusion procedures [189]. Originally, adding bone graft in the intervertebral space after nucleus discectomy had the advantage of a better blood supply, weight-bearing and facilitated bony fusion [380]. However, the associated morbidity and the risk of space collapse drove to the development of interbody cages or spacers which helps to prevent the collapse and pseudarthrosis seen with bone grafts [81][337]. There are many commercially available cages with a wide range of shapes and characteristics depending on the surgical approach, anterior [ALIF], posterior [PLIF] or transforaminal [TLIF], each one with their own advantages and disadvantages. ALIF has the advantage of avoiding nerve root damage that can occur with the posterior approach, but the disadvantage of potential damage to major vascular structures and sympathetic injury [39]. In turn, TLIF is a variation of the PLIF technique in which the disc space is accessed via the far lateral portion of the vertebral foramen. While less risky than the posterior approach, it can result in the removal of important stabilizing structures [155].

Despite lumbar fusion with supplementary posterior screw fixation has been widely used with high success rates [117] [134] [199], some biomechanical studies suggested that interbody cages are stable enough to be used as stand-alone devices [380], i.e. removing the screw fixation. Under the assumption that cages are introduced using a minimally invasive technique that ensures preservation of important stabilizing structures such as posterior musculature, anterior and posterior longitudinal ligaments, and facet joints [10][75], it could be thought that they will provide stability and, at the same time, the distraction of the ligaments will prevent the cage from migration. All in all, the effectiveness of stand-alone interbody cages has been questioned, with some investigators claiming that supplementary posterior fixation is required to produce better long-term clinical results [264].

One of the major concerns regarding the use of stand-alone constructs is the risk of subsidence of the device into the bone owing to the high contact pressures in the bony endplates. While low-grade subsidence is an expected outcome, high-grade subsidence could lead to a reduction in the intervertebral space height and eventually to persistent pain or the need for re-operation [223]. In order to achieve bony fusion, the disc and CEP are thoroughly removed and the underlying bleeding BEP is exposed avoiding gross violation of the EP before cage insertion [299]. The cross-sectional EP area available for cage and graft placement is an important factor because it allows for a larger surface for bone growth and for bearing cage pressure reducing the risk of subsidence [342]. In addition, the EP strength is highly variable depending on the region. While the center of the bone, where implants are usually placed, is the weakest part of the lumbar endplates, the posterolateral region of the endplate provides the greatest resistance to subsidence [122][213]. Furthermore, large scale clinical studies have also demonstrated no differences in reoperation rates between patients with stand-alone cages versus those with additional posterior fixation [196][295].

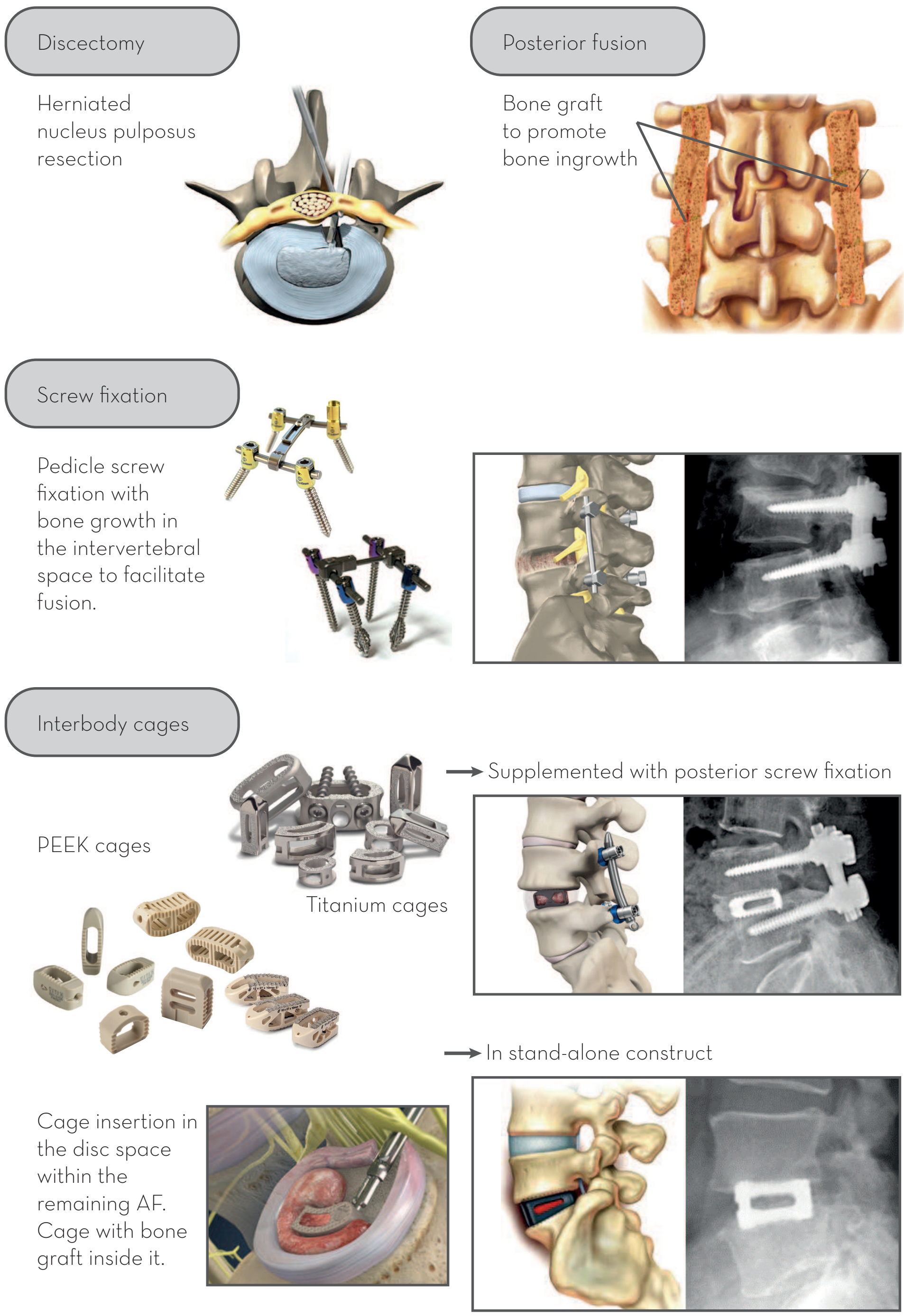

Figure 1.7: *Summary of the surgical options used to treat intervertebral disc herniation and degeneration.*

Indeed, interface strength in axial compression does not appear to be substantially enhance by supplementary instrumentation [264]. In conclusion, parameters such as the geometry of structural support and the position and preparation of the endplate can influence the resistance of an interbody cage to subside.

Cage material has been another key aspect of the evolution of interbody spacers. Cages are typically composed of titanium alloys or polymers such as PEEK[2], which has a markedly lower Young's modulus. An advantage that supports the use of PEEK is that it provides similar stability than titanium while reducing stresses on the endplates. Furthermore, because cages are commonly used in combination with bone graft (which is resorbed and replaced by bridge of trabecular bone), a cage that shares the load with the graft is preferable to promote bony fusion according to Wolff's law because load sharing is an important prerequisite for bone healing [356][240].

Although lumbar spinal fusion has yielded good clinical results in decreasing pain and fatigue with high union rates, it has been proposed that the immobilization of one segment may alter the biomechanics of the entire lumbar spine, especially in the upper and lower segments, leading to adjacent segment disease (ASD) [30][194]. Despite the exact mechanism remains uncertain, altered biomechanical stresses appear to play a key role in the development of ASD. The addition of posterior fixation, the use of pedicle screws, the number of segments fused, individual patient characteristics or age have emerged as risk factors [272]. The development of ASD is problematic because it often requires reoperation and has adverse effects on long-term clinical outcomes [61]. To avoid the cascade degeneration effect, several new technologies such as dynamic stabilization devices, interspinous process implants or total disc arthroplasty have been developed as alternatives to fusion.

1.3.3 Total disc replacement

Total disc replacement is intended to restore or preserve the natural biomechanics of the intervertebral segment and to reduce further degeneration of adjacent levels. Fernstron is considered as the pioneer of artificial disc replacement. He implanted a spherical stainless steel prosthesis in an attempt to restore disc spacing and articulation by creating a mobile center of rotation [96]. However, these balls were reported to have high failure rates because the sphere eroded the vertebral bodies as shown Figure 1.8.

[2] Polyether ether ketone (PEEK) is an organic thermoplastic polymer with a Young's modulus of 3.6 GPa that can be tailored to closely match cortical bone by preparing carbon-fibre-reinforced composites with varying fibre length and orientation. Its biocompatibility has brought it to be widely used in surgical applications [195].

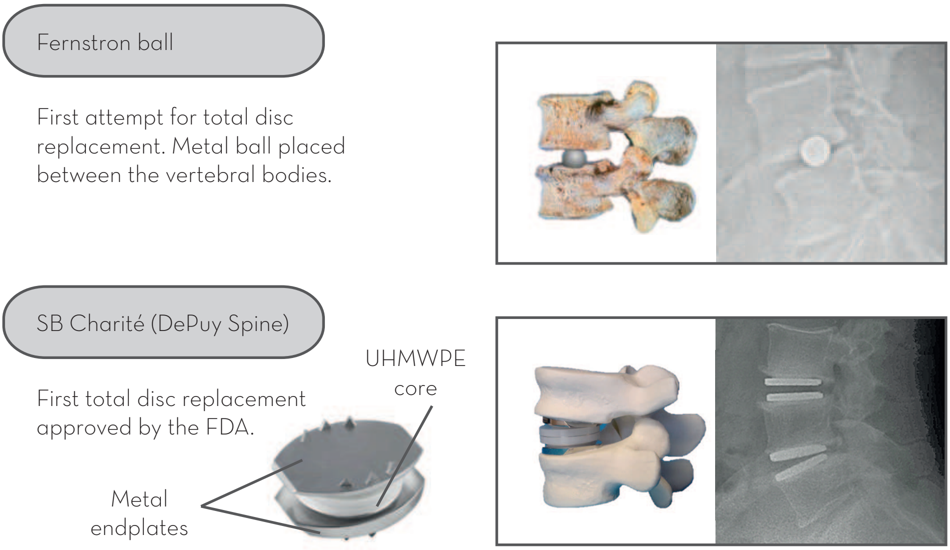

Figure 1.8: *Total disc replacement: Fernstron ball and SB Charité (DePuy Spine). Adapted from [96][310]*

From the time of Fernstron's balls, multiple designs for total disc replacement have been developed following two main principles: replace the motion characteristics of the discs with sliding plates and a central plastic core; or replicate the normal viscoelastic and hydrostatic properties of the nucleus, usually with hydrogels encased in a polymeric jacket [39][111]. The first disc prostheses approved by The United States Food and Drug Administration (FDA) was the Charité Artificial Disc (DePuy Spine, Raynham, MA). It consists of two cobalt chromium endplates with an ultra-high molecular weight polyethylene (UHMWPE) sliding core which allows the motion in all planes. It proved to have a quantitative clinical outcome equivalent to that with ALIF. Indeed, the range of motion (ROM) after surgery was restored and maintained while the disc space height was restored with less incidence of subsidence [38][230].

A literature review showed that ASD occur more likely after fusion procedures than after total disc replacements. However, the differences in the primary outcome parameters between both procedures were small and did not exceed clinical relevance. [168]. Furthermore, an increased facet joint loading after total disc replacement was found in human cadaveric studies [306]. This is why lumbar fusion remains the 'gold standard' technique for the treatment of intervertebral diseases.

1.3.4 Regenerative therapies

Even though the wide range of available treatments for low back pain presented above has proven to be successful, they only offer symptom's relief instead of addressing the underlying causes. Furthermore, those treatments are often accompanied by loss of function, mobility and altered biomechanics which could lead to ASD and further pain [298]. To overcome those limitations, current research efforts are focused on the development of biological therapies to repair or prevent the IVD degeneration. Cell-based therapies attempt to restore the structure and function of the tissue and potentially influence on native cells. Several studies have aimed to restore either nucleus, annulus or the whole IVD with the use of native NP cells, notochordal cells or mesenchymal stem cells (MSC) as reviewed elsewhere [60][298][260]. MSCs have been proposed as an ideal cell source for IVD regeneration with a large number of studies demonstrating their ability to differentiate into NP cells. However, these treatments are in early stages of translation into the clinic and much more effort is required to reach a feasible solution to lumbar diseases.

1.4 State of the art

Low back pain has been largely studied from different points of view. The understanding of IVD degeneration and the design of surgeries and new techniques to remove pain or restore functionality have been of great concern. Here, a brief review of the animal, clinical and computational studies developed so far is provided.

1.4.1 Animal experimentation

Over the past decades, animal models in different species have been widely used to investigate changes in structural, biological and biochemical properties along the degeneration as well as treatments to stop or even reverse this process [262][174][261]. Nonetheless, there are several important issues which should be considered in the translation of the results to human tissue due to the anatomical and biomechanical differences, changes with age, and loading conditions of the IVDs. For that reason, scaling is required in the interpretation of the findings, so the relationship between the geometrical factors and the behaviour being tested should be clear. In small quadrupeds the loads are probably smaller than in humans, however, since their discs are much smaller; the intradiscal pressure might be similar. In particular, the study of Beckstein et al. [33] compared normalized axial mechanical properties, GAG and water content among species and showed that once the measures were normalized, they did not present significant differences across species. Furthermore, in pilot preclinical studies the use of the rabbit disc model may still be relevant and cost effective [12].

Several methods have been used to induce IVD degeneration in large and small animals such as spontaneous initiation [200], chemical injections [16], biomechanical alterations [193] or disc lesions [329], among others. The most extensively used technique has been to provoke damage to the AF. In 1980 Lipson and Muir [208] were the first to induce degeneration through a stab with scalpel in the AF. In their experiment, they observed changes in proteoglycan and water content, and hyaluronic acid concentration over time. After that, many studies focused their efforts on achieving a slowly progressive degeneration model via stab incisions, needle punctures or percutaneous needle punctures. While stab injuries caused a quick degeneration or even an immediate herniation of the nucleus pulposus, annular punctures resulted in slow and reproducible degenerative process [89][335]. In most of the cases, the progression of IVD degeneration has been followed up with MRI and histologic evaluation along time showing a decrease in water content as well as a reduction of disc height and a loss in MRI signal intensity [182][383]. Later on, changes in mechanical behaviour were studied with dynamic compression [238], creep tests [205], tension/compression [131] and flexion/extension tests [139] seeing that degeneration alters the mechanical properties of the IVD tissues. A common limitation of these studies is that they performed different surgical procedures at each level of the spine preserving one level intact to serve as control and, therefore, the influence of degeneration over the adjacent segments was neglected.

An animal model capable of reproducing the biology of the degeneration process would be a powerful tool for the evaluation of new treatments such as regenerative therapies. An extensive review of the results achieved with the use of disc chondrocytes, MSCs, and other stem cells in different animal models was performed by Oehme et al. [260] who underlined the importance of the animal model selection based on biological processes, quadruped posture and economical and ethical constrains. He also pointed to the success of preclinical studies in disc height maintenance, increase in MRI signal and proteoglycan synthesis, and eventually, the deceleration in the degeneration process. These promising results have led to small clinical trials with cell treatments that are still in early stages. However, hydrogels functionalized with anti-angiogenic peptides and seeded with bone marrow cells failed to decelerate degeneration in merino sheep [296]. Growth factor's influence over degeneration has been another therapy extensively studied with the use of animal models. Osteogenic protein-1 [238], bone morphogenetic protein 2 (BMP2), tissue inhibitor of metalloproteinase 1 [205] and platelet-derived growth factor BB [265] have shown to be able of restoring disc height, increasing proteoglycan and collagen content, maintaining disc structure and biomechanical function and, therefore, delaying degenerative changes.

Apart from degeneration and gene therapies, large animal models have also been used for the assessment of bone fusion after different surgeries. A study in sheep comparing bone graft alone versus cylindrical and box-shaped cages filled with bone graft showed that the introduction of a cage improves significantly the distractive properties [175]. Other studies regarding the stiffness of the cage were carried on in goat models exhibiting that a reduced stiffness enhanced interbody fusion [358] but further experiments revealed that soft cages, such as the resorbable poly-(L-lactic acid) cages had insufficient stability when used as stand-alone and needed from supplementary fixation [191]. On the other side, different cage filling materials have been compared in sheep spines. RhBMP2 absorbable collagen sponge increased segment stiffness and fusion in comparison with autograft [346] Similarly, osteoconductive scaffold seeded with MSCs achieved similar or better fusion rates than autograft [370].

1.4.2 Clinical studies

From the beginning of lumbar surgery, a large number of case reports, prospective and retrospective clinical trials, and comparative studies have been published to show the effectiveness of different techniques and help in the selection of the optimal surgery. There is consistent evidence from this literature that lumbar spine fusion provides improvements in pain and function with acceptable patient satisfaction [279]. However, systematic reviews that adhere strictly to the principles and rigorous methodology of evidence-based medicine often conclude that there is insufficient evidence to demonstrate the superiority of a certain approach. This situation makes challenging to make decisions regarding the most appropriate treatment [136].

Most clinical studies based their conclusions in clinical and radiological outcomes. Oswestry Disability Index (ODI), which measures the degree of disability and estimates the quality of life in a person with low back pain [92], has emerged as the 'gold standard' measure for clinical results [115]. Visual Analogue Scale (VAS) and patient satisfaction are other questionnaires for the assessment of pain levels and treatment success, respectively. In the radiological images, fusion rate is usually assessed based on the amount and quality of bone formed after the surgery, which is quantified with scales like the one defined by Brantigan and Steffee [45]. Subsidence and migration are other important factors in the evaluation of surgery success when it involves the use of interbody devices. While the first is quantified as the disc height loss after cage insertion due to bone failure, the second accounts for the relative position of the cage between the vertebrae. Both of them could lead to the need of re-operation either to add supplementary fixation or to remove the device. Last but not least, lumbar instability, defined as abnormal lumbar motion during physiological loading of the spine, is measured with functional radiography. That is, performing X-rays with patients in flexion and extension bending postures and using the Cobb method [74] to measure the angle formed by the endplates [140].

Several studies suggested the ability of lumbar fusion to alleviate low back pain and achieve improvements in disability and quality of life. Randomized controlled trials (RCT) comparing surgery versus conservative treatments [188] have demonstrated that fusion is superior to conservative treatment irrespective of the patients degree of affectation. One of the first RCT regarding the effectiveness of lumbar fusion to treat low back pain compared non-surgical therapies with fusion interventions [101] in a cohort of 294 patients with radiological evidence of disc degeneration. ODI and VAS questionnaires were used as indicators of treatment's outcome during a 2-year follow-up period. Back pain was reduced in the surgical group by 33%, compared to 7% in the non-surgical group while ODI was reduced by 25% after surgery compared to 6% after physical therapy. Those results led to the conclusion that lumbar fusion can diminish pain and decrease disability more efficiently than commonly used non-surgical treatments. Recently, another study with a cohort of 304 patients randomly assigned to surgical (discectomy or fusion) or conservative treatments, showed a greater improvement in ODI score in the group subjected to lumbar surgery [369]. The decrease in disability occurred during the first six months and remained constant for two years. However, no available data after this period were provided.

In a clinical study published in 2015 examining the trends of surgical treatments of lumbar spine diseases in the United States it was seen that the most common diagnoses for low back pain were IVD degeneration, herniated NP, and spinal stenosis. For the treatment of all of them, the most common fusion method was PLIF with postero-lateral lumbar fusion (PLF) (45%) [271]. However, no statistical evidence of superior efficacy of any approach is provided in the literature. In a comparison between ALIF and PLF, no significant differences were found in clinical outcome or fusion rate [288]. Similarly, another comparative study of PLF, PLIF and PLIF+PLF reported no significant differences among them. Nevertheless, PLIF without PLF presented advantages such as the elimination of donor site pain, shorter operating time, and less blood loss [183]. Furthermore, although no differences in radiological and clinical outcomes have been noted, perioperative complications were more likely to appear when posterior or circumferential (posterior+anterior) approaches were used than when a transforaminal (TLIF) approach was considered [155][360]. Indeed, *The guideline for the performance of lumbar fusion for degenerative disease of the lumbar spine*, first published in 2005 and then updated in 2014, endorses the use of pedicle screw fixation (PSF) as a supplement to PLF only for patients in whom there is an increased risk of non-nunion when treated only with PLF [125]. Otherwise, no significant benefit is provided, as fusion rates were similar, and its use increases the costs and complication rates [100][71].

In regard to the use of interbody devices, the medical evidence continues to suggest that they are associated with higher fusion rates compared with PLF alone [244]. Moreover, for lumbar DDD without instability, there is moderate evidence that the stand-alone cage has better clinical outcomes than the open PLF instrumented with interbody device and PSF. Recent case reports with different cages placed in stand-alone construct have demonstrated good rates of fusion and improvements in clinical outcomes [10][75][223][13]. In a comparative study between ALIF in stand-alone and supplemented with PSF, better clinical outcomes were reported in the stand-alone group without differences in fusion rate [340]. However, the lack of large comparative clinical studies added to the subsidence and migration risk and the possible segment instability, make the stand-alone option a very controversial issue.

Comparative trials regarding cage material were also carried out to analyze the differences between PEEK and titanium. While titanium is an osteoconductive material which could promote bone growth [254], PEEK has mechanical properties which allow load sharing with the bone graft and reduce the rate of subsidence [67]. A promising alternative is a PEEK cage with a titanium surface coating, which has exhibited similar fusion rates and clinical outcomes compared to the current standard PEEK and added the benefit of a titanium interface for cellular attachment and osteoblastic phenotype expression [24].

A frequent criticism to the use of fusion is the possibility of increasing the rate of ASD, as observed by some authors reviewed by Radcliff et al. [293]. However, based on the available scientific literature, it is still unclear whether these radiographic and clinical findings are the result of the spinal fusion with the consequent segmental stiffening or whether these represent the natural history of the underlying degenerative disease [142]. Besides, in a study comparing total disc replacement versus ALIF+PSF the ROM measured in the adjacent segments did not present significant differences. Thus, the reoperation rate was not higher in the fusion group [132]. By contrast, a comparison of total disc replacement with circumferential fusion showed that the segment stiffening caused by fusion increased ROM in cranial segments, while the slight ROM decrease with total disc replacement was compensated with the caudal FSU [25], therefore maintaining a more physiological lumbar biomechanics.

1.4.3 In vitro studies

Accurate mechanical characterization of the IVD is required not only to understand how ageing and degeneration can influence the material properties, but also to obtain accurate data to input into finite element models with which develop and test surgical implants [255].

The constituents of AF [21], NP [160] and CEP [300] have been characterized by histological and microscopical observations. These studies have quantified water content, type of collagen or fibre organization of each tissue. From the mechanical point of view, the NP properties have been measured in confined compression [172], unconfined compression [73] and shear [159] giving the bulk, effective and shear moduli. Other studies have reflected the viscoelastic behaviour of the tissue [156] and the influence of the fluid inside it, which is responsible for the hydrostatic pressure that helps to withstand compressive loads [233]. The tensile properties of the AF lamellae have been investigated in tension tests [144] showing that along the fibre orientation the lamellae has the stiffest behaviour. Strain within the disc has been also studied under different loading cases [77]. Furthermore, Ebara et al. [87] explained the differences in tensile properties among the inner/outer and anterior/posterior regions of the AF and quantified them. The CEP has not been extensively studied, some authors have inspected its strength to understand failure mechanisms. Indentation tests have revealed that the underlying BEP is stiffer and stronger around the periphery of the vertebra than in the central region [122].

From the biomechanical point of view, Schultz et al. [321] were the first who analysed the lumbar response under flexion, extension, lateral bending and axial rotation. But the greatest contribution to the study of lumbar spine biomechanics was made by Panjabi and co-workers [267]. In their study, they measured the ROM of each segment in nine human lumbar spines under $\pm$10Nm in each of the three axes. The same author also defined the concept of neutral zone (NZ) [270] as the region around the neutral position where little resistance is offered to the movement. Some studies suggested that an increase in the NZ is a better indicator of clinical instability than an increase in the total ROM [237][112]. This led to the use of in vitro studies to analyse biomechanical alterations caused by IVD degeneration [110]. While some works showed an increment in spinal flexibility for early and mid degenerated discs [341] in axial rotations, others found an increase in segmental stiffness[3] with progressing degeneration [237][179]. Widely accepted results are the ones reported by Mimura et al. who showed reduced flexibility in flexion, extension and lateral bending and higher flexibility in axial rotation. At the same time, they observed an increase of the neutral zone size in all directions for degenerated discs, which may indicate clinical instability in severe degeneration stages.

In vitro testing has been also used to evaluate lumbar biomechanics after surgery. In a comparison among different approaches, it was shown that anterior plates, unilateral, and bilateral screw fixation significantly increased segment stiffness and decreased the NZ [201]. Furthermore, with bilateral PSF no differences were seen from one approach to the others. When rigid fixation was compared to dynamic instrumentation, it was observed that the last one allowed motion that was closer to the intact ROM indicating more natural and favourable kinematics [276]. In a recent study comparing among stand-alone constructs and different supplemental instrumentations (lateral plate, unilateral and bilateral PSF) it was shown that all conditions caused a

[3]The segment stiffness is defined as the applied force divided by the ROM achieved.

significant ROM reduction in comparison with the intact spine [51]. As mentioned before, in this study bilateral PSF provided the greatest reduction in segment motion with similar results among all approaches. In stand-alone construct, extreme lateral interbody fusion (XLIF) achieved more stiffness than ALIF [31] or TLIF [138].

To reveal motion changes in segments adjacent to lumbar surgery, three different approaches have been adopted. These test protocols mainly differ in the assumption on the postoperative motion behaviour of the patients. With the *flexibility protocol* a predefined load is applied to the top of the lumbar spine while maintaining the bottom part rigidly fixed. With the *stiffness protocol* a predefined displacement is applied instead of the load [269]. As a combination of both, the *hybrid protocol* takes the total ROM of the intact spine as a reference and applies a load on the surgical specimen until the reference ROM is reached [266]. It has been observed that with the flexibility protocol the motion of the adjacent segments remains unaltered, and hence the total ROM is reduced. By contrast, when the stiffness of hybrid protocol is used, there is an increase in ROM equally distributed among all the lumbar segments but the treated level. The only difference is that for the stiffness protocol the target ROM is predefined, whereas for the hybrid one it is defined by the intact movement of the patient.

Volkheimer et al. [362] reviewed the effects that a lumbar surgery has over the adjacent segments. Nearly all the studies which used the flexibility or stiffness protocols were not able to see any change at those levels. However, when the hybrid protocol was used, an increase in ROM, intradiscal pressure and applied load were registered at the caudal and cranial FSU adjacent to the fusion site. Yet, no such changes were reported in the levels adjacent to total disc replacement. Given that, the different protocols are defined by the assumption of postoperative motion behaviour, the stiffness and hybrid protocols do not appear to be correct as far as it was shown that the motion of the lumbar spine in patients tends to decrease after fusion [217]. The flexibility protocol could predict this motion decrease. Nonetheless, when used in combination with pure moments no differences can be observed in the adjacent segments and, therefore, no conclusions can be drawn.

1.4.4 Computational works

The finite element (FE) method, originated from the need for solving complex continuum elasticity and structural problems, has become a valuable complementary approach for the study of lumbar function and failure. Since the first application of the FE method to the biomedical field in 1972 [46] applied to a femur were reported, an enormous growth in these models has arisen [313]. The first to analyse the lumbar IVD were Belytschko et al. [34]. They used axisymmetric FE models with linear orthotropic properties to account for axial compression response. After that, the use of more accurate geometries emerged, including endplate curvature [315], 3D models [207] and real geometries extracted from computerized tomography (CT) [91]. In fact, there are parametric studies which have identified the disc height as the most influential parameter on the mechanical behaviour of the IVD [250][234]. Thus, it is important to accurately determine the disc height to estimate the spinal stiffness.

Regarding the material characterization, a tremendous evolution has been experienced since the first orthotropic models. The complexity has been increased incorporating the anisotropy of the annulus due to the collagen fibres, the fluid content, the osmotic pressure and the regional variation in tissue composition [173]. In simulating annulus behaviour, either truss elements within a matrix of solid elements [315], or anisotropic properties have been used to include the effect of fibre orientation [320]. Both options have proven to be equivalent [376]. However, as explained above, collagen fibre orientation and mechanical properties change depending on the region of the AF. Malandrino et al. [218] defined different fibre orientations for four different regions of the IVD: posterior outer, anterior outer, posterior inner and anterior inner and suggested that fibre variations might be an effective tool to calibrate IVD models. Further on, another study developed a model which defined a continuous variation of local annulus material properties based on radial-circumferential distribution and showed a strong influence of fibre distribution on disc biomechanics [224]. To simulate the time dependent response of the tissue, a biphasic behaviour should be defined including a porous solid phase to describe the collagen-proteoglycan components, and an incompressible fluid phase representing the interstitial fluid. The first who implement a poroelastic material behaviour for the disc were Simon et al. [328]. They used an axisymmetric model to study creep response. More complex mathematical models were thereafter implemented with non-linear fibres and a permeability dependence with deformation [22][320]. Besides, osmolarity regulates the swelling pressure and disc hydration contributing to the load-bearing. To include this phenomenon, the diffusion of mobile ions that interact with the fixed charges of the proteoglycans are required. Assuming an instantaneous chemical equilibrium throughout the tissue, swelling has been incorporated in biphasic formulation with osmotic pressure gradients expressed as a function of the fixed charge density that depends on volumetric deformations [320][108].

Finally, transport model studies have been carried on to investigate how the nutrients are supplied to the avascular disc tissues via endplates and peripheral annulus routes. Ferguson et al. [95] linked a convection/diffusion model with a poroelastic structural model to evaluate solute transport over a diurnal cycle. Soukane et al. [338] performed a parametric analysis of how EP area, EP properties, and the mechanical loads influence the diffusion of oxygen, glucose and lactic acid. Posteriorly a very detailed model described by Galbusera and co-workers showed how the endplate porosity, cell population, diffusivity and consumption rates affect considerably the glucose and oxygen concentrations [105].

To aid in the understanding of the degenerative process and biomechanical effects of lumbar treatments, a model of a complete FSU or even a whole lumbosacral FE model is required. As well as for the IVD, the geometries are often obtained from image data like CT or MRI, and then, some structures are simplified. For modelling of the FSU, other structures such as ligaments and facet joints should be considered. The ligaments are usually modelled as truss or spring elements with a cross-sectional area and either linear [183] or non-linear [94][372] elastic behaviour. However, some recent studies have modelled the ligaments as 3D solid structures with hyperelastic behaviour and proposed that this approach could reflect more effectively the mechanical behaviour of the FSU than using truss and spring elements [375]. In a sensitivity study about the parameters that influence more the movement of the spine, the authors reported that posterior ligaments play a dominant role in the response to flexion, whilst the capsular and anterior ligaments were more influential under extension [206]. Lastly, ligament pretension, which is often overlooked or not reported, was also found to have a significant impact in spine biomechanics. The facet joints have been modelled in different ways, chief of which are gap elements whose stiffness alters as the gap closes [304], and explicitly modelling of the cartilage layer with a frictionless contact or low coefficient of friction [314]. Furthermore, the facet morphology was found to have a considerable effect on the lateral bending and axial rotation of the segment [145]. A complete 3D non-linear poroelastic L1-L5 model was built by Schmidt et al. [318] to study the response under different diurnal loading cycles as well as disc recovery. However, they simplified the real geometry of the spine. In the same direction, Moramarco et al. developed a 3D non-linear poro-hyperelastic model with fibre anisotropy in a real lumbosacral geometry and studied the ROM of each segment and the stress distribution within the IVDs under different loads [241]. More accurate geometry segmentation processes for patient-specific modelling have been recently published [198][275], although these techniques have not been used to FE simulation yet.

One of the major goals of FE modelling in the lumbar spine is to help in the comprehension of the degenerative process initiation and progression. Commonly the degeneration process has been simulated by changing mechanical properties and disc morphology. Parameters such as disc height loss, endplate sclerosis, water content, tissue permeability and depressurization have been tested in FSU models [107]. It was seen that a decrease in disc height or water content caused a decrease in ROM and facet force, while a NP depressurization leads to an increase in disc stress possibly inducing failure. The same authors built a series of models with random combinations of degenerative changes and found a tendency of increasing segment stiffness with progressing degeneration and also a decrease in facet forces and fluid loss [106]. Other studies simulated the different grades of degeneration by varying the elastic properties and permeability in an axisymmetric model and suggested that changes caused by degeneration may lead to further structural changes in the tissues [228]. A simulation of a lumbosacral FE model using the hybrid loading protocol showed how degeneration at one level changed the motion patterns in the upper and lower segments. The ROM and facet forces of those levels increased, which could rise the risk of injury [307]. As already told, the nutrition of the disc plays a crucial role in maintaining the homeostasis of the tissues. Cell viability in the disc has been studied in a 3D geometry of the IVD coupled with mechanical deformation [167]. It was seen that, in the degenerated disc, the nutrient supply was bellow the levels required to maintain cell viability, and therefore, cell density decreased. A more detailed study based on a bio-mechano-eletro-chemical continuum mixture theory showed that a reduction in the nutrient supply had long-term effects on disc degeneration [129]. Lastly, the damage of the tissue was also simulated with a continuum damage formulation to investigate the initiation and progression of mechanical damage [292]. As the severity of degeneration increased, the number of cycles to failure decreased. A complete model of subject-specific geometry for different degeneration stages was recently published [219]. They included a validation of non-linear behaviour of the IVD tissues against in vitro creep tests, a transport cell viability model and tissue damage. With all of that, they found relationships of the disease with osmotic pressure, water loss, and disc fibrosis.

However, the FE models have not only been used for the study of the biomechanical function of the spine and its behaviour when healthy, diseased or damaged, but they also serve as a tool for the design and application of spinal instrumentation. Several computational works have been developed to evaluate and compare the effects of different surgical techniques and approaches over the affected and adjacent segments. Movements of the affected and adjacent segments, cage-endplate interface pressure and relative displacement, stress distribution within the disc, and facet joint forces have been primarily taken as output variables in the large number of studies regarding different surgical techniques. Implants such as dynamic pedicular devices [104], interspinous devices [210], nucleus replacements [312], TDR [85] or interbody cages (reviewed in [381]) have been computationally simulated and compared in an attempt to appraise for the benefits and drawbacks of each one.

This thesis is framed in the study of lumbar fusion using interbody cages with or without supplementary PSF. In this regard, some authors had simulated lumbar biomechanics after cage insertion in a single FSU [94][109][180] and others in a complete lumbar spine [67][70][93][209]. All of them agreed that PSF provides a higher segment stiffness [104][15], but segment stability was also reported when cages were placed as stand-alone devices. Since the goal of lumbar fusion is to stabilize the segment, restore the IVD space and maintain the lumbar lordosis, the major concerns regarding surgery complications are: segmental instability [151], cage subsidence into the vertebrae [229] and cage migration [65]. Furthermore, lumbar fusion has been associated with the risk of adjacent segment disease because it induces biomechanical alterations [61]. The change in stress distribution in the segments adjacent to the fused level were also considered in many studies [304][171]. However, there is a lack of a model of the whole lumbar spine with complex material behaviours that takes into account all these key-factors to design an improved device for the treatment of IVD degeneration and hernia.

Finally, computational mechano-biological models have been used to predict the healing process after surgery [14][242], so it could be possible to follow the tissue growth around the intervertebral cage. The relationship between the mechanical stimulus and the biological response was empirically obtained through the study of a long bone callus [72][197]. Many clinical applications of these models could be found in literature. However, there is only one recent model which study lumbar fusion after different cage insertions [286][29]. It consists of an axisymmetric model regulated by a mechano-differentiation process. Thus, it allows for the study under compressive loads but not under bending moments.

1.5 Motivation

Low back pain has become one of the most common causes of disability, with recent reports indicating a lifetime prevalence as high as 85% in industrialized countries [27]. As with many other musculoskeletal disorders, the prevalence of low back pain increases with age, suggesting that incidence is likely to increase due to a global ageing population, changes in lifestyle and occupational stresses.

In fact, according to the recent Global Burden of Disease study, low back pain is the most common musculoskeletal disorder and the leading cause of years lived with disability in all developed countries [363]. In Spain, it is the second main reason of chronic problems in the adult population (Fig. 1.9) and it is the main cause of work absenteeism, which increases the costs and worsens quality of life [56].

Those problems have a high social and economical cost. I.e. the total cost of back pain in the UK is estimated to be between 1% and 2% of gross domestic product, equating to between £14 and £28 billion lost per annum [220], while in the United States the costs have been estimated at around $85.9 billion [226].

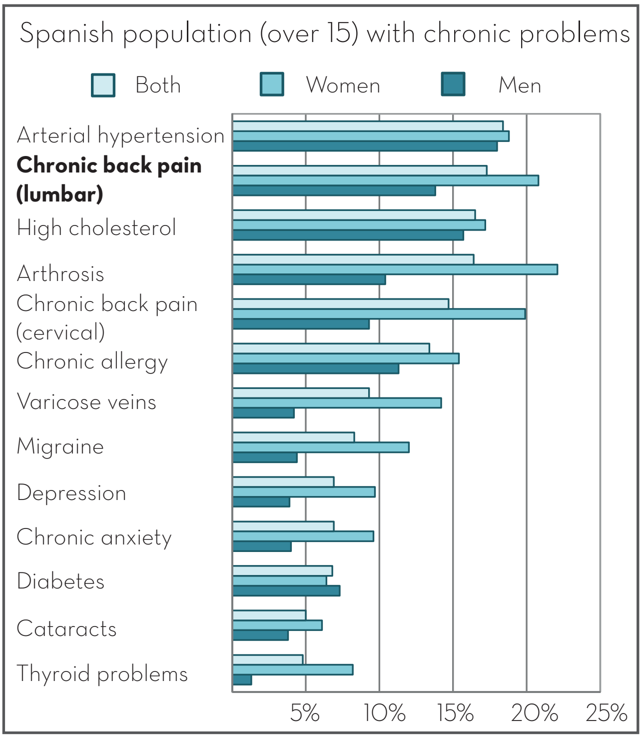

Figure 1.9: *Main causes of chronic problems in the adult Spanish population (INE 2014 [162]).*

In those cases where conservative treatments failed, a surgical intervention may be needed. However, until today no surgery has shown clear advantages over the others and, despite the large amount of clinical, in vitro and computational studies available, a big controversy is still present about the long-term consequences of lumbar fusion, which is the 'gold standard' technique. Thus, this thesis is motivated by the need to understand the underlying problems of lumbar pathologies and current surgeries. Furthermore, it is expected to overcome the demands of new implants thought specifically for each patient.

1.6 Objectives and thesis outline

The main objective of this thesis is to shed light on the biomechanical behaviour of the lumbar spine affected by different pathologies or surgeries and to suggest alternatives that may help to improve the long term clinical outcomes. To fulfil this principal goal, the following partial aims were defined:

- **Computational simulation of the intact lumbar spine biomechanics:** The development of a realistic FE model of the lumbar spine which will serve as a baseline for two purposes: build further models and act as the control.
- **Create an animal model of disc degeneration:** Understand the biological and biochemical changes that happen during IVD degeneration and how they correlate with the mechanical behaviour of the structures.
- **Computational simulations of the degenerated lumbar spine biomechanics:** Studying the influence that the degenerative process has over the affected and adjacent structures.
- **Computational simulations of the lumbar spine biomechanics after different surgeries:** Cross-compare among different surgical protocols and implant designs, as well as suggest alternatives or beneficial features from a mechanical point of view.
- **Development of an algorithm capable of predicting tissue growth and bone remodelling:** Expand the knowledge extant in other fields to the study of the tissue response after lumbar surgeries.

The results obtained during this thesis have been organized in seven chapters, including the present one as enumerated below:

Chapter 1: An introduction to the lumbar spine, its function, composition and behaviour; the intervertebral disc diseases; and the available surgical solutions, is presented. Then, a broad review of the work that has been done over the years on this particular topic is summarized. Finally, the motivation, goals and methodology in which are based this work are explained.

Chapter 2: The development of the intact FE model is detailed. This chapter gathers the geometrical aspects of the different structures, the mesh employed to discretized the geometry and the material behaviour used to characterize each tissue. Additionally, the loading and boundary conditions imposed to the model are explained, together with the validation of the model.

Chapter 3: This chapter shows the animal model created to understand the degeneration process of the IVD. New Zealand white rabbits were used to study the relationships among physical observations, mechanical properties and biomechanical behaviour by using MRI, mechanical testing and FE models.

Chapter 4: The influence of degenerative factors such as biphasic properties, morphological, and biomechanical changes are studied. A single IVD FE model was used to understand how the permeability, proteoglycan content and porosity altered the disc behaviour. MRI images from patients with different grades of degeneration were analysed to look for morphological changes. Finally, the model presented in Chapter 2 was modified to see the effect of degeneration on the lumbar spine.

Chapter 5: A comparison of the biomechanical behaviour of the lumbar spine after different surgeries is presented in this chapter. In particular, four different FE models of lumbar fusion are described and analysed: two different intervertebral cages (bean shape and two rectangular parallel cages) supplemented with posterior screw fixation or in a stand-alone construct (without any supplementary fixation). Additionally, a parametric investigation of different cage design features and positioning is presented in a single FSU with an inelastic characterization of the vertebral bone to study the risk of cage subsidence. Finally, the alternative of 3D printed PCL cages was studied and summarized.

Chapter 6: Two different algorithms for tissue healing are described and implemented in this chapter, together with a bone remodelling algorithm. A mechano-regulated and a bio-mechano-regulated theories were used to predict fusion after nucleotomy, internal fixation, anterior plate placement and stand-alone cage insertion. The role of disc height and loading protocol is discussed.

Chapter 7: In this chapter the main conclusions, original contributions and future works are summarized.

1 INTRODUCTION TO THE LUMBAR SPINE

2 FINITE ELEMENT MODEL

3 ANIMAL MODEL OF DISC DEGENERATION

4 DEGENERATION SIMULATION

5 SURGERIES

6 TISSUE HEALING AFTER SURGERY

7 CONCLUSIONS & FUTURE LINES

CHAPTER 2

FINITE ELEMENT MODEL DEVELOPMENT

The object of this chapter is to present in a detailed and comprehensive way the finite element model used to simulate the human lumbar spine. A description of the different tissues included, geometry reconstruction, meshing process, material characterization, and loading and boundary conditions applied is depicted.

Additionally, the biomechanical behaviour of the model is validated by comparison of the numerical results with in vitro and computational data from the literature.

2.1 Geometry definition

A computed tomography of the lumbar spine from an asymptomatic 46-year-old male subject was used to reconstruct the bone geometry [241]. The software Mimics®(Materialise, Belgium) was employed for the segmentation of the mineral tissue. Then, the soft tissues were modelled according to anatomical characteristics. The intervertebral discs were reconstructed from the surfaces of the vertebral bodies above and bellow the disc, 0.5mm layers were defined in the upper and lower ends of the disc to mimic the cartilaginous endplates. Additionally, the rest of the disc was divided into nucleus pulposus and annulus fibrosus considering that the NP occupies a 30% of the total disc volume [121]. Seven major ligaments, corresponding to anterior (ALL) and posterior longitudinal ligaments (PLL), intertransverse (ITL), interspinous (ISL) and supraspinous ligaments (SSL), capsular ligament (JC) and ligamentum flavum (LF) were defined according to anatomical descriptions. A view of the whole assembled model, as well as a split view of each component is shown in Figure 2.1.

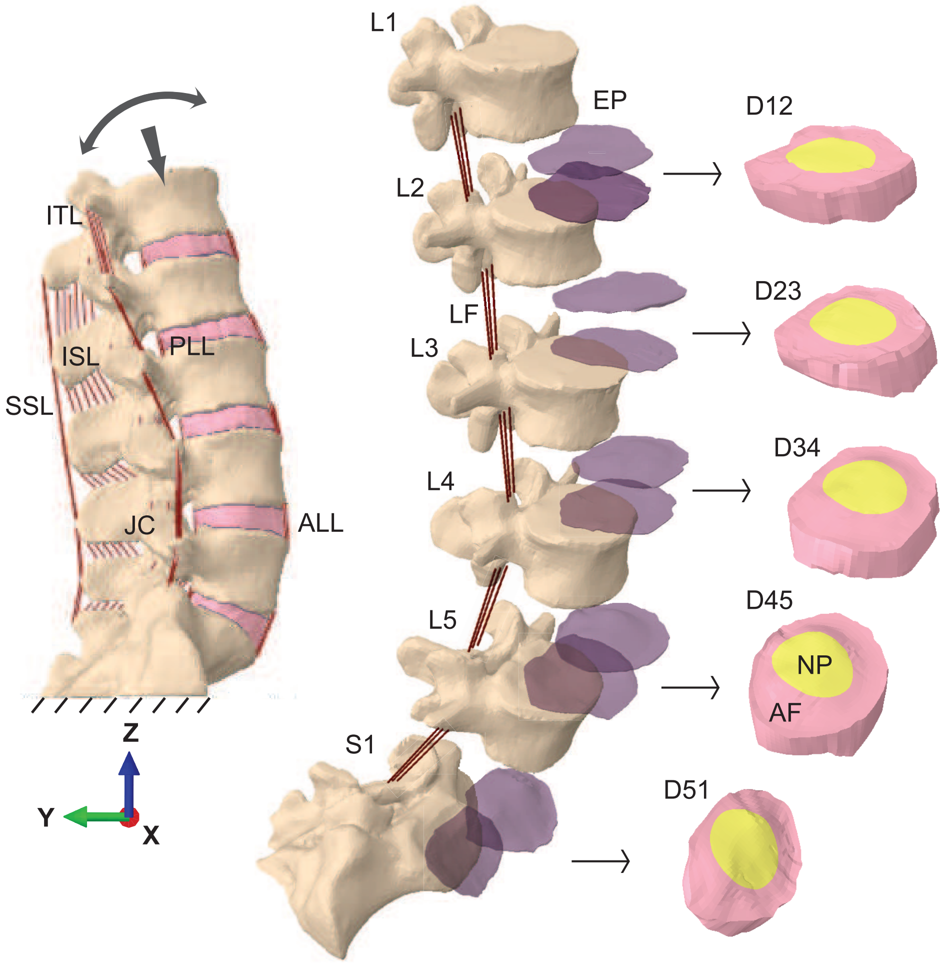

Figure 2.1: *Ligamentous lumbosacral lumbar spine. Lateral view and split view of the different components of the spine (vertebrae (from L1 to S1), intervertebral discs (from D12 to D51) composed of: endplates (EP), annulus fibrous (AF) and nucleus pulposus (NP); and ligaments)*

2.2 Finite element mesh

To build the finite element mesh, different element types have been used as explained below (Fig. 2.2). Linear tetrahedral elements were used to mesh the vertebrae. The mean size for these elements was 2mm at the surfaces which increased towards the centre of the vertebral body. The IVDs were meshed with linear hexahedral elements after a sensibility test to determine a mesh size of 1.5mm. In turn, the seven spinal ligaments were modelled as uniaxial truss elements with different cross-sectional areas shared among the number of elements employed to mimic each ligamentous membrane. Finally, triangular shell elements of 0.2mm thickness were used for the facet joints cartilage.

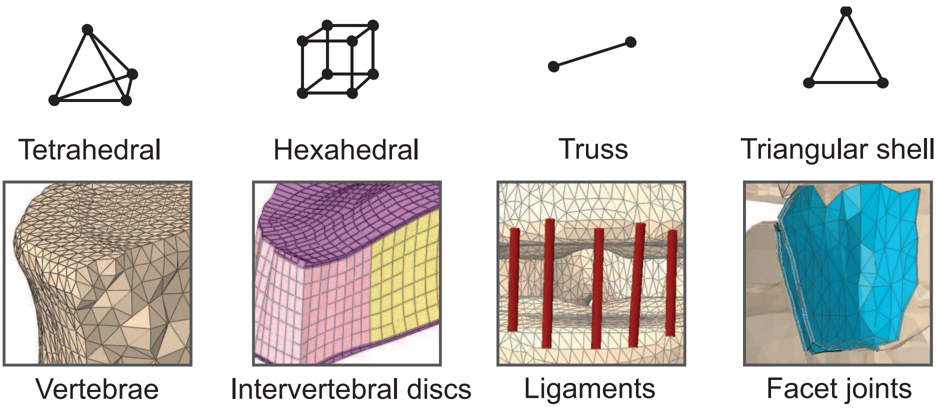

Figure 2.2: *Finite elements employed to mesh each structure of the model.*

2.3 Materials

Once the model was built and discretized, each material tissue has been characterized an introduced into the model as follows. Linear poro-elastic properties were assigned to the vertebral bodies differentiating between cortical and cancellous bone. Likewise, the cartilaginous EP were also characterized by a linear poro-elastic material. A poro-hyperelastic Neo-Hookean material was used for the NP, which strain energy density function was defined by Equation 2.1. Additionally, the osmotic behaviour (explained in detailed bellow) was included to account for the high water content present in the NP.

$$W = C_1(\overline{I_1} - 3) + D_1(J - 1)^2 \tag{2.1}$$

$\overline{I_1}$ is the first invariant of the isochoric part of $\overline{\mathbf{C}}$ (Eq. 2.2), $\mathbf{C}$ the deformation gradient $\mathbf{C} = \mathbf{F}^T\mathbf{F}$ and $\mathbf{F}$ the right Cauchy-Green deformation gradient.

$$\overline{I_1} = \overline{\mathbf{C}} = (det\mathbf{C})^{-1/3}\mathbf{C} = J^{-2/3} I_1 \tag{2.2}$$

The annulus fibrosus of human IVD presents a very particular structure. It consists of a solid porous matrix, saturated with water, which mainly contains proteoglycans and collagen fibres. To simulate its behaviour a 3D osmo-hyperelastic model reinforced with two families of fibres was constructed and implemented in a UMAT user Abaqus subroutine.

The strain energy density function (Eq. 2.3), initially presented by Eberlein et al. [88] to characterize fibre reinforced materials and extensively used for biological tissues, was modified to introduce the contribution of the osmotic pressure. This term takes into account the effect of the electrically charged proteoglycans and it can be coupled with the biphasic formulation.

$$\begin{aligned}
\Psi(\mathbf{C},\mathbf{A_1},\mathbf{A_2}) &= \Psi_{gs}(\mathbf{C}) + \Psi_f(\mathbf{C},\mathbf{A_1},\mathbf{A_2}) + \Psi_{vol}(J) \\
&= C_{10}(\overline{I_1} - 3) + C_{20}(\overline{I_1} - 3)^2 \\
&+ \frac{K_1}{2K_2}\left\{exp[K_2(\overline{I_4}^* - 1)^2] - 1\right\} + \frac{K_1}{2K_2}\left\{exp[K_2(\overline{I_6}^* - 1)^2] - 1\right\} \\
&+ \frac{1}{D}(J-1)^2
\end{aligned} \tag{2.3}$$

where the invariants are calculated as (Eq. 2.4)

$$\begin{aligned}
I_1 &= tr\mathbf{C}; \\
I_4 &= \mathbf{a_0}\mathbf{C}\mathbf{a_0}; \\
I_6 &= \mathbf{b_0}\mathbf{C}\mathbf{b_0}
\end{aligned} \tag{2.4}$$

considering that the vectors $\mathbf{a_0}$ and $\mathbf{b_0}$ define the initial direction of the two families of fibres (Eq. 2.5), which are distributed circumferentially in concentric layers forming an angle of $\phi = \pm 30°$with respect to the disc mid-height plane.

$$\mathbf{a_0} = \begin{pmatrix} \cos\phi \\ \sin\phi \\ 0 \end{pmatrix}; \mathbf{b_0} = \begin{pmatrix} \cos\phi \\ -\sin\phi \\ 0 \end{pmatrix} \tag{2.5}$$

The energy function is therefore divided into different components corresponding to the ground substance (gs), the fibres network (f), and the material compressibility (vol). Accordingly, the 2nd Piola-Kirchhoff stress tensor **S** is defined by the Equation 2.6, and the contribution of each part can be expressed as Eq. 2.7

$$\mathbf{S} = 2\frac{\partial \Psi}{\partial \mathbf{C}} = \mathbf{S}_{gs} + \mathbf{S}_f + \mathbf{S}_{vol} \tag{2.6}$$

$$\begin{aligned}\mathbf{S}_{gs} &= 2\frac{\partial \Psi_{gs}}{\partial \mathbf{C}} = 2\frac{\partial}{\partial \mathbf{C}}(C_{10}(\overline{I_1}-3) + C_{20}(\overline{I_1}-3)^2)\\ &= 2J^{2/3}\mathbb{P} : C_{10}\mathbb{I} + 4J^{2/3}\mathbb{P} : C_{20}\mathbb{I}\end{aligned} \tag{2.7}$$

$$\begin{aligned}\mathbf{S}_f &= 2\frac{\partial \Psi_f}{\partial \mathbf{C}} = 2\frac{\partial}{\partial \mathbf{C}}\sum_{n=1}^{2}\frac{K_1}{2K_2}\left\{exp[K_2(\overline{I_n}^* - 1)^2] - 1\right\}\\ &= 2J^{2/3}\mathbb{P} : \sum_{n=1}^{2} 2K_1\left\{exp[K_2(\overline{I_n}^* - 1)^2](\overline{I_n}^* - 1)\mathbf{A}_n\right\}\end{aligned}$$

$$\mathbf{S}_{vol} = 2\frac{\partial \Psi_{vol}}{\partial \mathbf{C}} = \frac{2}{D}J(J-1)\mathbf{C}^{-1} - J(\triangle\Pi + \mu_f)\mathbf{C}^{-1}$$

where the term relative to the material compressibility has been modified to incorporate the osmotic pressure contribution. Thus, the water chemical potential can be defined as Eq. 2.8 [320],

$$\mu_f = p - \Pi \tag{2.8}$$

while the osmotic pressure gradient (Eq. 2.9) is calculated by means of the external and internal osmotic pressures (Eq. 2.10):

$$\triangle\Pi = \Pi_{int} - \Pi_{ext} \tag{2.9}$$

$$\Pi_{ext} = 2\phi_{ext} RT c_{ext} \tag{2.10}$$

$$\Pi_{int} = \phi_{int} RT\sqrt{c_F^2 + 4c_{ext}^2}$$

Both external and internal osmotic pressures depend on the external and internal osmotic coefficients (ϕ), respectively, and on the external salt concentration (c_{ext}). Besides, the internal osmotic pressure depends also on the fixed charged density (c_F) that is related to the proteoglycans content as defined by Eq. 2.11

$$c_F = c_{F,0}\left(\frac{n_{F,0}}{n_{F,0} - 1 + J}\right) \tag{2.11}$$

Furthermore, as the tissue is compressed, the fluid is expelled diminishing the porosity. As a consequence, the decreasing hydraulic permeability (k) of the ground substance matrix can be assumed to be dependent on porosity changes in the following way (Eq. 2.12):

$$k = k_0\left(\frac{n}{n_0}\right)^m \tag{2.12}$$

where k_0 is the initial permeability, n_0 and n the initial and actual porosity, and m a positive coefficient equal to 15. All material parameters are listed in Table 2.1

Finally, the seven spinal ligaments were characterized with a strain-dependent behaviour under traction and without resistance to compression as summarized in Table 2.2.

Table 2.1: Material elastic and biphasic properties assigned to the different tissues of the lumbar spine.*[95][22] $^{\top}$[317] $^{\diamond}$[241][158][320].

	Elastic parameters					Biphasic parameters			
	E[MPa]			ν		k_0 [m^4/Ns]	e (void ratio)	$c_{F,0}$ [meq/mm^3]	$n_{F,0}$
Cortical bone*	17,000			0.3		5.77e-18	0.05	-	0.05
Cancellous bone*	100			0.2		5.55e-11	0.41	-	0.29
Endplate*	20			0.4		7.22e-13	4	-	0.8
Facet cartilage$^{\top}$	35			0.4					
	C_{10}	C_{20}	D [MPa^{-1}]	K_1 [MPa]	K_2				
Annulus$^{\diamond}$	0.1	2.5	0.306	1.8	11	1.85e-15	2.7	1.8e-4	0.72
Nucleus$^{\diamond}$	0.45	2.5	0.306	1.8	11	1.92e-16	4.8	2.4e-4	0.8

Table 2.2: Material properties [63][282] and initial pretension [302] of the lumbar spinal ligaments.

	E_1 [MPa]	E_2 [MPa]	ε_{12}	Number of elements	Area [mm^2]	Prestress [MPa]
ALL	7.8	20.0	0.12	10	32.9	0.804
PLL	1.0	2.0	0.11	9	5.2	0.019
LF	1.5	1.9	0.062	6	84.2	0.02
ITL	10.0	59.0	0.18	16	1.8	0.026
SSL	3.0	5.0	0.2	4	25.2	0.017
	Spine level	Stiffness [N/mm]	v	Number of elements	Area [mm^2]	Prestress [MPa]
	L1-L2	42.5±0.8				
	L2-L3	33.9±19.2				
JC	L3-L4	32.3±3.3	0.4	14	43.8	0.237
	L4-L5	30.6±1.5				
	L5-S1	29.9±22.0				
	L1-L2	10.0±5.2				
	L2-L3	9.6±4.8				
ISL	L3-L4	18.1±15.9	0.4	11	35.1	0.028
	L4-L5	8.7±6.5				
	L5-S1	16.3±15.0				

2.4 Loading & boundary conditions

The interactions among the different components of the model were defined as follows. All the elements were assumed to be tied but the facet joints, which were modelled as frictionless surface-to-surface contact combined with a penalty algorithm for normal contact, with a normal contact stiffness of 200N/m.

Initial ligament pre-strain was set as initial condition according to the experimental values from literature [302]: 5.3% in the anterior longitudinal ligament (ALL), and 4.3% in the interspinous ligament (ISL).

Once the model was built, a number of boundary and loading conditions were imposed to the model to simulate the body weight and bending movements. First of all, a total displacement and rotation restriction was imposed on the lower face of the sacrum. The first step consisted of 8 hours of free swelling during which the fluid came into the IVDs increasing the volume and intradiscal pressure. Then a follower pre-load of 100N was applied followed by ±10Nm moment load in flexion-extension, lateral bending (LB) and axial rotation (AR) [267][49][120]. All simulations were run and post-processed using ABAQUS 6.13 (SIMULIA, Providence, RI, USA).

2.5 Validation of the ROM

The material model used for the characterization of the intervertebral disc tissues was extensively tested and validated in previous works [241].

For that reason, in this thesis the ROM of the intact model was validated comparing the rotation of each segment with experimental and computational results from literature [267][130][273][50] as shown in Figure 2.3.

Comparing the moment-rotation curves in flexion, extension, lateral bending and axial rotation of each segment, the model presented in this thesis showed to be in agreement with the results from literature but in extension and axial rotation at the lower levels, where the movement reported in the in vitro literature was lower. The rotation in these directions was influenced by the contact at the facet joints which is geometry-dependent and may be the cause of this disagreement in the lower segments.

On the other hand, the total motion of the lumbar spine was in agreement for extension, lateral bending, and axial rotation (Fig. 2.3b). In flexion, the total rotation recorded in the presented lumbosacral FE model was above the range reported by Campbell et al., however, the segmental ROM matched closely the rest of the studies.

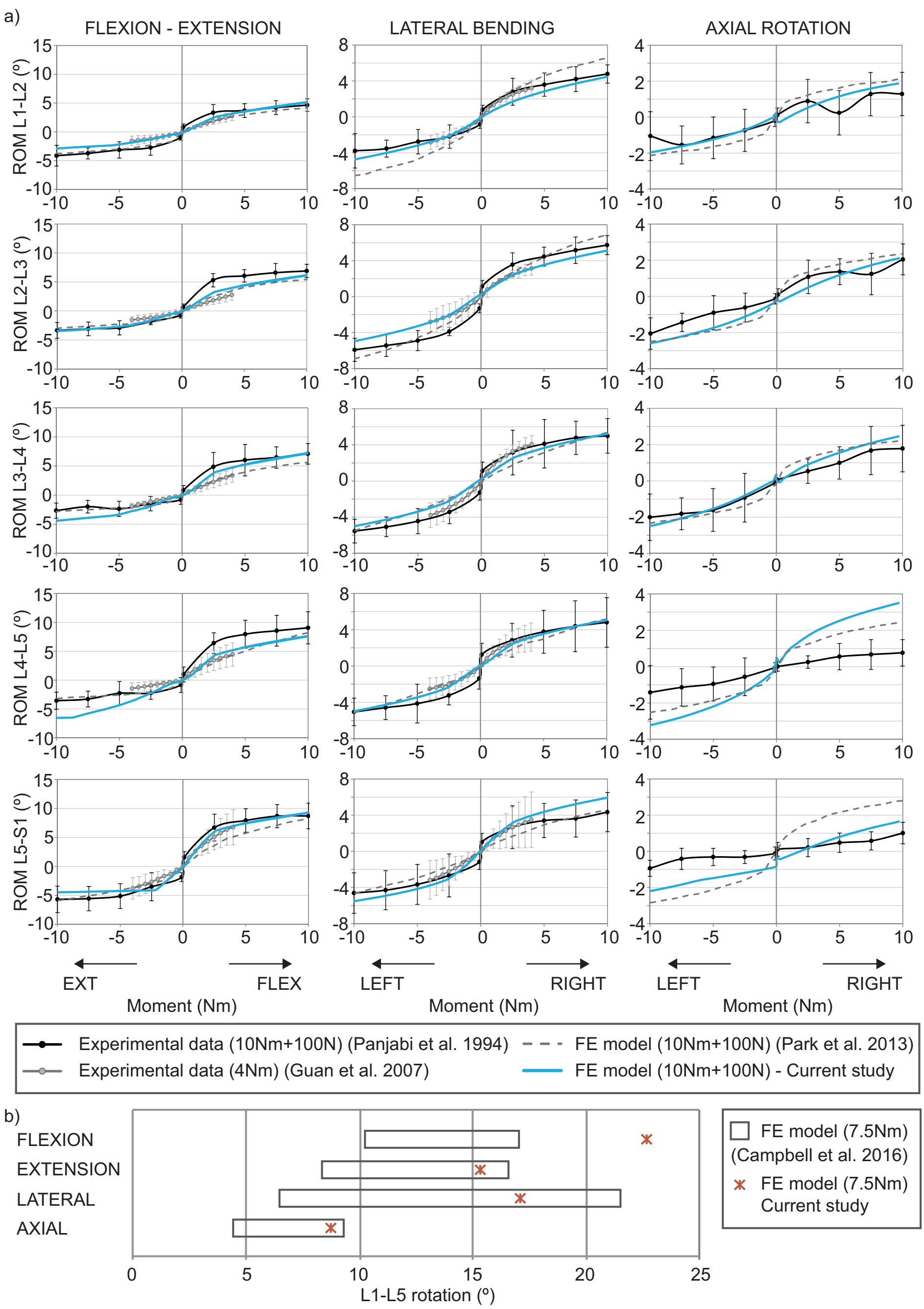

Figure 2.3: *a) Moment-rotation curves in flexion, extension, lateral bending, and axial rotation. ROM comparison of among FE results, in vitro and computational models from literature [267][130][273] in each segment of the intact spine. b) Total rotation of the lumbar spine in comparison with the results of 18 FE patient-specific models [50].*

CHAPTER 3

ANIMAL MODEL OF INTERVERTEBRAL DISC DEGENERATION

In this chapter, an animal model of disc degeneration is presented. Animal models have been extensively used for the study of degenerative diseases and evaluation of new therapies to stop or even reverse the disease progression. The aim of this study was to reproduce lumbar intervertebral disc degeneration in a rabbit model by performing a percutaneous annular puncture at L4-L5 level. The effect of this damage on the spinal behaviour was analysed combining three different techniques: imaging processing, mechanical testing, and computational modelling. A finite element model was built based on MRI and mechanical testing findings to add new biomechanical information that cannot be obtained experimentally.

Although extrapolation to humans should be carefully made, the use of numerical animal models combined with the experimental ones could give new insight of the overall mechanical behaviour of the spine.

**This study was carried out in strict accordance with the recommendations in the Royal Decree 1201/2005 of 10 October 2005 (BOE from Oct. 21) on protection of animals used for experimentation and other scientific purposes. Experimental protocols were approved by the Committee on the Ethics of Animal Experiments of Minimally Invasive Surgery Centre Jesús Usón and by the Council of Agriculture and Rural Development of the Regional Government of Extremadura, Spain.*

3.1 Introduction

Intervertebral disc degeneration is one of the most common causes of chronic disability and low back pain in the elderly population [149]. However, to date, few clinical options are available to manage the underlying problem of the degeneration and the treatment is limited to surgical joint replacement and pain relief due to the lack of knowledge of its aetiology and pathogenesis [361].

Urban and Roberts [352] described the degeneration of the IVD as “an aberrant cell-mediated response to progressive structural failure ”. To investigate changes in structural, biological and biochemical properties during the degenerative process as well as treatments to stop or even reverse this process, animal models of different species have been used [174][262][261][297]. Nonetheless, there are several important issues which should be considered in the translation of the results to human tissue due to: anatomical and biomechanical differences, changes with age and loading conditions of the IVDs. For this reason, scaling is required in the interpretation of the findings, so the relationship between the geometrical factors and the behaviour being tested should be clear. In small quadrupeds the loads are probably smaller than in humans, however, since their discs are much smaller; the intradiscal pressure might be similar. Thus, in pilot pre-clinical studies the use of the rabbit disc model may still be relevant and cost effective [12].

Several methods have been used to induce IVD degeneration in rabbit animal models such as spontaneous initiation [200], chemical injections [16], biomechanical alterations [193] or disc lesions [208], among others [329]. The most extensively used method has been to provoke damage to the annulus fibrosus. Within these techniques, stab with a scalpel was the first one used and described by Lipson and Muir [208] who observed changes in proteoglycan, water content, and hyaluronic acid concentration. After that, many studies focused their efforts on achieving a slow progressive degeneration model via stab incisions, needle punctures or percutaneous needle punctures. While stab injuries seemed to cause a quick degeneration or even an immediate herniation of the nucleus pulposus, annular punctures resulted in a slow and reproducible degenerative process [335][89]. In most of these works, the progression of degeneration was analysed using magnetic resonance imaging data and histologic evaluation over time showing a decrease in water content, a reduction of disc height and a decrease in MRI signal intensity [335][182][383]. However, these studies applied different surgical procedures at each level of the spine preserving one level intact to serve as control, and neglecting the influence of degeneration on the adjacent segments [184]. Furthermore, they did not assess changes in mechanical behaviour as was later on studied with dynamic compression [238], creep [205], tension/compression [131] and flexion/extension [139] tests showing significant alterations in mechanical properties with degeneration. In particular, the study done by

Beckstein et al. [33] compared normalized axial mechanical properties, glycosaminoglycan (GAG) and water content among species and showed that once the measures are normalized, they do not present significant differences across species.

On the other hand, the use of computational models could give significant information for in vivo studies and mechanical testing. Thus, a better understanding of internal pressures, local stresses and strains, which can be easily measured in finite element (FE) models, would be helpful to give new insight into IVD diseases. Previous studies [317] have built FE models in other species and proved that, when species-specific material properties are included, the human and animal discs are functionally adapted to produce similar internal stresses despite the large variation in geometry. Recently, some authors have developed animal FE models for the study of different disorders, e.g. a sheep cervical spine to serve as a model to test different treatments and surgeries [83], a porcine spine as a tool to test fusionless instrumentation for scoliosis treatment [133] or a compression-induced degeneration mouse model as an aid to interpret histologic and biologic data [211]. However, no FE model has been built to reproduce rabbit disc degeneration using data from an experimental protocol.

In this work, a disc degeneration animal model has been developed and analysed using MRI data, mechanical testing, and numerical modelling. As other authors [335][238], the New Zealand rabbit was used as the animal model. This degeneration model was obtained by performing a percutaneous puncture at one disc level remaining intact the rest of the rabbit spine. Thus, the progression of the degeneration in the whole spine was assessed by means of medical imaging and mechanical testing. These results have been used to construct a FE model of one specimen of rabbit spine to reproduce each step of the surgery. Thus, the goal of this study was to reproduce a progressive IVD degeneration in a rabbit model using a minimally invasive technique and to study the relationship between mechanical and structural changes seen experimentally and the stresses computed numerically.

3.2 Materials & Methods

Twenty mature female New Zealand White rabbits (5.5-6.5kg body weight) were used. The animals were randomly divided into two different groups: experimental (n=16), whereby the L4-L5 IVD was punctured; and control (n=4). The animals were followed up by MRI before surgery and three-six months after the surgery. In order to perform the mechanical test, half of the experimental group (randomly selected) were euthanized at three months and the rest of them at the end of the study. Data from MRI and mechanical testing were statistically analysed. Due to the small sample size, the non-parametric Mann Whitney U Test was used to test for differences [227]. Finally, a FE model of a rabbit spine was constructed to simulate the progression of the degeneration after surgery using the data from the experimental test. A summarized workflow of the whole study is shown in Figure 3.1. Each step is explained below in detail.

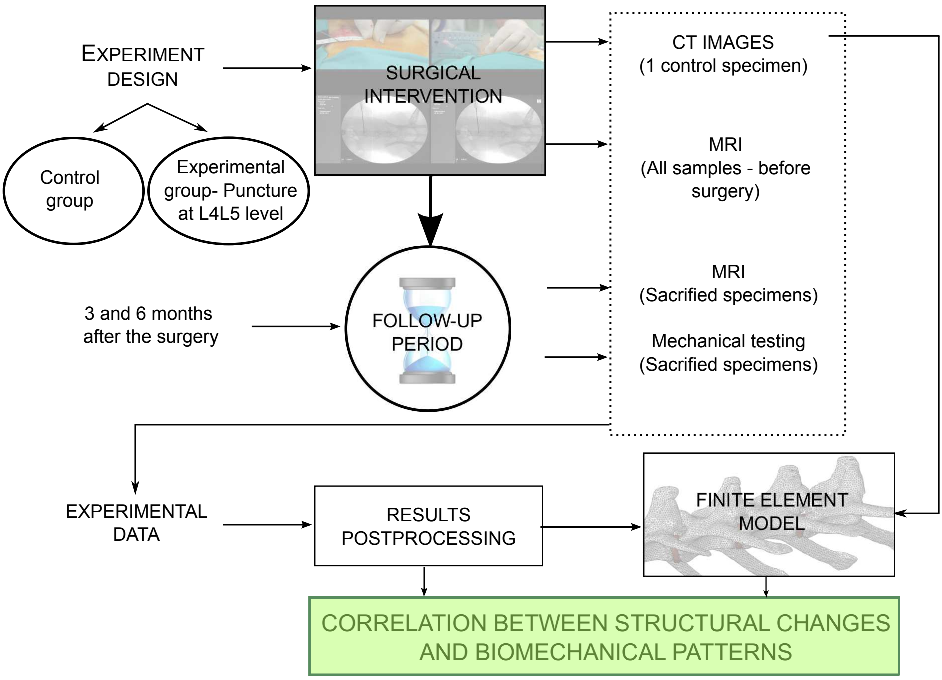

Figure 3.1: *The experimental protocol was designed using a control group (n=4) and an experimental group (n=16) in which a puncture was performed at L4L5 level. Three months after surgery the animals of the control and half of the experimental group were sacrificed. Six months after surgery, the remaining half of the experimental group was sacrificed. Spines were resected en bloc, harvested and conserved. Mechanical testing was performed on these spines to measure the evolution of the IVD mechanical properties with degeneration. The spines were followed up during all the study using MRI. Using the experimental data, a finite element model of a rabbit was developed to simulate the different steps of the surgery and the progression of the degeneration.*

3.2.1 Surgical technique

An 18-gauge hypodermic needle (Spinocan®B.Braun Melsunger AG, Germany) was used to induce disc injury at L4L5 level using a postero-lateral approach. The needle was inserted, in a percutaneous manner, at 30-35mm right to the midline spinous process and with an angle of 35-40°with respect to the horizontal plane. The penetration depth was checked under fluoroscopic control until reaching the nucleus pulposus, with a penetration depth between 35-40mm (Figure 3.2).

During the surgical procedures a sedation was induced and maintained with anaesthetic propofol (Diprivan®, Zeneca) (4mg/kg) through the marginal ear vein. The anaesthetic maintenance was performed via inhalation anaesthesia with sevoflurane (Sevorane®, Abbott) in a 1.1-1.2% concentration.

3.2.2 Image acquisition

The evolution of the degeneration process was followed up by MRI before surgery and three and six months after the surgery with a 1.5T equipment (MR System Intera Release 2.1, Philips Medical System Nederland B.V). For image acquisition rabbits were tranquilized with propofol (Diprivan®, Zeneca)(4mg/kg) administered via the intravenous route. A sagittal sequence TSE T1-weighted (slice thickness 1.5mm; TE=8ms; TR=400-600ms) and T2 (slice thickness 1.5mm; TE=100ms; TR=2500-4000ms) were taken. In addition, a transversal T2 Balance TFE was made to the discs of interest (slice thickness 1mm; TE shortest; TR shortest). The DICOM image data were processed with MicroDicom®and 3D Slicer4.3.0®to obtain: area, disc height, and mean signal intensity of nucleus pulposus. Since the MRI of the nucleus pulposus of a degenerating disc potentially could show changes in area, signal intensity, or both simultaneously, an additional MRI outcome measure named “MRI index ”, defined by Sobajima et al. [335], was computed to serve as a more comprehensive measure of the degenerative changes. This index was calculated as the product of nucleus pulposus area and its average signal intensity. Thus, it amplifies the differences along the experiment when both events take place at the same time.

3.2.3 Mechanical testing

To perform the mechanical test, lumbar spines were resected en bloc, harvested and conserved at a temperature of 193K embedded in physiological saline serum after each sacrifice. Twenty-four hours prior to dissection, the specimen was transferred from âĹŠ80°Cto âĹŠ20°C. Twelve hours prior to dissection, the specimen was placed at room temperature to continue thawing. Three functional spinal units (FSU) (the injured level L4L5 and its adjacent ones: L3L4 and L5L6, for the experimental group and the three levels L3-L6 for the control group) were analysed from each spine (Figure 3.3a). The FSUs were obtained cutting the vertebral bodies with a circular saw, perpendicular to the longitudinal axis. Then, all posterior and anterior elements were carefully removed with a scalpel. The superior and inferior cut surfaces of the complex were rasped in order to align them parallel and to make both end plates thin enough

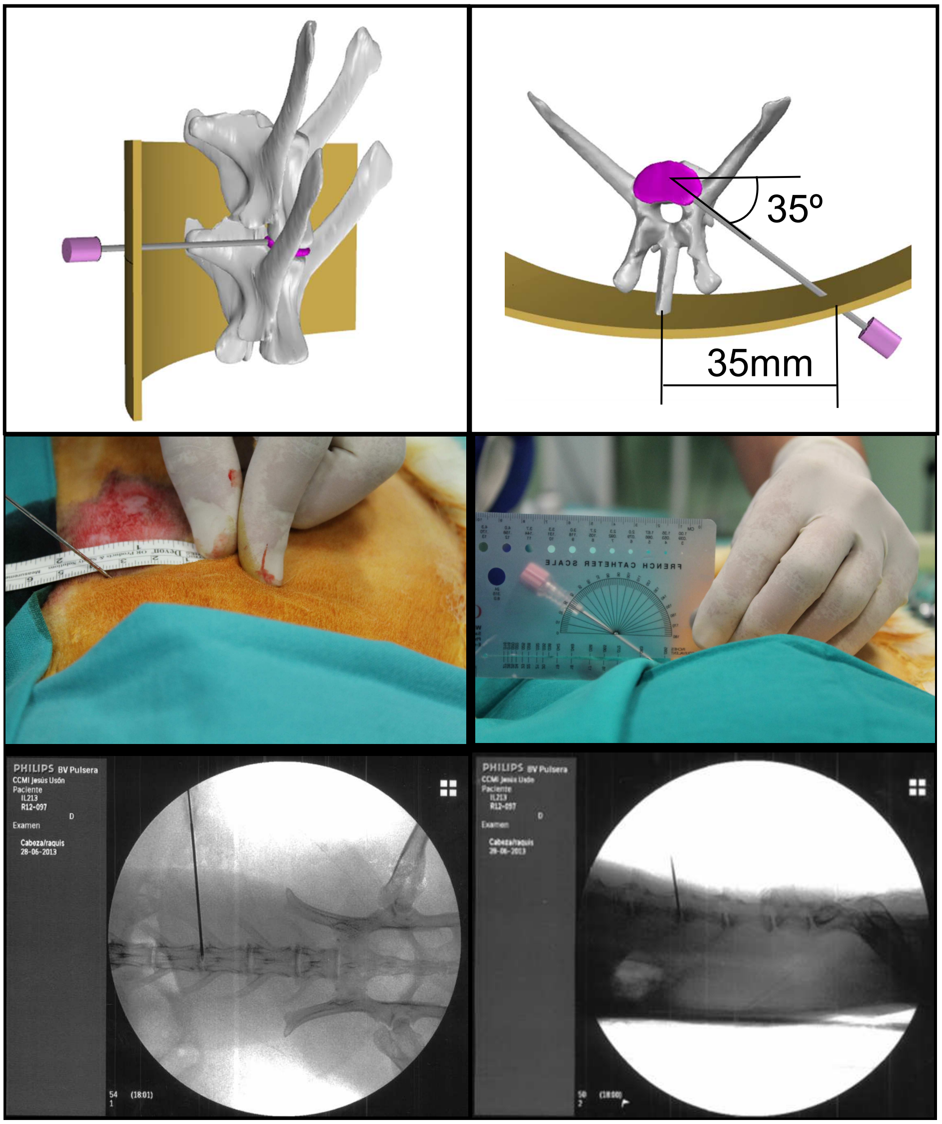

Figure 3.2: *The needle was inserted, in a percutaneous manner, at 30-35mm right to the midline spinous process and with an angle of 35-40°with respect to the horizontal plane. The penetration depth was checked under fluoroscopic control until reaching the centre of the IVD.*

(~2 mm) to maintain the integrity of the whole disc as a functional unit. Each disc was tested in an INSTRON 5548 (INSTRON, Canton, Massachusetts) equipment between two 316L stainless steel porous pucks (100 μm pore size; Mott Corporation; Farmington, CT) and covered with physiological serum as shown in Figure 3.3b.

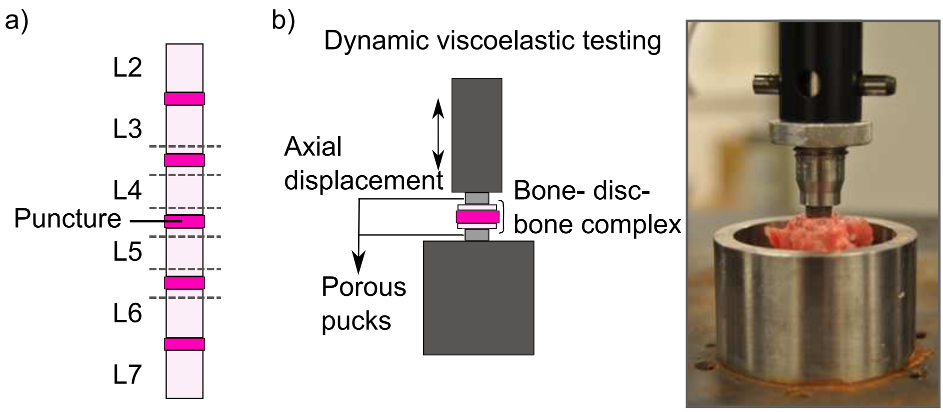

Figure 3.3: *a) Three FSU were analysed: the punctured level (L4L5) and its adjacent ones (L3L4 and L5L6) for the experimental group and L3L4, L4L5 and L5L6 for the control group; b) Samples preparation for the viscoelastic test; The dynamic viscoelastic test of the IVD has been made placing the bone-disc-bone complex in an INSTRON equipment between two porous pucks and surrounded by physiological saline solution.*

A dynamic compressive test was carried out following an oscillatory curve in accordance with the protocol described by Miyamoto and co-workers [238]. The loading shaft was slowly loaded onto the disc (0.005 mm/s) until the contact criterion of 5N compression was reached to maintain contact with the disc during the unloading cycle of the test. The samples were preconditioned by applying 10 sinusoidal strain cycles at 1Hz with an amplitude of 10% of the disc height. After a 3-minute recovery from preconditioning, three compressive loading cycles (10% disc height) were applied at different frequencies (0.05, 0.2 and 1Hz). Each load cycle was followed by a 3 minutes recovery.

The viscoelastic properties of each IVD were quantified in accordance with the well-known Maxwell viscoelastic model [236] defined by Eq 3.1,

$$\mid E^* \mid = \frac{\sigma_0}{\gamma_0} \tag{3.1}$$

where σ_0 is the maximum stress, γ_0 is the maximum strain in each compression cycle, and E^* is the complex modulus vectorially divided into storage (E') and loss (E'')

moduli which are defined as $E' = \mid E^* \mid cos\delta$ and $E'' = \mid E^* \mid sen\delta$, where δ is the phase angle between the stress and strain curves.

3.2.4 Finite element model

A three-dimensional L2-L7 FE model was created using data from a computer tomography (CT) performed to a rabbit of the experimental group at the beginning of the experiment (slices obtained by 0.5 mm intervals of 512x512 resolution). The vertebral bodies were segmented using the software Mimics®(Materialise, Belgium). The cortical and trabecular parts of the vertebra were identified by grey scale. The intervertebral discs were reconstructed based on the upper and lower vertebral endplates using Rhinoceros 5.0®(McNeil, Seattle, USA). The final dimensions of the intervertebral discs were checked by a trained neurosurgeon using the MRI data of the same rabbit. In this model, no muscles or ligaments were introduced since only a pure compression test was analysed and no reliable data of these elements can be found in the literature. The model is shown in Figure 3.4a.

This model was then modified to simulate the different stages of the surgery and the degeneration process (Figure 3.4b). Four different scenarios were simulated: 1) preoperative situation when the spine was intact; 2) immediately after surgery: a hole was performed at L4L5 level following the same protocol explained in Section 2.2 (35mm right to the midline with an angle of 35°and a penetration depth of 40mm (see Figure 3.2) and the height of the punctured disc was kept intact; 3) three months after the surgery the height of the punctured disc was decreased by 15% to take into account its flattening measured from MRI data and 4) six months after the surgery the height was decreased by 30%.

The entire model was meshed using linear tetrahedral elements of 0.8mm length for the vertebra and 0.4mm length for the IVDs using Abaqus 6.13 (SIMULIA, Providence, RI, USA). The size was determined after a mesh sensitivity analysis. With regard to the interaction between elements, all the discs were assumed to be fixed to the endplates, therefore, no relative movement between them may exist. Moreover, facet joints were modelled using gap elements with a non-penetration condition.

As mentioned before, the viscoelastic properties obtained by mechanical testing were used to simulate the different stages of the surgery and the degeneration progress. Taking into account that higher frequencies correspond to physiological values, here the data from 1Hz test was used for the intervertebral discs (see Table 3.1). The material behaviour was implemented as a viscoelastic material in a frequency domain using the Prony series. The four scenarios described before were simulated using the following mechanical properties: 1) and 2) all the discs were considered intact;

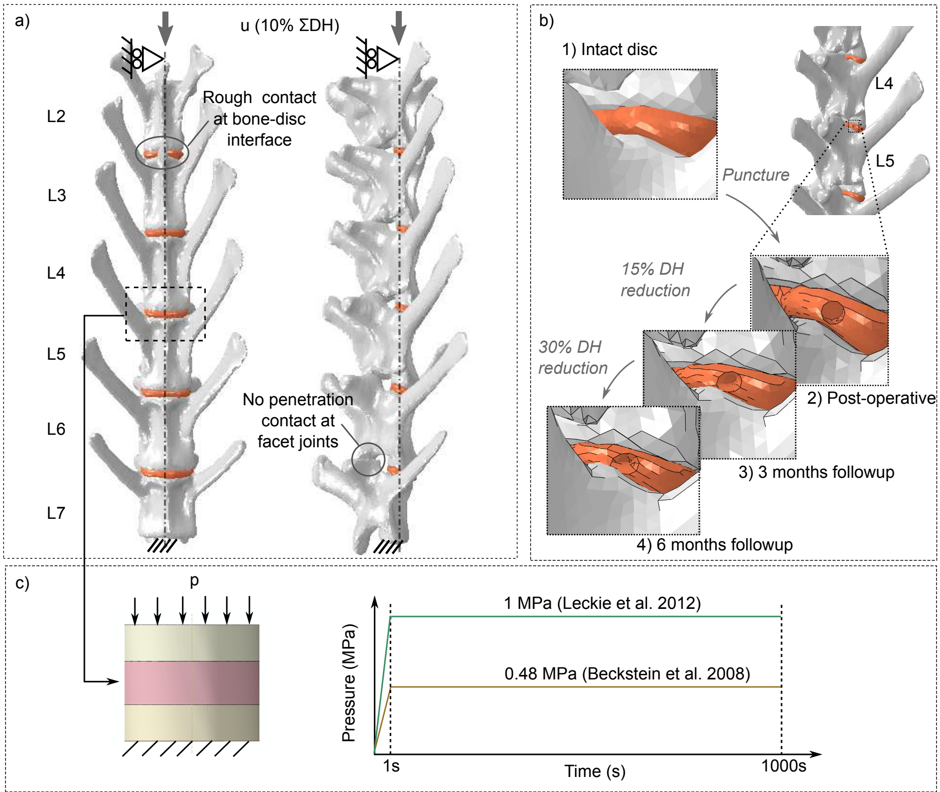

Figure 3.4: *a) FE model of the whole rabbit spine; b) A schematic diagram of the 4 analysed scenarios. The disc height reduction at 3 and 6 months has been applied to the initial height; c) Schematic diagram of a functional spinal unit for its validation using the data from Leckie et al. [205] and Beckstein et al. [33].*

3) the viscoelastic properties measured 3 months after surgery were assigned to the punctured disc and its adjacent ones. The rest of the discs were considered intact; 4) exact methodology as in 3) but with viscoelastic properties measured 6 months after surgery. Thus, the disc was treated as a continuous material neglecting the different behaviour of the annulus and the nucleus. On the other hand, vertebral bodies were simplified using elastic and homogeneous material taking into account the cortical and trabecular parts of the bone.

Taking into account that the experimental protocol was design as a pure compression test, and since there is scarce data in the literature about the biomechanics

Table 3.1: Mechanical properties of the materials involved in the finite element simulation. Intervertebral discs properties are collected from the experimental setup. Vertebra mechanical properties are obtained from literature [317][83].

			Viscoelastic model	
			E' [MPa]	E" [MPa]
Intervertebral discs	Intact discs		2.89	0.35
	3 months after surgery	L3L4	4.96	0.49
		Punctured- L4L5	4.67	0.53
		L5L6	5.11	0.59
	6 months after surgery	L3L4	5.25	0.56
		Punctured- L4L5	5.39	0.61
		L5L6	4.51	0.57

		Elastic model	
		E [MPa]	ν
Vertebra	Cortical bone	10,000	0.3
	Trabecular bone	100	0.2

of the spine rabbit, a FE model of L4L5 FSU was validated in compression using the results of the literature. Data from Beckstein et al. [33] and Leckie et al. [205] was used to check the viscoelastic behaviour. In both works, a spinal unit of a rabbit spine was mechanically loaded under a creep test (Figure 3.4c).

Finally, a pure compression displacement of 0.6mm, equivalent to the summation of 10% disc height of the five discs, was applied to the whole model on the upper face of L2 in 1s and was maintained during 10 minutes. The displacements and rotations at the lower face of L7 were completely restrained through the simulation. Abaqus 6.13 (SIMULIA, Providence, RI, USA) was used to analyse and post-process the results.

3.3 Results

3.3.1 MRI analysis

Degeneration of punctured discs (L4L5) with time was qualitatively observed using MRI as shown in Figure 4a with a reduction of the nucleus area and signal intensity. In Figure 3.5b, the evolution of the nucleus area, signal intensity (SI), MRI index and disc height (DH) for the punctured disc (L4L5) and for its adjacent ones (L3L4 and L5L6) are shown.

Regarding the punctured disc, a significant reduction (p-value<0.05) in area, MRI index and DH was found at three months. Moreover, six months after the surgery, all parameters measured showed a significant reduction (p-value<0.001) from the beginning of the experiment. In addition, the flattening of this disc during the progression of the degeneration was measured. Thus, an average decrease of 15% was obtained at 3 months, and it decreased by 30% of the initial height at 6 months. These values were used to feed the FE simulation as explained in section 2.5.

In turn, adjacent discs did not show significant changes at three months in area, SI of MRI index, however six months after the surgery both discs experienced a significant decrease in all MRI parameters (p-value<0.01). Meanwhile, the adjacent disc height progressively decreased and it was statistically significant at both time points.

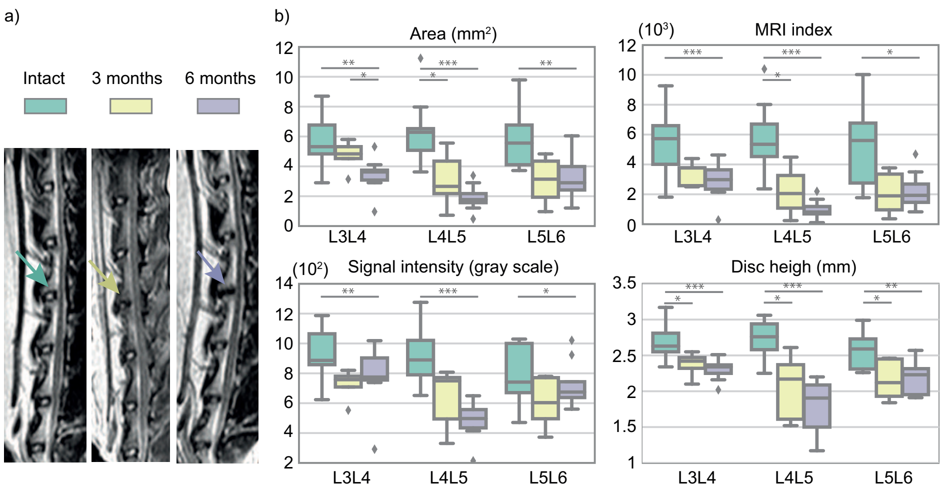

Figure 3.5: *a) Slices from MRI in the median sagittal plane showing IVD degeneration at the punctured level (arrows) over time (intact, 3 months and 6 months). b) Boxplots showing the evolution of disc characteristics with time: nucleus area, mean signal intensity (SI), MRI index, and disc height (DH). These values are measured using MRI data for punctured and adjacent discs. [*p-value<0.05; **p-value<0.01; ***p-value<0.001].*

3.3.2 Experimentally measured mechanical properties

Regarding the punctured discs, the evolution of the viscoelastic properties measured at 1Hz is shown in Figures 5a and 5b. It was obtained that the storage modulus

(E') gradually increased with degeneration by 56% (Figure 3.6a). Significant differences (p<0.05) were obtained in the first 3 months, but no significant differences were obtained between 3 and 6 months follow-ups. On the other hand, the phase angle δ was slightly lower as the degeneration progressed (Figure 3.6b). However, due to the high dispersion of the data, no significant differences could be found.

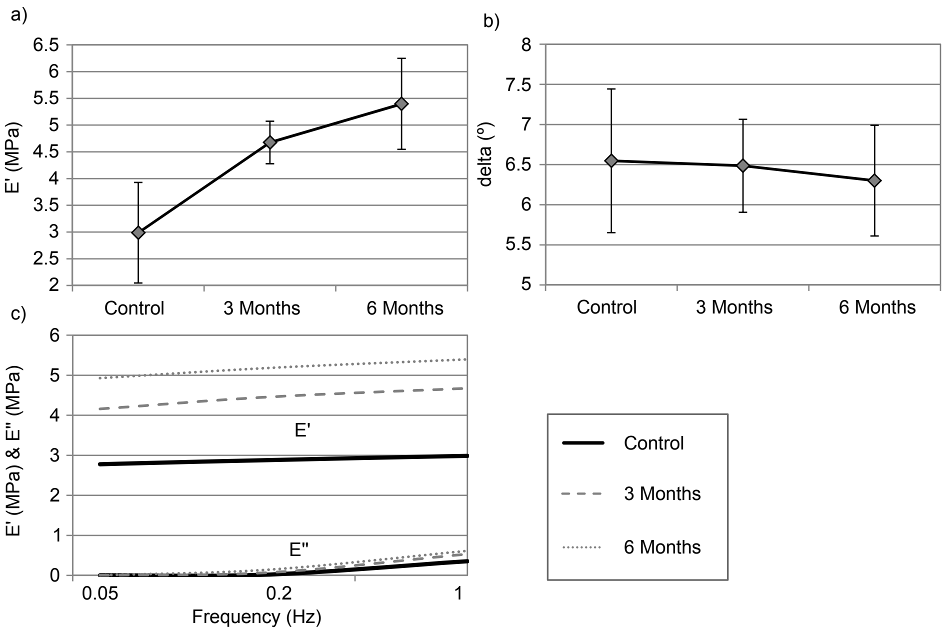

Figure 3.6: *Evolution with degeneration in the punctured discs: (a) Storage modulus (E') at 1Hz; (b) phase angle (δ) at 1Hz; (c) Effect of loading frequency on storage (E') and loss (E'') moduli.*

On the other hand, the influence of loading frequency on storage (E') and loss moduli (E'') showed in Figure 5c, was not significant for neither of the two parameters in any of the follow-ups. However, storage and loss moduli increased with increasing frequencies. Moreover, the elastic component, characterized as the ability to store deformational energy, was much greater than the viscous component, understood as the energy dissipation during deformation.

Likewise, the viscoelastic properties of the caudal and cranial adjacent discs changed with degeneration. As can be seen in Table 3.2 this change was more significant at L3L4 level than at L5L6 level. As occurred at the punctured level, it was obtained that for the adjacent discs both viscoelastic parameters increased with the degeneration.

Table 3.2: Mean (± std dev) values of storage (E'[MPa]) and loss (E''[MPa]) moduli obtained in the viscoelastic frequency dependent test for the discs in the control and experimental group at both follow-ups. For the experimental group a distinction was made between damaged, upper adjacent and lower adjacent discs.

	E'[MPa]			E''[MPa]		
Frequency [Hz]	0.05	0.2	1	0.05	0.2	1
Control	2.77±1.1	2.88±1.3	2.89±1.3	0.001±7e-4	0.023±3e-2	0.350±0.18
3 months						
L3L4	4.59±1.5	4.82±1.7	4.96±1.7	0.002±1e-3	0.076±0.03	0.487±0.24
Punctured	4.15±0.5	4.46±0.4	4.67±0.3	0.002±1e-3	0.073±8e-3	0.533±0.08
L5L6	4.73±1.5	4.97±1.5	5.11±1.5	0.017±3e-3	0.074±0.02	0.593±0.17
6 months						
L3L4	4.85±2.5	5.08±2.6	5.25±2.7	0.016±2e-3	0.080±0.03	0.564±0.35
Punctured	4.92±2.0	5.18±2.1	5.39±2.1	0.003±1e-3	0.146±0.07	0.614±0.32
L5L6	4.29±2.2	4.43±2.3	4.51±2.3	0.013±2e-3	0.096±0.05	0.526±0.31

3.3.3 Finite element model

The FSU was validated in relaxation and frequency oscillatory tests. Relaxation behaviour was compared with data from literature [205][33] by testing two different levels of pressure. In both cases a good agreement between experimental and computational curves was obtained (Figure 3.7a). The greatest difference appeared at the stabilization time, where the FE model predicted higher displacements for the same load because of the lower stiffness registered in our experiments in comparison with that of the literature. However, our results are comprised between the limits defined by Beckstein et al. [33]. Besides, the mechanical experiment at three different frequencies (0.05, 0.2 and 1 Hz) performed in this study was numerically reproduced and the reaction force was compared with the experimental data. As shown in Figure 3.7b, the FE model was capable of predicting the average force in each group of discs: intact, punctured and adjacent at the different follow-ups.

The results of the pure compression test of the whole rabbit spine are shown in Figure 3.8 for the four simulated scenarios. Minimum principal stresses were chosen as the output variables to plot given that they were the greatest ones after the compression load. Nonetheless, the maximal principal stresses were analysed to observe that the tensile stresses did not show a significant variation with degeneration apart from the boundaries of the puncture (see Figure 3.9 for more information). The most remarkable outcome was the transient behaviour. Just after the loading period, the outer part of the disc suffered tensile stresses while the inner part compressive ones. However, during the relaxation period, the tensile stresses appeared in the inner part

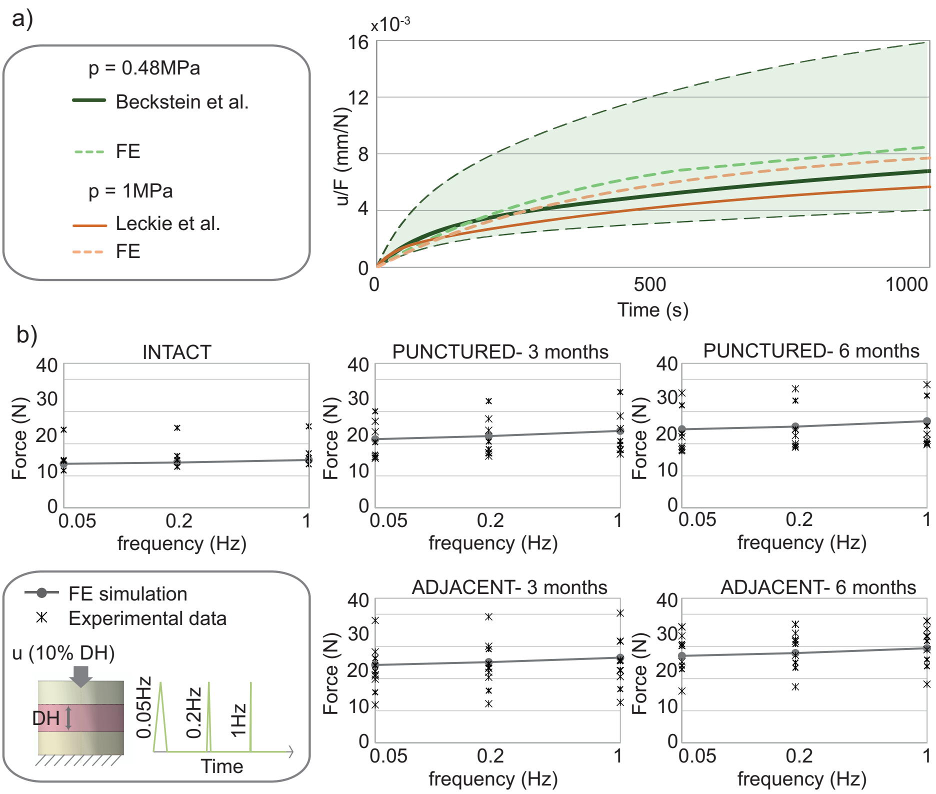

Figure 3.7: *a) Compression relaxation test at 0.48 and 1MPa for validation with data from literature [205][33]. The shaded area shows the limits of the experimental data from Beckstein et al. b) Force needed to achieve a 10% of DH displacement at different frequencies for each group of discs tested in the study.*

and the periphery was relaxed. Figure 3.8a shows the stress distribution along the laterolateral direction of a frontal cut of the IVD. The stresses are shown for the punctured disc and for its adjacent ones. Figure 3.8b shows a colour map distribution of the minimum principal stresses on the discs. Firstly, the instantaneous response just when the load is applied was analysed. It can be observed that at the puncture level, a slight increase in compressive stresses occurred just after the surgery. Three and six months before surgery, these stresses were increased by 70% respect to the pre-operative stage. Regarding the adjacent segments, the same trend was observed but the stress increase was less marked (an increase of 65% in L3L4 disc and 35% in L5L6 disc). Moreover, it was seen that at every level the most significant change took place the first three months and after this period the degeneration was smoother. Regarding the eigenvector corresponding to the minimal principal stress, it was uniformly distributed in the vertical direction through the disc while the eigenvector corresponding to the maximal principal stress had an antero-posterior direction in the centre of the disc and a circumferential component in the periphery. The eigenvectors were altered by the needle puncture making them circumferential at the hole boundaries but they were not affected by the degeneration.

Attending to the transient response, the stress relaxation was larger where the puncture was performed. There were no significant differences between the adjacent levels. Although the punctured level underwent higher stresses when the displacement was applied, the final stress value after relaxation was more similar to the adjacent discs. However, comparing again with the intact situation, the minimum principal stresses increased by 100% at the punctured level and by 45%-40% at L3L4 and L5L6 disc respectively.

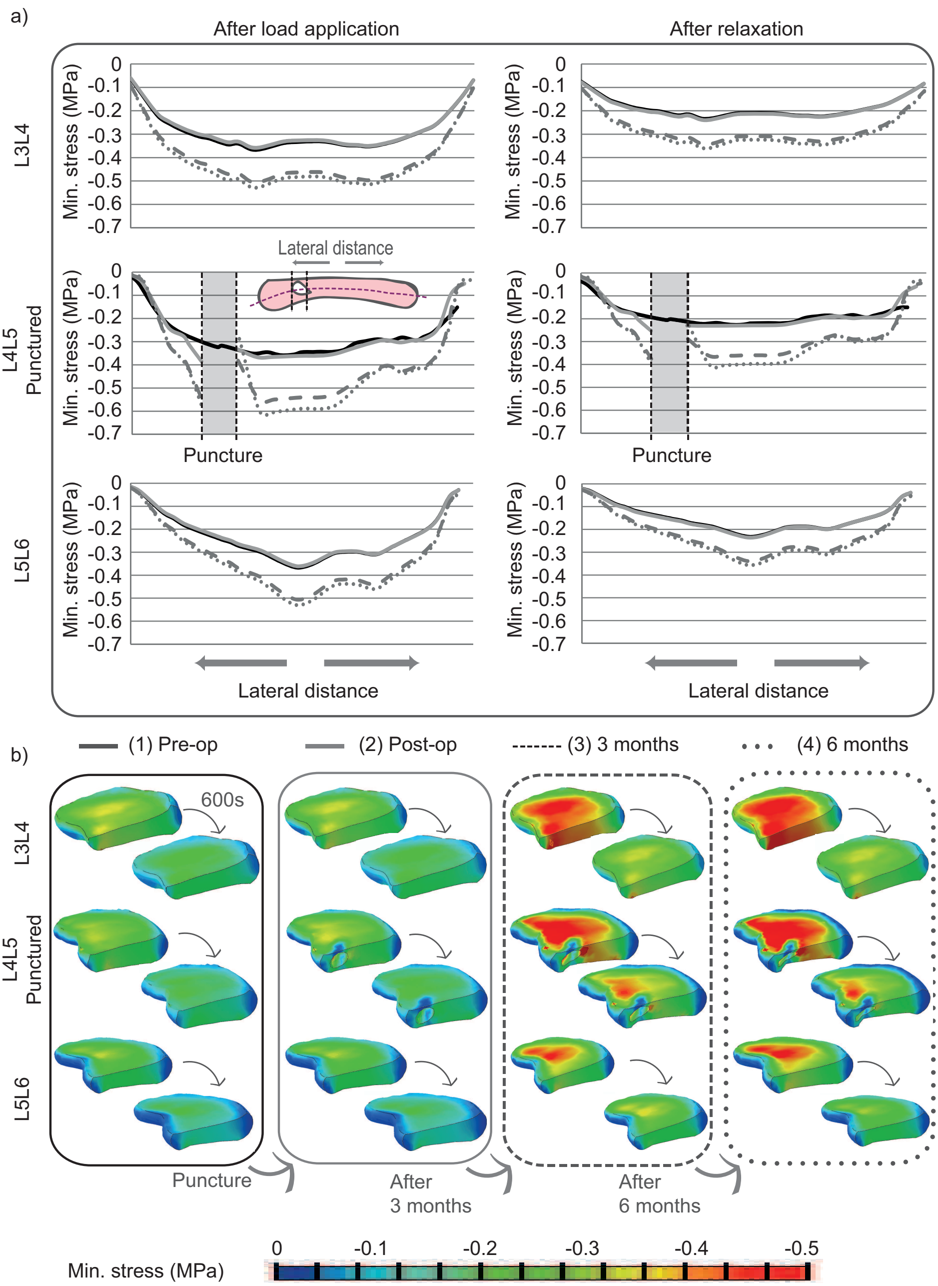

Figure 3.8: *Comparison between the minimum principal stresses at the four stages ((1) Pre-operatively, (2) post-operatively, (3) 3 months after the surgery and (4) 6 months after the surgery) at the punctured level (L4L5) and its adjacent ones (L3L4 and L5L6). (a) Minimum principal stresses variation across a laterolateral line that lies on a frontal cut of the intervertebral disc. The discontinuities are due to the puncture. Data shown for instant and transient response. (b) Colour maps of minimum principal stress distribution after loading and after relaxation period.*

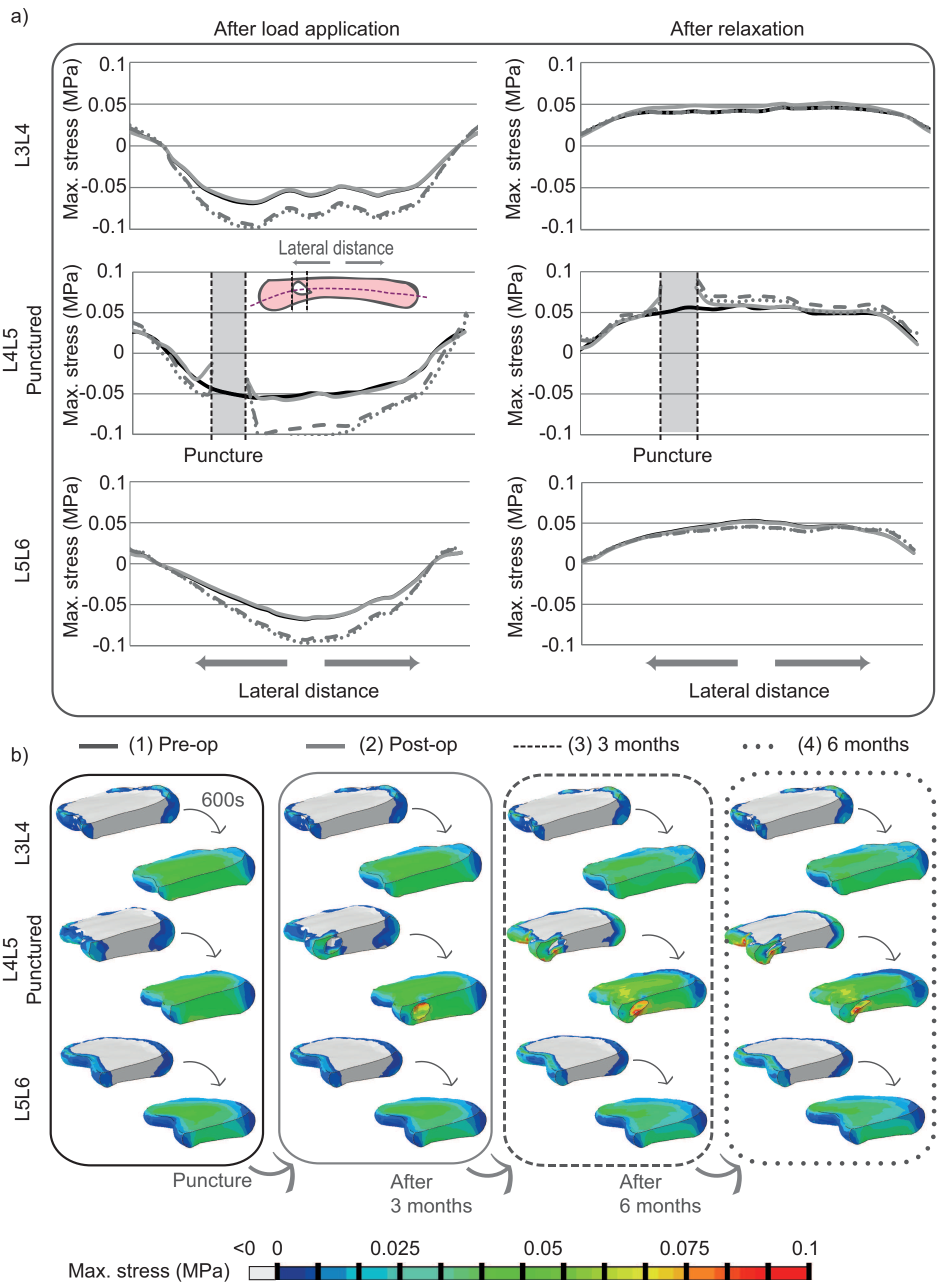

Figure 3.9: *Comparison between the maximal principal stresses at the four stages ((1) Pre-operatively, (2) post-operatively, (3) 3 months after the surgery and (4) 6 months after the surgery) at the punctured level (L4L5) and its adjacent ones (L3L4 and L5L6). (a) Maximal principal stresses variation across a laterolateral line that lies on a frontal cut of the intervertebral disc. The discontinuities are due to the puncture. Data shown for instant and transient response. (b) Colour maps of minimum principal stress distribution after loading and after relaxation period.*

3.4 Discussion

The main purpose of this study was to reproduce IVD degeneration in a rabbit model taking into account that the degeneration of one disc alters the behaviour of the whole spine, and to study the relationships between mechanical and structural changes. A percutaneous minimally invasive surgery was performed at one lumbar level and the disease progression was followed-up during six months by MRI and mechanical testing. After that, a FE model was built based on the experimental data to evaluate the spine biomechanics during the degeneration process.

Firstly, the degeneration progression was analysed by MRI. The height of the punctured disc decreased by 30% of the initial IVD height six months after the surgery, which is in accordance with the data presented in literature [182][181], where a 25% of disc height reduction was reported. The disc height of the adjacent discs was also affected by degeneration showing a significant decrease three months after the surgery. All MRI parameters in the damaged discs were significantly affected by the degeneration three months after the surgery apart from SI which did not show a significant decrease until six months. These findings are in accordance with the results showed by Sobajima et al [335]. The reduction of all the MRI parameters at the 6 months follow-up can be related with the degeneration process as it has been described in the literature. With degeneration, the nucleus pulposus loses its hydrophilic nature [3][156]. Moreover, the collagen proportion increases and, therefore, the tissue becomes more fibrotic and does not behave in the same manner as a healthy disc [3][6][344]. Degenerative changes in structural properties may be represented as consequences of these changes in material properties of the substructure of the disc [161].

To relate the MRI findings with the mechanical properties of the disc, an experimental set up focused on the analysis of the degenerative changes in viscoelastic properties of the whole disc was developed. As it is known, the storage modulus, loss modulus, and δ are important parameters in evaluating viscoelasticity of tissues and biomaterials. The storage modulus reflects the elasticity, the loss modulus reflects the viscosity, and tan δ, the ratio of the storage and loss modulus. When the compression loads on the disc, the viscoelasticity enables the disc to absorb the energy and dissipate to surrounding tissue via shape changes. After the load disappears, the viscoelasticity enables the disc to release energy and dissipate to surrounding tissue via recovery of shape.

The values obtained in the mechanical tests for the storage modulus were similar to those obtained in previous works [19]. It was observed that, six months after the surgery, the storage modulus of specimens in the degenerated discs was statistically greater than those in the control group revealing that the degeneration made the disc tissue significantly stiffer. These results can be correlated with the MRI findings and support the hypothesis that the tissue is more fibrotic as the degeneration progresses. On the other hand, the phase angle related to the lag between the applied stress and the resulting strain slightly decreased during the study. However, the loss modulus significantly increased with degeneration. This result is more controversial since there are different studies that support this finding [384][159][98] but others which just showed the opposite trend [82][48]. It is known that a degenerated disc becomes stiffer due to the fibrosis of the nucleus. The high collagen content might contribute to maintain the viscoelastic behavior of the disc during degeneration, although the nucleus has lost a large amount of water. This explanation can be proved using the data obtained from Freeman et al. [98] where both storage and loss moduli were obtained from nucleus, annulus and fibrous repair tissue. It was seen that the viscoelastic contribution by means of the loss modulus was very similar in the annulus and the fibrous tissue and even slightly greater than for the nucleus.

Finally, the mechanical testing was designed to analyse the influence of frequency in the viscoelastic mechanical properties of the discs. Both storage and loss moduli experimented a significant increase with frequency. Although these results are contrary to Miyamoto and co-workers [238] who found that loss modulus decreased at higher frequencies, it is in accordance with several other studies [156][159][98][76][204]. The results of the dynamic frequency sweep indicate that the store and bulk moduli increased with frequency indicating that the tissue became stiffer and more dissipative as frequency increased. Thus, disc tissue was found to be sensitive to loading rate and this behaviour was generalized for intact and degenerated discs. This sensitivity may be a consequence of the biphasic composition of the disc. When the load is applied, the incompressible interstitial fluid absorbs it and then transmitted it to the solid phase as the fluid drain. Under higher loading rates, the load transmission between fluid and solid phases is not instantaneous creating a higher resistance to deformation, and therefore a stress increase.

To complete this animal model study, a FE model was built to add new information that cannot be obtained experimentally. A complete rabbit lumbar spine FE model was developed and a pure compression relaxation test was performed. Due to the several assumptions done to construct this kind of computational models, the derived conclusions should be always considered as qualitative trends. Here, we tried to simulate the different stages of the evolution of the degeneration after performing the surgery. For the four scenarios analyzed, data from MRI and experimental testing were used. MRI data were used to reproduce the morphological changes in the rabbit intervertebral discs during the 6 months follow-up, while the experimental testing was used to assign the mechanical properties that were measured in each stage of the study. The novelty of this research is that it allows us to qualitative compare the mechanical behaviour of the intervertebral discs of this rabbit spine in a virtual simulation of the surgery with the behaviour of an intact spine. It was obtained that the influence of the puncture at one level modified the biomechanics of the rest of the spine. This result has been widely proved using experimental set-up as it has been done in the present paper, but as far as the author's knowledge it has not been numerically simulated. Several authors have numerically demonstrated the different biomechanical behaviour of degenerated versus healthy segments, modifying the disc height, the mechanical properties or even the nutrition and cell viability [107][106][307][219], but a multisegmental FE model of the spine including MRI and experimental findings has not yet been constructed. Here, the change of the magnitude of the minimum principal stresses (that can be assumed as compressive stresses) along the degeneration progress has been evaluated for every segment using an animal model. Although these values can only be used for cross comparison, relevant consequences could be derived. First of all, the instantaneous response of the spine under a pure compression displacement was studied. The higher increase (70%) of compressive stresses was undergone by the punctured disc but the adjacent discs also suffered larger stresses (L3L4 disc âĂŞ 65%; L5L6 disc âĂŞ 35%). This behaviour was practically obtained only 3 months after surgery, revealing that the progression of the degeneration to the adjacent discs was very fast [205][139]. Moreover, the transient response of the spine provides more information to the degeneration progress, since it was obtained that after the relaxation period the most loaded disc was the punctured one (a 100% increase relative to the preoperative situation) while the adjacent ones underwent smaller increases (L3L4 disc âĂŞ 45%; L5L6 disc âĂŞ 40%). This result implies that although the degeneration progresses to one level affects to its adjacent ones, this change is not as sudden as the instantaneous response seems to be. The viscoelastic behaviour of either healthy or degenerated intervertebral disc prevents the tissue from suffering too high stresses, and therefore the changes in the biomechanical behaviour of the spine are very progressive.

3.4.1 Assumptions and limitations

As with any model that attempts to simulate the complexity of an animal body, this study has several limitations and underlying assumptions.

Firstly, the number of rabbit spine specimens was limited by ethical issues and they must be separated into two different groups in order to compare the evolution of the degeneration with the control group. Furthermore, it was necessary to sacrifice half of them at the middle control point for mechanical testing. Due to the small sample size and the high variability intrinsic to the biological experiments some changes could not be proven to be statistically significant.

Additionally, the size of the control group was lower than the experimental one because it was considered that it would have less inter-specimen variation given that no surgical procedure was applied to them. Moreover, the biomechanical test used in this study was performed on a bone-disc-bone complex and the material behaviour considered, which included nucleus, annulus and terminal endplates, was a viscoelastic one. Since it was not possible to separate each tissue in this particular test, the multidirectional behaviour of the disc could not be taken into account. However, although nucleus and annulus which are composed of the same basic components differ in their organization and relative amounts, the clear distinction between the two tissues disappears with degeneration [359]. Finally, the biomechanical testing was performed applying uniaxial compression only. Because the human spine has multidirectional flexibility, supported by the mechanical properties of the IVDs, several variations in the biomechanical testing on in vivo rabbit IVDs need to be performed in the future.

Attending to the FE simulation, there are several assumptions that have to be addressed. First of all, a FSU was used for validation in compression. To validate it in flexion only data from Grauer et al. [124] could be used. The cited work reported multi-directional flexibility tests in rabbit L4-L7 spine. However, this model includes the ligaments and the joint capsules and, since there is no available data about the mechanical properties of these elements for the rabbit spine, a non-accurate FE model would have been constructed. Here, as the mechanical properties were obtained using a pure compression test, only a compression load case, neglecting the ligaments contribution, was taken into account and therefore the FSU validation can be considered suitable. This validation allowed us to construct a FE model to infer qualitative trends and to cross compare. On the other hand, the spatial resolution of the images may affect the geometry of the spine model. While the vertebral body is not expected to have a significant influence in the outcome, the curvature and gap size of the facet joints could change the range of motion allowed in each segment. Moreover, a co-registration between MRI and CT images would allow for a more precise segmentation of the soft tissues. However, given that the goal of this work was to qualitatively study the possible relationship between mechanical and structural changes, the quantitative results from the finite element model should be interpreted as trends instead of absolute values.

Regarding the mechanical properties of the different tissues involved, some simplifications were also made. Vertebrae were considered elastic and no change with degeneration was considered. Bone tissue is a very complex material that presents a poroelastic behaviour and adapts to its mechanical environment. Here, we have focused on the IVD degeneration and therefore the complexity of bone structure has been simplified. Concerning the IVD, as mentioned previously, neither annulus nor nucleus was distinguished. As these authors have simulated in previous papers [241][59] an accurate constitutive modelling of these components is essential to construct reliable FE spinal models. If the differentiation between annulus fibrosus and nucleus pulposus would have been considered, the stress distribution shown in Figure 7a would present a different profile, with higher stresses in the annulus and lower stresses inside the nucleus. Additionally, considering the anisotropy of the tissue, the circumferential lamellas would have had higher stresses in the outer part of the annulus, increasing confining of the nucleus and therefore its internal pressure. Nevertheless, the stiffening of the tissues seen experimentally indicated that the stress would follow the same trend with degeneration. Furthermore, the purpose of this work was to use the mechanical testing and the MRI data to construct a FE model capable of simulating the different stages of the experiment, and therefore the disc was treated as a viscoelastic homogeneous material. Finally, the fibrous tissue that appears before the puncture was not taken into account but it could be added in future works.

Chapter 4

Modelling the degeneration and ageing of the lumbar spine

In this chapter, a deep study of the events which may trigger the intervertebral disc degenerative process is presented. A simplified FE model of an intervertebral disc is used to investigate the difference in the mechanical behaviour for each degree of degeneration. Then, a series of patients with different grades of degeneration were analysed to look for morphologic changes in the IVD which may change the spine biomechanics. Finally, one IVD of the complete lumbar spine have been considered to be degenerated and the mechanical consequences on the spinal motion and the adjacent segments have been compared with the healthy spine. An additional comparison of a lumbar spine with a fused segment was performed with the purpose of searching for possible reasons of adjacent segment degeneration.

4.1 Introduction

Degenerative disc disease is a progressive pathology that alters the biochemistry and morphology of the IVD leading to low back pain. Although its aetiology is not well understood [23], it has been suggested that the degeneration may mimic the age-related changes of the disc but at an accelerated rate [6][203]. The main pathologic mechanism of ageing is the loss of proteoglycan content [7][8][21][330]. The cell metabolism is regulated by growth factors, particularly the IGF-1, secreted by the cells, which stimulates cell proliferation and proteoglycan synthesis [289]. With ageing, the decrease in IGF-1 receptors and the production of IGFBP, that void the IGF-1, diminish the proteoglycan production. This loss of proteoglycan and water content leads to a decrease of swelling pressure inside the nucleus pulposus originating a more fibrotic and stiffer tissue due to the change of collagen I into collagen II [353][161][135]. The gradual changes in collagen type and the disorganization of the annulus fibrosus structure suggest a mechanical influence of the degeneration, translated as a change of permeability [319][128]. As the degeneration progress, some tears appear in different regions of the annulus increasing the risk of nucleus herniation.

On the other hand, the DDD seems to be related to the modification of the biomechanical functioning of the spine. Abnormal mechanical loads and/or motion patterns have been related to the risk of injury to the spine [4][339]. Despite the numerous studies on the mechanics of the degenerated disc, there is limited data on how this condition affects the adjacent caudal and cephalic segments or the lumbar spine stability contributing to the progression of disc degeneration [6][158][2][21][303][248][251] [330]. The results of these studies vary considerably. Similarly to Kirkaldy-Willis & Farfan [186], some authors report instability during the early stages of degeneration [103][341] while others rather show the opposite [192][237].

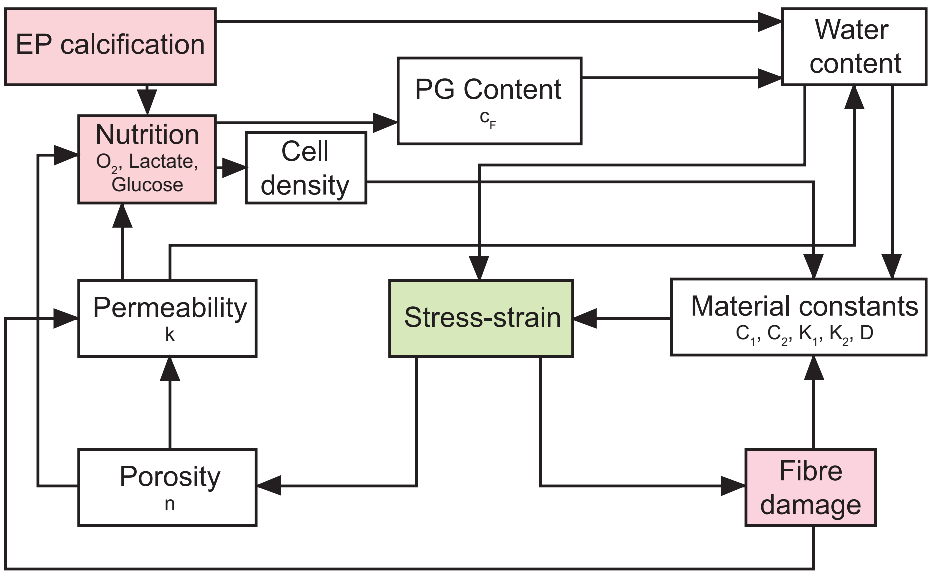

Figure 4.1: *Flow-chart of the degeneration process on an IVD depending on the possible effects which may trigger the initiation of the disease.*

Endplate calcification has been pointed as another possible trigger for DDD [352].

This calcification hinders the nutrient diffusion [300], provoking a decrease of the pH and glucose content and, in turn, accelerating cell apoptosis [245][355][36]. Furthermore, the decrease in cell concentration is again connected with a decrease in proteoglycan production and a change in the ground matrix synthesis. All of those interconnected events are depicted in Figure 4.1, where the possible initiators of degeneration are related to the mechanical behaviour of the disc.

To better understand the mechanical changes that take place in the degenerated invertebral disc and how these changes affect the adjacent discs, the chapter has been divided into three partial goals:

- First of all, a FE model of an ideal intervertebral disc was used to investigate the influence of the **biphasic properties** in the behaviour of the disc.
- Secondly, a **morphologic analysis** of the disc was performed based on MRI images of 18 patients with different grades of degeneration in each lumbar level.
- Finally, the **lumbar FE model** presented in Chapter 2 was modified to include a degenerated segment and in a further step a fused segment. The purpose was to describe how DDD or surgical procedures at one single level alter the **adjacent discs**. The range of motion and loading patterns in the whole lumbar spine were measured for a healthy, degenerated and fused spine to cross-compare.

4.2 Materials & Methods

4.2.1 Single disc FE model

A simplified FE model of a single disc was built to investigate the influence of the biphasic properties into the mechanical response of the IVD. The model consisted of bony and cartilaginous endplates with an elliptic cross-sectional area of 1235 mm^2, the nucleus pulposus and the annulus fibrosus (divided into inner and outer part) with a constant height of 12.5mm. Linear hexahedral elements of 1mm mean size were used to mesh all the tissues. The materials used to characterize the behaviour of each tissue are defined in Chapter 2. Only the biphasic properties of the nucleus and annulus were changed to represent four grades of degeneration in accordance with the data presented in Figure 4.2.

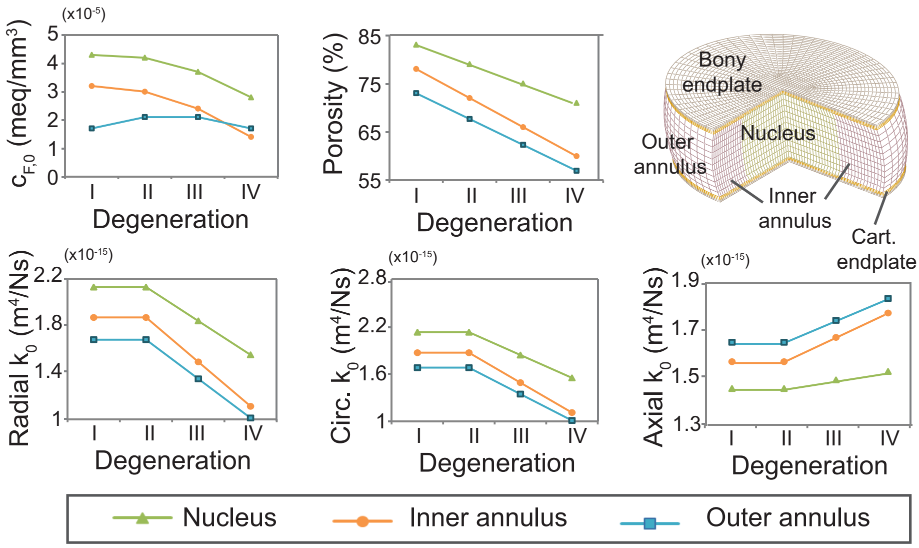

Figure 4.2: *Variation of the biphasic properties: fixed charge density, porosity and initial permeability in the three principal directions, with the progression of degeneration in the nucleus, inner annulus and outer annulus [21][128][249].*

The bottom surface of the model was completely constrained while an axial distributed load of 1,000N was applied, after 8h of free swelling, and maintained during 16h. Once the stability was reached for the first grade of degeneration, the biphasic parameters were modified to simulate the second grade of degeneration. And it was continued in the same way until the last degeneration grade.

4.2.2 Patient-specific data for the morphologic study

MRI images of a total of 18 patients with ages ranging from 31 to 64 years old were taken and analysed in collaboration with an expert neurosurgeon to assess the grade of degeneration of each segment in accordance with Thopmson scale [344] (Table 4.1).

A high prevalence of severe degeneration was encountered in the lower segments (D45 and D51), while the upper IVDs presented a healthy or mid degenerated state. This difference, also reported by most of the clinical studies may indicate that the higher loads supported by those segments, together with the lordosis of this region could accelerate the ageing process.

Table 4.1: Number of discs affected by each grade of degeneration differentiating among each lumbar level.

	Grade I	Grade II	Grade III	Grade IV	Grade V
D12	12	3	3	0	0
D23	11	4	3	0	0
D34	6	6	4	2	0
D45	3	3	8	0	4
D51	1	0	4	7	6

Additionally, the mid-sagital slice of each MRI was analysed to measure the following dimensions using a DICOM viewer (Fig. 4.3): Total disc area, nucleus area, disc height at the central position and antero-posterior distance. In order to make the magnitudes comparable, the nucleus area was calculated as a percentage of the total disc area, the antero-posterior distance was divided as well by the disc area, and the height was divided by the antero-posterior distance.

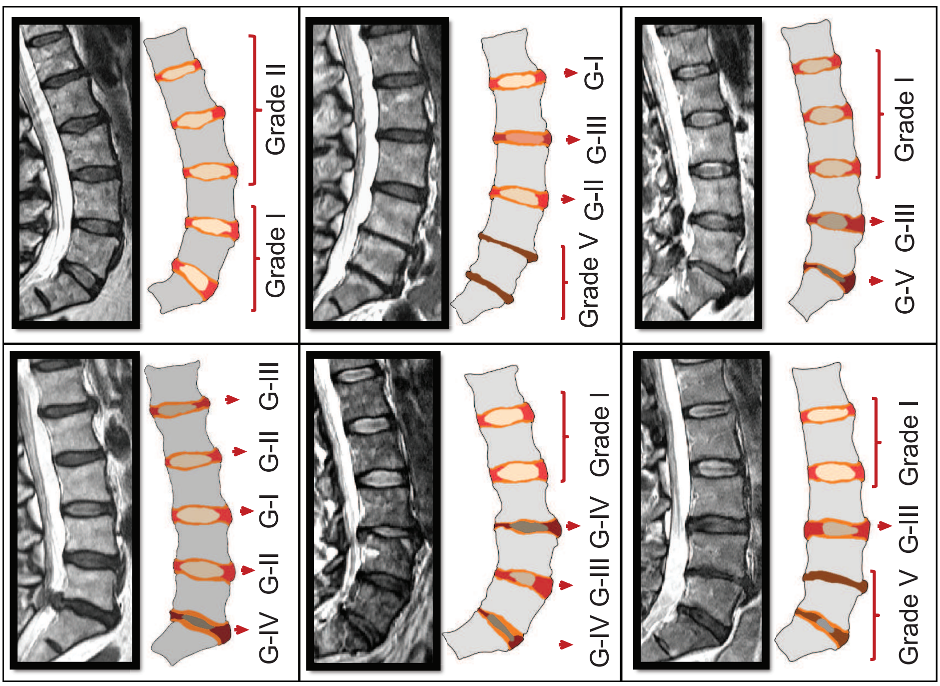

Figure 4.3: *Mid-sagital slice of MRI images taken from six patients with different degrees of degeneration on the lumbar IVDs.*

4.2.3 Lumbar spine FE model including degeneration

As shown above, during degeneration annulus stiffness increases and annulus permeability decreases due to a reduction in proteoglycans and water content. On the other hand, in the nucleus, proteoglycan content decreases while its permeability increases [157]. In agreement with the prevalence of high degeneration grades in the lower segments seen in Section 4.2.2 and the prevalence of interventions reported in the literature at L4-L5 segment [322], a Grade IV degeneration based in Thompson grading system was simulated at this level [344]. Starting from the intact model described in Chapter 2, D45 IVD was degenerated changing its elastic and biphasic material properties in accordance with the values presented in Table 4.2. Therefore, the risk of cascade degeneration effect was studied in L3-L4 and L5-S1 segments.

Table 4.2: Material properties of the degenerated nucleus pulposus and annulus fibrosus [158][251][320][59][228]

	Elastic parameters					Biphasic parameters			
	C_{10} [MPa]	C_{20} [MPa]	D [MPa^{-1}]	K_1 [MPa]	K_2	$c_{F,0}$ [meq/mm^3]	k_0 [m^4/Ns]	$n_{f,0}$	e (void ratio)
Annulus	0.45	2.5	0.306	1.8	11	0.9e-4	1.45e-15	0.7	2.4
Nucleus	0.0314	0	0.36	-	-	1.5e-4	1.3e-15	0.78	2.45

For comparison, a lumbar FE model with a fused segment (L4-L5) was created adding a posterior screw fixation. The fixation consisted of four screws (one per pedicle) and two rods, all of them of 5mm diameter and made of titanium (E= 100,000MPa, ν= 0.33) [373]. Linear tetrahedral elements of 1mm size were used to mesh the implant. Before screw insertion, L4 and L5 vertebrae were perforated and a tied contact was assumed at the bone-screw interface.

A hybrid method was applied for the loading conditions considering the hypothesis that people try to bend their spines in the same way independently of their surgical or healthy state [66][70]. Therefore, a pure moment of ±4Nm was applied at the centre of L1 vertebra in flexion-extension and lateral bending directions in the intact model. In the degenerated and fused models, the magnitude of the load needed to achieve a total lumbar rotation equivalent to that of the intact one was calculated resulting in the loads showed in Figure 4.4.

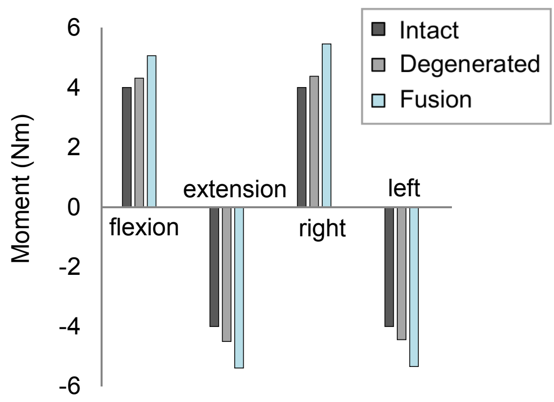

Figure 4.4: *Moment needed to reach the same motion in the whole lumbar spine in the healthy, degenerated and fused cases under flexion-extension and lateral bending.*

4.3 Results

4.3.1 Effect of degeneration on disc biomechanics

A loading-relaxation cycle was simulated mimicking a diurnal cycle of 16h of activity and 8h of rest for a single disc with changing biphasic properties. With the degeneration of the IVD, a progressive decrease in the disc height was observed (Fig. 4.5a). It may be a consequence of the less proteoglycan content in the nucleus, which reduced the water attraction capacity decreasing the swelling of the disc in the relaxation state.

The same response could be observed in the osmotic pressure (Fig.4.5b), where it was shown that the more degeneration, the less osmotic pressure in the centre of the nucleus. Therefore, the fluid influx decreased not only because of the permeability reduction but also because of the osmotic gradient.

In turn, the intradiscal pressure of the disc showed significant variations with degeneration (Fig. 4.5c). The higher the grade, the higher the pressure created inside the disc. Furthermore, after 16h of maintained load, the disc with severe degeneration presented a higher pressure, uniformly distributed throughout the disc, than the healthy one. Just after load removal, a high negative pressure occurred in the healthy state, which means that the ground substance was subjected to traction allowing the fluid to fill the pores. Meanwhile, the negative pressure in the severely degenerated nucleus was lower.

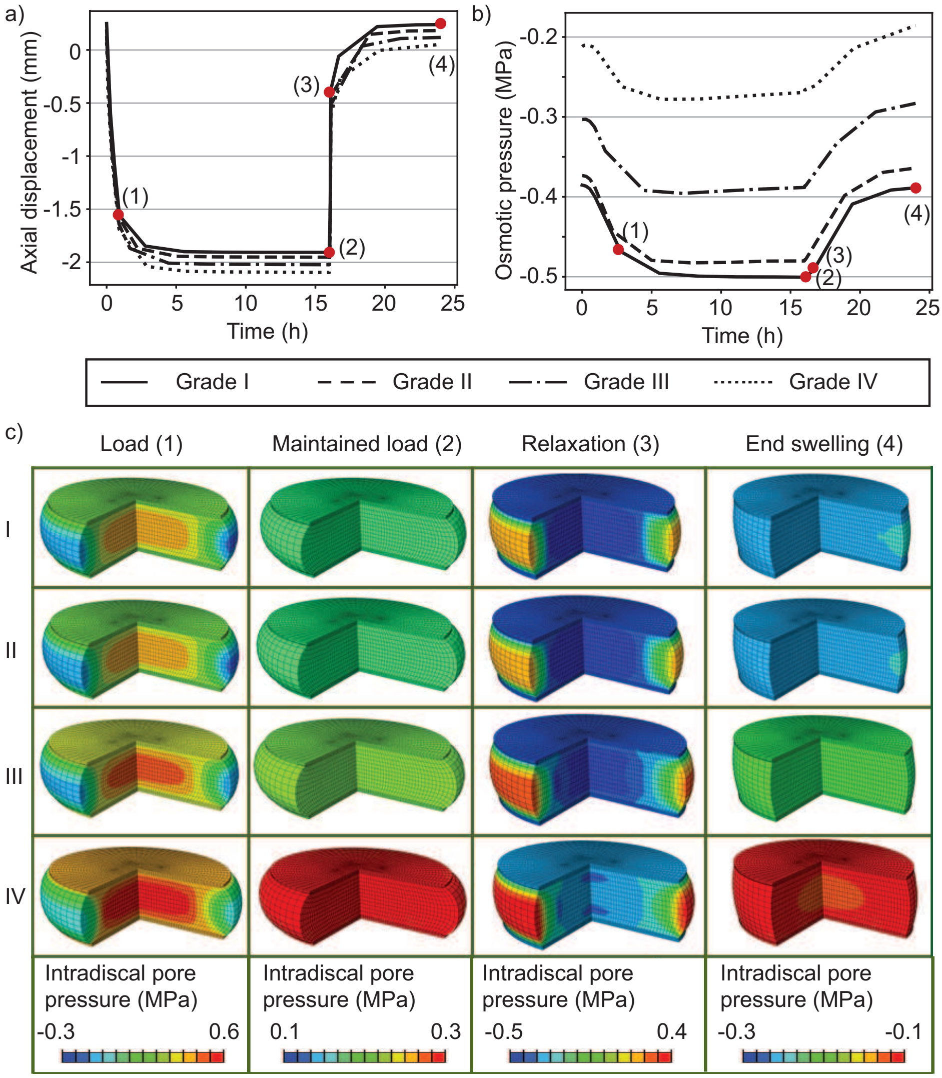

Figure 4.5: *a) Axial displacement, b) variation of osmotic pressure at the centre of the NP, and c) intradiscal pore pressure distribution at different points of the cycle for different grades of degeneration.*

4.3.2 Effect of degeneration on disc morphology

A morphologic study of the degenerated disc exhibited how the first signs of degeneration were not very noticeable. Conversely, the discs with severe degeneration presented a completely different geometry as shown in Figure 4.6a.

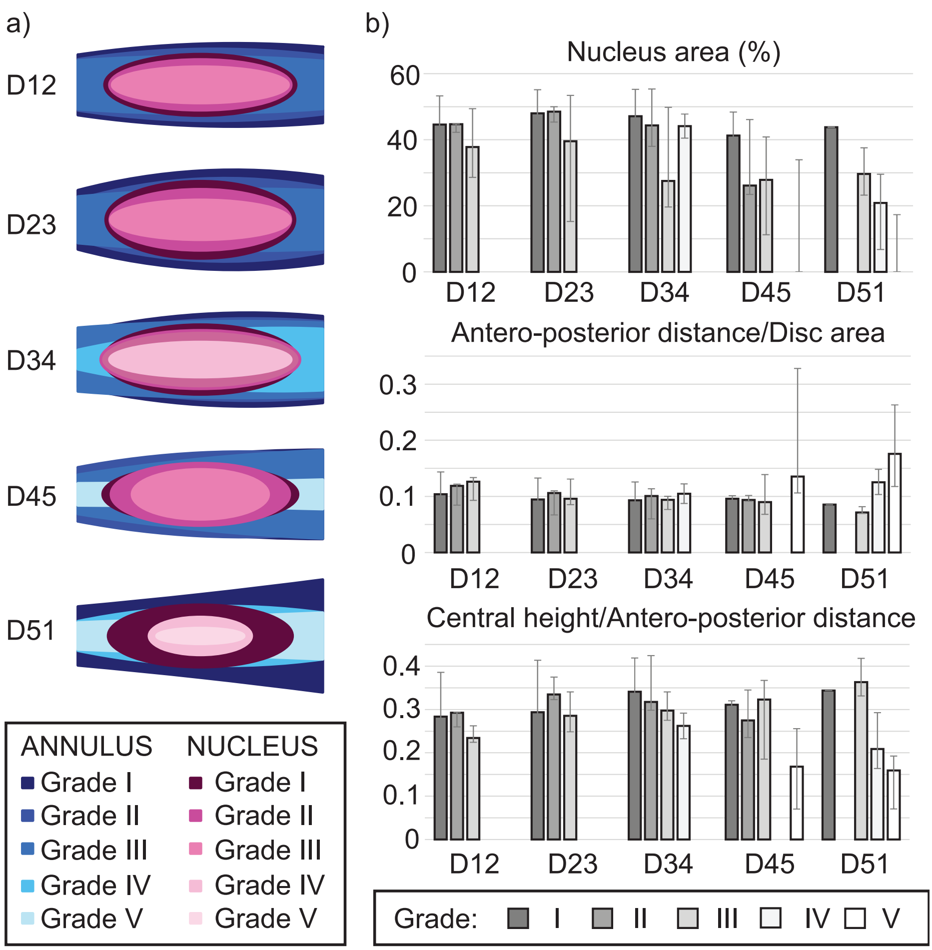

__Figure 4.6:__ a) Graphic representation of the mean morphology change of each disc differentiating between annulus and nucleus. b) Quantification of the effect of degeneration in the area of each disc occupied by the nucleus, the antero-posterior distance and the central height. The last two magnitudes have been normalized to make them comparable among patients.

It was observed that with the progression of degeneration the area occupied by the nucleus pulposus decreased until be unrecognisable at Grade V. This change could be related with the loss of water retained by the nucleus which, in turn, is linked to a reduction of proteoglycan content and therefore, with the gradient of osmotic pressure. The relation between the antero-posterior distance and the total disc area was less affected by the degeneration. However, in high grades, it presented an increase which may be understood as a bulging annulus due to the loss of height. On the contrary, the disc height presented a progressive decrease with degeneration, clearly visible in segment D34 (Fig 4.6b). In the latest degeneration states, not only the height was decreased, but also the lordosis was rectified turning the disc into a flat structure.

4.3.3 Effect of degeneration on the overall behaviour of the lumbar spine

Figure 4.7 compares the motion of the affected segment (L4-L5) in the healthy, degenerated and fused stages. A slight decrease of the ROM in the degenerated disc was observed while the fused model had a stronger reduction of the rotation.

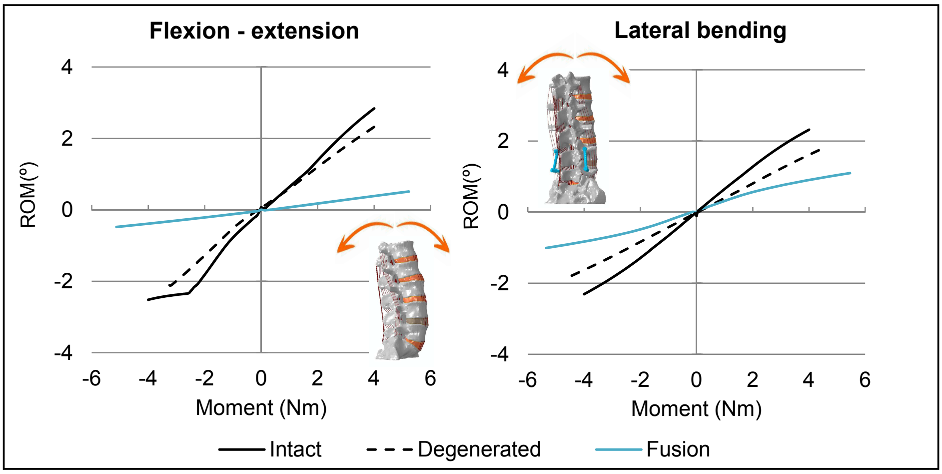

Figure 4.7: *Comparison among the ROM of the affected disc (L4-L5) of the healthy, degenerated and fused lumbar spine under flexion-extension and lateral bending.*

The use of screws also reduces the pore pressure in the operated disc achieving the decompression goal as reported in Table 4.3. This pressure loss was higher in lateral bending than in flexion-extension which was also seen for maximal and minimal principal stresses and strains in the affected disc.

Table 4.3: Intradiscal pressure of D45 in the healthy, degenerated and fused model under different loading conditions.

Intradiscal pressure [kPa]	Intact	Degenerated	Fused
Flexion	3.84	2.95	2.47
Extension	2.59	2.53	0.09
Right bending	3.75	2.9	0.14
Left bending	3.57	2.62	0.218

As shown in Figure 4.8, the changes in one segment altered the biomechanics of the whole spine. In fact, the effect over the adjacent discs was accentuated by the segment fixation. The ROM increased with degeneration in order to compensate the reduction in the pathologic segment. With the screw fixation, this effect was magnified reaching the highest ROM growth in flexion movement for both, the upper (55%) and lower (70%) adjacent discs. The variation in lateral bending was lower, around 20%.

Attending to the pore pressure results, the degeneration did not have a significant effect over adjacent discs in comparison with the fused model. Flexion movement was the worst loading condition, like in ROM analysis, for the cranial disc. However, the caudal disc was nearly unaffected by this movement.

It is also possible to note that, the stresses were more influenced by the immobilization of one segment than the pore pressure. They showed a 20-30% of increase in most cases, reaching the increment peak with right bending for D51 in the fused model (42%). The maximal principal stress distribution maps plotted in Figure 4.9 reflect the areas with more traction stresses for upper and lower discs in flexion movement. The stress peaks were found in the antero-lateral part of the discs near to the inferior endplate increasing the risk of annulus disruption and nucleus retropulsion. It is important to observe that the stress levels in the lower adjacent disc are considerably higher than in the upper one.

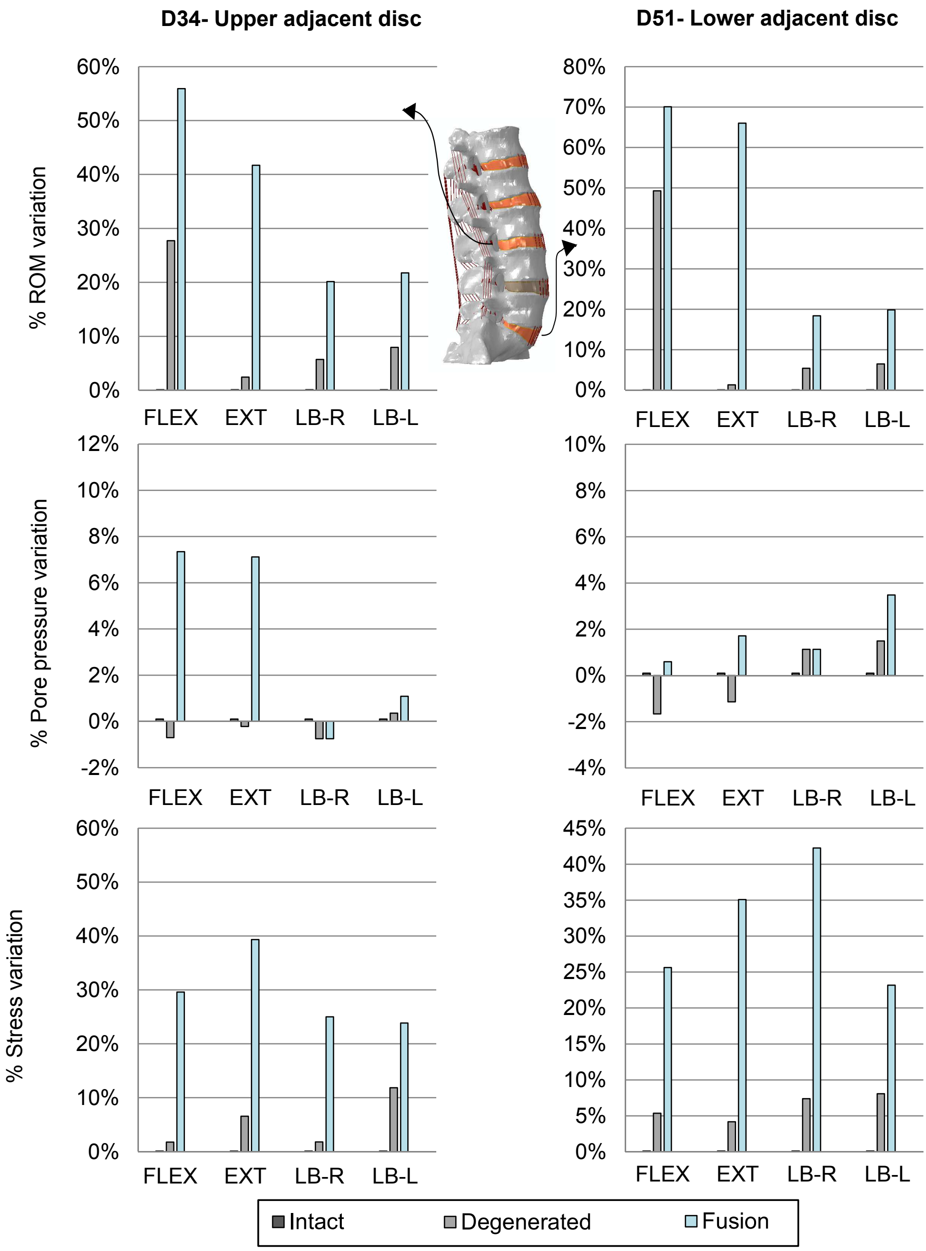

__Figure 4.8:__ Influence of the degeneration and fusion over the upper and lower adjacent discs quantified as percentage over the intact values for the ROM, pore pressure and maximal stress parameters.

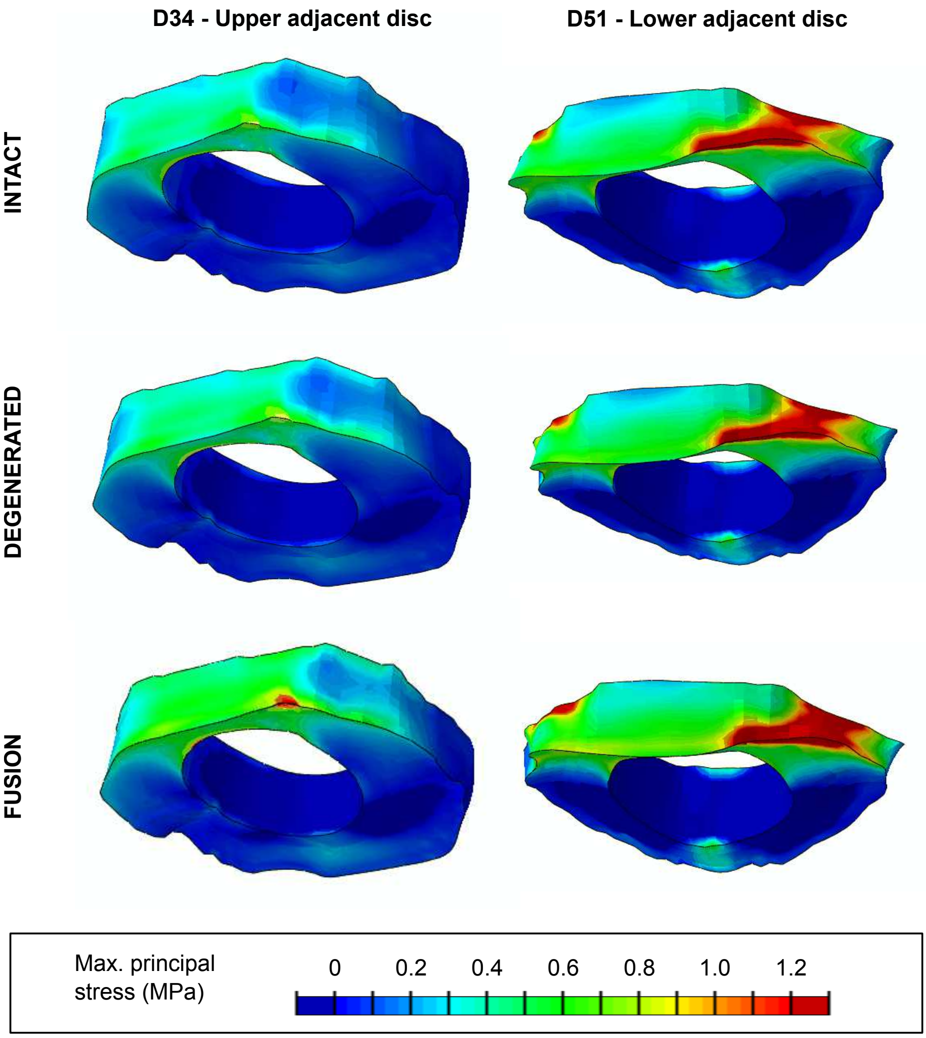

Figure 4.9: *Stress distribution maps for upper and lower adjacent discs in flexion movement for the healthy, degenerated and fused models.*

4.4 Discussion

The main goal of this chapter was the study of one of the most common pathologies which affects the invertebral disc and which is a recurrent source of pain and discomfort for the patients. With that purpose, three different studies were carried on. In the first one, the influence of the biphasic properties on the mechanical behaviour of a single disc was analysed. In the second one, the geometrical changes that undergo the IVD during the progression of the disease were examined using MRI from 18 patients. Finally, the lumbar spine FE model was used to compare the influence that the degeneration or fusion of one segment has over the adjacent ones.

The variation of the fixed charge density and permeability with the degeneration caused a variation of the axial displacement in accordance with experimental and numerical data [228][22] reported in the literature. Disc height decreases with degeneration [95] due to less recovery of axial displacement which may be caused by a decrease in permeability and proteoglycan content. Furthermore, the osmotic pressure in the nucleus, directly related to the proteoglycan content, decreased with the latest states of degeneration. Therefore, the amount of water which was attracted back to the disc was reduced avoiding the disc swelling and height recovery. Additionally, the intradiscal pore pressure variation followed the same trend and magnitudes than those reported in previous studies [318]. The decrease in the radial and circumferential permeability, together with the loss of water content caused a higher pore pressure in the nucleus centre in the loaded state and a less negative pore pressure in the relaxed state.

After the evaluation of the 18 patients afflicted by different grades of DDD, it was observed, in agreement with previous clinical studies [322][69], that the lower segments had a higher prevalence for severe degeneration while the upper ones just showed the first signs. With regard to the morphologic changes, no significant effect over IVD geometry was observed for the first grades of degeneration. However, when severe degeneration affected the disc, three main changes were noticed: a marked reduction in the nuclear area, even unrecognisable in the more degenerated discs, which may be a result of the tissue fibrosis; a decrease in the disc height together with a lordosis rectification; and an increase in the antero-posterior distance, which may be related with an increase in the axial disc area because of the disc bulging. Equivalent to these observations, Peloquin et al. [275] found a decrease in disc height and an increase in the axial area with the progression of degeneration. In fact, the height reduction was in agreement with the results of the previous section, where a less height recovery was predicted for the most degenerated disc. These geometrical changes have exhibited to highly influence the biomechanical response of the spine. In a parametric study, Niemeyer et al [258] found that the disc height was one of the most influential parameters in a FSU FE model. In addition, Malandrino et al. [219] showed in a recent study how disc geometry determines cell nutrition.

Studying the effect of the degeneration and fusion over the lumbar spine, a drastic loss of motion in the fused segment was seen (Fig. 4.7) together with a reduction in the nucleus intradiscal pore pressure as evidenced in Table II. Previous clinical reports showed that spinal fusion with pedicle screw instrumentation demonstrates good stability and reduces the disc overload at the surgical level [216][42][155] in agreement with the findings presented here. It is important to note that the magnitude of the pore pressure was lower than the values reported in other studies [171][318] because the velocity of the applied load was slower. Despite this fact, the disc decompression with surgeries could be noticed.

To perform the analysis it has been taken into account the hypothesis presented by Goel et al. [118] who suggested that in real life people bend their spines until achieving a similar movement regardless of whether their spine is healthy or has undergone spinal surgery. Therefore, different moment loads, reported in Figure 4.4, have been applied so that the same overall ROM was reached for all the models. The necessary load was around 30-50% over the initial load, which is in accordance with other FE studies [80].

It has been also hypothesized in previous studies that screw fixation could trigger a cascade degeneration effect over the adjacent discs. Randomized clinical studies reported a rate of clinical ASD between 10-30% at different follow-up periods [64][116]. Sears et al. [322] gathered in their study that a 13% of the procedures required further surgery after the development of DDD at an adjacent level. It may be possible to find a relationship between the increased load seen above and the ASD presented in the clinical data.

In order to distinguish the effect in the adjacent discs, ROM, pore pressure, and maximal stresses were analysed as a percentage of the intact value. Those results showed an increase in ROM, nucleus pore pressure and maximal stress in all loading directions more pronounced in the lower adjacent segment. Other authors showed the same trend in their studies [364][326]. Chen et al. [66] remarked that the stresses on the adjacent disc annulus increased and were concentrated at the outermost layers close to the endplate regions, which was also reported in this work as can be seen in Figure 4.9.

Some limitations of this work should be addressed. First of all, the geometry used for mimicking the pathologic disc was the same as for the healthy one, contrary to the findings of the morphologic analysis. The variation of disc height with degeneration would be an important factor and should be analysed in a posterior research. However, the main goal of this work was to compare between surgeries and their effect on the global spine biomechanics. In a first approximation, the disc height loss in the degenerated spine could be neglected assuming that the fusion techniques attempt to restore the physiologic IVD space. Also, a reduction of the disc height would reduce the ROM of this segment, and in turn, increase the motion of the adjacent segments and their stresses. On the other hand, the stiffening process was introduced changing the material properties and neglecting the fibre re-orientation and damage. The changes in the collagen type and its structure are key aspects for reproducing the different degeneration grades but, as well as for the previous limitation, they did not have a significant contribution in the surgeries comparison.

To summarized, in this chapter, the different aspects of the intervertebral disc degeneration were studied showing that both material behaviour and geometry had an important role in the pathology and, therefore, they should be considered in combination. In fact, a relation may be found between the less capacity of swelling and the reduction of the disc height. Finally, an effect of the degeneration on the adjacent segments was predicted. This change in the mechanics of the discs may lead to a cascade of degeneration which might be aggravated by the use of posterior fixation.

Chapter 5

Surgical procedures simulation: from commercial cages to new intersomatic cage designs

Segment fusion using interbody cages supplemented with pedicle screw fixation is the most common surgery for the treatment of low back pain. However, in the last years, a controversy regarding the use of cages in a stand-alone fashion has arisen. The goal of this chapter is to compare the influence that each surgery has into lumbar biomechanics. Given that one of the major concerns about the use of stand-alone cages is the risk of subsidence of the device into the bone, a parametric study is presented to understand the effects of intervertebral cage design and placement on the biomechanical vertebral bone damage. Finally, the possibility of a 3D-printed cage was experimentally studied and evaluated under lumbar spinal loads.

5.1 Introduction

Segment fusion with intradiscal cage and pedicle screw fixation is the "gold standard "treatment for lumbar hernia and degenerative intervertebral disc diseases. However, stand-alone interbody cages have shown to be a feasible surgical technique for the treatment of discogenic back pain [75][10]. The aim of these surgeries is to stabilize the segment and restore the intervertebral disc height. A simple discectomy without cage insertion reduces the disc height creating slack in all longitudinal ligaments [216]. Nevertheless, if the IVD space is distracted by a cage insertion, the ligaments are pre-strained contributing to spine stabilization [380]. Furthermore, using a minimally invasive approach, important stabilizing structures such as posterior musculature, anterior and posterior longitudinal ligaments and facet joints are preserved helping to control segment kinematics [309][190][256]. In spite of that, some physicians advocate for the use of supplementary PSF to assure long-term stabilization and to avoid the risk of non-union [264][254]. However, this additional fixation, apart from being more invasive, has been reported to present some complications such as screw loosening or implant failure.

However, few clinical prospective randomized studies have been made comparing stand-alone construct versus fusion with supplemental PSF [357][244]. These studies did not show significant differences in clinical outcomes while several advantages were reported for the use of cages as stand-alone in degenerated lumbar segments without previous instability: the surgical technique is less demanding, it takes less time, the implant cost is lower and pedicle screw-related complications are avoided. Besides, different cohorts of patients undergoing a stand-alone cage implantation have been followed up showing good clinical outcomes, a high rate of fusion and a low incidence of cage subsidence and migration [75][10][252][223][202][13]. In vitro studies comparing among different cages and fixations have shown that additional fixation substantially reduced the range of motion in all loading directions but segmental stability was also reported for stand-alone cages [113][51][120].

On the other hand, several computational works have been developed using finite element models to simulate lumbar biomechanics after cage insertion in single functional spinal unit [94][109][180] or complete lumbar spine [70][67][209][93]. All of them studied the spinal movement showing that PSF provides a higher segment stiffness than stand-alone cages [171][108], but segment stability was also reported for the last ones. Since the goal of lumbar surgery is not only to stabilize the segment but also to restore the IVD space and maintain the lumbar lordosis, the major concerns regarding surgery complications are: segmental instability [151], cage subsidence [380] and cage migration [65]. Furthermore, lumbar fusion has been associated with the risk of adjacent segment disease because it alters the biomechanical environment of the whole spine [61]. However, all these key factors have not been studied together yet in a complete lumbar spine model with accurate constitutive material models.

Additionally, the ligaments play an important role in segment behaviour, particularly in bending. Ligament pre-strain is thought to be responsible for spinal stability in the absence of active muscle contraction [173]. However, ligament pretension is often overlooked or not reported in lumbar spine FE models because of the lack of experimental data. Recently, some FE studies have introduced the experimentally characterized pre-strain of some spinal ligaments in healthy lumbar spines [302][148] showing its influence on the overall spine biomechanics. Despite the importance that the ligament pre-strain may have on lumbar surgery success, few computational works have considered this condition after cage insertion [94].

As mentioned above, one of the major concerns about the use of stand-alone cages is the risk of subsidence of the device into the bone owing to the high contact pressures on the bony endplates. For this reason, a deeper investigation of the bony structures behaviour has been performed for possible solutions of cages in stand-alone construct. Although subsidence in early postoperative stage may increase the contact area, avoid the peak pressures caused by irregularities and prevent the progression of subsidence, high-grade subsidence can lead to a reduction in the intervertebral space height [223]. Thus, the use of an appropriate constitutive material of the vertebral bone incorporating a plasticity formulation would lead to a better prediction of the risk of subsidence in a stand-alone fashion. In previous studies, Von Mises equivalent stress has been used as the criterion for bone yielding. However, considering that the tensile strength of bone is smaller than its compressive strength, bone should be treated as a brittle material and the Von Mises criteria would not be suitable [35]. Furthermore, compressing collapse of crushable bone cells allowed for a gradual decrease of the stresses and a local hardening of the tissue. This behaviour was studied by Kelly et al. [178] who proved that a crushable foam plasticity formulation with pressure dependent yield behaviour provided the best approximation to the stress-strain curve of the bone. Other studies [35][278] have shown that the Druker−Prager formulation is able to predict the post-yield behaviour of the bone that can be improved by the definition of the hardening. Therefore, the modified Drucker−Prager Cap model, which takes the contribution of hydrostatic stress into consideration as the yield criterion, was used in this model.

On the other hand, cage characteristics such as shape, material and positioning were also expected to have a significant influence on subsidence risk. Previous studies have used FE models to compare among commercial cages, but only some of them have discussed the influence of cage material [109] or shape [150][62] using parametric or optimization methods. In their study, Hsu et al.[150] used a genetic algorithm to find the cage shape with an optimal subsidence resistance. However, they assumed flat endplates instead of real geometry which may lead to a more uniform pressure distribution and an underestimation of subsidence risk. Later on, a study comparing a standard cage with a custom-fit one showed that patient-specific cage geometry could reduce the stress concentration on the endplates [62]. However, these studies provided a limited prediction of subsidence as they used elastic material models.

Lastly, in the last years, some efforts have been made to develop patient-specific devices based on 3D-printed technologies. Applying this technique to the intervertebral spacers would allow to individualize the implant design in accordance with the predicted biomechanical behaviour. Moreover, the use of scaffolds offers the opportunity of functionalise the material with osteoinductive proteins to achieve a quicker and more solid bony fusion. However, the relatively weak initial material strength compared to permanent materials may be problematic. In addition, although degradability is a desirable feature of orthopedic implants for bone healing, the reduction in material properties due to degradation should be timed to coincide with the increase in mechanical stability resulting from bone growth. Previous studies showed the suitability of these devices following the evolution of bony fusion in animal models [1][377]. Other researchers found that cages printed by integrated global-local topology optimization were able to withstand typical human lumbar spinal loads and analysed computationally the mechanical integrity of the cage within the spine [176].

This chapter aims to fulfil three different goals:

- First of all, a FE model of the whole human lumbar spine was simulated in the intact stage and after surgery with the cage placed in a **stand-alone** fashion or in combination **with PSF**. In addition, two different cage designs corresponding to postero lateral interbody fusion (PLIF) and transforaminal interbody fusion (TLIF) were compared. The role that ligament pre-strain and cage-endplate interface play in spinal behaviour was discussed in a FSU. Thus, the biomechanics of the affected and adjacent segments were investigated and, whether a stand-alone cage is a feasible option for the treatment of lumbar disc diseases or not, was discussed.
- Secondly, the influence of different **cage parameters** on segment stability and **subsidence risk** was studied in a patient-specific FSU. The main contribution of this study was the evaluation of cage subsidence with an elasto-plastic material formulation with different behaviour for traction and compression for the bone. This work may provide a useful tool for the preclinical evaluation of the device and the prediction of surgery outcomes in each specific patient.
- Finally, different **scaffolds designs**, manufactured using additive 3D-printed techniques, were built and mechanically tested to evaluate whether it may be a suitable option to build patient-specific implants or not.

5.2 Materials & methods

5.2.1 FE models of the surgical treated lumbar spine

The poro-hyperelastic FE model of the whole lumbar spine (L1-S1) presented in Chapter 1 was modified to create four different post-surgical models adding instrumentation as shown in Figure 5.1. These models can be summarized as follows: 1)

Intact; 2) Stand-alone cage (TLIF); 3) Stand-alone cage (PLIF); 4) Cage (TLIF) + PSF; and 5) Cage (PLIF) + PSF.

5.2.1.1 Stand-alone cage

Two different commercial cages were modelled using Rhinoceros 5.0 (Robert McNeil & Associates, USA): the first one, used for TLIF approach was a single bean shape piece (OLYS®, Scient'x, Alphatec Spine Inc., France); the second, used for PLIF approach, consisted of two rectangular parallel pieces (NEOLIF®, Biomet, Germany). Both of them were made of PEEK (E=3,600MPa, ν= 0.38) [346] and meshed with tetrahedral elements with a mean element size of 0.5mm. For both cases, a discectomy was simulated, the NP was completely removed and the AF was adapted to the cage geometry. The cages were placed as shown in Figure 5.1b, maintaining the facet joints and all ligaments intact as described elsewhere [28]. Penetration of the cage through the annulus was avoided, whereas a surface-to-surface sliding-contact with a 0.5 friction coefficient [348] was set to the cage-endplate interface considering the effect of the serrated faces of the cage. The implant size was determined by an expert physician according to the patient spine geometry: 12mm height for OLYS cage and 10mm height for NEOLIF. The remaining AF was characterized as Grade IV degenerated tissue based on the Thompson grading system [344] with the material properties outlined in Table 5.1. A 5% of intervertebral space distraction was considered [94] and the corresponding ligament pre-stress was introduced in the model as initial conditions (Table 2.2).

Table 5.1: Material elastic and biphasic properties of grade IV degenerated annulus [251][228].

	Elastic parameters					Biphasic parameters			
	C_{10}[MPa]	C_{20}[MPa]	D[MPa^{-1}]	K_1[MPa]	K_2	k_0[m^4/Ks]	e (void ratio)	$c_{F,0}$	$n_{f,0}$
Degenerated annulus (grade IV)	0.45	2.5	0.306	1.8	11	1.45e-15	2.4	0.9e-4	0.7

Additionally, the sensibility of the lumbar segment motion to ligament pre-stress was studied in a FSU instrumented with a stand-alone OLYS cage. The FSU motion was tested in all loading directions for distractions ranging from 0 to 20% of the disc height, and taking into account that each distraction caused a different initial pre-stress of the ligaments (Table 5.2). Moreover, to check the influence of friction on cage migration, three different friction coefficients (0.1; 0.3; 0.5) were simulated in the same FSU without distraction to study the influence on cage migration.

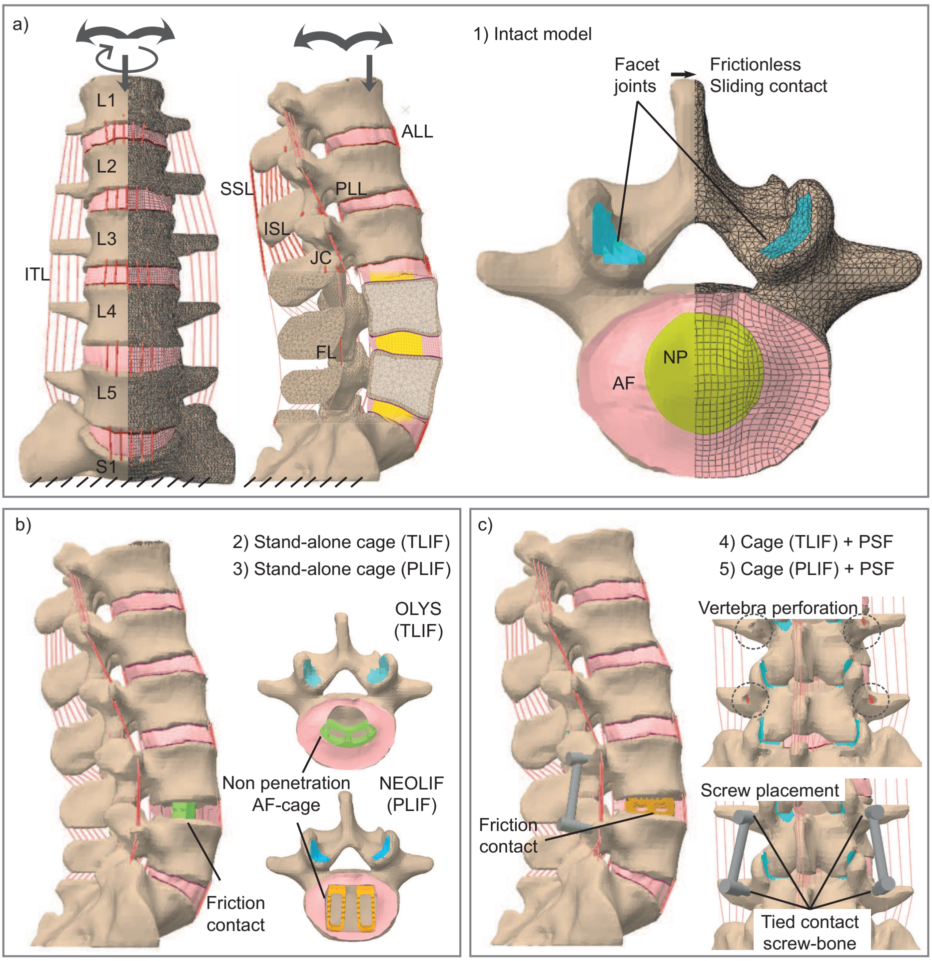

Figure 5.1: *a) (1) Intact model (L1-S1). Frontal and lateral view of the whole lumbar spine with a schematic representation of the boundary and loading conditions and the ligaments [Antero longitudinal ligament (ALL); Postero longitudinal ligament (PLL); Intertransverse ligament (ITL); Interspinous ligament (ISL) capsular ligaments (JC); flaval ligament (FL); Supraspinous ligament (SSL)] (left). Top view of L5 and the disc between L4L5 (right). b) Stand-alone models. Two different cages were introduced in the L4L5 interbody space: (2) TLIF cage (OLYS) and (3) PLIF cage (NEOLIF). A lateral view of the whole lumbar spine and the top view of cages placement are shown. c) Cage + PSF models. The stand-alone models have been supplemented with PSF after the perforation of L4 and L5 vertebrae: (4) TLIF + PSF and (5) PLIF + PSF.*

Table 5.2: Ligament pre-stress in stand-alone models caused by intervertebral space distraction (from 0 to 20% of the intact IVD height) during cage insertion.

Pre-stress	Intervertebral space distraction									
[MPa]	0%	1%	2%	3%	4%	5%	7.5%	10%	15%	20%
ALL	0	0.168	0.344	0.499	0.663	0.804	1.227	1.620	2.410	3.160
PLL	0	0.003	0.007	0.011	0.015	0.019	0.034	0.051	0.097	0.016
LF	0	0.003	0.007	0.011	0.015	0.020	0.035	0.053	0.101	0.169
ITL	0	0.004	0.009	0.014	0.020	0.026	0.052	0.085	0.199	0.387
JC	0	0.051	0.104	0.150	0.197	0.237	0.358	0.471	0.673	0.848
ISL	0	0.006	0.012	0.017	0.023	0.028	0.042	0.056	0.081	0.105
SSL	0	0.003	0.006	0.009	0.013	0.017	0.030	0.046	0.090	0.154

5.2.1.2 Cage with PSF

To provide additional stability, the previous models were supplemented with PSF. L4 and L5 vertebrae were perforated before screw insertion as shown in Figure 5.1c. A tied contact was assumed at the bone-screw interface. The fixation (diameter of rods and screws of 5mm) was made of titanium (E= 100,000MPa, ν= 0.33) [373] and meshed with tetrahedral elements of 1mm size.

5.2.2 Parametric study of subsidence risk

5.2.2.1 FE model of a FSU

L4-L5 segment was isolated from the model presented in Chapter 2 to evaluate the influence of cage insertion (Figure 5.2a). The model was remeshed to increase the accuracy of the results in the bone. The cortical bone was assumed to have a constant thickness of 0.5mm [325] and meshed with quadratic hexahedral elements of 2mm size. The cancellous bone was meshed with tetrahedral elements of 2mm mean size. Bone was characterized as a transversal isotropic material with a Druker−Prager cap plasticity formulation (see Section 5.2.2.3). The free space between the AF and the cage was filled with granulation tissue and meshed with tetrahedral elements. The mechanical properties for the cortical and cancellous bone are summarized in Table 5.3.

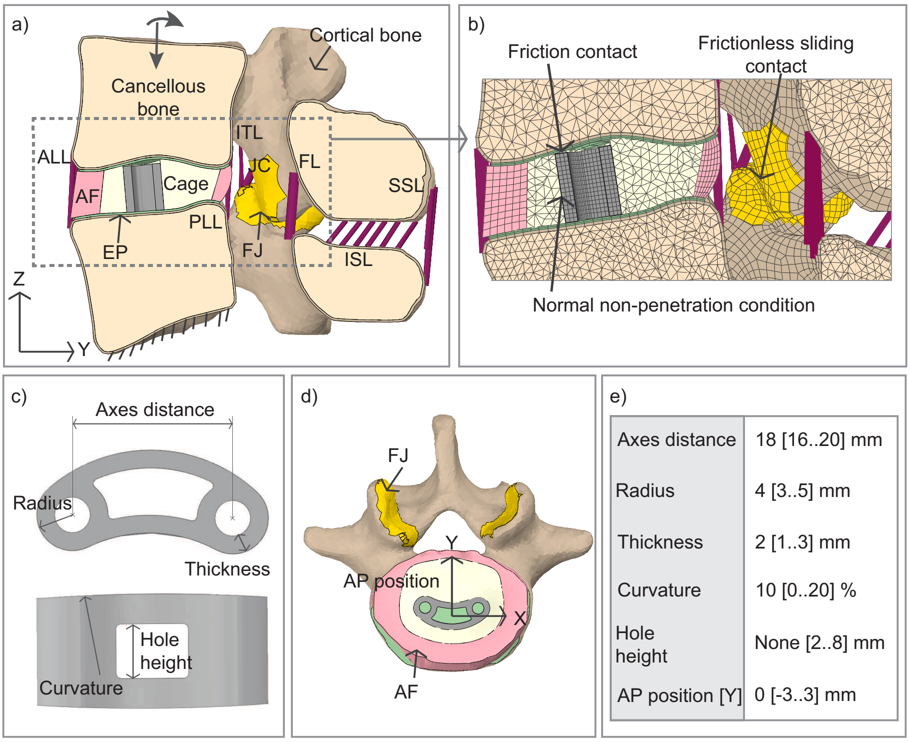

Figure 5.2: *a) FSU model including cortical and cancellous bone, endplates (EP), annulus fibrosus (AF), ligaments. b) Details of the mesh and contact definitions of the FE model. c) Interbody cage design and parametrization. d) Cage placement on L5 vertebra, the cage was moved along the anteroposterior direction. Granular tissue was considered between the annulus fibrosus (AF) and the cage. The facet joint (FJ) cartilage of L5 is shown. e) Parameter variation (Neutral values [min..max]).*

5.2.2.2 Parametric FE model of the intervertebral cage

A parametric model of a bean-shaped cage was created using Python scripting in ABAQUS 6.13 (SIMULIA, Providence, RI, USA) (Figure 5.2c). The nucleus pulposus was removed and the annulus scraped to host the cage. Furthermore, due to the lateral approach, no ligament was resected. The cage was placed at a central position and moved along the anteroposterior direction as shown in Figure 5.2d. Different features were modified: the axes distance, radius and thickness modified the cage size and cross-sectional area; the curvature, defined as the percentage of the difference

Table 5.3: Elastic and inelastic material properties of the vertebral bone. *[214][185] ⊤[214][187]

	Young modulus [MPa]	Poisson coef.		Yield stress [MPa]	Ultimate yield strain [%]
Cortical bone*	E_{XX}=E_{YY}=11,300 E_{ZZ}=22,000 G_{XY}=3,800 G_{YZ}=G_{XZ}=5,400	ν_{XY}=0.0484 ν_{YZ}=ν_{XZ}=0.203	Tension	155	-
			Compression	173	
Cancellous bone⊤	E_{XX}=E_{YY}=140 E_{ZZ}=200 G_{XY}=G_{YZ}=G_{XZ}=48.3	ν_{XY}=0.045 ν_{YZ}=ν_{XZ}=0.315	Tension	1.75	1.59
			Compression	1.92	1.45

between the central and the lateral height of the cage, varied the congruence between the cage and the vertebral bodies. In addition, a transversal hole (7mm width) with a modifiable height was introduced to vary the effective stiffness of the cage. Each parameter was varied uniformly between minimum and maximum values with a total of 9 values per parameter. Neutral parameter values corresponded to the standard shape of commercial implants. One parameter was varied at a time while maintaining neutral values for all other parameters. The upper and lower limits and the neutral values for each parameter are summarized in Figure 5.2e. The cage was meshed with linear hexahedral elements after a sensitivity mesh analysis (0.7mm size) and made of PEEK (E=4100MPa, ν=0.36, Yield stress=100-115MPa)(PEEK-OPTIMA®, InvibioTM Biomaterials Solutions).

5.2.2.3 Druker−Prager Cap plasticity formulation

The plasticity model presented by Drucker & Prager in 1952 [86] has been extended including modifications such as the Cap surface. The addition of that cap allows plastic consolidation modelling. The yield surface in the meridional (p-q) stress plane is defined by a line representing yielding in shear (F_s), and an arc representing yielding in compression (F_c) as shown in Figure 5.3.

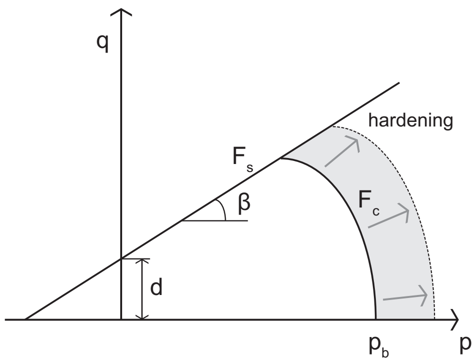

Figure 5.3: *Drucker-Prager Cap yield surface.*

According to the diagram, p is the equivalent pressure stress (Eq 5.1) and q the Mises equivalent stress (Eq 5.2).

$$p = -\frac{1}{3} trace(\sigma) \tag{5.1}$$

$$q = \sqrt{\frac{3}{2}(\mathbf{S}:\mathbf{S})} \tag{5.2}$$

Where **S** is the stress tensor.

The shear yielding surface is defined by Eq 5.3 with t representing the yield surface in the deviatoric plane (Eq 5.4), β the friction angle (43°for bone [235]) of the material and d the cohesion of the material related to the uniaxial compression yield stress (Eq 5.5).

$$F_s = t - p\tan\beta - d = 0 \tag{5.3}$$

$$t = \frac{1}{2}\left[1 + \frac{1}{K} - \left(1 - \frac{1}{K}\right)\left(\frac{r}{q}\right)^3\right] \tag{5.4}$$

Where K is the ratio of the yield stress in triaxial tension to the yield stress in triaxial compression and r the third invariant of deviatoric stress.

$$d = \left(1 - \frac{1}{3}\tan\beta\right)\sigma_c \tag{5.5}$$

On the other hand, the compression cap yielding surface is defined by Eq 5.6.

$$F_c = \sqrt{(p - p_a)^2 + \left[\frac{Rq}{1 + \alpha - \alpha/\cos\beta}\right]^2} - R(d + p_a\tan\beta) = 0 \tag{5.6}$$

Where α is a small number to define a smooth transition between the cap and the shear surface, R a material parameter which defines the cap shape, and p_a represents the volumetric plastic strain driven by hardening. For this model, α and R were arbitrarily set to 0.07 and 0.5, respectively. Instead of assuming ideal plasticity, a hardening law was defined by the evolution of p_b with the volumetric inelastic strain. After an element underwent compressive yield, Young's modulus was reduced to the post yield modulus, which was set to 5% the initial elastic modulus [257].

5.2.2.4 Boundary conditions

For the whole lumbar spine, the loading and boundary conditions were those explained in Section 2.4. For the parametric model an axial preload of 500N was applied followed by $\pm$7.5Nm moment load in flexion-extension, lateral bending and axial rotation at the centre of L4 while movement at the lower portion of L5 was restricted [119]. A surface-to-surface contact with a friction coefficient of 0.5 was assigned to the cage-endplate interface [356]. The penetration of the cage into the granulation tissue was avoided with a normal non-penetrating contact (Fig 5.2b).

5.3 Results

5.3.1 Comparison among cages alone or in combination with PSF

5.3.1.1 Movement of the affected segment

Moment-rotation curves were analysed and compared for all the models to see the effect of surgery over the segment mobility as shown in Figure 5.4. When PSF was used, a dramatic loss of motion occurred regardless the load direction or surgical approach, although the immobilization was more pronounced in flexion, extension and LB than in AR. Meanwhile, the stand-alone cages allowed for a wider ROM without exceeding the movement of the intact segment. The stiffness, defined as the moment applied divided by the ROM achieved, of L4-L5 segment in models (2) and (3) were greater in extension and AR movements (around 75%) than in flexion and LB (around 25%). Comparing between cages, the one used for TLIF approach (2) showed a higher ROM restriction in AR, whereas the one used for PLIF (3) approach reduced more the extension rotation. In flexion and LB the behaviour of the spine with both surgeries was similar.

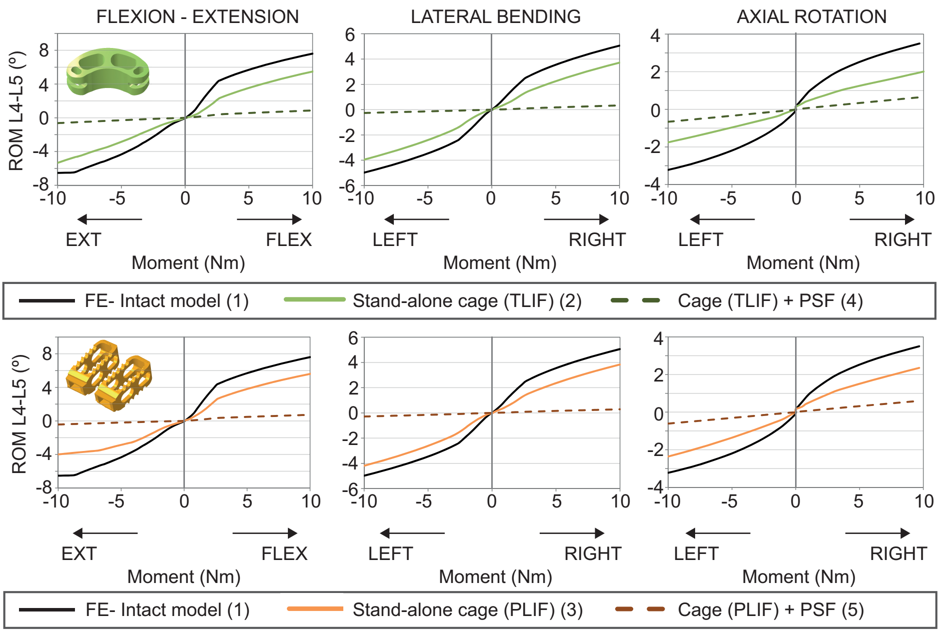

Figure 5.4: *Range of motion in L4-L5 segments in flexion, extension, lateral bending and axial rotation for TLIF (top) and PLIF (bottom) approaches in comparison with the intact movement.*

Regarding the influence of ligament pre-stress, the sensibility study showed that ALL, JC and, at high distraction levels, ITL were the most affected by space distraction (Table 5.2). The movement was reduced in all loading directions by increasing the distraction, contributing to segment stabilization. ALL affected the extension movement, while JC decreased the rotation primarily in flexion and AR. LB movements were the less influenced by the pre-stress (Figure 5.5).

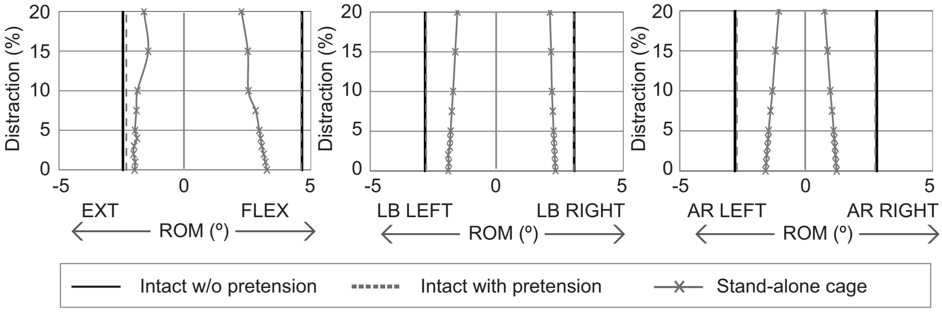

Figure 5.5: *Influence of intervertebral space distraction (from 0 to 20% of the intact IVD height) on the FSU motion with OLYS stand-alone cage in all load directions. (EXT: Extension; FLEX: Flexion; LB: Lateral bending; AR: Axial rotation)*

5.3.1.2 Subsidence risk

To evaluate the risk of subsidence, and therefore, the intervertebral space height reduction, the contact pressure in the cage-endplate interface was studied for the stand-alone models (2) and (3). With both cages the magnitude of contact pressure was similar; however, as shown in Figure 5.6, the footprint left by each cage differed. When NEOLIF was used, the pressure was more concentrated at the corners of the cages, while with the OLYS cage the contact pressures were distributed in a larger area on the central region. These results suggest that the cage geometry and placement may be important parameters in the prevention of the subsidence risk.

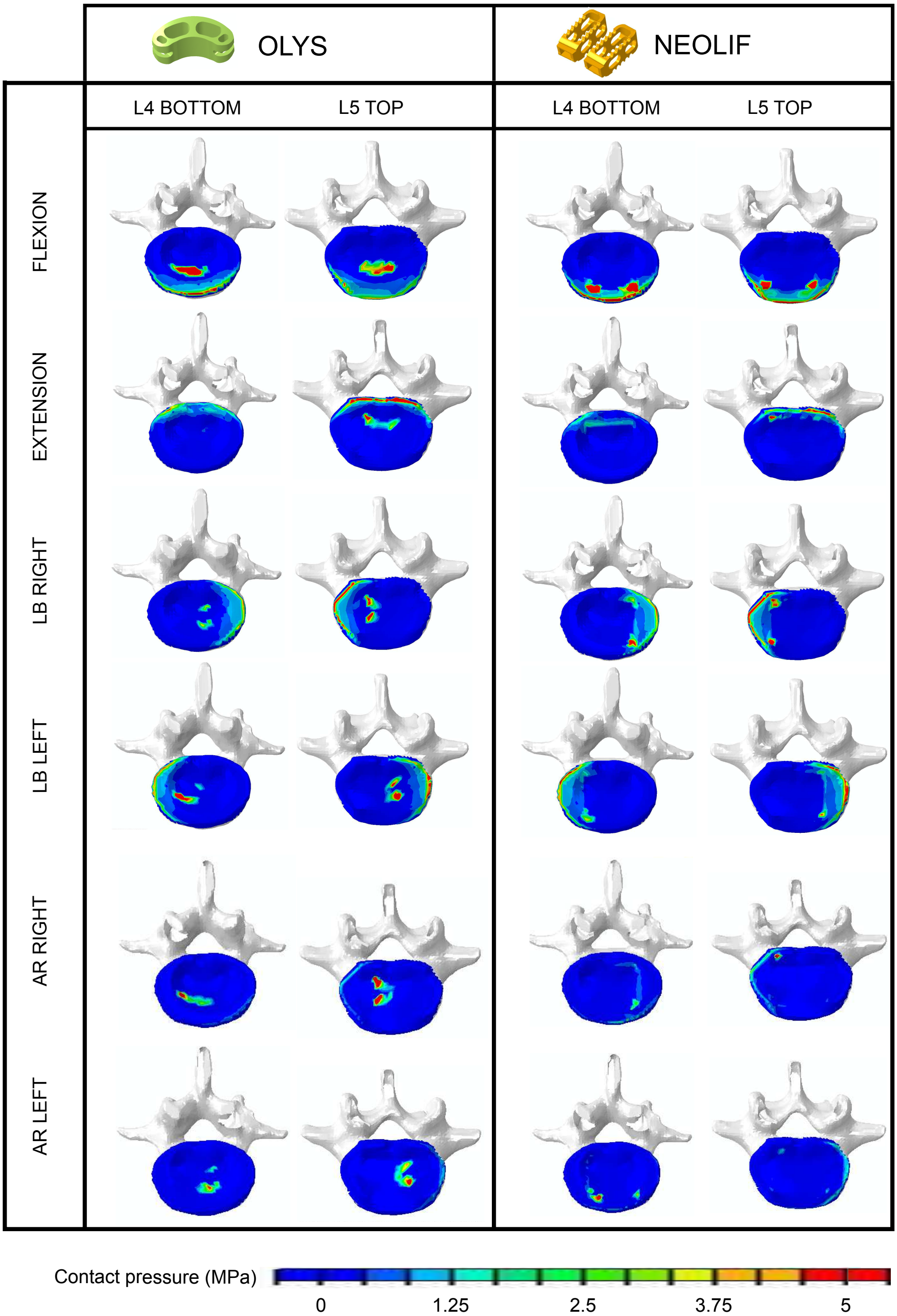

Figure 5.6: *Contact pressure distribution on the top endplate of L5 and bottom endplate of L4 for both stand-alone cages in each rotation movement.*

5.3.1.3 Cage migration risk

The relative displacement of the cages within the vertebrae, summarized in Table 5.4, was smaller when the OLYS cage was used excluding flexion. The highest slip distances were reported in AR with NEOLIF cage, which are the only ones exceeding 150μm. Furthermore, as expected, the displacement direction of the cage depended on the applied loads: for flexion-extension movements the highest slip occurred in antero-posterior direction; while for LB and AR, the cage slipped in lateral direction.

Table 5.4: Maximum relative displacement between cage and endplate at the top and bottom surfaces in flexion, extension, lateral bending (LB) and axial rotation (AR). The direction of the displacement was represented in brackets: (AP) Antero-posterior and (LAT) Lateral.

Relative displacement [μm]	OLYS (2)	NEOLIF (3)
FLEXION	79 (AP)	36 (AP)
EXTENSION	54 (AP)	75 (AP)
LB RIGHT	27 (LAT)	94 (LAT)
LB LEFT	7 (LAT)	83 (LAT)
AR RIGHT	88 (LAT)	295 (LAT)
AR LEFT	92 (LAT)	452 (LAT)

In the study of the FSU, the relative movement showed to be greatly dependent on cage-endplate friction coefficient. By decreasing the friction, the relative displacement of the implant increased as shown in Figure 5.7.

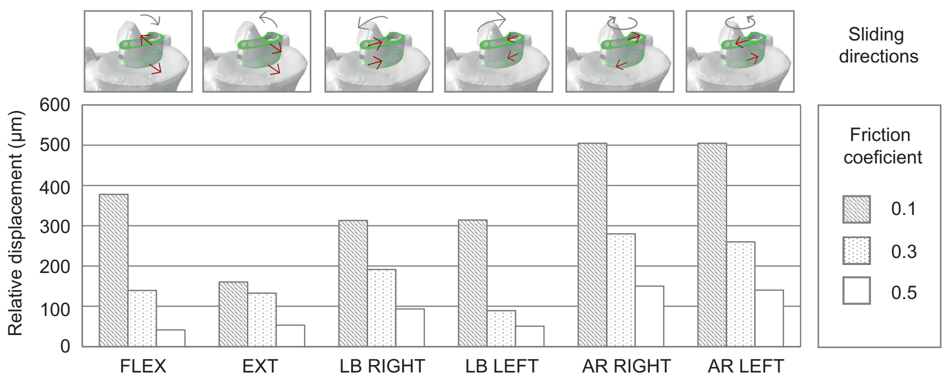

Figure 5.7: *Influence of cage-endplate interfacial friction on the relative displacement of the stand-alone OLYS cage and the directions where the maximum displacement took place. (EXT: Extension; FLEX: Flexion; LB: Lateral bending; AR: Axial rotation)*

5.3.1.4 Biomechanical changes in affected and adjacent IVD.

In the remaining AF of the affected segment (L4L5), the maximal and minimal principal stresses almost disappeared when PSF was used in flexion-extension and LB and were reduced to a half in AR, as shown in Figure 5.8. On the other hand, the models with stand-alone cages suffered compressive stresses higher than those of the intact discs and tension stresses lower with the exception of NEOLIF cage in right rotation.

Attending to the adjacent segments, the PSF caused a higher increase of principal stresses as shown in Figure 5.8. In flexion, the increase in stresses was more pronounce in the upper adjacent disc than in the lower one. However, in LB and AR the influence over upper and lower discs was similar but depends on the load direction and surgical approach. The adjacent discs to stand-alone constructs experienced a smaller change but it was also higher in the cranial disc during flexion.

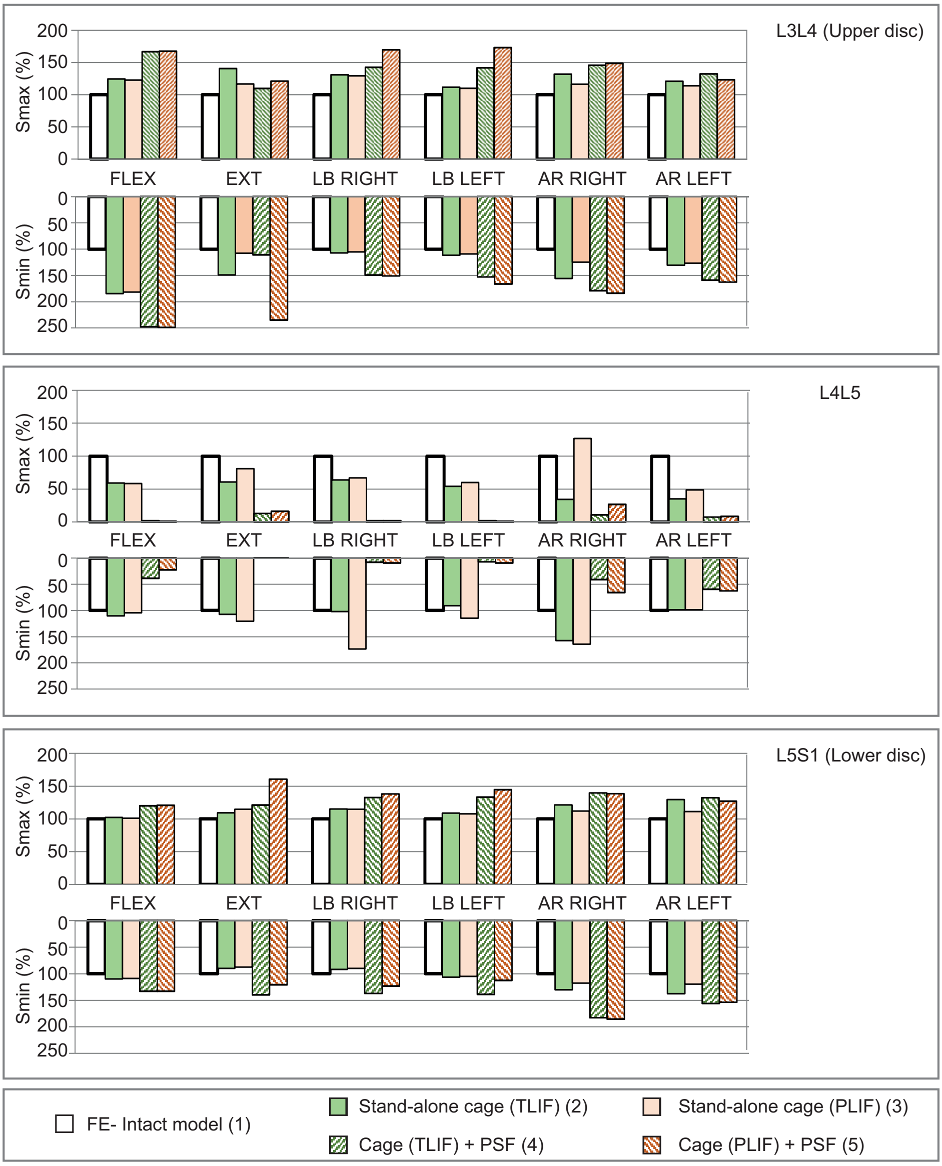

Figure 5.8: *Maximal and minimal principal stresses in the remaining AF (L4L5) and the adjacent discs (L3L4 and L5S1) in flexion, extension, lateral bending (LB) and axial rotation (AR) as percentage of the intact values for each simulated model. For comparison, the stresses were measured at the same IVD location along the models.*

5.3.2 Parametric study of the cage design and placement

5.3.2.1 Segmental stability

The range of motion (ROM) of the FSU for each cage design and position is shown in Figure 5.9 together with the rotation of the intact segment. The parameters exerting the strongest effects were radius and anteroposterior position. The segment stability was improved increasing the radius, which means a wider cage, in all loading directions. A longer cage, increasing the axes distance, improved the stability in extension and lateral bending while a higher curvature led to the opposite outcome. In addition, in axial rotation a flat cage was more unstable than a biconvex one. On the other hand, the antero-posterior positioning of the cage had a different impact depending on the load direction: an anteriorly placed cage increased the stability in flexion, lateral bending and axial rotation but decreased it in extension. However, an extreme posterior placement also increased the rotation in extension.

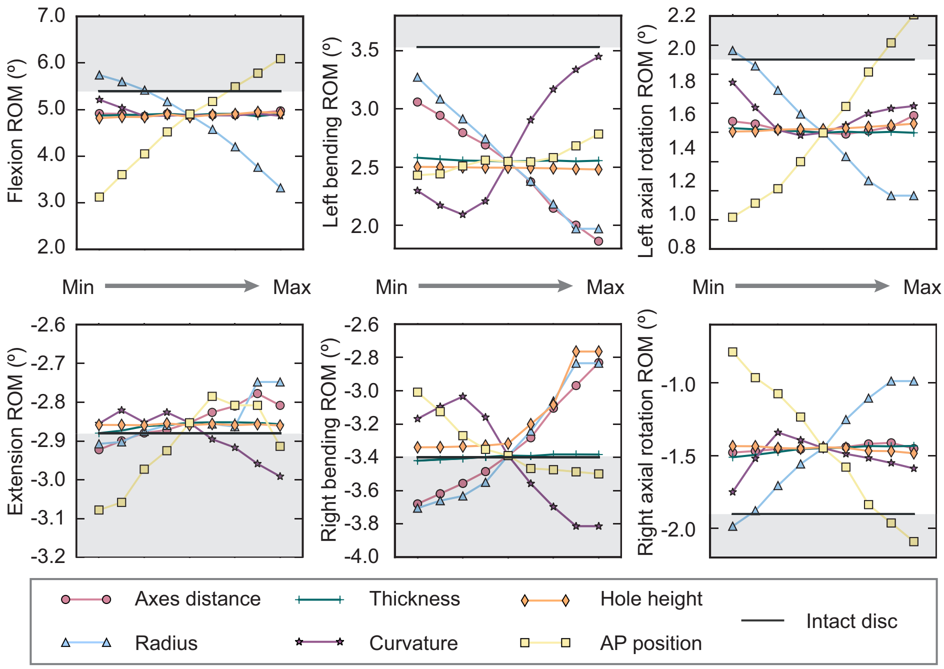

__Figure 5.9:__ Change of the final rotation of the FSU due to the variation of each parameter in flexion, extension, lateral bending (LB) and axial rotation (AR). The rotation of the intact segment under the same conditions is shown as reference. The shaded area denotes the ROM for which the segment would be unstable.

5.3.2.2 Facet joint forces

In flexion, the facet joints remained unloaded for the intact model. However, the presence of a cage led to the appearance of facet forces, which were not significant in comparison with those depicted in Figure 5.10 for extension, lateral bending, and axial rotation. As mentioned before, short cages and high curvatures caused instability of the segment increasing the facet forces more than 20% in extension and lateral bending, and more than 30% in axial rotation. On the contrary, a drastic reduction of the facet forces was obtained when the cage was posteriorly placed because most of the load was transmitted through the endplates instead of through the posterior elements. Although in general, more stability was accompanied by a facet force reduction, this force was in many cases higher than in the intact segment. This increment is related to the displacement of the instantaneous centre of rotation (ICR).

5.3.2.3 Risk of cage subsidence

After a careful analysis of the results, it was observed that the maximum peak contact pressures appeared for flexion and lateral bending movements at the bottom endplate. Due to the irregularities of the endplate geometry, these peak pressures took place on small areas and did not follow a uniform trend with the variations of the parameters. Therefore, the nominal contact pressures were analyzed. Once again, flexion and lateral bending transmitted the highest forces through the endplates and: radius, curvature and anteroposterior positioning, exerted the greatest influence. Regarding the bone integrity, it was observed that these parameters also had the greatest influence in the appearance of inelastic strains. Furthermore, caudal vertebra presented a higher volume of failed bone. Here the most significant results are shown; more details can be found in the Online resource 2. Figure 5.11 depicts the change in bone volume that had undergone inelastic strains with the most influential cage parameters. In flexion, it was observed that a cage with a curvature higher than 12.5% or a radius higher than 4.25mm caused bone failure preceding cage subsidence. In turn, an anteriorly placed cage also led to bone failure.

On the other hand, in extension, the yield zone moved backward to the vertebral arch and the facet joints, where the inelastic strains in the arch were primarily caused by tensile stresses due to the contact between the facet joints. Furthermore, plastic strains on the endplates were obtained with a posterior positioning of the cage.

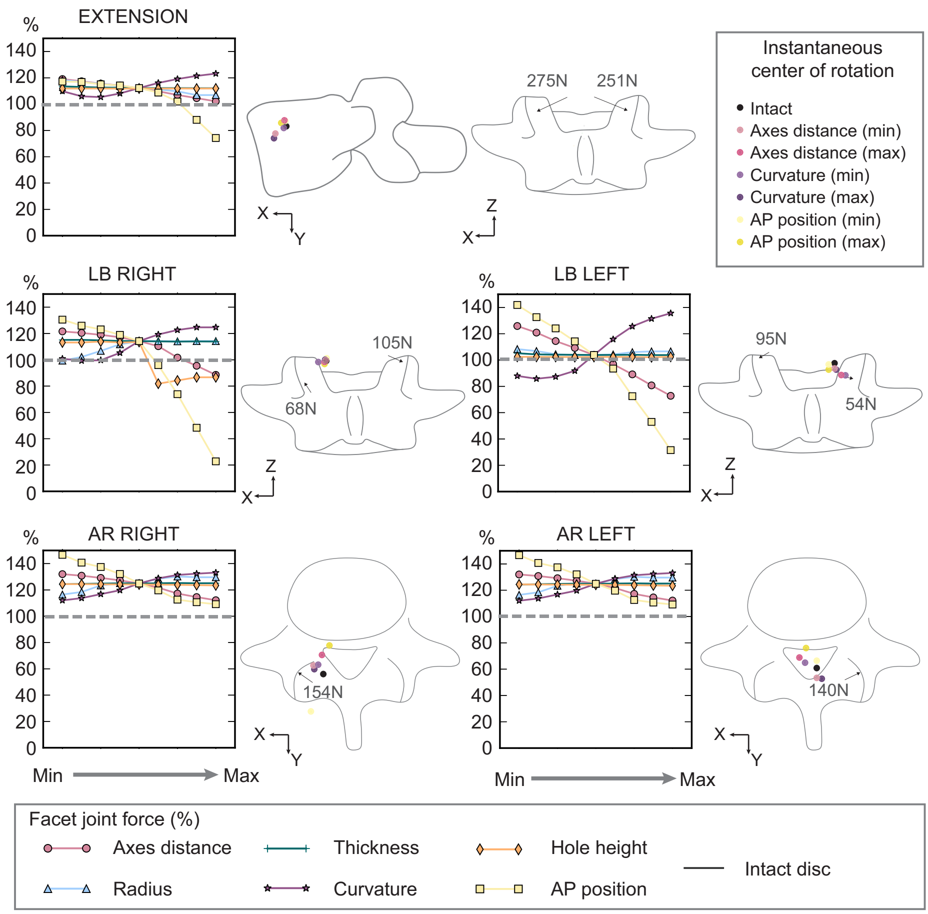

Figure 5.10: *Change in the force supported by the most loaded facet joint due to the variation of each parameter under extension, lateral bending (LB) and axial rotation (AR) in percentage of the intact force. At the right of each graph, the scheme of L5 has been depicted with the direction and value of the facet joint forces in the intact FSU. The instantaneous center of rotation has been plotted for the intact case, and the maximum and minimum values of the parameters which affect the most the facet joint forces (axes distance, curvature and AP position).*

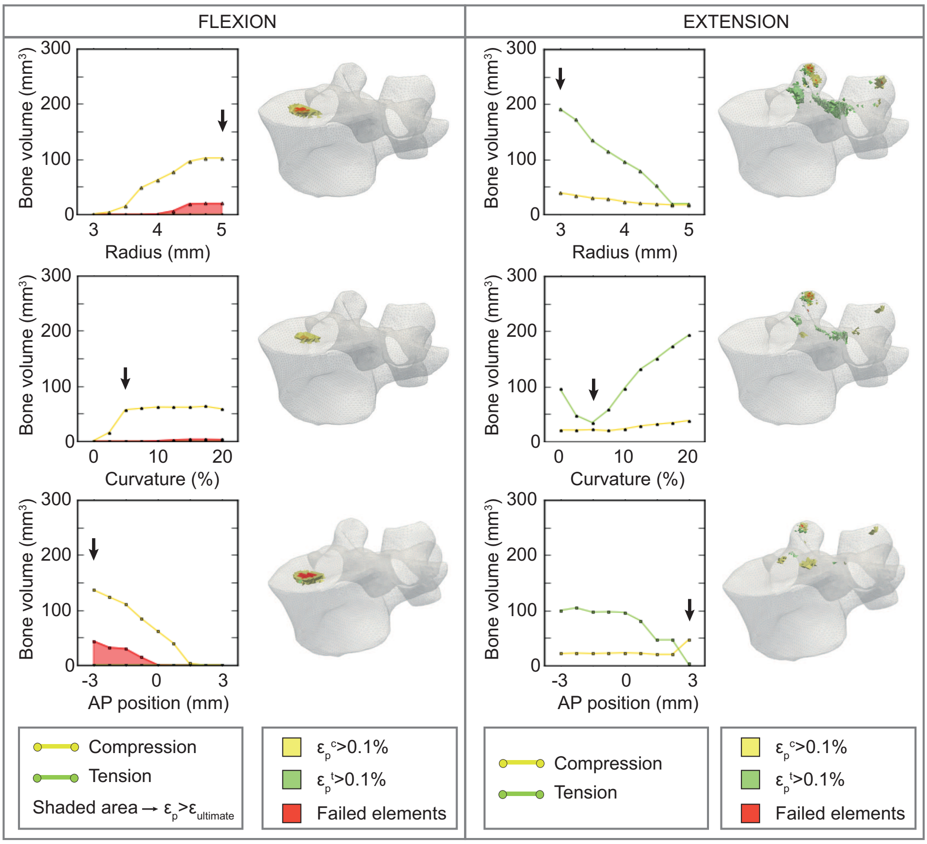

Figure 5.11: *Change in the bone volume that undergone plastic strains due to the variation of radius, curvature and AP position.* ε_p^c *and* ε_p^t *are the plastic strains in compression and tension respectively (see Table 1). The volume of failed bone has been represented as a shaded area. At the right of each graph, the distribution of plastic strain is shown in L5 for the case marked by the arrow.*

5.4 Discussion

5.4.1 Comparison among cages alone or in combination with PSF

The first aim of this chapter was to compare among intervertebral lumbar cage surgeries with and without supplemental PSF and argue whether a stand-alone cage is a feasible solution for lumbar disc degeneration and hernia or not. The analysis of ligament pre-stress and cage-endplate interface behaviour has allowed for a deep discussion of segment stability and cage migration. Five different variations of a whole lumbar spine FE model were built to compare between cages commonly used for two different approaches (TLIF and PLIF) and those in combination with PSF. Additionally, a FE model of a single FSU was used to test the sensibility of lumbar motion to changes in ligament pre-stress, and the relative displacement due to variations in cage-endplate friction.

The results revealed a drastic reduction in ROM when PSF was used in flexion, extension and LB. In AR the addition of posterior fixation considerably reduced the movement but it allowed for around 1°of rotation. Meanwhile stand-alone cages allowed for a greater ROM. The segment stiffness increased around 25-35% in flexion and LB and approximately 70% in extension and AR. Considering that spine instability occurs if the ROM of the affected segment exceeds that of the intact segment for the same moment load [263], all the surgeries kept the segment stable as the stiffness increased in all cases. And, although the PSF achieved a much more stable union, stand-alone cages have proven to be sufficient for intervertebral fusion when used in combination with bone graft [10][223][222]. Furthermore, when no graft is added, a fibrosis occurred around the implant preventing from migration and preserving some segmental motion [28]. Other authors have evaluated the ROM for a variety of cage designs and load magnitudes from a computational and experimental point of view. In vitro studies reported ROM reductions with stand-alone cages between 6 and 70% of the intact movement in flexion-extension and LB for complete lumbar spines [51][343] or FSUs [49]. This wide range in experimental findings may be caused by the different cages and surgical approaches used. However, all of them agreed in showing that the restriction in the AR is lower and, in some cases, it was even higher than the intact movement. Moreover, all of them reported a significantly greater segmental stiffness when the cage was augmented with PSF. As well as in vitro studies, FE models from literature also reported a broad range of ROM reduction depending on cage design, material and simulation simplifications in whole lumbar spines [70][67] and FSU [94][180]. But, as happened in experimental works all of them showed a less stabilization for AR and more rigid segments with the use of PSF, which is in accordance with the results of this work except in AR with stand-alone cages. In this work the segment was stiffer in AR, which could be a consequence of ligament pre-stress, specially the capsular ligaments. Here the role of ligament pre-stress due to cage insertion in the stabilization of the segment was considered. ALL and JC ligaments, which are dominant under extension [206], were the most affected by space distraction. Consequently, the ROM in extension was reduced with increasing distraction. The capsular ligaments also restricted flexion and AR movements, providing additional stability.

Apart from stability, the interaction between cage and endplate was studied. Cage subsidence and migration are the most common causes of failure in lumbar surgeries [223][171] and contact pressure and slip distance can be related to these phenomena [336]. Herein, both parameters were analysed to assess the risk of failure for each cage design. The OLYS cage showed an homogeneous contact pressure distributed in a large contact area. On the contrary, the NEOLIF cage exhibited concentrated contact pressures at the cage edges, as shown in other studies [348][67]. However, while OLYS cage laid in the central part of the endplate, NEOLIF contact pressures were located in the outer part of the bony endplate, where its strength is higher [213]. It is known that subsidence risk depends on bone properties and is different for each patient [264][123][178], so a deeper analysis including the local strength of the bony endplate would be necessary to discuss which cage is more likely to subside.

On the other hand, relative micromotions on the cage-endplate interface were in the range reported by Chen et al. (2008) [68]. The slip distances found were under the critical level of relative micromotion of 150μm for bone ingrowth [280] except for AR with NEOLIF cage, thus no risk of migration was encountered for stand-alone cages. In general, LB is the less risky movement, while AR has a higher probability of causing relative displacements of the cages. In fact, cage retropulsion is more likely to be caused by flexion, where the slip distances were under the above-said threshold. For this analysis, a friction coefficient of 0.5 was assumed because of the serrated cage surfaces. A study of the influence that friction has in the relative displacement of the cage showed that decreasing friction coefficient increased the slippage, especially for very low friction values.

Finally, the stress distribution in the affected and adjacent segments was analysed. The addition of PSF reduced the maximal and minimal principal stresses in the remaining annulus by more than 50%. The stand-alone construct also caused a reduction in the maximal stresses around 30%, however the minimal principal stresses were increased in some movements. Additionally, it has been hypothesized that the addition of PSF could lead to the development of IVD degeneration in the segments adjacent to the fused level due to alterations in the stress-strain distribution [90][117][352]. In this work, a greater increase in tension and compression stresses has been reported for the models with PSF, while the stand-alone slightly alters the stress distribution in the adjacent segments, which is also seen in the literature [68]. Moreover, the change in stresses in the cranial segment was greater than in the caudal one, which matches with the incidence of reoperations reported clinically [322].

Although special care has been taken in reproducing the physiological behaviour of the tissues and the events after the surgery, this work has several limitations. Despite spinal ligaments exhibit a non-linear, anisotropic and viscoelastic response [302] [44][63][147], they have been simulated as non-linear uniaxial elements. A shell or 3D model of the ligaments would allow for the implementation of a more accurate material behaviour and for taking into account the tension caused by disc bulging [147]. However, the pre-stress has been demonstrated to influence more than anisotropy in intersegmental motion. Furthermore, few experimental data are available regarding spinal ligament pretension. For deeper studies more experimental work is needed. A tie contact was defined at bone-screw interface assuming bone growth. This assumption is valid if the surgeries are evaluated in a long-term state. Only quasi-static loads were applied to the models. For a more accurate evaluation of the surgical technique, cyclic and impact loading should be considered.

5.4.2 Parametric study of the cage design and placement

The second goal of this chapter was to investigate the effect of varying interbody cage design and placement on the risk of subsidence. FE models with a post-yield characterization of the vertebral bone were used to achieve this purpose. Because this work aims to provide a useful tool for preoperative evaluation: stability, facet forces and bone integrity have been studied as key factors to achieve a successful fusion surgery.

Historically, supplementary fixation has proved to provide greater stability, however, recent clinical studies have shown successful fusion using stand-alone cages [10][357]. In this study, a stand-alone cage was tested using a patient specific geometry and a movement exceeding the physiological ROM was deemed unacceptable. Thus, better stability was predicted for wider and longer cages in agreement with in vitro and clinical findings [223][281]. Nonetheless, the maximum cage width would be ultimately determined by the risk of neural injury during the insertion. Cage placement has also demonstrated a high impact in segmental stability. As seen in clinical practice an anterior positioning of the cage makes for a more stable construct [58]. In our study, all rotations were reduced when the cage was anteriorly placed except for extension movement. Similarly, previous studies reviewed elsewhere [264] have shown greater instabilities in extension. In these studies, the instability may be caused by the removal of stabilizing structures such as ALL and facet joints while, here, these structures were preserved, simulating a minimally invasive surgery, and allowed to achieve a stable construct by varying the device design and placement.

Besides, an alteration in the load transmission through the posterior elements was observed with the variation of the interbody cage design. In their study, Schmidt et al. [316] showed how these forces strongly depend on the total disc replacement design. Our results showed that the higher the stabilization achieved the less the forces except for position variation. However, facet forces were higher than the intact ones for most of the analysed cases, which seems to be inconsistent with the idea of load sharing between posterior elements and a stiff interbody spacer. This inconsistency may be explained by the displacement of the ICR. In axial rotation, where the highest load increment was reported, the ICR moved towards the centre of the disc, in agreement with Schmidt's findings, changing the motion pathway of the upper vertebra and, therefore, the contact through the facet joints. In fact, when the cage was posteriorly placed the facet forces significantly decreased in all movements because the load was mainly transmitted through the implant.

Finally, cage subsidence risk has been previously predicted based on contact pressures [109], Von Misses stresses [62] and total reaction forces [150]. However, none of these outcomes account for bone failure which is the actual cause of subsidence. Here, the maximum peak pressures were similar to those obtained previously [109], but no constant trend was found with the variation of the cage design parameters. The irregularities of the endplates naturally result in small contact areas with high loads, which may explain why the pressures did not show any trend when varying the design. Thus, they hindered the discussion of which parameters will enhance subsidence resistance. However, these pressures provoke stresses in the underlying bone which may cause inelastic strains. In our model, the implementation of a Drucker-Prager cap plasticity material behaviour allowed to predict bone failure and, therefore, cage subsidence. Contrary to other studies [170] which found more inelastic strains in extension or lateral bending, in our model plastic strains were more prone to occur in the anterior part of the caudal vertebra during flexion. This difference may be related to the use of posterior fixation by Jalil et al. which restricted the flexion motion decreasing the compressive force on the anterior part of the endplates. Regarding the cage parameters, the inelastic strains increased for cages with: high radius, high curvature and an anterior position. Thus, a wider cage enhanced stability at the same time that increased the risk of subsidence, and the same occurred with an anteriorly placed cage. So an equilibrium between stabilization and subsidence should be reached to determine the best cage design. In agreement with our results, previous FE studies showed that a higher cage stiffness would increase the risk of subsidence [109]. By contrast, clinical studies have shown that a wider cage increases the subsidence resistance [223][202] because they lay in the peripheral region where the structural properties of the lumbosacral endplates are superior [213]. This disagreement is due to the fact that in this study uniform properties have been considered due to the lack of material data. Lastly, in extension, the yield zone moved backward to the vertebral arch and is mainly caused by tensile stresses. Here a constant cortical thickness was considered for the entire vertebra, however, the arch has actually a thicker cortical layer and, therefore, the stiffness of this part is higher and the inelastic strains would decrease.

This study has a number of limitations. Firstly, a high friction coefficient at the cage-endplate interface was used, assuming that the surfaces of the cages are prepared with a serrated geometry or roughness to avoid slippage of the device [68]. Nevertheless, this parameter would be more important for the risk of cage migration than for cage subsidence which is the goal of this work. Secondly, when modelling the mechanical behaviour of the endplates linear elasticity and constant thickness were assumed. Modelling using a hyperelastic material and irregular thickness would allow for a more accurate analysis of endplate behaviour. Regarding the facet joints, the properties were taken in accordance with other previous studies, however, slight changes in the gap distance, the degree of curvature or the facet orientation can lead to different results. In this study, the results have been normalized with the intact data for comparison. In the model, the cage insertion canal was not explicitly modelled. Given that the simulated surgery corresponded to a TLIF approach an anterolateral annular defect should have being included for a more actual prediction. However, although it is expected to cause some asymmetry in the results, the largest part of the load was transmitted through the cage and the posterior elements so it was assumed that the difference would not be significant. Furthermore, the distraction of the segment due to the cage press-fit was not included. If the cage height would be higher than the initial disc height, all the surrounding structures such as ligaments, muscles and annular fibres would present a pre-strain which would increase the load in the cage and, therefore, the contact pressures on the endplates. Nevertheless, considering that this pre-strain would affect all the cases, the predicted trends with varying parameters is expected to be unaltered. For a more deep understanding of the effect of segment distraction, a further parametric study should be performed varying cage height, and also considering that the segment would adapt to the cage differently in each position depending on the specific geometry, so that the pre-strain state of each structure would change from one to another. Furthermore, subsidence is directly related to bone quality which must be cautiously evaluated preoperatively. In this model, the material properties chosen for bone modelling corresponded with the lowest ones found in the literature [187] to create the worst possible scenario. Moreover, they were considered uniform along the endplates. A characterization of the local thickness and bone mineral density of the cortical and cancellous bone would improve the subsidence prediction. Besides, as was shown in other studies [9] the vertebral endplate morphology follows the bone remodelling principles. When an implant is placed, the load sharing among the different regions of the endplate modified the mechanical environment of the bone forming cells initiating a remodelling process which may lead to a new situation. In further studies, the adaptive bone response to mechanical alterations should be studied in combination with its inelastic behaviour. Finally, a quasistatic load was applied to cross compare among implants while the physiologic environment of the lumbar segment would be better reproduced by a cyclic loading. It is expected that the elements which underwent inelastic strains accumulate damage over time driving to the progressive sinking of the implant into the vertebral body. Nevertheless, this study aims for the comparison between cage designs, so it is expected that the higher the inelastic strains in the static case, the higher the accumulated damage during time.

This model goes a step forward in subsidence prediction with the possibility to discern if the bone will fail under the cage pressure or not. It was seen that cage design and placement played an important role in the biomechanical behaviour of the FSU after lumbar surgery. A compromise between stabilization and bone integrity should be reached by modifying the width, length, curvature and position of the cage for each specific patient. For that purpose, the model presented above may be a useful tool for the preoperative evaluation of patient-specific surgery outcome.

5.4.3 3D-printed cages

A bean shape cage was printed with a geometry similar to those cages previously studied (1)(Fig 5.12). Posteriorly, a porous structure was added into the gaps with a mean pore size around 300-400μm, which is thought to promote bone growth (2). Finally, transversal holes were made in the mid-height of the cage varying the cage stiffness and the possibility of bone growth (3).

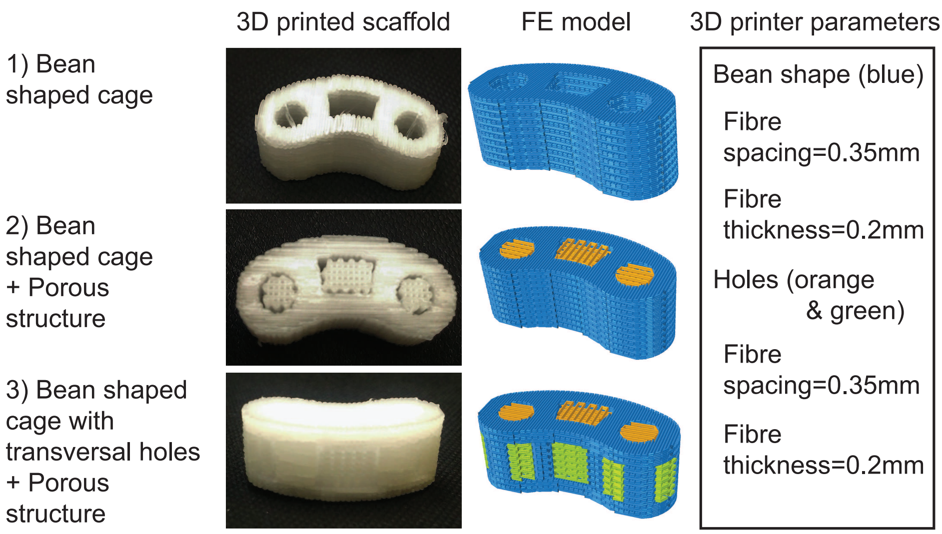

Figure 5.12: *Three different designs for 3D-printed cages and their corresponding FE models, built with the listed printer parameters.*

A 3D bioplotter from RegenHU (3D Discovery) was used to print two cages of each type. Polycaprolactone (PCL), Mw = 45,000 (Sigma-Aldrich) was melted at 68°Cin the printing chamber. A screw driven piston (24rev/min, screw diameter 1cm) extruded the PCL onto a coverslip at a pressure of 0.45MPa. A 25 Gauge straight needle was used throughout to plot PCL resulting in fibre diameters of approximately

200μm. Compressive mechanical tests were performed using an INSTRON 3366 (Instron®, Massachusetts, USA) with a 10kN load cell until 50% of strain or 4,000N load was reached.

A FE model was built for each cage and inserted into the lumbar spine model to study the mechanical behaviour of the structure under lumbar loads.

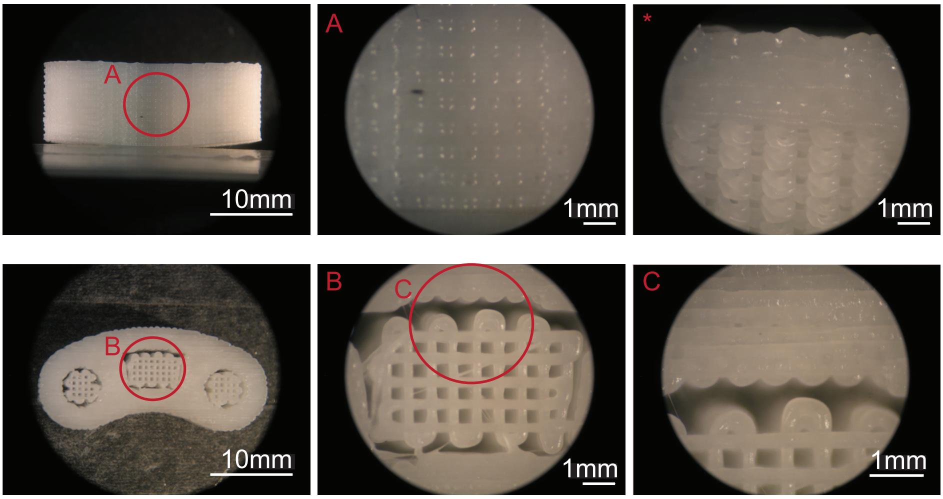

Figure 5.13: *Microscopic images of the porous structure. All the images correspond to the cage (2) but the one marked with *, which shows the transversal hole of the cage (3).*

A compressive mechanical test was performed to the printed cages as explained in Section 5.2.3 obtaining the stress-strain curves showed in Figure 5.14a. After the toe region, a similar elastic modulus was recorded for all the samples, giving a higher value for one of the cages (1) and (2). However, the elastic limit was clearly lower for the cages with transversal holes (3), which were not able to withstand lumbar physiological loads without inelastic strains.

A FE analysis of each structure was run assuming uniform properties of the PCL (E=470MPa), which were experimentally measured by a traction test of a single fibre. Similar to the results obtained in the experiments, the porous structure introduced in (2) did not affect the effective elastic modulus as it did the transversal holes. In all the cases, the effective modulus was underestimated using FE models. This may be a consequence of the manufacturing method because the melted PCL fibres may fused with the previous layer during the process decreasing the pore size.

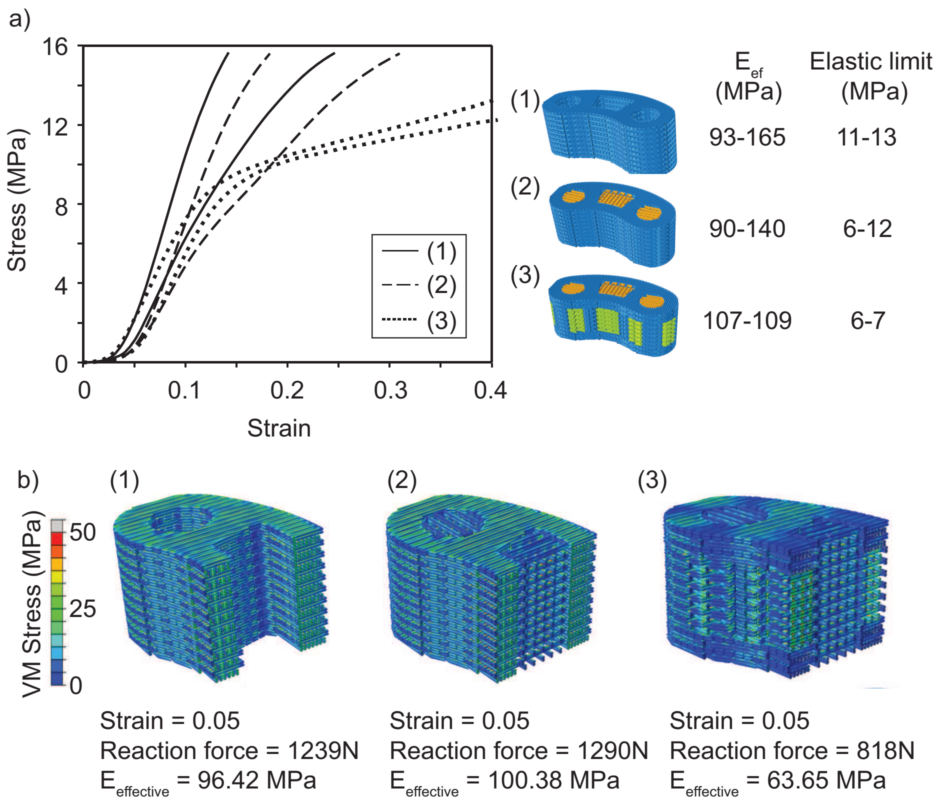

Figure 5.14: *a) Stress-strain curves obtained from the compressive mechanical test of the PCL cages. b) Von Misses stresses in the PCL fibres of the different FE models.*

CHAPTER 6

TISSUE HEALING DURING LUMBAR FUSION

After lumbar surgery, the blood clots and progenitor cells liberated by the damage of the surrounding tissues create an environment prone to generate new tissues. In this chapter, two algorithms for tissue healing were implemented. A mechano-regulated theory and a bio-mechano-regulated theory were used to predict fusion after nucleotomy, internal fixation, anterior plate placement and stand-alone cage insertion. Additionally, the bone remodelling inside the vertebral bodies due to changes in the mechanical environment was predicted.

6.1 Introduction

Bone healing can occur through two different pathways depending on the conditions. If primary healing takes place, usually under optimal conditions, the bone tissue is directly repaired without the formation of a fracture callus. However, the most common pathway is the secondary healing which consists of three main phases: inflammatory, reparative and remodelling phase. When the tissue is damaged, it's inflammatory response, together with the blood influx, formates a granulation tissue in the area around the damage. After that, the mesenchymal stem cells (MSC) invade the granulation tissue and differentiate, driven by biological and mechanical factors, into different cell phenotypes. During the reparative phase, those cells formate fibrous tissue, cartilage or bone. Finally, the unnecessary areas of regenerated bone are resorbed during the remodelling phase [55].

Several computational models have tried to predict the secondary healing process from two points of view: mechanical and biological [40]. The mechano-regulated models relate the mechanical variables with the phenotype to which the cell would morph. For instance, the model proposed by Claes & Heigele [72] determines whether bone, cartilage or fibrous tissue will be formed based on the hydrostatic pressure and the strain. Differently, Lacroix & Prendergast developed a model based on the poroelastic behaviour of the tissues. In particular, shear strains and fluid velocity are the variables which control the differentiation process [197]. On the contrary, the bio-regulated models are controlled by biological factors such as precursor cells and growth factors, and some of them introduced processes as angiogenesis [26][114]. However, there are some models in the literature that combine both approaches such as the one developed by Andreikiv et al. [18]. Starting from the mechano-regulation theory proposed by Prendergast et al. [290], they included cells diffusion, proliferation and differentiation as well as tissue formation applied to a long bone callus.

Big efforts have been made to computationally simulate the healing process of different structures for the widely studied long bone callus [197][164], to mandibular symphyseal distraction [41] or lumbar vertebral fracture [40]. However, the fusion process, which takes place after lumbar surgery, has ussually been neglected, although the pattern of bone growth or the appearance of fibrotic tissue are key factors for surgery success or failure. Only one model was found in the literature that studied the development of lumbar fusion after different cages insertion in an asisymmetric mechano-regulated model [286][29].

With a long and distinguished history, the nucleotomy is considered a gold standard for the surgical treatment of disc herniation [225][285]. Although widely debated, up to now there is no consensus about the amount of nucleus tissue to be removed during surgery to find the ideal compromise between the beneficial relief of painful nerve root impingement and potential adverse effects like segmental instability that boost the degenerative cascade and thus the recurrence of pain [165]. The endplate between the vertebral body and the intervertebral disc is an important structure for the nutrition of the disc [143][354], which is also known to deform significantly under compressive loads [47]. It seems reasonable that abnormal deformation patterns following nucleotomy [99] may induce remodelling processes in the endplate and underlying trabecular bone, thus affecting nutrition pathways.

To avoid the progression of disc degeneration following nucleotomy dynamic stabilization systems were shown to be a promising tool [291]. However, different animal model studies have shown a recovery of segmental stability without the need of additional stabilizing instrumentation [79][347]. Rather, controlled instability (by allowing 2 mm of anterior-posterior segmental translations) was found to enhance bone formation in sheep [97]. Additionally, in humans, facetectomy is a part of noninstrumented posterolateral fusion approaches with equal postoperative patients'satisfaction compared to instrumented surgeries [287] and can result in stabilization in patients with proven degenerative spondylolisthesis [274]. Making use of the natural reparative capacities of the body would avoid implant-related complications with significant reductions of surgical time, blood loss etc. [247][345].

Intervertebral disc cages appeared in an attempt to supplement the dynamic stabilization increasing the stability of the segment and enhancing the bone formation. When they were used in a stand-alone fashion, the non-fusion rate was a source of disagreement, with varying rates from 5% to 40% depending on the use of additional fixation [13][223], cage material [254], cage design [175][332] and the type and amount of bone graft used [378][20].

Recent animal studies on sheep have shown a stiffening effect of spinal segments after destabilizing interventions like facetectomy and nucleotomy six month postoperatively [297]. With regard to nucleotomy, various hypotheses for the initiation of a remodelling cascade have been proposed: i) osteoblastic progenitor cell invasion due to the opening of the subchondral vascular network as a consequence of endplate damage, ii) the osteogenic transformation of residing cells within the nucleus pulposus due to degeneration by increased OPG levels and immunopositivity of Runx2, the presence of ALP activity and/ or iii) a progressive ossification of the peridiscal ligaments due to increased segmental motion with subsequent inflammation, fibrosis, calcification by significant up-regulation of angiopoietin-like protein 2 (Angptl2) and TGF- β [246][365].

The overall goal of this chapter was to describe comprehensively the mechanics of the lumbar functional spinal unit and to search for possible explanations that may trigger the bone formation. To this end, two different approaches have been developed:

- A **mechano-regulated model** based on the theory presented by Claes & Heigele [72] including vertebral **bone remodelling** according to the theory of Huiskes et al. [153]. With this model, the possibility of segmental fusion after nucleotomy, internal fixation, and anterior plate placement was investigated, as well as the role of disc height loss.
- A **bio-mechano-regulated model** based on the theory proposed by Prendergast et al. [290] adding the diffusion, proliferation, and differentiation of different cell's populations. The fusion after stand-alone cage placement was analysed with this model under different loading conditions.

6.2 Materials & Methods

6.2.1 Mechano-regulated model

6.2.1.1 Finite element model

Due to the high computational cost associated to the iterative process implemented in this Chapter and the complexity of the patient specific model, a finite element model of an intact L4-L5 ligamentous FSU was built based on anatomical landmarks instead of using the segmented geometry. The geometrical parameters were taken from [270] [268]. Since both, the anatomy and the loading conditions, were symmetrical with respect to the sagittal plane, only half of the structure was simulated. The model consists of distinct structural regions, namely cancellous bone, cortical bone, posterior bony elements, annulus fibrosus (AF), nucleus pulposus (NP), cartilaginous and bony endplates (EP) and seven major ligaments. Additionally, an anterior plate (AP) and an internal fixator (IF) were modelled to simulate two different stabilization scenarios after nucleotomy.

Except for the collagen fibres and ligaments, first-order hexahedral elements were used for the intact model. The annulus fibres, organized in concentric layers, and the spinal ligaments (anterior and posterior longitudinal ligaments, intertransverse, interspinous and supraspinous ligaments, capsular ligament and ligamentum flavum) were represented by membrane elements with rebar nonlinear properties. Twelve criss-cross annular fibre layers were considered in the radial direction where each layer contained nonlinear tension-only fibres. The fibre angles to the disc mid-height plane varied from ±45°at the innermost layer to ±30°at the outer periphery [144]. The articulating facet surfaces were modelled using frictionless surface-to-surface contacts. For the current study, the initial gap between the articulating surfaces was taken to be 0.2 mm. After mesh convergence studies, the model consists of 28.324 solid elements and 1.996 membrane elements with a total of 1.387.496 degrees of freedom (Fig. 6.1). The AP was modelled using 6 mm-thick shell elements while the posterior screws and rods were meshed with 5 mm-diameter beam elements.

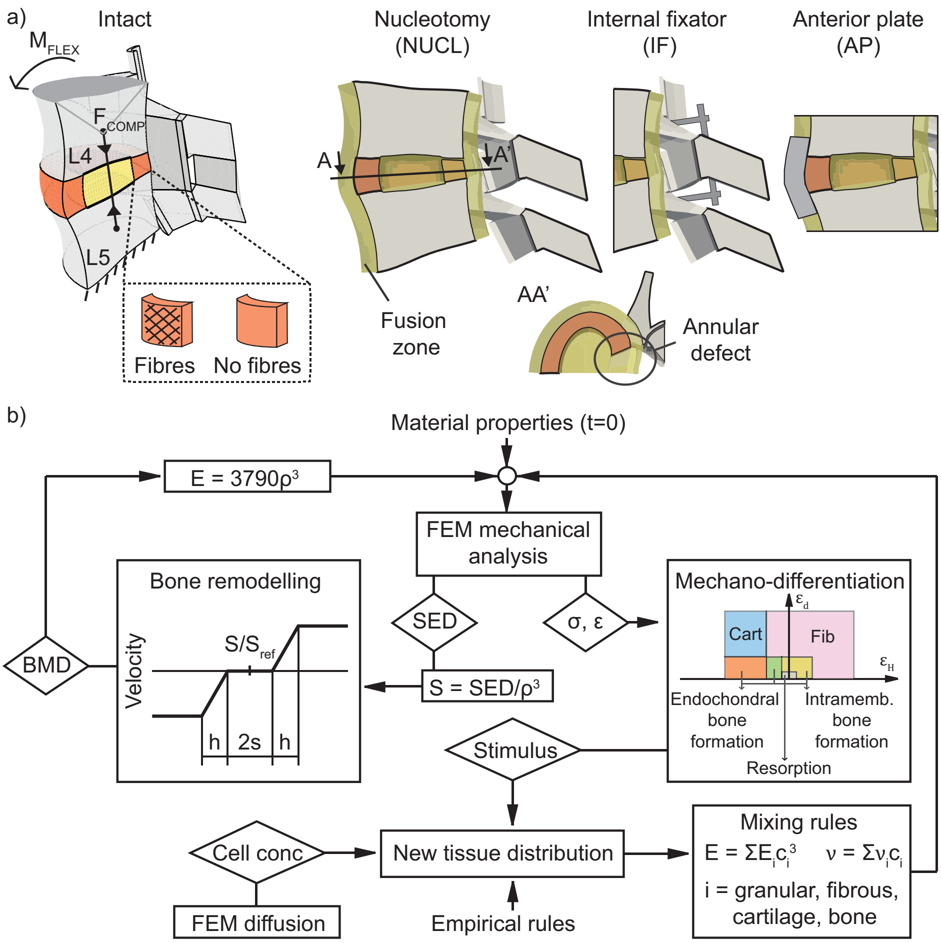

Figure 6.1: *Finite element model of the intact, nucleotomized and instrumented FSU (a). The fusion zone delimitates the region where new tissue can be formed. (b) Flow chart of the bone remodelling and tissue healing processes. The remodelling process and the mechano-differentiation algorithm are based on the works of Huiskes et al. [154] and Claes & Heigele [72], respectively.*

The annulus ground substance and the nucleus pulposus were modelled using Mooney-Rivlin hyperelastic material model (Eq. 6.1). The stress-strain behaviour of the annular fibres and ligaments were described by non-linear curves taken from previous elastostatic studies [315][314]. The material properties are summarized in Table 6.1.

$$W = C_1(\overline{I_1} - 3) + C_2(\overline{I_2} - 3) + D(J-1)^2 \tag{6.1}$$

Table 6.1: Material properties used for the different spinal structures, new formed tissues and implants in the healing model.

Materials	**E [MPa]**		ν	**Ref.**
Cortical bone	10,000		0.325	[22]
Cancellous bone	100		0.325	[22]
Posterior elements	3,500		0.325	[22]
Cartilaginous endplates	23		0.4	[214]
Facet cartilage	35		0.4	[317]
Titanium	100,000		0.33	[373]
	C_1	**C_2**	ν	**Ref**
Nucleus pulposus	0.12	0.09	0.499	[331]
Annular matrix	0.56	0.14	0.45	[118]
Annular fibres	*non-linear stress-strain curves*			[324]
Ligaments	*non-linear stress-strain curves*			[63][282]
Tissue healing	**E [MPa]**		ν	**Ref**
Granular tissue	0.2		0.167	[197]
Fibrous tissue	2		0.167	[197]
Cartilage	10		0.167	[197]
New bone	1,000		0.325	[197]

6.2.1.2 Bone remodelling algorithm

An adaptive bone remodelling algorithm [153] was implemented to regulate the bone mineral density (BMD) ρ of the vertebrae according to the strain energy density (SED) [53][243]. A cubic relationship between BMD and Young's modulus E was employed according to Carter and Hayes [54] (Eq. 6.2):

$$E = 3790\rho^3 \tag{6.2}$$

The SED divided by the cube of the BMD was used as the mechanical stimulus to avoid diverging solutions typical for stress-driven models. A piecewise-linear relationship between the stimulus and the rate of BMD change (Fig. 6.1b) was assumed (Eq.6.3):

$$\frac{\mathrm{d}BMD}{\mathrm{d}t} = \begin{cases} \triangle tC(1+s+h) & S^i \geq (1+s+h)S^{ref} \\ \triangle tC(S^i/S^{ref} - (1+s)) & (1+s+h)S^{ref} > S^i > (1+s)S^{ref} \\ 0 & (1+s)S^{ref} \geq S^i \geq (1-s)S^{ref} \\ \triangle tC(S^i/S^{ref} - (1-s)) & (1-s)S^{ref} > S^i > (1-s-h)S^{ref} \\ \triangle tC(1-s-h) & S^i \leq (1-s-h)S^{ref} \end{cases} \tag{6.3}$$

Where C is the slope of the remodelling rate, h is the width of the positive slope zones and *2s* the width of the “lazy zone”, in which bone structure stays unchanged and the rate of BMD change is likely limited by mechanical strength [52][32]. Here, C was set to 0.1 and the value of both h and s, was set to 0.15. The reference stimulus was computed as the average of the stimulus in the intact model. The simulations with the intact model started with a uniform BMD of 0.4g/cm^3 and run until an equilibrium density distribution was reached. Upper and lower limits of 1.6g/cm^3 and 0.1g/cm^3 were defined, beyond which no change in bone density was allowed.

6.2.1.3 Tissue healing algorithm

In the nucleotomized models, the space left by the removed tissue (nucleus, cartilage endplates and annular defect) as well as a 5-mm-thick area around the segment were assumed eligible for new tissue formation. Except for the remaining annulus tissue, fully vascularized granulation tissue was assumed to initially occupy these regions. Precursor cells migration from the bone marrow into the granulation tissue was modelled as a diffusive process (Eq. 6.4).

$$\frac{\mathrm{d}n}{\mathrm{d}t} = D\nabla^2 n \tag{6.4}$$

where the cell density n is determined from the diffusion coefficient D, which was specifically chosen as D=0.8mm/iteration for the granulation tissue and as D=0.2mm/iteration for the remaining annulus [177]. The cell origin was modelled as a constant concentration at the center of the vertebral endplates, whereas the maximal cell density was normalized to 1.

In each iteration, the mechanical stimuli (distortional equivalent strain ε_d and hydrostatic strain ε_H, equations (6.5), (6.6)) were calculated according to the adapted mechano-regulation theory proposed by Claes and Heigele [72]:

$$\varepsilon_d = \frac{2}{3}\sqrt{[(\varepsilon_1-\varepsilon_2)^2+(\varepsilon_2-\varepsilon_3)^2+(\varepsilon_1-\varepsilon_3)^2]} \tag{6.5}$$

$$\varepsilon_H = \frac{1}{3} trace(\epsilon) \tag{6.6}$$

where ε_1,ε_2 and ε_3 are principal strains and ϵ is the strain tensor. The threshold values of $\pm1\%$ for hydrostatic strain and 5% for equivalent strain were used for bone formation. The resorption limits were set to 0.1% and 1% for hydrostatic strain and for equivalent strain, respectively [286]. Additional empirical rules defined by Shefelbine et al. [323] were added to complement the model. i.e., hydrostatic strains higher than 5% or equivalent strains beyond 15% were considered to cause tissue destruction morphing any tissue into granular tissue and a differentiation was made between intramembranous and endochondral bone formation as indicated in Figure 6.1b. Based on the mechanical stimulus the precursor cells could differentiate into fibroblasts, chondrocytes, and osteoblasts and produce their respective tissue phenotypes. At the same time, cartilage could also turn into bone during endochondral ossification and fibrous tissue could morph into cartilage. The differentiation rates are 0.1 it^{-1}, 0.1 it^{-1} and 0.2 it^{-1} for the precursor cells, chondroblast and, fibroblast, respectively, while the resorption rate was 0.05 it^{-1}, adjusted from [163] to avoid instabilities.

The Young's modulus was calculated depending on the volumetric fractions of the tissues, according to [53] (Eq. 6.7):

$$E = E_{gran}c_{gran}^3 + E_{fib}c_{fib}^3 + E_{cart}c_{cart}^3 + E_{bone}c_{bone}^3 \tag{6.7}$$

where c_{gran}, c_{fib}, c_{cart}, and c_{bone} are the volumetric fractions of granular tissue, fibrous tissue, cartilage, and bone, respectively, in an element. Poisson's ratio ν was calculated as follows [323] (Eq. 6.8):

$$\nu = \nu_{gran}c_{gran} + \nu_{fib}c_{fib} + \nu_{cart}c_{cart} + \nu_{bone}c_{bone} \tag{6.8}$$

with $c_{gran} + c_{fib} + c_{cart} + c_{bone} = 1$. It was assumed that new bone formation only occurs on the surfaces of extant bone (in the initial fusion phase at the vertebral surface), similar to the fracture healing processes [72][350][311]. Therefore, bone apposition was allowed when the concentration of bone in a neighbouring element was above 25%.

6.2.1.4 Boundary and loading conditions

An iterative procedure (Fig. 6.1b) was implemented to model bone remodelling and tissue healing processes in a lumbar FSU. The load was applied in two steps: first axial compression of 500N was applied as a follower load; then, flexion moment of 7.5Nm was added in the following step. The stimulus was calculated as the weighted average of the results considering 75% of pure compression and 25% compression plus flexion. To investigate the role of annular fibres, the bone remodelling simulation of the intact segment was run with and without fibres. After BMD reached the equilibrium, the entire NP and cartilaginous EP were removed, a 1cm-wide defect was created in the posterior portion of the AF and an external region for possible osteophyte formation was added. Consequently, the disc height was reduced to 75 and 50% of the initial height to mimic the disc height loss caused by material removal. In additional simulations, the models were supplied with either AP or IF to study the effects of these devices in the healing process. The described algorithms were implemented in python and the simulations were run in ABAQUS 6.13 (SIMULIA, Providence, RI, USA).

6.2.2 Bio-Mechano-regulated model

To simulate the bio-mechano-regulated healing process, an iterative process was implemented with two separate analyses in each iteration: a mechanical analysis to calculate the mechanical stimulus; and a diffusion-differentiation model to compute the evolution of cell's concentration. Both analysis were solved using the FE method. A user defined code was used to manage the data exchange between both analyses in each iteration, which represented one day. The flow-chart outlined in Figure 6.2a shows the implementation of the model. At the beginning, all the gap was assumed to be filled with granular tissue. After the mechanical simulation, the mechanical stimulus was calculated and used as an input for the diffusion-differentiation model. An initial condition of MSC saturation in the endplates was set during the first seven days. Once the cell concentrations and tissue fractions were updated, the material properties used in the granular tissue were recalculated according to the rules of mixtures. The models are explained in detail below.

6.2.2.1 Finite element model

The 3D finite element models were built using linear hexahedral elements with a couple pore-displacement formulation in Abaqus6.13 (SIMULIA, Providence, RI, USA).

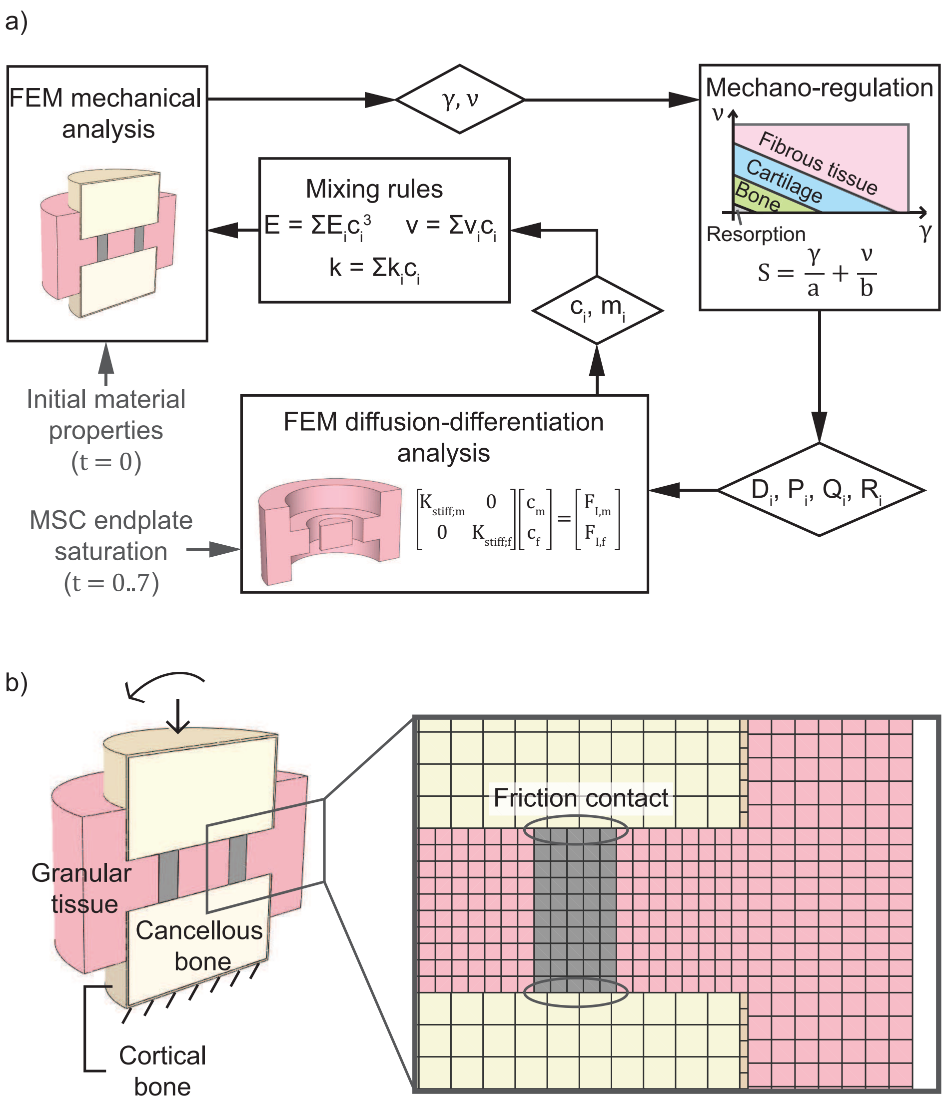

__Figure 6.2:__ a) Flow chart of the bio-mechano-regulated tissue healing model based on the study of Prendergast et al. [290]. The biological and mechanical parameters were calculated for i=granular, fibrous, cartilage and bone precursor cells (c) and mass fractions (m). b) Finite element model of the FSU used for the mechanical analysis. Only the granular tissue was used in the diffusion-differentiation analysis.

The FE model (Fig 6.2b) consisted on two vertebrae modelled according with the average geometry of a L4-L5 segment [270], an intervertebral cage laying at the center of the space and the region defined for possible tissue formation. Each vertebra was considered to be formed by an outer layer of cortical bone and an inner core of cancellous bone. The bony endplates, as well as all the IVD (nucleus, annulus and cartilage endplates), were removed before the insertion of the PEEK stand-alone cage. The intervertebral disc space and an additional area around were assumed to be filled with granular tissue and, therefore, eligible for tissue formation. All the tissues were characterized as poro-elastic materials with the properties summarised in Table 6.2. The properties (elastic modulus, Poisson's coefficient and permeability) of each element of this region were updated in each iteration according to the rules of mixtures (Eq. 6.7, 6.8 and 6.9).

$$k = k_{gran}c_{gran} + k_{fib}c_{fib} + k_{cart}c_{cart} + k_{bone}c_{bone} \tag{6.9}$$

Symmetry boundary conditions were applied at the mid-sagittal plane while the bottom surface of the vertebra was constrained. The healing process was simulated for two different loading conditions: an axial load of 500N applied on the upper part of the vertebra in 0.5s and a 10Nm rotation combined with 500N axial preload. All the parts were assumed to be tied but at the bone-cage interface, where a surface-to-surface contact with a friction coefficient of 0.5 was defined. Additionally, the fluid flow at the cage/granular and bone/cage interfaces was not allowed.

Table 6.2: Poroelastic mechanical properties characterizing the tissues in the bio-mechano-regulated model [332][197][29][72][290].

	E [MPa]	v	k [m4/Ns]	Porosity
Cortical bone	15,750	0.325	1e-17	0.8
Cancellous bone	400	0.325	1e-14	0.04
Granular tissue (gran)	0.4	0.167	1e-14	0.8
Fibrous tissue (fib)	2	0.167	1e-14	0.8
Cartilage (cart)	10	0.167	5e-15	0.8
New bone (bone)	6,000	0.325	3.7e-13	0.8
PEEK	3,600	0.4	-	-

6.2.2.2 Tissue healing algorithm

When secondary healing process takes place the cells migrate and differentiate depending on the local mechanical and biological environment. In this model, the relationship between mechanical stimulus and cell differentiation defined by Prendergast et al. [290] was used. Therefore, the mechanical stimulus was defined by the octahedral shear strain (γ) (Eq. 6.10) and the relative fluid/solid velocity (v) as defined by Equation 6.11.

$$\gamma = \frac{2}{3}\sqrt{\left[(\varepsilon_1-\varepsilon_2)^2+(\varepsilon_2-\varepsilon_3)^2+(\varepsilon_1-\varepsilon_3)^2+6\left(\left(\frac{\varepsilon_{12}}{2}\right)^2+\left(\frac{\varepsilon_{23}}{2}\right)^2+\left(\frac{\varepsilon_{13}}{2}\right)^2\right)\right]} \tag{6.10}$$

$$S = \frac{\gamma}{a}+\frac{v}{b} \tag{6.11}$$

where *a=0.0375* and *b=3μm/s* [152]. According to the model, a low stimulus ($S < S_{min}$) would promote bone tissue formation, a medium stimulus ($S_{min} < S < S_{max}$) would stimulate cartilage formation and a high stimulus ($S > S_{max}$) would benefit fibrous tissue formation. With the thresholds S_{min} and S_{max} equal to 1 and 3 respectively. Additionally, a resorption limit ($S_{resorp} = 0.01$) was set to avoid bone formation when the mechanical stimulus was not enough to stimulate tissue production [164]. For the differentiation analysis, only the region initially filled with granular tissue was considered eligible for tissue formation. The MSC migrated from the endplates into the region depending on the tissue composition. A bone border condition, similar to that explained for the mechano-regulated model was included to force bone apposition in the surrounding of extant bone.

Similar to the model presented by Andreykiv et al. [18], the concentration of MSC and fibroblast were considered as the degrees of freedom in each integration point giving a total of 16 degrees of freedom in each element. Both cell phenotypes were able to diffuse, proliferate and differentiate. In the case of MSC, they could morph into fibroblast, chondroblast and osteoblast (Eq. 6.12). Meanwhile, fibrous progenitor cells could differentiate into cartilage or bone forming cells and apart from diffusion and proliferation their density increase because of differentiation from MSC (Eq. 6.13).

$$\frac{\mathrm{d}c_m}{\mathrm{d}t} = D_m\nabla^2 c_m + P_m(1-c_{tot})c_m - F_f(1-c_f)c_m - F_c(1-c_c)c_m - F_b(1-c_b)c_m \tag{6.12}$$

$$\frac{\mathrm{d}c_f}{\mathrm{d}t} = D_f\nabla^2 c_f + P_f(1-c_{tot})c_f + F_f(1-c_f)c_m - F_c(1-c_c)c_f - F_b(1-c_b)c_f \tag{6.13}$$

Where c_m and c_f represent the concentration of MSC and fibroblasts, respectively. The diffusion coefficients (D_i) and proliferation rates (P_i) were assumed to vary with the tissue composition at each time point as $D_i = D_{i,0}(1 - m_c - m_b)$ and $P_i = P_{i,0}(1 - m_c - m_b)$ being $i = m \; and \; b$, respectively.

In turn, chondroblasts and osteoblasts were not considered to diffuse, so they were calculated as explicit parameters in accordance with Eq. 6.14 and 6.15.

$$\frac{\mathrm{d}c_c}{\mathrm{d}t} = P_c(1 - c_{tot})c_c + F_c(1 - c_c)(c_m + c_f) - F_b(1 - c_b)c_c \tag{6.14}$$

$$\frac{\mathrm{d}c_b}{\mathrm{d}t} = P_b(1 - c_{tot})c_b + F_b(1 - c_c)(c_m + c_f + c_c) \tag{6.15}$$

With c_c and c_b the concentration of chondroblasts and osteoblasts, respectively.

On the other hand, the tissue fractions were determined as a function of the cell densities and the tissue fractions in the previous iteration as defined by Eq. 6.16, 6.17 and 6.18.

$$\frac{\mathrm{d}m_b}{\mathrm{d}t} = Q_b(1 - m_b)c_b \tag{6.16}$$

$$\frac{\mathrm{d}m_c}{\mathrm{d}t} = Q_c(1 - m_b - m_c)c_c - R_b c_b m_c m_{tot} \tag{6.17}$$

$$\frac{\mathrm{d}m_f}{\mathrm{d}t} = Q_f(1 - m_{tot})c_f - (R_b c_b + R_c c_c)m_f m_{tot} \tag{6.18}$$

Where $m_{tot} = m_f + m_c + m_b$ and the granulation tissue fraction was calculated as $m_g = 1 - m_{tot}$. The parameters used to characterize the model are summarized in Table 6.3.

Table 6.3: Cell's diffusion, proliferation and differentiation coefficients and tissue production and resorption rates to characterize the bio-mechano-regulated healing model. The non-stimulated (N-S) value refers to the value that takes the parameter when the mechanical stimulus is under the threshold of each specific cell phenotype.[1] [127]; [2] [26]; [3] [327]; [4] [239]; [5] [382] [374]; [6] [18]

	MSC	Fibroblast	Chondroblast	Osteoblast
Diffusion coef. $D_{i,0}$ [mm^2/day]	0.3456[1]	0.1152[2]	-	-
Proliferation rate $P_{i,0}$ [day^{-1}]	1.2 (N-S)[3] 0.5[3]	0.1 (N-S)[4] 0.6[4]	0.75 (N-S)[5] 0.925[5]	0.75[6]
Differentiation rate F_i [day^{-1}]	-	0.01[6]	0.3[6]	0.15[6]
Production rate Q_i [day^{-1}]	-	0.06[6]	0.2[6]	0.1[6]
Resorption rate R_i [day^{-1}]	-	-	0.2[6]	0.1[6]

The diffusion-differentiation algorithm presented above was implemented in an Abaqus user subroutine (UEL) defining a linear hexahedral element with eight integration points.

According with the weak formulation, the Eq. 6.12 and 6.13 were multiplied by an arbitrary function (w_m and w_f respectively) and integrated over the whole domain (Eq. 6.19 and 6.20).

$$\begin{aligned}\int \mathbf{w}_m^T \Bigg[\frac{\mathrm{d}c_m}{\mathrm{d}t} - D_m \nabla^2 c_m - P_m(1-c_{tot})c_m \\ + F_f(1-c_f)c_m + F_c(1-c_c)c_m + F_b(1-c_b)c_m \Bigg] \mathrm{d}\Omega = 0\end{aligned} \tag{6.19}$$

$$\begin{aligned}\int \mathbf{w}_f^T \Bigg[\frac{\mathrm{d}c_f}{\mathrm{d}t} - D_f \nabla^2 c_f - P_f(1-c_{tot})c_f \\ - F_f(1-c_f)c_m + F_c(1-c_c)c_f + F_b(1-c_b)c_f \Bigg] \mathrm{d}\Omega = 0\end{aligned} \tag{6.20}$$

The degrees of freedom were approximated by multiplying the nodal values by the shape functions (Eq. 6.21) an the divergence operator eliminated applying Green's theorem (Eq. 6.22). Besides, the time derivatives were discretized with finite differences and in each equation a variable was solved implicitly (Eq. 6.23)

$$N_i = \frac{1}{8}(1 \pm \xi_0 \xi)(1 \pm \eta_0 \eta)(1 \pm \mu_0 \mu) \qquad i = 1..8 \tag{6.21}$$

$$\int_\Omega w \overline{\nabla} \overline{q} \mathrm{d}\Omega = \oint_\Gamma \overline{qn} \mathrm{d}\Gamma - \int_\Omega \overline{\nabla} w \overline{q} \mathrm{d}\Omega \tag{6.22}$$

$$\frac{\mathrm{d}c_i}{\mathrm{d}t} = \frac{\triangle c_i}{\triangle t} = \frac{(c_{i,n+1} - c_{i,n})}{\triangle t} \tag{6.23}$$

Obtaining (Eq. 6.24 and 6.25):

$$\begin{aligned} &\mathbf{C}\frac{(\mathbf{c}_{\mathbf{m},n+1} - \mathbf{c}_{\mathbf{m},n})}{\triangle t} + \mathbf{K_m}\mathbf{c}_{\mathbf{m},n+1} \\ &- \left[P_m(1 - c_{c,n} - c_{b,n}) - F_f - F_c(1 - c_{c,n}) - F_b(1 - c_{b,n})\right]\mathbf{C}\mathbf{c}_{\mathbf{m},n+1} \\ &+ (P_m - F_f)\mathbf{p_{mix}}(\mathbf{c}_{\mathbf{m},n+1}, \mathbf{c}_{\mathbf{f},n}) + P_m \mathbf{p_n}(\mathbf{c}_{\mathbf{m},n+1}) = 0 \end{aligned} \tag{6.24}$$

$$\begin{aligned} &\mathbf{C}\frac{(\mathbf{c}_{\mathbf{f},n+1} - c_{f,n})}{\triangle t} + \mathbf{K_f}\mathbf{c}_{\mathbf{f},n+1} \\ &- \left[P_f(1 - c_{c,n} - c_{b,n}) - F_c(1 - c_{c,n}) - F_b(1 - c_{b,n})\right]\mathbf{C}\mathbf{c}_{\mathbf{f},n+1} \\ &+ F_f \mathbf{C}\mathbf{c}_{\mathbf{m},n} + (P_f + F_f)\mathbf{p_{mix}}(\mathbf{c}_{\mathbf{m},n}, \mathbf{c}_{\mathbf{f},n+1}) + P_f \mathbf{p_n}(\mathbf{c}_{\mathbf{f},n+1}) = 0 \end{aligned} \tag{6.25}$$

With:

$$\mathbf{C} = \int_{V_{el}} \mathbf{N}^T \mathbf{N} \, \mathrm{d}V_{el} \tag{6.26}$$

$$\mathbf{K_i} = \int_{V_{el}} \nabla \mathbf{N}^T D_i \mathbf{N} \, \mathrm{d}V_{el} \qquad i = m, f \tag{6.27}$$

$$\mathbf{p_n} = \int_{V_{el}} \mathbf{N}^T (\mathbf{c_i}\mathbf{N})^2 \, \mathrm{d}V_{el} \qquad i = m, f \tag{6.28}$$

$$\mathbf{p_{mix}} = \int_{V_{el}} \mathbf{N}^T (\mathbf{c_m N})(\mathbf{c_f N}) \, \mathrm{d}V_{el} \tag{6.29}$$

Finally, the non-linear terms ($\mathbf{p_n}$ and $\mathbf{p_{mix}}$) were linearized. The resultant finite element formulation of the problem is shown in Eq. 6.30

$$\begin{bmatrix} \mathbf{K_{stiff;m}} & 0 \\ 0 & \mathbf{K_{stiff;f}} \end{bmatrix} \begin{bmatrix} \mathbf{c_{m,n+1}} \\ \mathbf{c_{f,n+1}} \end{bmatrix} = \begin{bmatrix} \mathbf{F_{I;m}} \\ \mathbf{F_{I;f}} \end{bmatrix} \tag{6.30}$$

Where $\mathbf{K_{stiff;m}}$ and $\mathbf{K_{stiff;f}}$ were introduced in the stiffness matrix (**AMATRX**) and the residual vector **(RHS)** was defined as the difference between the external force vector and the internal force vector evaluated at the current iteration as defined by Eq. 6.31

$$\mathbf{RHS} = \mathbf{F_{I;i}} - \mathbf{K_{stiff;i} U_i} \tag{6.31}$$

6.3 Results

6.3.1 Mechano-regulated model

6.3.1.1 Bone remodelling of the intact segment

The remodelling process started with a uniform increase of BMD in the whole vertebral body. Progressively, dense cortical shells and endplates formed around a softer inner core (Fig 6.3). In the last stages, bone resorption occurred in the anterior and posterior portions of the cancellous bone close to the endplates of the adjacent segments. After 100 iterations the equilibrium had been reached in the intact models with and without fibres. Although in some areas of the cortical shell and the endplates the stimulus remained high (Fig 6.3a), the maximum BMD had been already reached in those regions and no further density change was possible (Fig 6.3b). Removal of the fibres shifted the load sharing in the disc towards the annulus from 43.8% to 49.6%. Accordingly, the BMD decreased in the middle region and increased in the periphery except in the posterior part of the top vertebra, where a decreased was seen (Fig 6.3c). However, the variation of the median values was less than 3% in the intact model and the difference was even lower after nucleotomy. Since the fibres showed only minor influence in the intact and nucleotomy models, in the following only results from the models with fibres are shown.

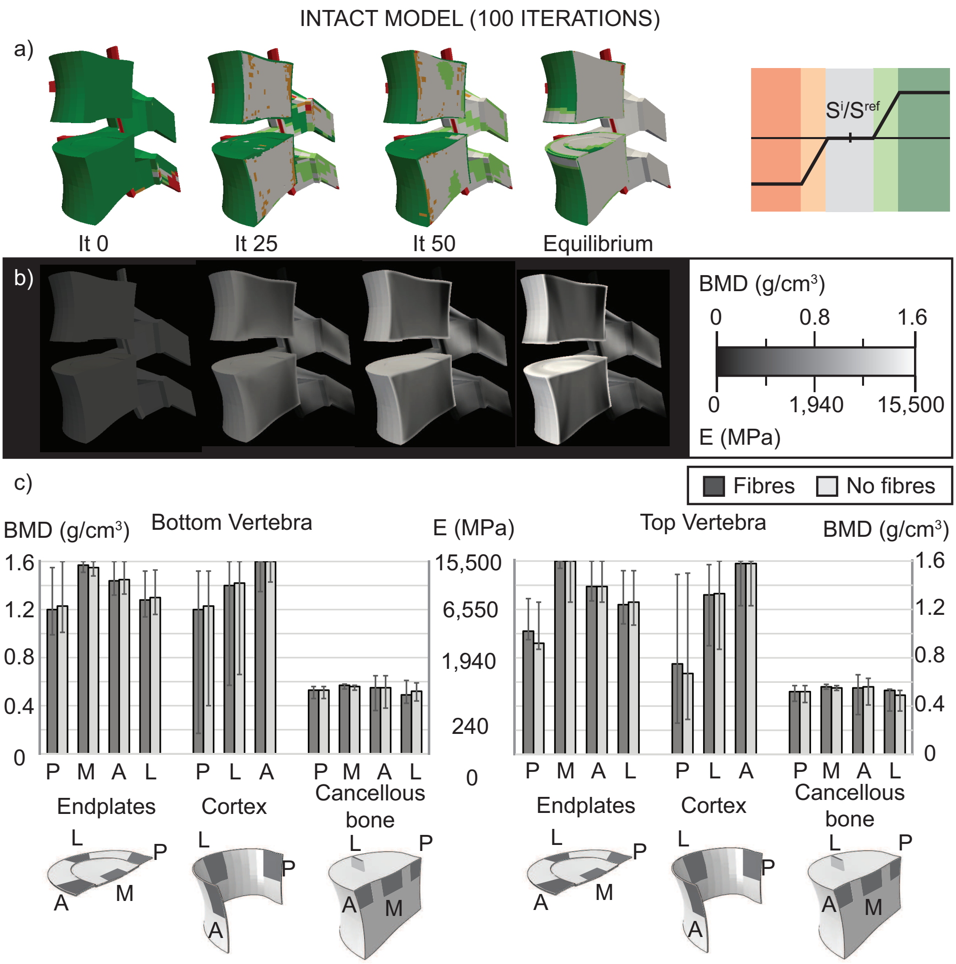

__Figure 6.3:__ Distribution of the mechanical stimulus (a) which drives the BMD change (b) during the bone remodelling process of the intact segment with fibres. (c) BMD in different regions of the endplates, cortex and cancellous bone (P-posterior; M-middle; A-anterior; L-lateral) with and without fibres. Median and range values are shown.

6.3.1.2 Tissue healing after nucleotomy with and without stabilization.

New bone formation, as well as BMD distributions in the vertebrae, showed different patterns for each investigated case (Fig. 6.4). When retaining the initial disc height (100% DH) in the nucleotomy without instrumentation and with IF, both models failed to converge after 15 iterations due to excessive distortion of the anterior annulus elements. On the contrary, AP produced solid bone within the annular defect, which resulted in unloading of the facets and reduction of BMD in the pedicles. With increasing DH loss, a gradual increase of BMD in the pedicles was predicted indicating higher facet loads. In turn, while AP resulted in a higher bone density posteriorly, IF predicted higher BMD anteriorly. A simple nucleotomy showed little differences to IF. With 50% DH reduction, marked anterior and posterior osteophyte formations were predicted in both NUCL and IF while a layer of cartilage and fibrous tissue remained in the mid-height disc region. The models with AP did not show any signs of osteophytes.

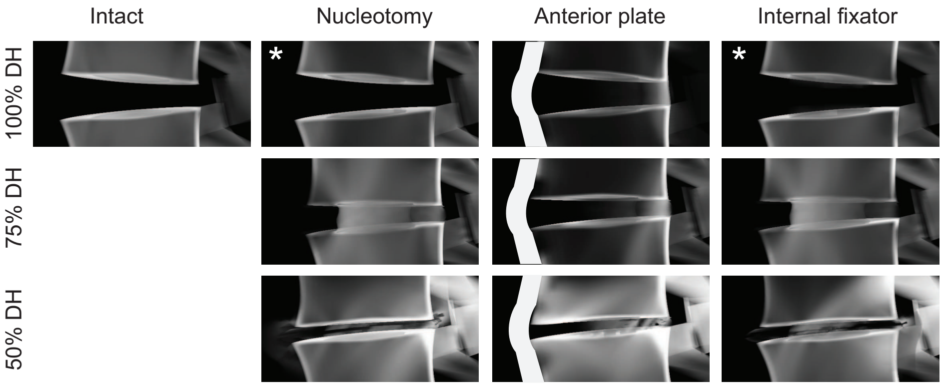

Figure 6.4: *Bone mineral density images of the intact FSU and after equilibrium (no further changes in either vertebrae BMD nor new tissue formation) for each treatment and disc height reduction. ∗Simulation failed due to excessive distortion resulted from the loss of stiffness.*

The tissue composition at the end of each simulation was analysed in different regions of interests (RoI) (Fig. 6.5). These were defined to cover the anterior portion of the intact AF, the annular defect in the posterior region, the space left by the NP and endplates, and the area around the segment.

Considering the intact disc height after nucleotomy, annular tissue destruction was predicted anteriorly due to high strains without instrumentation and with IF. By reducing the disc height to a 75%, bone fusion occurred in the posterior and central parts of the intervertebral space (RoIs II and III), with bone volume fractions between 40 and 50%. Adding anterior instrumentation the mechanical stimulus was highly reduced promoting intramembranous ossification in the posterior part of the annulus (RoI II).

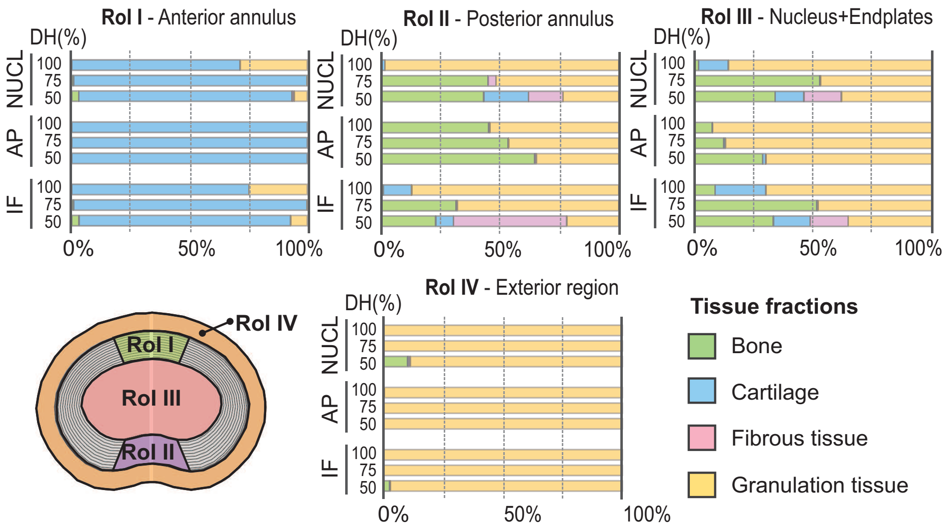

Figure 6.5: *Tissue distribution in each RoI after reaching the equilibrium in each simulated scenario. The posterior annulus corresponds to the annular defect. The values were calculated as percentage of the total volume of each RoI. Bone existing in RoI IV indicates osteophyte formation.*

Figure 6.6 illustrates the healing process for the NUCL model with 75% DH. The mechanical stimulus (1st row) determined the tissue phenotype that could potentially be formed in each element in each iteration, however, the progenitor cells diffusion (2nd row) limited the tissue formation in the initial stage of the process. In turn the vascularization, which was kept constant throughout the simulation in the granular tissue and the outermost layer of the annulus (3rd row) and the bone neighbour condition (4th row), which was activated when bony tissue filled 25% of element volume, were necessary for bone formation. In this case, cartilage was formed in the spaced left by the resected tissue and then it was replaced by new bone through an endochondral ossification process which started in the vertebral endplates and progressed towards the mid-height disc section until fused the segment. No bone formation occurred in the remaining annulus due to the lack of vascularization.

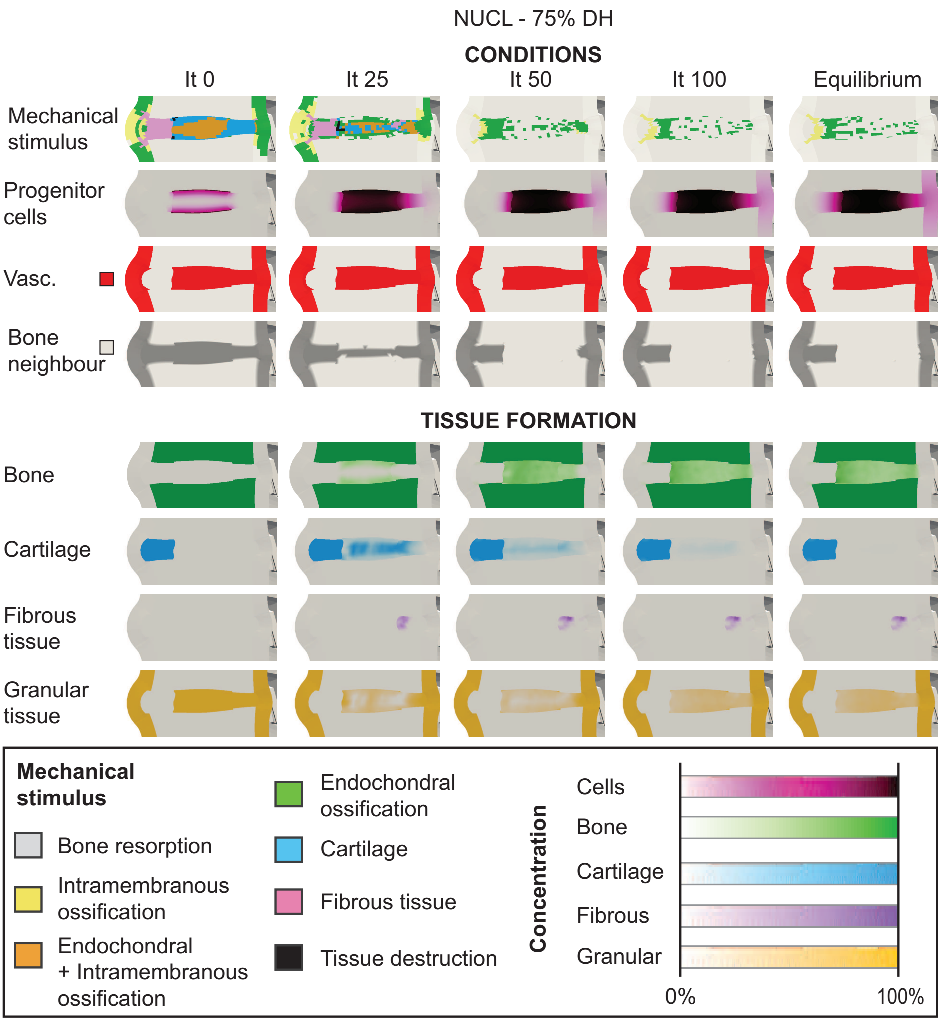

Figure 6.6: *Tissue healing evolution in the model with nucleotomy and 75% DH. When all conditions for a tissue phenotype were met in an element, this tissue was formed proportional to the amount of precursor cells available.*

Immediately after nucleotomy, the mechanical environment of the segment changed determining the progression of tissue healing (Fig 6.7). Tissue destruction due to excessive strains led to a progressive increase in the flexibility for NUCL and IF models with the intact disc height (Fig. 6.7) and, consequently, to a failure of both models.

However, the reduction in disc height resulted in increased stiffness of the FSU, which developed further with tissue formation in all models. For NUCL, axial displacement initially increased to ~130% for 75% DH and gradually decreased to ~18% as the process progressed. Segmental rotation decreased initially to ~70% and further to ~13% of the intact value. Placing an IF for 75% DH both axial displacement and segmental rotation decreased after the surgery and were reduced down to 13 and 9% once the tissue healed. For the models with 50% DH the axial and rotational stiffness stayed nearly constant throughout the simulation as a result of predicted non-union. On the other hand, AP resulted in stabilisation of the FSU under all DH conditions with resulting axial displacement and segmental rotation below 10% of the intact values for 100 and 75% DH and 3% for 50% DH.

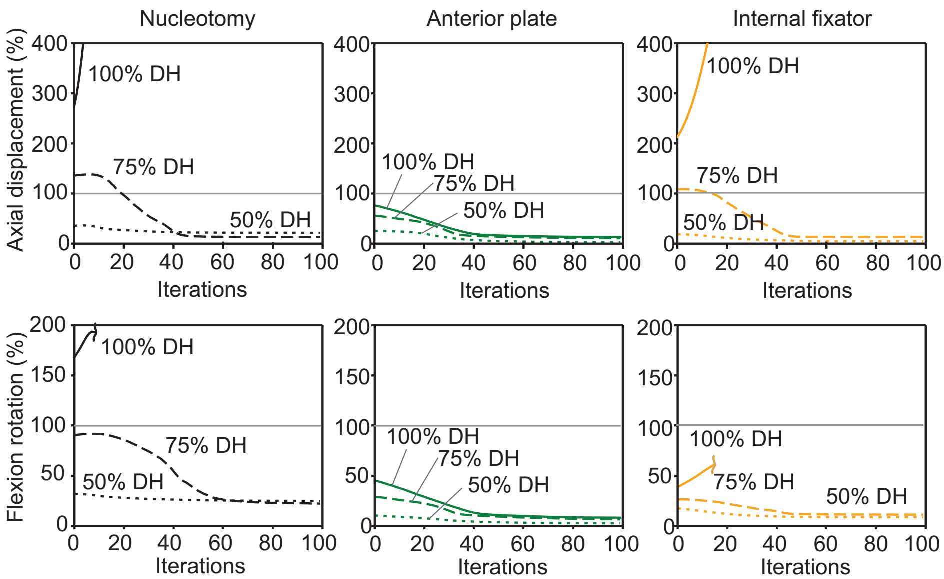

Figure 6.7: Temporal evolution of axial displacement under compressive load and rotation under flexion moment with respect to the corresponding ranges of motion of the intact segment.

6.3.1.3 Bone remodelling after surgery

The models predicted the BMD adaptation within the vertebrae according to the altered mechanical environment to favour the force flow through the FSU (Fig. 6.4). In general, the BMD increased in the areas above and underneath the bone bridge and decreased in the regions where no bone formation was predicted. As such, application of the AP resulted in bone resorption anteriorly and increased BMD posteriorly (Fig.

6.8a). The changes were not symmetrical about the disc mid-plane. So, AP resulted in a decrease in BMD in the central part of the lower endplate, but in an increased BMD in the central part of the upper endplate. For 50% DH most of the models predicted maximal BMD in all endplate regions. Only the IF predicted lower BMD in both endplates anteriorly for 50 and 75% DH. On the other hand, the endplates deformation decreased in the regions where the tissue was resected (NP and Post AF) (Fig 6.8b) and increased in the anterior portion of the annulus just after nucleotomy. The adaptive response of the bony endplates tried to restore the intact deformation state. However, the formation of osteophytes provoked deflection of the cranial endplate in the model with 50% disc height leading to denser endplates.

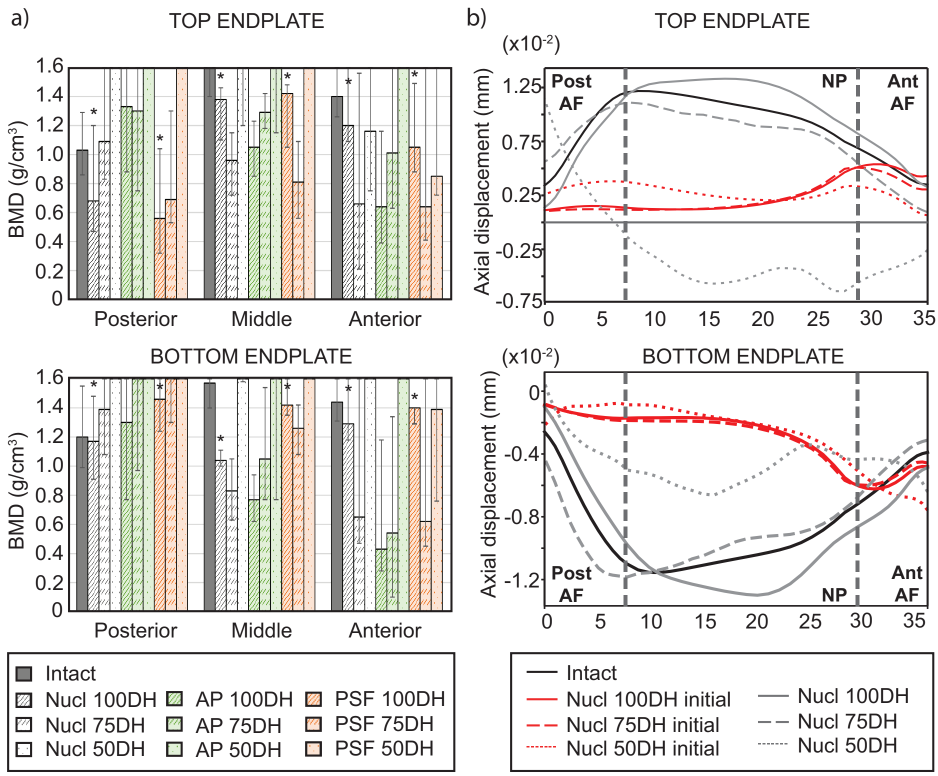

Figure 6.8: *(a) BMD in different regions of the top and bottom endplates (EP) at the end of tissue healing. Median and ranges values are shown. ∗Simulation failed due to excessive distortion resulted from the loss of stiffness, therefore the corresponding values are not representative. (b) Axial displacement profiles in the mid-sagital plane for the nucleotomy models just after the surgery and after the healing process.*

6.3.2 Bio-Mechano-regulated model

New tissue formation occurred in a different manner depending on the loading protocol (Fig. 6.9). When a cage is placed in a stand-alone fashion, some flexion rotation may take place in addition to pure compression. Bone grew uniformly from the vertebral endplates towards the mid-height disc plane when only pure compression was considered reaching a solid bone bridge in the circumferential part of the space. By contrast, adding flexion movement, the pattern of bone growth changed considerably. It started to grow inside the cage and then it extended radially creating osteophytes bigger in the anterior than in the posterior part.

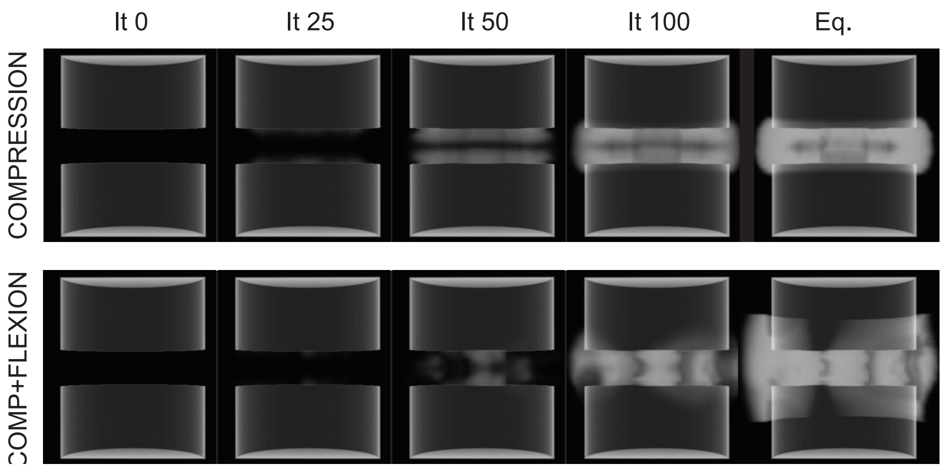

Figure 6.9: *Bone mineral density images of the fusion process after cage insertion with the bio-mechano-regulated model. The anterior part corresponds to the left side of the images.*

The tissue composition at the end of each simulation was analysed in different RoI (Fig 6.10). These were defined to cover the region inside the cage, the anterior, posterior and lateral part of the annular region and the area around the segment.

In agreement to what was shown in the X-ray images, a solid and uniform bone bridge was formed in all the annular region with 90% of the volume filled with new bone. However, only 70% of the region inside the cage was ossified. Neither cartilage nor fibrous tissue formation was predicted when pure compression was applied. On the other hand, when flexion was added, bone apposition was more pronounced in the anterior part (98% of the volume), while the posterior part was formed by a mixture of bone (64%), cartilage (19%) and granular tissue (17%). Furthermore, almost 50%

of the exterior region was composed by new bone, which reflects the big osteophyte formation predicted.

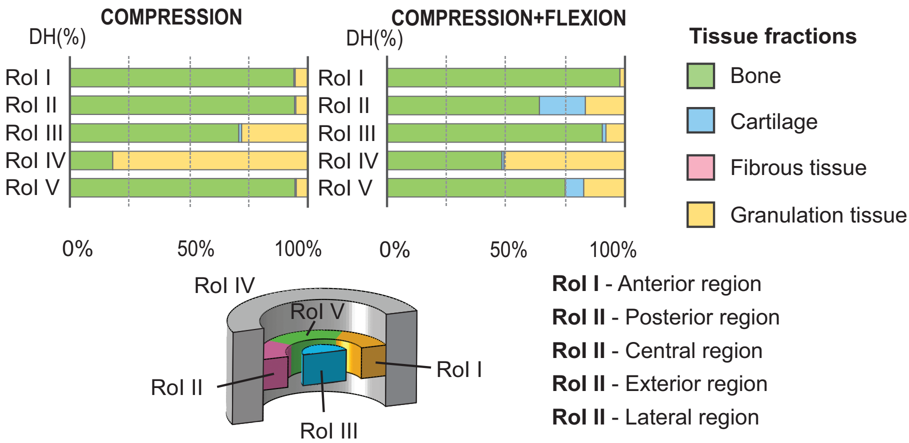

Figure 6.10: *Tissue distribution in each RoI after reaching the equilibrium under different loading conditions with the bio-mechano-regulated model. The values were calculated as percentage of the total volume of each RoI. Bone existing in RoI I indicates osteophyte formation.*

Figure 6.11 ilustrates the healing process after stand-alone cage insertion considering a compression and flexion as athe loading protocol. The mechanical stimulus (1st row) determined the proliferation and differentiation rates of the different cell phenotypes. In turn, the bone neighbour condition (2nd row) limited the elements in which new bone could be formed depending on the surrounding elements composition. In this case, MSC diffused from the vertebral endplates filling all the region during the first 25 iterations and then morphed into different cell types. Bone forming cells were also distributed throughout the entire region, however new bone formation was limited by the bone neighbour condition. Cartilage was firstly developed in the posterior region and, further on, an endochondral ossification turned it into bone.

Figure 6.11: *Tissue healing in the bio-mechano-regulated model under flexion+compression. The mechanical stimulus conditioned the differentiation of the cells which, together with the bone neighbour condition, determined tissue formation. The anterior part corresponds to the left side of the images.*

6.4 Discussion

The self-repairing ability of the tissue is a key factor to achieve a stable bony fusion of a lumbar segment. The conditions which may trigger this healing from a mechanical point of view has been analysed together with the effect that each surgery has on the vertebral bone density. An excessive ROM has shown to lead to tissue destruction and segment instability. Conversely, a lack of strains prevented from tissue formation. Bone bridging promotion was shown to be possible by changing the mechanical scenario adding instrumentation and/or decreasing the disc height.

The adaptive bone remodelling of the intact segment predicted denser bone in the anterior than in the posterior part of the vertebrae in agreement with previous FE studies [126] and medical image observations [19][325]. However, contrary to previous findings, a higher BMD appeared at the central region of the endplates than at the periphery, which may be explained by the imposed lower thickness of the central endplate. Furthermore, the loading conditions, which were chosen to represent the average daily load, influenced the bone density distribution.

On the other hand, small influence (less than 3%) of the annular fibres in the bone density distribution was seen in the intact model and it was even lower after nucleotomy. Therefore, the hypothesis stated by Reitmaier et al. [297], that the bone bridging could be initiated by chronic inflammation due to increased segmental motion and microtrauma in the AF and peridiscal ligaments could not be proven with the current model. The inclusion of biological events such as possible fibrosis and calcification of the ligaments may help to shed light on this particular issue.

Progenitor cell invasion due to the opening of the subchondral vascular network as a consequence of endplate damage shown to be a possible trigger for bone bridging. So, as was seen in animal studies a nucleotomy with access to the vertebral vascular network might be as successful as instrumented fusion approaches [79][347][97][297]. Not only animal studies have shown the possibility of self-fusion, but some clinical studies have been focus on the ability of the tissue to heal itself showing similar outcomes with and without additional fixation [287][169]. In the present study, similar radiographic results were predicted for lone nucleotomy and internal fixation. Considering an intact disc height, the segmental instability after both surgeries was too high preventing tissue healing. A higher diameter rod in the IF may help to reduce the ROM and promote bone fusion, but may also increase the risk of fixation loosening or breakage. Therefore, if the goal is to restore the disc height the use of an intervertebral spacer may be necessary. By contrast, anterior plate placement was stiff enough to promote posterior bony fusion.

The removal of intervertebral disc tissue, together with possible tissue damage and further degeneration was thought to cause a decrease in height. McGirt et al. [232] found that large annular defects and less disc removal increased the risk of reherniation while higher disc volume removal accelerated disc height loss (up to 26% two years after surgery). Thus, two different scenarios were simulated decreasing the intact disc height to 75 and 50%. A degree of controlled instability, as shown in the models with 75% DH, enhanced endochondral ossification in agreement with ovine fusion models [97]. However, a strong reduction of the disc height may lead to heterotopic bone formation, as was the case of the osteophytes formed with 50% DH, similar to the last stages of disc degeneration [344].

Endplate defection is a defining feature of vertebral fracture and is associated with properties of the underlying trabecular bone [166]. After surgery, endplates densification occurred in the regions above and underneath the bone bridge while resorption took place where no bone was formed in accordance with clinical observations [19] and other FE studies which shown the correlation between the endplate's BMD and the state of the disc [9][146]. This bone remodelling restored the deformation of the endplates which was reduced following surgery. However, while the bone resorption in case of 100% DH increased the inward deflection of the endplates with respect to the intact ones, the osteophytes formation in case of 50% DH caused an outward deflection on the cranial endplate. Those abnormal deformation patterns may increase the risk of fracture and affect the nutrition pathways [99].

On the other hand, when a bio-mechano-regulated model was used to simulate the lumbar fusion after stand-alone cage insertion, solid fusion was predicted. In agreement with other FE studies [286][29], under pure compressive loads, the formation of bone started at the vertebral endplates in the proximity of the cage and developed along the intervertebral space to the transversal mid-plane. Subsequently, the bone apposition continued toward the periphery.

However, despite the large amount of studies adressing for the fusion rate [10][252], few of them have analysed the bone growth pathway. Marchi et al. [223] showed how the bone grew initially inside the cage and then towards the anterior region. In agreement with these results, in this chapter the same behaviour was predicted in case of applying compression plus flexion, which may indicate the necessity to consider a loading protocol representative of the mean daily load.

6.4.1 Limitations and assumptions

6.4.1.1 Mechano-regulated model

Although computational models may provide insight into bone healing after surgery they have some assumptions and limitations. Given that stress-driven models have a positive feedback system [367], which usually leads to a diverging solution and are therefore not suitable for macro scale simulations, the mechanical stimulus S has been calculated in each element as the quotient of the SED divided by the cube of the BMD [308][349]. The mentioned stimulus as well as the values chosen for the parameters C, s and, h influence in the final BMD distribution. A future sensitivity analysis should be performed to study this influence. The loading and boundary conditions also affected the final bone distribution. A single FSU was modelled, so the loads applied by the adjacent discs, ligaments and facet joints were not considered. Therefore, the results could only be interpreted in the central region far from the boundaries.

The tissue healing algorithm employed was based on the theory of Claes & Heigele [72] defining linear elastic materials. Other healing theories proposed the inclusion of fluid flow [290] to calculate the mechanical stimulus taking into account time dependent effects in the behaviour of the tissue. However, since both theories have shown to be able to predict spinal fusion [286], the less expensive computationally was employed.

The vascularization progress was not explicitly modelled and was maintained constant throughout the simulation preventing from bone formation in the remaining annular tissue. The degeneration of the tissue could cause tissue disruption and blood income, allowing for additional bone formation in those regions. The sensitivity of the result due to changes in the threshold for bone neighbour activation and the boundaries of the differentiation diagram should also be address in future studies. Finally, a constant source of progenitor cells was considered at the endplates, which may cause and overestimation of cell's concentration and tissue formation. Since the goal of this study was to investigate for possible explanations that trigger the bone formation, all the above mentioned assumptions were considered acceptable to cross-compare among different mechanical scenarios. Validation with clinical data would be necessary for more reliable predictions.

6.4.1.2 Bio-mechano-regulated model

The bio-mechano-regulated model presented in this chapter is a preliminary study of the suitability of this kind of models to predict the healing process after lumbar surgery. For that reason, the geometry used was simplified idealizing the segment geometry to cylindrical shape and removing the posterior elements and ligaments. For a more accurate prediction, the inclusion of the posterior elements and ligaments, which would modify the load requirements, would be mandatory.

All the parameters used to characterized the model (cell diffusion, proliferation, formation rates, etc.) were mostly taken from bone healing in long bone callus studies. More clinical studies in the field of radiologic outcomes of lumbar fusion would be necessary to adjust and validate the model.

In conclusion, this study showed that fusion may be self-induced by controlling the mechanical stabilization without the need of additional fixation. Thus, reducing surgery costs and implant related complications. It was also seen that both models were able to predict fusion patterns, however whether the higher computational cost introduced by the bio-mechano-regulated model, increases or not the quality of the prediction can not be discuss without the necessary clinical data to validate the models. Further studies should be focused on the following questions arisen from this chapter, can the bone fusion be triggered by altering the mechanical environment? Is it possible to control the mechanical environment by resecting disc tissue? And if so, which is the optimal amount of nucleus tissue to be removed to promote this fusion?

Chapter 7

General conclusions

A brief summary of the work developed along with the main conclusions drawn as a result of this thesis is presented in this chapter. Furthermore, the original contributions to the field of intervertebral lumbar surgery are enumerated. Finally, the future work lines are outlined.

7.1 Conclusions

Several FE models have been developed over the course of this thesis to comprehensively understand the biomechanical behaviour of the lumbar spine. First of all, the degenerative process of the intervertebral disc has been studied from different points of view. An in-vivo animal model was used to examine the biological and mechanical changes which underwent the discs structures. Then, a FE model of the animal spine was built to correlate the alterations and to search for possible explanations that may trigger the initiation of the disease. Further on, human FE models were used to analyse the influence of the disease on the disc and lumbar spine biomechanics covering three different aspects: the influence of the biphasic properties, the changes in morphology, and the effect of the degeneration over the adjacent segments.

Later on, the available surgical processes for lumbar fusion were analysed. In particular, posterior screw fixation, intervertebral disc cage supplemented with pedicle screw fixation and intervertebral disc cage in a stand-alone fashion. The main drawbacks of these surgeries were deeply investigated. First of all, a hybrid loading protocol was used to analyse the possibility of adjacent disc disease with each type of surgery. Then, a parametric FE model of a single segment with a complex bone characterization was used to search for the parameters which would decrease the risk of subsidence in case of stand-alone cages.

Finally, the fusion process in itself was simulated. To this end, two different algorithms were proposed: a mechano-regulated model and a bio-mechano-regulated model. The healing response after nucleotomy, internal fixation, anterior plate placement and stand-alone cage was predicted.

A combination of the findings derived from this thesis could be a powerful tool for the preclinical evaluation of surgery outcomes. Furthermore, a patient-specific surgery design is possible insofar this allows to predict the potential risk of subsidence, adjacent segment disease and non-union, leading to the best-personalised option for a specific subject.

The main conclusions extracted from this work are listed bellow:

- The in-vivo animal study provided quantitative and qualitative measures on the bio-mechanical alterations during degeneration of the rabbit intervertebral disc. It was seen that the degeneration altered the mechanical properties and the stress patterns of both the degenerated and the adjacent discs by decreasing its water content and increasing its stiffness.

  Notwithstanding the fact that the extrapolation to humans should be carefully made, the developed methodology could give new insight into the human intervertebral disc degeneration knowledge and serve as a tool for the evaluation of new treatments.

- Through the study of the degenerative process of the intervertebral disc it was concluded that both, material behaviour and geometry, had an important role in the pathology, and therefore they should be considered in combination. In fact, a relation may be found between the less capacity of swelling and the reduction of the disc height.

  Finally, an effect of the degeneration over the adjacent segments was predicted. This change in the IVD's mechanics may lead to a cascade of degeneration which might be aggravated by the use of posterior fixation.

- By the use of different FE models to compare among surgical options it was concluded that stand-alone cages could be a minimally invasive alternative to posterior screw fixation in carefully selected patients without previous signs of instability.

Special attention should be taken when choosing the cage size to cause a certain amount of ligament pre-strain and avoid cage migration but without provoking damage to the ligaments or the bony endplates.

- The parametric FE model allowed for subsidence prediction with the possibility to discern if the bone will fail under the cage pressure or not. It was seen that cage design and placement played a key role in the biomechanical behaviour of the FSU after lumbar surgery. A compromise between stabilization and bone integrity should be reached by modifying the width, length, curvature and position of the cage for each specific patient. A preoperative evaluation of the patient-specific geometry and bone quality using this tool would predict the optimal cage design.
- Regarding the healing process after lumbar surgery, it was shown that fusion may be self-induced by controlling the mechanical stabilization without the need of additional fixation. Thus, reducing surgery costs and implant related complications.
- Mechano-regulated model as well as bio-mechano-regulated model were able to predict fusion patterns. However, whether the higher computational cost introduced by the bio-mechano-regulated model improves or not the quality of the prediction can not be discuss without the necessary clinical data to validate the models.

7.2 Original contributions

The original contributions carried out during the period of this thesis are exposed below:

- Animal study of the degenerative changes induced in a single disc and how they influence on the cranial and caudal segments.
- Quantification of morphological changes which underwent IVDs with progressive degeneration.
- Simulation of the healthy and degenerated lumbar spine biomechanics, emphasizing the alterations in the segments adjacent to the affected disc.
- Computational simulation of different segmental fusion procedures (TLIF and PLIF cages supplemented with pedicle screw fixation or in stand-alone construct) and comparison of the biomechanical changes in the entire lumbar spine.

- Analysis of the role of ligament pre-strain after cage insertion on the stability of the operated segment.
- Inclusion of a Drucker-Prager Cap plasticity formulation to characterize the inelastic behaviour of the transversal isotropic vertebral bone.
- Parametric study of cage design features and placement when used as stand-alone. Analysis of the stability, facet joint forces and risk of cage subsidence.
- Design and mechanical testing of PCL scaffolds to use as lumbar intervertebral spacer in fusion surgeries.
- Implementation of a bone remodelling theory to study the vertebral bone density distribution and its evolution after fusion surgery.
- Study of the role of annular fibres in the vertebral bone density distribution.
- Development of an algorithm to predict lumbar fusion after nucleotomy, internal fixation and anterior plate fixation based on a mechano-regulation theory. Study of the role of disc height on the healing process.
- Development of an algorithm to predict lumbar fusion after stand-alone cage insertion based on a bio-mechano-regulation theory. Study of the role of the loading protocol on the healing process.

7.2.1 Publications

Cegoñino, J., Moramarco, V., Calvo-Echenique, A., Pappalettere, C. and A. Pérez Del Palomar (2014). A constitutive model for the annulus of human intervertebral disc (IVD): implications for developing a degeneration model and its influence on lumbar spine functioning. *Journal of Applied Mathematics.*

Cegoñino, J., Calvo-Echenique, A. and A. Pérez Del Palomar. (2015) Influence of different fusion techniques in lumbar spine over the adjacent segments: a 3D finite element study. *Journal of Orthopaedic Research*, 33(7), 993-1000.

Calvo-Echenique, A., Cegoñino, J., Correa-Martín, L., Bances, L. and A. Pérez-del Palomar (AÑO). (2017) Intervertebral disc degeneration: an experimental and numerical study using a rabbit model. *Medical & Biological Engineering & Computing.*

Calvo-Echenique, A., Cegoñino, J. and A. Pérez-del Palomar. Biomechanical comparison between stand-alone interbody cages and their benefits over posterior screw fixation. *Submitted to BMC Musculoskeletal Disorders.*

Calvo-Echenique, A., Cegoñino, J., Chueca, R. and A. Pérez-del Palomar. Influence of stand-alone cage design on subsidence and lumbar biomechanics: a parametric finite element study. *Submitted to Computer methods & programs in biomedicine.*

Calvo-Echenique, A., Bashkuev M., Reitmaier S., Pérez-del Palomar A. and Schmidt H. Numerical Simulations of Bone Remodelling and Formation after Nucleotomy. *Submitted to The Spine Journal.*

7.2.2 Conferences

Oral communications

Calvo-Echenique, A., A. Pérez-del Palomar and J.Cegoñino. Surgical techniques in lumbar spine related to intervertebral disc disorders. A finite element study. *Spanish Chapter of the European Society of Biomechanics (ESB)*, Barcelona (Spain) 2013.

Calvo-Echenique, A., Cegoñino, J., Correa-Martín, L., Bances, L. and A. Pérez-del Palomar. A rabbit model for mimicking the intervertebral disc degeneration An experimental and computational study. *21st Congress of the European Society of Biomechanics (ESB)*, Prague (Czech Republic) 2015.

Calvo-Echenique, A., Cegoñino, J. and A. Pérez-del Palomar. Biomechanical Comparison between Stand-alone Interbody Cages and their Benefits over Posterior Screw Fixation. *IV Jornada jóvenes investigadores del I3A*, Zaragoza (Spain) 2015.

Calvo-Echenique A. Biomecánica de la columna lumbar humana. Estudio de patologías y diseño de nuevos procedimientos quirúrgicos. *II Jornadas Doctorales Campus Iberus*, Jaca (Spain) 2015.

Calvo-Echenique, A., Cegoñino, J., Kelly, D. and A. Pérez-del Palomar. A 3D mechanobiological model to simulate tissue growth around implants. *23st Congress of the European Society of Biomechanics (ESB)*, Seville (Spain) 2017.

Calvo-Echenique, A., Bashkuev M., Reitmaier S., Pérez-del Palomar A. and Schmidt H. Numerical simulations of bone remodelling after nucleotomy. *CMBBE. Computer Methods in Biology and Biomedical Engineering*, Lisbon (Portugal) 2018.

Poster communications

Calvo-Echenique, A., Cegoñino, J., Bances, L. and A. Pérez-del Palomar. Finite element study of healthy, pathological and surgical lumbar spine biomechanics. *WCCM XI & ECCM V & ECFD VI*, Barcelona (Spain) 2014.

Calvo-Echenique, A., Cegoñino, J., Chueca, R. and A. Pérez-del Palomar. A parametric finite element study for prosthesis design. *23st Congress of the European Society of Biomechanics (ESB)*, Seville (Spain) 2017.

7.2.3 Awards

Mimics Innovation Award for Best Poster Communication 2015 *awarded by Materialise (Belgium)*

Best Poster Communication in the II Doctoral Meeting of Campus Iberus 2015 *awarded by the comitee of Campus Iberus.*

7.3 Future work

As exposed throughout the entire document, a large number of studies have been done over the last decades in relation to the biomechanical behaviour of the lumbar spine from animal, clinical and computational points of view. However, there is still a high controversy regarding the use of one or another fusion surgical procedure. In this thesis, those conflicting topics have been tackled with the aim of discuss the suitability and indications of each technique. Nonetheless, the results found in this thesis opened new questions that may be addressed in future works:

- The study of degeneration including biphasic, morphologic and tissue changes in a broad range of patients would allow for the statistical analysis of the probability of adjacent segment disease occurrence.
- Building a data base of the alterations derived from progressive lumbar disc degeneration may help to predict, using machine learning tools, the possibility of severe degeneration by the analysis of medical images at the first signs of the disease.
- A multidisciplinary project combining clinical trials and computational simulations to study the healing process after different surgeries with frequent follow-ups would allow for the validation of the implemented models which may serve as a predictor tool of the successful fusion rate.
- The development of a software combining the different models presented in this thesis (patient-specific geometry, bone inelastic behaviour characterization, bone remodelling algorithm and tissue healing algorithm) would allow for the preclinical evaluation of different intervertebral spacers with and without

supplementary instrumentation in each specific cage providing personalized treatment guidance.

RESUMEN Y CONCLUSIONES

De acuerdo a la normativa vigente para la obtención de mención de doctorado internacional, en el presente capítulo se recoge el resumen, las principales conclusiones de la tesis y sus aportaciones originales en español.

7.4 Resumen

Esta tesis tiene como objetivo arrojar luz en el proceso que tiene lugar en la columna lumbar como resultado de la degeneración de disco intervertebral y las diferentes cirugías lumbares, prestando especial atención a los principales factores de riesgo y como superarlos.

El dolor de espalda es el trastorno musculo-esquelético más frecuente en todos los países desarrollados generando grandes costes a los sistemas sanitarios. La degeneración de disco intervertebral es una de las causas más comunes del dolor lumbar. Cuando los tratamientos conservativos no consiguen mitigar este dolor es necesario recurrir a la cirugía. Y, en este aspecto, la fusión lumbar es la técnica más utilizada para recuperar la estabilidad y descomprimir las raíces nerviosas.

La enfermedad degenerativa del disco ha sido estudiada a través de dos aproximaciones diferentes. Un modelo animal fue reproducido en vivo y seguido con imágenes de resonancia magnética y ensayos mecánicos para observar cómo, con el progreso de la degeneración, decrecía el contenido de agua y aumentaba la rigidez del tejido. Después, esta degeneración fue inducida en un disco de la columna lumbar humana y sus efectos sobre los discos adyacentes fueron investigados utilizando modelos de elementos finitos.

Más adelante, se simularon computacionalmente diferentes procedimientos para la fusión del segmento. Una comparación entre diferentes cajas intersomáticas, suplementadas con fijación posterior o colocadas sin fijación, mostró cómo el uso de fijación suplementaria redujo drásticamente el movimiento del segmento afectado incrementando el riesgo de degeneración en los segmentos adyacentes. Sin embargo, una de las mayores preocupaciones acerca del uso de cajas sin fijación adicional es la posibilidad de hundimiento del dispositivo en el hueso vertebral. Un estudio paramétrico de las características y el posicionamiento de las cajas apuntó a la anchura, la curvatura y la posición como los parámetros más influyentes en la estabilidad y el enclavamiento.

Finalmente, dos algoritmos diferentes para la cicatrización de tejido fueron implementados y aplicados por primera vez a la predicción de la fusión lumbar en modelos 3D. La capacidad auto-reparadora del hueso fue comprobada tras una nucleotomía simple y tras la instrumentación con fijación interna, placa anterior y colocación de caja intersomática. De acuerdo con estudios previos tanto en animales como en casos clínicos, se predijo que la instrumentación podría no ser necesaria para promover la fusión del segmento. En particular, se vio que la altura del disco intervertebral juega un papel importante en la formación de puente óseo o de osteofitos.

Resumiendo, esta tesis se ha centrado en los temas más controvertidos relativos a la degeneración del disco intervertebral y la fusión lumbar como son: el proceso degenerativo, la progresión de la degeneración a los segmentos adyacentes, la estabilidad del segmento, el enclavamiento de la caja intersomática o la formación de puente óseo. Todos los modelos descritos en esta tesis pueden servir como una poderosa herramienta para la evaluación pre clínica de la respuesta a la cirugía de cada paciente dando apoyo a la decisión del cirujano.

7.5 Conclusiones

Varios modelos de elementos finitos han sido desarrollados a lo largo de esta tesis con el propósito de entender de forma exhaustiva el comportamiento biomecánico de la columna lumbar. En primer lugar, el proceso degenerativo del disco intervertebral ha sido estudiado desde diferentes perspectivas. Se utilizó un modelo animal in-vivo para examinar los cambios biológicos y mecánicos que sufrieron las estructuras del disco. Después, se construyó un modelo de elementos finitos de la columna del animal estudiado para correlacionar las alteraciones observadas y buscar posibles explicaciones a los desencadenantes de la enfermedad. A continuación, se utilizaron diferentes modelos de elementos finitos para analizar la influencia de la degeneración en el disco intervertebral y en la biomecánica de la columna lumbar cubriendo tres aspectos: la influencia de las propiedades bifásicas, los cambios en la morfología, y el efecto de la degeneración sobre los segmentos adyacentes.

En el siguiente estudio, se analizaron los procedimientos quirúrgicos disponibles para la realización de la fusión lumbar. En particular, la fijación de tornillos posterior, la caja intersomática suplementada con fijación de tornillos pediculares, y la utilización de la caja intersomática sin fijación. Las principales desventajas de cada una de estas técnicas han sido investigadas en profundidad. En primer lugar, se utilizó un protocolo de carga híbrido para analizar la posibilidad de inducción de la enfermedad en los discos adyacentes con cada tipo de cirugía. Luego, un análisis paramétrico de elementos finitos con una caracterización compleja del hueso permitió determinar que parámetros reducirían el riesgo de enclavamiento en cajas intersomáticas colocadas sin fijación adicional.

Finalmente, se simuló el proceso de fusión en sí mismo. Para ello, se propusieron dos algoritmos diferentes: un modelo mecano-regulado y un modelo bio-mecano-regulado. Ambos permitieron predecir la respuesta de la cicatrización tras las cirugías de nucleotomía, fijación interna, fijación con placa anterior y caja intersomática sin fijación adicional.

La combinación de los resultados derivados de esta tesis puede conformar una potente herramienta para la evaluación pre-clínica de los resultados quirúrgicos. Además, permitiría el diseño personalizado para un paciente específico en tanto en cuanto permite predecir el riesgo de enclavamiento, la posibilidad de degeneración en los segmentos adyacentes y el riesgo de no-unión.

Las principales conclusiones extraídas de este trabajo se listan a continuación:

- El modelo animal in-vivo permitió obtener medidas tanto cualitativas como cuantitativas de las alteraciones biomecánicas que tuvieron lugar durante el proceso de regeneración del disco intervertebral. Se observó como la degeneración alteró las propiedades mecánicas y los patrones de tensión tanto de los discos degenerados como de los adyacentes, decreciendo la cantidad de agua e incrementando la rigidez del tejido.

  A pesar de que la extrapolación de los resultados al caso humano debe hacerse de forma cuidadosa, la metodología desarrollada puede aportar nueva luz al conocimiento de la degeneración del disco intervertebral y servir como herramienta para la evaluación de nuevos tratamientos.

- A través del estudio del proceso degenerativo del disco intervertebral se concluyó que ambos: el comportamiento del material y la geometría, tuvieron un papel importante en el desarrollo de la patología y, por tanto, en adelante deben ser considerados conjuntamente. De hecho, quizá sea posible establecer una relación entre la menor capacidad del disco para hincharse y la reducción de su altura.

  Finalmente, se observó un efecto de la degeneración sobre los segmentos adyacentes. Este cambio en la mecánica del disco podría conducir a un efecto de degeneración en cascada que sería agravado con el uso de fijación posterior.

- Mediante el uso de diferentes modelos de elementos finitos se comparó entre distintas técnicas quirúrgicas llegando a la conclusión de que una caja intersomática podría ser colocada de forma mínimamente invasiva sin la necesidad de fijación posterior en pacientes cuidadosamente seleccionados sin signos previos de inestabilidad.

  Especial atención debe ser tomada al elegir la altura de la caja para producir la cantidad de distracción de los ligamentos adecuada para evitar la migración del dispositivo sin provocar daños en los ligamentos o en las placas óseas.

- El modelo paramátrico de elementos finitos permitió la predicción del enclavamiento, brindando la posibilidad de discernir si el hueso fallará o no bajo la presión creada por el espaciador. Se vio cómo el diseño de la caja intersomática, así como su posicionamiento, son esenciales en el comportamiento biomecánico del segmento lumbar después de la cirugía. Se debe alcanzar un compromiso entre la estabilización y la integridad del hueso mediante la modificación de la anchura, longitud, curvatura y posición del implante para cada paciente. Además, la evaluación pre-clínica de la geometría del paciente, así como de la calidad ósea de las vértebras permitiría, utilizando esta herramienta, conocer un diseño óptimo personalizado.

- En cuanto al proceso de cicatrización tras la intervención quirúrgica. Se ha mostrado como la fusión puede ser auto-inducida controlando la estabilización mecánica sin necesidad de introducir fijaciones adicionales. Esto implica la reducción de costes relacionados con la cirugía así como las complicaciones relacionadas con el implante.

- Tanto el modelo mecano-regulado como el bio-mecano-regulado fueron capaces de predecir patrones de fusión, sin embargo, discutir si el coste computacional añadido al implementar el modelo bio-mecano-regulado es necesario o no para mejorar la precisión de la predicción no es posible debido a la falta de datos clínicos que permitan la validación del modelo.

7.6 Contribuciones originales

Las contribuciones originales aportadas durante esta tesis se exponen a continuación:

- Estudio animal de los cambios degenerativos inducidos en un solo disco y cómo influyen en los segmentos caudal y craneal.

- Cuantificación de los cambios morfológicos que experimentan los discos intervertebrales a lo largo del proceso de degeneración.
- Simulación de la columna lumbar sana y patológica enfatizando las alteraciones producidas en los segmentos adyacentes al disco afectado.
- Simulación computacional de los diferentes procedimientos de fusión segmentaria (cajas intersomáticas para TLIF y PLIF suplementadas con tornillos pediculares o sin fijación adicional) y comparación de los cambios biomecánicos experimentados por la columna lumbar completa.
- Análisis de la influencia de la pre-tensión de los ligamentos tras la inserción del espaciador intersomático en la estabilidad del segmento intervenido.
- Inclusión de la formulación Drucker-Prager modificada para incluir el comportamiento inelástico del hueso transversalmente isótropo con el que se caracterizan las vértebras.
- Estudio paramétrico de los aspectos de diseño y posicionamiento de la caja intersomática cuando se coloca sin fijación adicional. Análisis de la estabilidad, las fuerzas facetarias y el riesgo de enclavamiento.
- Diseño y examen mecánico de los *scaffolds* de PCL para ser utilizados como espaciador intervertebral en las operaciones de fusión.
- Implementación de un modelo de regeneración ósea para el estudio de la distribución de densidad mineral ósea vertebral y su evolución tras la cirugía.
- Estudio de la influencia de las fibras del anillo del disco intervertebral en la distribución de densidad mineral ósea.
- Desarrollo de un algoritmo para predecir la fusión lumbar tras una nucleotomía, una fijación interna y una fijación con placa anterior, basado en una teoría de mecano-regulación. Estudio del papel que tiene la altura del disco en el proceso de cicatrización.
- Desarrollo de un algoritmo para predecir la fusión lumbar tras la inserción de una caja intersomática sin fijación basado en una teoría de bio-mecano-regulación. Estudio del papel que tiene el protocolo de carga en el proceso de cicatrización.

7.7 Futuras líneas de investigación

Como se ha expuesto a lo largo de todo el documento, un gran número de estudios han sido realizados a lo largo de las últimas décadas en relación con el comportamiento biomecánico de la columna lumbar desde el punto de vista de experimentación animal, ensayos clínicos y trabajos computacionales. Aun así, sigue existiendo una gran controversia en cuanto al uso de una cirugía u otra. En esta tesis, se han abordado los temas más conflictivos con el propósito de discutir acerca de la idoneidad e indicaciones de cada una de las técnicas. Sin embargo, los resultados obtenidos en la presente tesis abren nuevas preguntas que pueden ser respondidas en futuros trabajos:

- El estudio de la degeneración incluyendo los cambios bifásicos, morfológicos y de tejido en un rango amplio de pacientes permitiría el análisis estadístico de la probabilidad de ocurrencia de degeneración de los segmentos adyacentes.
- Construir una base de datos de las alteraciones derivadas de la degeneración progresiva del disco lumbar que pueda ayudar a predecir, utilizando técnicas de aprendizaje automático, la posibilidad de degeneración avanzada mediante el análisis de imágenes médicas ante los primeros signos de la enfermedad.
- Un proyecto multidisciplinario combinando ensayos clínicos y simulaciones computacionales para el estudio del proceso de cicatrización tras diferentes cirugías con una alta frecuencia de seguimientos permitiría la validación de los modelos implementados. Y a su vez, podría ser una herramienta de predicción de éxito de la cirugía.
- El desarrollo de un software que combine los diferentes modelos presentados en esta tesis (geometría paciente-específica, caracterización inelástica del comportamiento del hueso, remodelación ósea y cicatrización de tejidos) permitiría la evaluación pre-clínica de diferentes espaciadores intervertebrales con y sin fijación suplementaria en cada paciente de forma específica proveyendo guías para el tratamiento personalizado.

Bibliography

[1] Sunny A. Abbah, Christopher X.F. Lam, Amit K. Ramruttun, James C.H. Goh, and Hee-Kit Wong. Fusion Performance of Low-Dose Recombinant Human Bone Morphogenetic Protein 2 and Bone Marrow-Derived Multipotent Stromal Cells in Biodegradable Scaffolds. *Spine*, 36(21):1752–1759, 2011.

[2] E.R. Acaroglu, J.C. Iatridis, L.A. Setton, R.J. Foster, V.C. Mow, and M. Weidenbaum. Degeneration and aging affect the tensile behavior of human lumbar anulus fibrosus. *Spine (Phila Pa 1976)*, 1995.

[3] M A Adams, D S McNally, and P Dolan. 'Stress' distributions inside intervertebral discs. The effects of age and degeneration. *The Journal of bone and joint surgery.*, 78(6):965–972, 1996.

[4] Michael A. Adams, Brian J C Freeman, Helen P. Morrison, Ian W. Nelson, and Patricia Dolan. Mechanical initiation of intervertebral disc degeneration. *Spine*, 25(13):1625–1636, 2000.

[5] Michael A Adams and William C Hutton. The mechanical function of the lumbar apophyseal joints. *Spine (Phila Pa 1976)*, 8(3):327–330, 1983.

[6] Michael A Adams and Peter J Roughley. What is intervertebral disc degeneration, and what causes it? *Spine*, 31(18):2151–61, aug 2006.

[7] P. Adams, D.R. Eyre, and H. Muir. Biochemical aspects of development and ageing of human lumbar intervertebral discs. *Rheumatology*, 16(1):22–29, 1977.

[8] P Adams and H Muir. Qualitative changes with age of proteoglycans of human lumbar discs. *Annals of the rheumatic diseases*, 35(4):289–96, 1976.

[9] Aakash Agarwal, Anand K Agarwal, and Vijay K Goel. The Endplate Morphology Changes with Change in Biomechanical Environment Following Discectomy. *International Journal of Clinical Medicine*, 04(07):8–17, 2013.

[10] Amir Ahmadian, Konrad Bach, Bryan Bolinger, Gregory M. Malham, David O. Okonkwo, Adam S. Kanter, and Juan S. Uribe. Stand-alone minimally invasive lateral lumbar interbody fusion: Multicenter clinical outcomes. *Journal of Clinical Neuroscience*, 22(4):740–746, 2015.

[11] FH Albee. Transplantation of a portion of the tibia into the spine for Pott's disease: a preliminary report. *Journal of the American Medical Association*, 57(11):885–886, 1911.

[12] Mauro Alini, Stephen M. Eisenstein, Keita Ito, Christopher Little, A. Annette Kettler, Koichi Masuda, James Melrose, Jim Ralphs, Ian Stokes, and Hans Joachim Wilke. Are animal models useful for studying human disc disorders/degeneration? *European Spine Journal*, 17(1):2–19, 2008.

[13] Jérôme Allain, Joël Delecrin, Jacques Beaurain, Alexandre Poignard, Thierry Vila, and Charles Henri Flouzat-Lachaniette. Stand-alone ALIF with integrated intracorporeal anchoring plates in the treatment of degenerative lumbar disc disease: a prospective study on 65 cases. *European Spine Journal*, 23(10):2136–2143, 2014.

[14] Dominique Ambard and Pascal Swider. A predictive mechano-biological model of the bone-implant healing. *European Journal of Mechanics A/Solids*, 25(6):927–937, 2006.

[15] Divya V. Ambati, Edward K. Wright, Ronald A. Lehman, Daniel G. Kang, Scott C. Wagner, and Anton E. Dmitriev. Bilateral pedicle screw fixation provides superior biomechanical stability in transforaminal lumbar interbody fusion: a finite element study. *Spine Journal*, 15(8):1812–1822, 2015.

[16] Greg D Anderson, Xudong Li, Tony Tannoury, Gina Beck, and Gary Balian. A fibronectin fragment stimulates intervertebral disc degeneration in vivo. *Spine*, 28(20):2338–45, 2003.

[17] G. BJ Andersson and A.B. Schulze. Effects of fluid injection on mechanical properties of intervertebral discs. *Journal of Biomechanics*, 12(6):453–458, 1979.

[18] A. Andreykiv, F. Van Keulen, and P. J. Prendergast. Simulation of fracture healing incorporating mechanoregulation of tissue differentiation and dispersal/proliferation of cells. *Biomechanics and Modeling in Mechanobiology*, 7(6):443–461, 2008.

[19] M.D. Antonacci, D.S. Hanson, A. Leblanc, and M.H. Heggeness. Regional variation in vertebral bone density and trabecular architecture are influenced by osteoarthritic change and osteoporosis. *Spine (Phila Pa 1976)*, 22(20):2393–2402, 1997.

[20] Maxime Antoni, Yann Philippe Charles, Axel Walter, Sébastien Schuller, and Jean-Paul Steib. Fusion rates of different anterior grafts in thoracolumbar fractures. *Journal of spinal disorders & techniques*, 28(9):528–533, 2015.

[21] John Antoniou, Thomas Steffen, Fred Nelson, Neil Winterbottom, Anthony P. Hollander, Robin A. Poole, Max Aebi, and Mauro Alini. The human lumbar intervertebral disc: Evidence for changes in the biosynthesis and denaturation of the extracellular matrix with growth, maturation, ageing, and degeneration. *Journal of Clinical Investigation*, 98(4):996–1003, 1996.

[22] M. Argoubi and A. Shirazi-Adl. Poroelastic creep response analysis of a lumbar motion segment in compression. *Journal of Biomechanics*, 29(10):1331–1339, 1996.

[23] Shihab Asfour, Francesco Travascio, Shady Elmasry, and Juan Pablo de Rivero Vaccari. A computational analysis on the implications of age-related changes in the expression of cellular signals on the role of IGF-1 in intervertebral disc homeostasis. *Journal of Biomechanics*, 48(2):332–339, 2015.

[24] Yusuf Assem, Ralph J. Mobbs, Matthew H. Pelletier, Kevin Phan, and William R. Walsh. Radiological and clinical outcomes of novel Ti/PEEK combined spinal fusion cages: a systematic review and preclinical evaluation. *European Spine Journal*, January:1–13, 2016.

[25] Joshua D Auerbach, Kristofer J Jones, Andrew H Milby, Okechukwu a Anakwenze, and Richard a Balderston. Segmental Contribution Toward Total Lumbar Range of Motion in Disc Replacement and Fusions. *Spine*, 34(23):2510–2517, 2009.

[26] Alicia Bailón-Plaza and Marjolein C.H. Vander Meulen. A Mathematical Framework to Study the Effects of Growth Factor Influences on Fracture Healing. *Journal of Theoretical Biology*, 212(2):191–209, 2001.

[27] Federico Balagué, Anne F. Mannion, Ferran Pellisé, and Christine Cedraschi. Non-specific low back pain. *The Lancet*, 379:482–491, 2012.

[28] Luciano Bances. *Interbody cage without instrumentation for the treatment of lumbar disc hernia.* PhD thesis, University of Zaragoza, 2016.

[29] Maxim Bashkuev, Sara Checa, Sergio Postigo, Georg Duda, and Hendrik Schmidt. Computational analyses of different intervertebral cages for lumbar spinal fusion. *Journal of Biomechanics*, 48(12):3274–3282, 2015.

[30] Leonard Bastian, Uta Lange, Christian Knop, Guenter Tusch, and Michael Blauth. Evaluation of the mobility of adjacent segments after posterior thoracolumbar fixation: A biomechanical study. *European Spine Journal*, 10(4):295–300, 2001.

[31] Brian P. Beaubien, Alihan Derincek, William D. Lew, and Kirkham B. Wood. In vitro, biomechanical comparison of an anterior lumbar interbody fusion with an anteriorly placed, low-profile lumbar plate and posteriorly placed pedicle screws or translaminar screws. *Spine*, 30(16):1846–1851, 2005.

[32] G S Beaupré, T E Orr, and D R Carter. An approach for time-dependent bone modeling and remodeling-application: a preliminary remodeling simulation. *Journal of orthopaedic research : official publication of the Orthopaedic Research Society*, 8(5):662–670, 1990.

[33] Jesse C Beckstein, Sounok Sen, Thomas P. Schaer, Edward J. Vresilovic, and Dawn M. Elliott. Comparison of Animal Discs Used in Disc Research to Human Lumbar Disc: Torsion Mechanics and Collagen Content. *Spine*, 33(6):E166–E173, 2008.

[34] T Belytschko, RF Kulak, and AB Schultz. Finite element stress analysis of an intervertebral disc. *Journal of Biomechanics*, 7(3):277–285, 1974.

[35] Masahiko Bessho, Isao Ohnishi, Juntaro Matsuyama, Takuya Matsumoto, Kazuhiro Imai, and Kozo Nakamura. Prediction of strength and strain of the proximal femur by a CT-based finite element method. *Journal of Biomechanics*, 40(8):1745–1753, 2007.

[36] S. R S Bibby, J. C T Fairbank, Martin R. Urban, and J. P G Urban. Cell viability in scoliotic discs in relation to disc deformity and nutrient levels. *Spine*, 27(20):2220–2227, 2002.

[37] A. Blamoutier. Surgical discectomy for lumbar disc herniation: surgical techniques. *Orthopaedics & traumatology, surgery & research : OTSR*, 99(1 Suppl):S187–S196, 2013.

[38] Scott Blumenthal, Paul C McAfee, Richard D Guyer, Stephen H Hochschuler, Fred H Geisler, Richard T Holt, Rolando Garcia, John J Regan, and Donna D Ohnmeiss. A prospective, randomized, multicenter Food and Drug Administration investigational device exemptions study of lumbar total disc replacement with the CHARITE artificial disc versus lumbar fusion: part I: evaluation of clinical outcomes. *Spine*, 30(14):1565–75; discussion E387–91, 2005.

[39] Scott L. Blumenthal and Donna D. Ohnmeiss. Intervertebral cages for degenerative spinal diseases. *Spine Journal*, 3(4):301–309, 2003.

[40] Antonio Boccaccio, Daniel J Kelly, and Carmine Pappalettere. A mechano-regulation model of fracture repair in vertebral bodies. *Journal of orthopaedic research*, 29(3):433–43, 2011.

[41] Antonio Boccaccio, Luciano Lamberti, and Carmine Pappalettere. Effects of aging on the latency period in mandibular distraction osteogenesis: a computational mechanobiological analysis. *Journal of Mechanics in Medicine and Biology*, 08(02):203–225, jun 2008.

[42] N. Boos and J. K. Webb. Pedicle screw fixation in spinal disorders: A European view. *European Spine Journal*, 6(1):2–18, 1997.

[43] A C Bourgeois, A R Faulkner, A S Pasciak, and Y C Bradley. The evolution of image-guided lumbosacral spine surgery. *Ann Transl Med*, 3(5):69, 2015.

[44] RJ Bradshaw, AC Russell, and Anton E. Bowden. Spinal ligaments: anisotropic characterization using very small samples. *Experimental and applied mechanics*, 6:429–436, 2011.

[45] JW Brantigan and AD Steffee. A carbon fiber implant to aid interbody lumbar fusion. Two-year clinical results in the first 26 patients. *Spine (Phila Pa 1976)*, 18(14):2106–7, 1993.

[46] W. A. M. Brekelmans, H. W. Poort, and T. J. J. H. Slooff. A New Method to Analyze the Mechanical Behavior of Skeletal Parts. *Acta Orthopaedica Scandinavica*, 43(February):301–317, 1972.

[47] P. Brinckmann, W. Frobin, E. Hierholzer, and M. Horst. Deformation of the vertebral end-plate under axial loading of the spine. *Spine (Phila Pa 1976)*, 8:851–856, 1983.

[48] J. L. Bron, G. H. Koenderink, V. Everts, and T. H. Smit. Rheological characterization of the nucleus pulposus and dense collagen scaffolds intended for functional replacement. *Journal of Orthopaedic Research*, 27(5):620–626, 2009.

[49] Glenn R. Buttermann, Brian P. Beaubien, Andrew L. Freeman, James E. Stoll, and James L. Chappuis. Interbody device endplate engagement effects on motion segment biomechanics. *Spine Journal*, 9(7):564–573, 2009.

[50] J Q Campbell, D J Coombs, M Rao, P J Rullkoetter, and A J Petrella. Automated finite element meshing of the lumbar spine : Verification and validation with 18 specimen-specific models. *Journal of Biomechanics*, 49:2669–2676, 2016.

[51] Andrew Cappuccino, G Bryan Cornwall, Alexander W L Turner, Guy R Fogel, Huy T Duong, Kee D Kim, and Darrel S Brodke. Biomechanical analysis and review of lateral lumbar fusion constructs. *Spine*, 35(26 Suppl):S361–S367, 2010.

[52] D R Carter. Mechanical loading histories and cortical bone remodeling. *Calcified tissue international*, 36 Suppl 1:S19–24, jan 1984.

[53] D R Carter, D P Fyhrie, and R T Whalen. Trabecular bone density and loading history: regulation of connective tissue biology by mechanical energy. *Journal of biomechanics*, 20(8):785–94, jan 1987.

[54] D. R. Carter and W. C. Hayes. The Compressive Behavior of Bone as a Two-Phase Porous Structure. *The Journal of Bone & Joint Surgery*, 59(7):954–962, 1977.

[55] Dennis R Carter, Gary S Beaupré, Nicholas J Giori, and Jill A Helms. Mechanobiology of Skeletal Regeneration. *Clinical Orthopaedics and Related Research*, 355, 1998.

[56] María Casado, Jenny Moix, and Julia Vidal. Aetiology, chronification, and treatment of low back pain. *Clinica y Salud*, 19(3):379–392, 2008.

[57] W. Caspar. A new surgical procedure for lumbar disc herniation causing less tissue damage through a microsurgical approach. *Advanced Neurosurgery*, 4:74–77, 1977.

[58] Alejandro Castellvi, Shankar Thampi, Daniel Cook, Matthew Yeager, Yuan Yao, Qing Zou, Donald Whiting, Michael Oh, Edward Prostko, and Boyle Cheng. Effect of TLIF Cage Placement on In Vivo Kinematics. *International Journal of Spine Surgery*, pages 1–7, 2015.

[59] J. Cegoñino, V. Moramarco, A. Calvo-Echenique, C. Pappalettere, and A. Pérez Del Palomar. A constitutive model for the annulus of human intervertebral disc (IVD): implications for developing a degeneration model and its influence on lumbar spine functioning. *Journal of Applied Mathematics*, 2014.

[60] Samantha C W Chan and Benjamin Gantenbein-Ritter. Intervertebral disc regeneration or repair with biomaterials and stem cell therapy - Feasible or fiction? *Swiss Medical Weekly*, 142(MAY):1–12, 2012.

[61] Wilsa M S Charles Malveaux and Alok D. Sharan. Adjacent segment disease after lumbar spinal fusion: A systematic review of the current literature. *Seminars in Spine Surgery*, 23(4):266–274, 2011.

[62] Lillian S. Chatham, Vikas V. Patel, Christopher M. Yakacki, and R. Dana Carpenter. Interbody Spacer Material Properties and Design Conformity for Reducing Subsidence During Lumbar Interbody Fusion. *Journal of Biomechanical Engineering*, 139(May):1–8, 2017.

[63] J. Chazal, A. Tanguy, M. Bourges, G. Gaurel, G. Escande, M. Guillot, and G. Vanneuville. Biomechanical properties of spinal ligaments and a histological study of the supraspinal ligament in traction. *Journal of Biomechanics*, 18(3):167–176, jan 1985.

[64] Gene Cheh, Keith H. Bridwell, Lawrence G. Lenke, Jacob Buchowski, Michael D. Daubs, Yongjung Kim, and Christy Baldus. Adjacent segment disease followinglumbar/thoracolumbar fusion with pedicle screw instrumentation: A minimum 5-year follow-up. *Spine (Phila Pa 1976)*, 32(20):2253–2257, 2007.

[65] Liang Chen, Huilin Yang, and Tiansi Tang. Cage migration in spondylolisthesis treated with posterior lumbar interbody fusion using BAK cages. *Spine*, 30(19):2171–2175, 2005.

[66] S. Chen, Z. Zhong, C. Chen, W. Chen, and C. Hung. Biomechanical comparison between lumbar disc arthroplasty and fusion. *Medical engineering & physics*, 31:244–253, 2009.

[67] Shih-Hao Chen, Ming-Chieh Chiang, Jin-Fu Lin, Shang-Chih Lin, and Ching-Hua Hung. Biomechanical comparison of three stand-alone lumbar cages– a three-dimensional finite element analysis. *BMC musculoskeletal disorders*, 14(1):281, 2013.

[68] Shih-Hao Chen, Ching-Lung Tai, Chien-Yu Lin, Pang-Hsing Hsieh, and Weng-Pin Chen. Biomechanical comparison of a new stand-alone anterior lumbar interbody fusion cage with established fixation techniques - a three-dimensional finite element analysis. *BMC Musculoskeletal Disorders*, 9, 2008.

[69] K M C Cheung, J Karppinen, D Chan, D W H Ho, Y Q Song, P Sham, K S E Cheah, J C Y Leong, and K D K Luk. Prevalence and pattern of lumbar magnetic resonance imaging changes in a population study of one thousand forty-three individuals. *Spine (Phila Pa 1976)*, 34(9):934–940, 2009.

[70] Kyung-Chul Choi, Kyeong-Sik Ryu, Sung Jae Sang-Ho Lee, Yeong Hyeon Kim, Sung Jae Sang-Ho Lee, and Chun-Kun Park. Biomechanical comparison of anterior lumbar interbody fusion: stand-alone interbody cage versus interbody cage with pedicle screw fixation – a finite element analysis. *BMC musculoskeletal disorders*, 14(1):220, jan 2013.

[71] Finn Bjarke Christensen, Ebbe Stender Hansen, Malene Laursen, Karsten Thomsen, and Cody E Bünger. Long-Term Functional Outcome of Pedicle Screw Instrumentation as a Support for Posterolateral Spinal Fusion. Randomized Clinical Study With a 5-Year Follow-up. *Spine (Phila Pa 1976)*, 27(12):1269–1277, 2002.

[72] L. E. Claes and C. A. Heigele. Magnitudes of local stress and strain along bony surfaces predict the course and type of fracture healing. *Journal of Biomechanics*, 32(3):255–266, 1999.

[73] Jordan M. Cloyd, Neil R. Malhotra, Lihui Weng, Weiliam Chen, Robert L. Mauck, and Dawn M. Elliott. Material properties in unconfined compression of human nucleus pulposus, injectable hyaluronic acid-based hydrogels and tissue engineering scaffolds. *European Spine Journal*, 16(11):1892–1898, 2007.

[74] JR Cobb. Outline for the study of scoliosis. *In instructional course lectures. The american academy of orthopaedic surgeons*, 5:261–275, 1948.

[75] Francesco Costa, Marco Sassi, Alessandro Ortolina, Andrea Cardia, Roberto Assietti, Alberto Zerbi, Martin Lorenzetti, Fabio Galbusera, and Maurizio Fornari. Stand-alone cage for posterior lumbar interbody fusion in the treatment of high-degree degenerative disc disease: Design of a new device for an "old" technique. a prospective study on a series of 116 patients. *European Spine Journal*, 20(SUPPL. 1):46–56, 2011.

[76] JJ Costi, IA Stokes, M Gardner-Morse, and James C. Iatridis. Frequency-dependent behavior of the intervertebral disc in response to each of six degree of freedom dynamic loading: solid phase and fluid phase contributions. *Spine (Phila Pa 1976)*, 33(16):173–1738, 2008.

[77] JJ Costi, IA Stokes, M Gardner-Morse, JP Laible, HM Scoffone, and J C Iatridis. Direct measurement of intervertebral disc maximum shear strain in six degrees of freedom: Motions that place disc tissue at risk of injury. *Journal of Biomechanics*, 40(11):2457–2466, 2007.

[78] Gregory D. Cramer. General Characteristics of the spine. In *Clinical Anatomy of the Spine, Spinal Cord and Ans*, chapter 2, pages 15–64. Elsevier, 2014.

[79] J.J. Crisco, M.M. Panjabi, E. Wang, M.A. Price, and R.R. Pelker. The injured canine cervical spine after six months of healing. An in vitro three-dimensional study. *Spine (Phila Pa 1976)*, 15:1047–1052, 1990.

[80] F. J. de Cos Juez, F. Sánchez Lasheras, C. Ordóñez Galán, and P. J. García Nieto. Study of posterolateral lumbar arthrodesis by means of a finite element model. *Mathematical and Computer Modelling*, 50(5-6):680–694, 2009.

[81] S Dennis, R Watkins, MD Stephen, W Dillin, and D Springer. Comparison of disc space heights after anterior lumbar interbody fusion. *Spine (Phila Pa 1976)*, 14(8):876–878, 1989.

[82] Suzanne E L Detiger, Roel J W Hoogendoorn, Albert J. Van Der Veen, Barend J. Van Royen, Marco N. Helder, Gijsje H. Koenderink, and Theo H. Smit. Biomechanical and rheological characterization of mild intervertebral disc degeneration in a large animal model. *Journal of Orthopaedic Research*, 31(5):703–709, 2013.

[83] Nicole A DeVries Watson, Anup A Gandhi, Doug C Fredericks, Joseph D Smucker, and Nicole M Grosland. Sheep cervical spine biomechanics: a finite element study. *The Iowa orthopaedic journal*, 34:137–43, 2014.

[84] RA Deyo and JE Bass. Lifestyle and low-back pain: the influence of smoking and obesity. *Spine (Phila Pa 1976)*, 14(5):501–506, 1989.

[85] Marcel Dreischarf, Hendrik Schmidt, Michael Putzier, and Thomas Zander. Biomechanics of the L5-S1 motion segment after total disc replacement - Influence of iatrogenic distraction, implant positioning and preoperative disc height on the range of motion and loading of facet joints. *Journal of Biomechanics*, 48(12):3283–3291, 2015.

[86] DC Drucker and W Prager. Soil mechanics and plastic analysis of limit design. *Quarterly of Applied Mathematics*, 10:157–165, 1952.

[87] Sohei Ebara, James Iatridis, Lori A. Setton, Robert J. Foster, Van C. Mow, and Mark Weidenbaum. Tensile properties of nondegenerate human lumbar anulus fibrosus. *Spine*, 21(4):452–461, 1996.

[88] Robert Eberlein, Gerhard a. Holzapfel, and Christian a. J. Schulze-Bauer. An Anisotropic Model for Annulus Tissue and Enhanced Finite Element Analyses of Intact Lumbar Disc Bodies. *Computer Methods in Biomechanics and Biomedical Engineering*, 4(3):209–229, 2001.

[89] Dawn M Elliott, Chandra S Yerramalli, Jesse C Beckstein, John I Boxberger, Wade Johannessen, and Edward J Vresilovic. The effect of relative needle diameter in puncture and sham injection animal models of degeneration. *Spine*, 33(6):588–596, 2008.

[90] S Etebar and D W Cahill. Risk factors for adjacent-segment failure following lumbar fixation with rigid instrumentation for degenerative instability. *Journal of neurosurgery*, 90(Spine 2):163–169, 1999.

[91] M J Fagan, S Julian, D J Siddall, and a M Mohsen. Patient-specific spine models. Part 1: Finite element analysis of the lumbar intervertebral disc - A material sensitivity study. *Proceedings of the Institution of Mechanical Engineers, Part H: Journal of Engineering in Medicine*, 216:299–314, 2002.

[92] J C Fairbank and Paul B Pynsent. The Oswestry Disability Index. *Spine*, 25(22):2940–52; discussion 2952, 2000.

[93] Ahmad Faizan, Ali Kiapour, Ata M Kiapour, and Vijay K Goel. Biomechanical analysis of various footprints of transforaminal lumbar interbody fusion devices. *Journal of spinal disorders & techniques*, 27(4):E118–27, 2014.

[94] Alfonso Fantigrossi, Fabio Galbusera, Manuela Teresa Raimondi, Marco Sassi, and Maurizio Fornari. Biomechanical analysis of cages for posterior lumbar interbody fusion. *Medical engineering & physics*, 29(1):101–9, 2007.

[95] Stephen J. Ferguson, Keita Ito, and Lutz P. Nolte. Fluid flow and convective transport of solutes within the intervertebral disc. *Journal of Biomechanics*, 37(2):213–221, 2004.

[96] Christian Fisahn, Brittni Burgess, Joe Iwanaga, Jens R Chapman, Rod J Oskouian, and R Shane Tubbs. Ulf Fernström (1915âĂŞ1985) and his Contributions to the Development of Artificial Disc Replacements. *World Neurosurgery*, 98:278–280, 2017.

[97] M.R. Foster, M.J. Allen, J.E. Schoonmaker, H.A. Yuan, A. Kanazawa, S.A. Park, and B. Liu. Characterization of a developing lumbar arthrodesis in a sheep model with quantitative instability. *The spine journal*, 2:244–250, 2002.

[98] Andrew L. Freeman, Glenn R. Buttermann, Brian P. Beaubien, and Willie E. Rochefort. Compressive properties of fibrous repair tissue compared to nucleus and annulus. *Journal of Biomechanics*, 46(10):1714–1721, 2013.

[99] H Frei, T R Oxland, G C Rathonyi, and L P Nolte. The effect of nucleotomy on lumbar spine mechanics in compression and shear loading. *Spine*, 26(19):2080–2089, 2001.

[100] Peter Fritzell, Olle Hägg, Per Wessberg, Anders Nordwall, and the Swedish Lumbar Spine Study Group. Chronic Low Back Pain and Fusion : A Comparison of Three Surgical Techniques A Prospective Multicenter Randomized Study From the Swedish Lumbar Spine Study Group. *Spine (Phila Pa 1976)*, 27(11):1131–1141, 2002.

[101] Peter Fritzell, Per Wessberg, Anders Nordwall, and Swedish Lumbar Spine Study Group. 2001 Volvo Award Winner in Clinical Studies : Lumbar Fusion Versus Nonsurgical Treatment for Chronic Low Back Pain Lumbar Spine Study Group. *Spine (Phila Pa 1976)*, 26(23):2521–2534, 2001.

[102] W. Frobin, P. Brinckmann, M. Biggemann, M. Tillotson, and K. Burton. Precison measurement of disc height, vertebral height and sagittal plane displacement

from lateral radiographic views of the lumbar spine. *Clinical Biomechanics*, 12(SUPPL. 1):S1–S64, 1997.

[103] A Fujiwara, T H Lim, H S An, N Tanaka, C H Jeon, G B Andersson, and V M Haughton. The effect of disc degeneration and facet joint osteoarthritis on the segmental flexibility of the lumbar spine. *Spine*, 25(23):3036–3044, 2000.

[104] Fabio Galbusera, Chiara Maria Bellini, Federica Anasetti, Cristina Ciavarro, Alessio Lovi, and Marco Brayda-Bruno. Rigid and flexible spinal stabilization devices: A biomechanical comparison. *Medical Engineering and Physics*, 33(4):490–496, 2011.

[105] Fabio Galbusera, Antje Mietsch, Hendrik Schmidt, Hans-Joachim Wilke, and Cornelia Neidlinger-Wilke. Effect of intervertebral disc degeneration on disc cell viability: a numerical investigation. *Computer Methods in Biomechanics and Biomedical Engineering*, 16(3):328–337, 2013.

[106] Fabio Galbusera, Hendrik Schmidt, Cornelia Neidlinger-Wilke, Andreas Gottschalk, and Hans Joachim Wilke. The mechanical response of the lumbar spine to different combinations of disc degenerative changes investigated using randomized poroelastic finite element models. *European Spine Journal*, 20(4):563–571, 2011.

[107] Fabio Galbusera, Hendrik Schmidt, Cornelia Neidlinger-Wilke, and Hans-Joachim Wilke. The effect of degenerative morphological changes of the intervertebral disc on the lumbar spine biomechanics: a poroelastic finite element investigation. *Computer methods in biomechanics and biomedical engineering*, 14(March):729–739, 2011.

[108] Fabio Galbusera, Hendrik Schmidt, Jérôme Noailly, Andrea Malandrino, Damien Lacroix, Hans Joachim Wilke, and Aboulfazl Shirazi-Adl. Comparison of four methods to simulate swelling in poroelastic finite element models of intervertebral discs. *Journal of the Mechanical Behavior of Biomedical Materials*, 4(7):1234–1241, 2011.

[109] Fabio Galbusera, Hendrik Schmidt, and Hans-Joachim Joachim Wilke. Lumbar interbody fusion: A parametric investigation of a novel cage design with and without posterior instrumentation. *European Spine Journal*, 21(3):455–462, 2012.

[110] Fabio Galbusera, Marc Van Rijsbergen, Keita Ito, Jacques M. Huyghe, Marco Brayda-Bruno, and Hans Joachim Wilke. Ageing and degenerative changes of the intervertebral disc and their impact on spinal flexibility. *European Spine Journal*, 23(SUPPL. 3):324–332, 2014.

[111] Seth C. Gamradt and Jeffrey C. Wang. Lumbar disc arthroplasty. *Spine Journal*, 5(1):95–103, 2005.

[112] Ralph E. Gay, Brice Ilharreborde, Kristin Zhao, Emir Boumediene, and Kai Nan An. The effect of loading rate and degeneration on neutral region motion in human cadaveric lumbar motion segments. *Clinical Biomechanics*, 23(1):1–7, 2008.

[113] Mark Gerber, Neil R Crawford, Robert H Chamberlain, Mary S Fifield, Jean-Charles LeHuec, and Curtis A Dickman. Biomechanical assessment of anterior lumbar interbody fusion with an anterior lumbosacral fixation screw-plate: comparison to stand-alone anterior lumbar interbody fusion and anterior lumbar interbody fusion with pedicle screws in an unstable human cadaver. *Spine*, 31(7):762–768, 2006.

[114] Liesbet Geris, Alf Gerisch, Jos Vander Sloten, Rüdiger Weiner, and Hans Van Oosterwyck. Angiogenesis in bone fracture healing: a bioregulatory model. *Journal of theoretical biology*, 251(1):137–58, mar 2008.

[115] Zoher Ghogawala, Daniel K Resnick, William C Watters, Praveen V Mummaneni, Andrew T Dailey, Tanvir F Choudhri, Jason C Eck, Alok Sharan, Michael W Groff, Jeffrey C Wang, Sanjay S Dhall, and Michael G Kaiser. Guideline update for the performance of fusion procedures for degenerative disease of the lumbar spine. Part 2: Assessment of functional outcome following lumbar fusion. *Journal of neurosurgery. Spine*, 21(1):7–13, 2014.

[116] P. Gillet. The Fate of the Adjacent Motion Segments After Lumbar Fusion. *Clinical Spine Surgery*, 16(4):338–345, 2003.

[117] John Glaser, Mark Stanley, Hutha Sayre, Joyce Woody, Ernest Found, and Kevin Spratt. A 10-year follow-up evaluation of lumbar spine fusion with pedicle screw fixation. *Spine*, 28(13):1390–1395, 2003.

[118] VK Goel, BT Monroe, LG Gilbertson, and P Brinckmann. Interlaminar Shear Stresses and Laminae Separation in a Disc: Finite Element Analysis of the L3-L4 Motion Segment Subjected to Axial Compressive Loads. *Spine*, 20(6):689–698, 1995.

[119] VK Goel, MM Panjabi, AG Patwardhan, AP Dooris, H Serhan, , and American Society for Testing Materials. Test protocols for evaluation of spinal implants. *Journal of Bone and Joint Surgery American*, 88(Suppl 2):103–109, 2006.

[120] Sabrina A Gonzalez-Blohm, James J Doulgeris, Kamran Aghayev, William E Lee, Andrey Volkov, and Frank D Vrionis. Biomechanical analysis of an interspinous

fusion device as a stand-alone and as supplemental fixation to posterior expandable interbody cages in the lumbar spine. *Journal of neurosurgery of the Spine*, 20:209–219, 2014.

[121] K Goto, N Tajima, E Chosa, K Totoribe, S Shinichiro, and H Kukori. Mechanical analysis of the lumbar vertebrae in a three-dimensional finite element method model in which intradiscal pressure in the nucleus pulposus was used to establish the model. *Journal of orthopaedic science*, 8:577–584, 2003.

[122] J P Grant, T R Oxland, and M F Dvorak. Mapping the structural properties of the lumbosacral vertebral endplates. *Spine*, 26(8):889–896, 2001.

[123] J. P. Grant, Thomas R. Oxland, Marcel F. Dvorak, and Charles G. Fisher. The effects of bone density and disc degeneration on the structural property distributions in the lower lumbar vertebral endplates. *Journal of Orthopaedic Research*, 20(5):1115–1120, 2002.

[124] J N Grauer, J S Erulkar, T C Patel, and M M Panjabi. Biomechanical evaluation of the New Zealand white rabbit lumbar spine: a physiologic characterization. *European spine journal*, 9(3):250–255, 2000.

[125] Michael W Groff, Andrew T Dailey, Zoher Ghogawala, Daniel K Resnick, William C Watters, Praveen V Mummaneni, Tanvir F Choudhri, Jason C Eck, Alok Sharan, Jeffrey C Wang, Sanjay S Dhall, and Michael G Kaiser. Guideline update for the performance of fusion procedures for degenerative disease of the lumbar spine. Part 12: pedicle screw fixation as an adjunct to posterolateral fusion. *Journal of neurosurgery. Spine*, 21(1):75–8, 2014.

[126] Nicole M Grosland and Vijay K Goel. Vertebral endplate morphology follows bone remodeling principles. *Spine*, 32(23):E667–E673, 2007.

[127] H Gruler and BD Bültmann. Analysis of cell movement. *Blood Cells*, 10:61–77, 1984.

[128] W. Y. Gu, X. G. Mao, R. J. Foster, M. Weidenbaum, V. C. Mow, and B. A. Rawlins. The anisotropic hydraulic permeability of human lumbar anulus fibrosus: Influence of age, degeneration, direction, and water content. *Spine*, 24(23):2449–2455, 1999.

[129] Weiyong Gu, Qiaoqiao Zhu, Xin Gao, and Mark D. Brown. Simulation of the Progression of Intervertebral Disc Degeneration Due to Decreased Nutritional Supply. *Spine*, 39(24):E1411–E1417, 2014.

[130] Yabo Guan, Narayan Yoganandan, Jason Moore, Frank A. Pintar, Jiangyue Zhang, Dennis J. Maiman, and Purushottam Laud. Moment-rotation responses

of the human lumbosacral spinal column. *Journal of Biomechanics*, 40:1975–1980, 2007.

[131] Sarah E. Gullbrand, Beth G. Ashinsky, John T. Martin, Stephen Pickup, Lachlan J. Smith, Robert L. Mauck, and Harvey E. Smith. Correlations between quantitative T2 and T1?? MRI, mechanical properties and biochemical composition in a rabbit lumbar intervertebral disc degeneration model. *Journal of Orthopaedic Research*, 34(8):1382–1388, 2016.

[132] Richard D. Guyer, Paul C. McAfee, Robert J. Banco, Fabian D. Bitan, Andrew Cappuccino, Fred H. Geisler, Stephen H. Hochschuler, Richard T. Holt, Louis G. Jenis, Mohamed E. Majd, John J. Regan, Scott G. Tromanhauser, Douglas C. Wong, and Scott L. Blumenthal. Prospective, randomized, multicenter Food and Drug Administration investigational device exemption study of lumbar total disc replacement with the CHARITÉ artificial disc versus lumbar fusion: Five-year follow-up. *Spine Journal*, 9(5):374–386, 2009.

[133] Bahe Hachem, Carl-Eric Aubin, and Stefan Parent. Porcine spine finite element model: a complementary tool to experimental scoliosis fusionless instrumentation. *European Spine Journal*, 26(6):1610–1617, 2017.

[134] Lars Hackenberg, Henry Halm, Viola Bullmann, Volker Vieth, Marc Schneider, and Ulf Liljenqvist. Transforaminal lumbar interbody fusion: A safe technique with satisfactory three to five year results. *European Spine Journal*, 14(6):551–558, 2005.

[135] M. Haefeli, F. Kalberer, D. Saegesser, A. G. Nerlich, N. Boos, and G. Paesold. The course of macroscopic degeneration in the human lumbar intervertebral disc. *European Cells and Materials*, 31(14):1522–1531, 2006.

[136] Scott Haldeman and Simon Dagenais. What have we learned about the evidence-informed management of chronic low back pain? *The spine journal : official journal of the North American Spine Society*, 8(1):266–277, 2008.

[137] Kap Soo Han, Antonius Rohlmann, Seok Jo Yang, Byeong Sam Kim, and Tae Hong Lim. Spinal muscles can create compressive follower loads in the lumbar spine in a neutral standing posture. *Medical Engineering and Physics*, 33(4):472–478, 2011.

[138] B M Harris, A S Hilibrand, P E Savas, A Pellegrino, A R Vaccaro, S Siegler, and T J Albert. Transforaminal lumbar interbody fusion: the effect of various instrumentation techniques on the flexibility of the lumbar spine. *Spine*, 29(4):E65–70, 2004.

[139] Robert A. Hartman, Kevin M. Bell, Bichun Quan, Yao Nuzhao, Gwendolyn A. Sowa, and James D. Kang. Needle puncture in rabbit functional spinal units alters rotational biomechanics. *Journal of spinal disorders & techniques*, 28(3):E146–E153, 2015.

[140] Dennis Hey, Eugene Tze Chun Lau, Joel-Louis Lim, Denise Choong, Chuen-Seng Tan, Gabriel Ka-Po Liu, and Hee-Kit Wong. Slump sitting X-ray of the lumbar spine is superior to the conventional flexion view in assessing lumbar spine instability. *The Spine Journal*, 17(3):360–368, 2016.

[141] R Hibbs. An operation for progressive spinal deformities. *Clinical Orthopaedics and Related Research*, 35:4–8, 1964.

[142] Alan S. Hilibrand and Matthew Robbins. Adjacent segment degeneration and adjacent segment disease: The consequences of spinal fusion? *Spine Journal*, 4(6 SUPPL.):190–194, 2004.

[143] S. Holm. Pathophysiology of disc degeneration. *Acta Orthopaedica Scandinavica*, Supplement:13–15, 1993.

[144] G. A. Holzapfel, C. A J Schulze-Bauer, G. Feigl, and P. Regitnig. Single lamellar mechanics of the human lumbar anulus fibrosus. *Biomechanics and Modeling in Mechanobiology*, 3(3):125–140, 2005.

[145] Gerhard A. Holzapfel and Michael Stadler. Role of facet curvature for accurate vertebral facet load analysis. *European Spine Journal*, 15(6):849–856, 2006.

[146] Jasper Homminga, Rene Aquarius, Vera E. Bulsink, Christiaan T J Jansen, and Nico Verdonschot. Can vertebral density changes be explained by intervertebral disc degeneration? *Medical Engineering and Physics*, 34(4):453–458, 2012.

[147] Mitchell Hortin, Sarah Graham, Kara Boatwright, Peter Hyoung, and Anton Bowden. Transversely isotropic material characterization of the human anterior longitudinal ligament. *Journal of the Mechanical Behavior of Biomedical Materials*, 45:75–82, 2015.

[148] Mitchell S. Hortin and Anton E. Bowden. Quantitative comparison of ligament formulation and pre-strain in finite element analysis of the human lumbar spine. *Computer Methods in Biomechanics and Biomedical Engineering*, 19(14):1505–1518, 2016.

[149] Damian Hoy, Lyn March, Peter Brooks, Anthony Woolf, Fiona Blyth, Theo Vos, and Rachelle Buchbinder. Measuring the global burden of low back pain. *Best Practice and Research: Clinical Rheumatology*, 24(2):155–165, 2010.

[150] Ching Chi Hsu. Shape optimization for the subsidence resistance of an interbody device using simulation-based genetic algorithms and experimental validation. *Journal of Orthopaedic Research*, 31(7):1158–1163, 2013.

[151] Dueng-Yuan Hueng, Tzu-Tsao Chung, Wen-Hsien Chuang, Chi-Pin Hsu, Kuan-Nien Chou, and Shang-Chih Lin. Biomechanical effects of cage positions and facet fixation on initial stability of the anterior lumbar interbody fusion motion segment. *The Spine Journal*, 39(13):E770–6, 2014.

[152] R. Huiskes, W. D. Van Driel, P. J. Prendergast, and K. Søballe. A biomechanical regulatory model for periprosthetic fibrous-tissue differentiation. *Journal of Materials Science: Materials in Medicine*, 8(12):785–788, 1997.

[153] R Huiskes, H. Weinans, H.J. Grootenboer, M. Dalstra, B. Fudala, and T.J. Slooff. Adaptative bone-remodeling theory applied to prosthetic-design analysis. *Journal of Biomechanics*, 20(11):1130–1150, 1987.

[154] RIK Huiskes, HARRIE Weinans, and BERT VAN Rietbergen. The relationship between stress shielding and bone resorption around total hip stems and the effects of flexible materials. *Clinical Orthopaedics and Related Research*, 274:124–134, 1992.

[155] S C Humphreys, S D Hodges, a G Patwardhan, J C Eck, R B Murphy, and L a Covington. Comparison of posterior and transforaminal approaches to lumbar interbody fusion. *Spine*, 26(5):567–571, 2001.

[156] J C Iatridis, M Weidenbaum, L a Setton, and V C Mow. Is the nucleus pulposus a solid or a fluid? Mechanical behaviors of the nucleus pulposus of the human intervertebral disc. *Spine*, 21(10):1174–1184, 1996.

[157] James C. Iatridis, Steven B. Nicoll, Arthur J. Michalek, Benjamin A. Walter, and Michelle S. Gupta. Role of biomechanics in intervertebral disc degeneration and regenerative therapies: What needs repairing in the disc and what are promising biomaterials for its repair? *Spine Journal*, 13(3):243–262, 2013.

[158] James C. Iatridis, Lori A. Setton, Robert J. Foster, Bernard A. Rawlins, Mark Weidenbaum, and Van C. Mow. Degeneration affects the anisotropic and nonlinear behaviors of human anulus fibrosus in compression. *Journal of Biomechanics*, 31(6):535–544, 1998.

[159] James C. Iatridis, Lori A. Setton, Mark Weidenbaum, and Van C. Mow. The viscoelastic behavior of the non-degenerate human lumbar nucleus pulposus in shear. *Journal of Biomechanics*, 30(10):1005–1013, 1997.

[160] H Inoue and T Takeda. Three-dimensional observation of collagen framework of lumbar intervertebral discs. *Acta orthopaedica Scandinavica*, 46(6):949–956, 1975.

[161] N Inoue and Aa Espinoza Orias. Biomechanics of intervertebral disc degeneration. *Orthop Clin North Am*, 42(4):487–499, 2011.

[162] Insituto Nacional de Estadística. Encuesta europea de salud en España, 2014.

[163] Hanna Isaksson, Corrinus C. van Donkelaar, Rik Huiskes, and Keita Ito. A mechano-regulatory bone-healing model incorporating cell-phenotype specific activity. *Journal of Theoretical Biology*, 252(2):230–246, 2008.

[164] Hanna Isaksson, Wouter Wilson, Corrinus C. van Donkelaar, Rik Huiskes, and Keita Ito. Comparison of biophysical stimuli for mechano-regulation of tissue differentiation during fracture healing. *Journal of Biomechanics*, 39(8):1507–1516, 2006.

[165] M.F. Ivicsics, N.E. Bishop, K. Puschel, M.M. Morlock, and G. Huber. Increase in facet joint loading after nucleotomy in the human lumbar spine. *Journal of Biomechanics*, 47:1712–1717, 2014.

[166] Timothy M. Jackman, Amira I. Hussein, Alexander M. Adams, Kamil K. Makhnejia, and Elise F. Morgan. Endplate deflection is a defining feature of vertebral fracture and is associated with properties of the underlying trabecular bone. *Journal of Orthopaedic Research*, 32(7):880–886, 2014.

[167] Alicia R Jackson, Chun-Yuh C Huang, Mark D Brown, and Wei Yong Gu. 3D Finite element analysis of nutrient distributions and cell viability in the intervertebral disc: Effects of deformation and degeneration. *Journal of Biomechanical Engineering*, 133(9):091006, 2011.

[168] Wilco Jacobs, Alexander Tuschel, Kleuver Marinus De, Cumhur Oner, Wilco Peul, and A J Verbout. Total disc replacement for chronic low-back pain. *Jacobs.Wilco., Tuschel.Alexander., de Kleuver.Marinus., Oner.Cumhur., Peul.Wilco., Verbout.AJ.Total disc.replacement.for.chronic.low back pain.Cochrane Database of Systematic Reviews: Protocols.2010.Issue.1 John.Wiley.& Sons., Ltd.Chichester, UK DOI.: 1*, 38(1):24–26, 2012.

[169] Marcus Jäger, Konrad Seller, Peter Raab, Rüdiger Krauspe, and Alexander Wild. Clinical outcome in monosegmental fusion of degenerative lumbar instabilities:instrumented versus non-instrumented. *Medical science monitor : international medical journal of experimental and clinical research*, 9(7):CR324–CR327, 2003.

[170] Muhammad Hilmi Jalil, Muhammad Hazli Mazlan, and Mitsugu Todo. Biomechanical Comparison of Polymeric Spinal Cages Using Ct Based Finite Element Method. *International Journal of Bioscience, Biochemistry and Bioinformatics*, 7(2):110–117, 2017.

[171] Yong Jun Jin, Young Eun Kim, Jung Ho Seo, Hae Won Choi, and Tae Ahn Jahng. Effects of rod stiffness and fusion mass on the adjacent segments after floating mono-segmental fusion: A study using finite element analysis. *European Spine Journal*, 22(5):1066–1077, 2013.

[172] Wade Johannessen and Dawn M Elliott. Effects of degeneration on the biphasic material properties of human nucleus pulposus in confined compression. *Spine*, 30(24):E724–E729, 2005.

[173] Alison C. Jones and Ruth K. Wilcox. Finite element analysis of the spine: Towards a framework of verification, validation and sensitivity analysis. *Medical Engineering and Physics*, 30(10):1287–1304, 2008.

[174] E Kääpä, S Holm, X Han, T Takala, V Kovanen, and H Vanharanta. Collagens in the injured porcine intervertebral disc. *Journal of Orthopaedic Research*, 12(1):93–102, 1994.

[175] Frank Kandziora, Georg Schollmeier, Matti Scholz, Jan Schaefer, Alexandra Scholz, Gerhard Schmidmaier, Ralf Schröder, Herman Bail, Georg Duda, Thomas Mittlmeier, and Norbert P Haas. Influence of cage design on interbody fusion in a sheep cervical spine model. *Journal of neurosurgery*, 96(3 Suppl):321–32, 2002.

[176] Heesuk Kang, Scott J Hollister, Frank La Marca, Paul Park, and Chia-Ying Lin. Porous biodegradable lumbar interbody fusion cage design and fabrication using integrated global-local topology optimization with laser sintering. *Journal of biomechanical engineering*, 135(10):101013–8, 2013.

[177] D. J. Kelly and P. J. Prendergast. Mechano-regulation of stem cell differentiation and tissue regeneration in osteochondral defects. *Journal of Biomechanics*, 38(7):1413–1422, 2005.

[178] Nicola Kelly, Noel M. Harrison, Pat McDonnell, and J. Patrick McGarry. An experimental and computational investigation of the post-yield behaviour of trabecular bone during vertebral device subsidence. *Biomechanics and Modeling in Mechanobiology*, 12(4):685–703, 2013.

[179] Annette Kettler, F. Rohlmann, C. Ring, C. Mack, and H. J. Wilke. Do early stages of lumbar intervertebral disc degeneration really cause instability? Evaluation of an in vitro database. *European Spine Journal*, 20(4):578–584, 2011.

[180] A Kiapour, MA Kiapour, M Kodigudla, GM Hill, S Mishra, and VK Goel. A Biomechanical Finite Element Study of Subsidence and Migration Tendencies in Stand-Alone Fusion Procedures âĂŞ Comparison of an In Situ Expandable Device with a Rigid Device. *Journal of Spine*, 01(04):1–5, 2013.

[181] Dong Won Kim, Hyoung Joon Chun, and Sang Kook Lee. Percutaneous needle puncture technique to create a rabbit model with traumatic degenerative disk disease. *World Neurosurgery*, 84(2):438–445, 2015.

[182] Keun Su Kim, S Tim Yoon, Jun Li, Jin Soo Park, and William C Hutton. Disc degeneration in the rabbit: a biochemical and radiological comparison between four disc injury models. *Spine*, 30(1):33–37, 2005.

[183] Ki-Tack Kim, Sang-Hun Lee, Young-Ho Lee, Sung-Chul Bae, and Kyung-Soo Suk. Clinical outcomes of 3 fusion methods through the posterior approach in the lumbar spine. *Spine (Phila Pa 1976)*, 31(12):1351–1357, 2006.

[184] Y E Kim, V K Goel, J N Weinstein, and T H Lim. Effect of disc degeneration at one level on the adjacent level in axial mode. *Spine*, 16(3):331–335, 1991.

[185] Young Kim. Finite element analysis of anterior lumbar interbody fusion: threaded cylindrical cage and pedicle screw fixation. *Spine*, 32(23):2558–68, 2007.

[186] WH Kirkaldy-Willis and HF Farfan. Instability of the lumbar spine. *Clinical orthopaedics and related research*, 165:110–123, 1982.

[187] David L. Kopperdahl and Tony M. Keaveny. Yield strain behavior of trabecular bone. *Journal of Biomechanics*, 31(7):601–608, 1998.

[188] Francisco M Kovacs, Gerard Urrútia, and José D. Alarcón. Surgery Versus Conservative Treatment for symptomatic lumbar spinal stenosis. *Spine (Phila Pa 1976)*, 36(20):1335–1351, 2011.

[189] J A Kozak, A E Heilman, and J P O'Brien. Anterior lumbar fusion options. Technique and graft materials. *Clinical orthopaedics and related research*, 300:45–51, 1994.

[190] RM Kretzer, C Molina, N Hu, H Umekoji, AA Baaj, H Serhan, and BW Cunningham. A comparative Biomechanical analysis of stand alone versus facet screw and pedicle screw augmented lateral interbody arthrodesis: an in vitro human cadaveric model. *Clinical Spine Surgery*, 29(7):336–343, 2016.

[191] Matthijs R Krijnen, Margriet G Mullender, Theo H Smit, Vincent Everts, and Paul I J M Wuisman. Radiographic, histologic, and chemical evaluation of bioresorbable 70/30 poly-L-lactide-CO-D, L-lactide interbody fusion cages in a goat model. *Spine*, 31(14):1559–1567, 2006.

[192] M. Krismer, C. Haid, H. Behensky, P. Kapfinger, F. Landauer, and F. Rachbauer. Motion in lumbar functional spine units during side bending and axial rotationmoments depending on the degree of degeneration. *Spine (Phila Pa 1976)*, 25(16):2020–2027, 2000.

[193] Markus W Kroeber, Frank Unglaub, Haili Wang, Carsten Schmid, Marc Thomsen, Andreas Nerlich, and Wiltrud Richter. New in vivo animal model to create intervertebral disc degeneration and to investigate the effects of therapeutic strategies to stimulate disc regeneration. *Spine*, 27(23):2684–2690, 2002.

[194] Malhar N. Kumar, Frederic Jacquot, and Hamilton Hall. Long-term follow-up of functional outcomes and radiographic changes at adjacent levels following lumbar spine fusion for degenerative disc disease. *European Spine Journal*, 10(4):309–313, 2001.

[195] Steven M. Kurtz and John N. Devine. PEEK biomaterials in trauma, orthopedic, and spinal implants. *Biomaterials*, 28(32):4845–4869, 2007.

[196] SD Kuslich, CL Ulstrom, SL Griffith, JW Ahern, and JD Dowdle. The Bagby and Kuslich method of lumbar interbody fusion. History, techniques, and 2-year follow-up results of a United States prospective, multicenter trial. *Spine (Phila Pa 1976)*, 23(11):1267–78, 1998.

[197] D Lacroix, P J Prendergast, G Li, and D Marsh. Biomechanical model to simulate tissue differentiation and bone regeneration: application to fracture healing. *Medical and Biological Engineering and Computing*, 40(1):14–21, 2002.

[198] Nadine Michele Lalonde, Yvan Petit, Carl Eric Aubin, Eric Wagnac, and Pierre Jean Arnoux. Method to geometrically personalize a detailed finite-element model of the Spine. *IEEE Transactions on Biomedical Engineering*, 60(7):2014–2021, 2013.

[199] Sebastian Lauber, Tobias Ludger Schulte, Ulf Liljenqvist, Henry Halm, and Lars Hackenberg. Clinical and radiologic 2-4-year results of transforaminal lumbar interbody fusion in degenerative and isthmic spondylolisthesis grades 1 and 2. *Spine*, 31(15):1693–1698, 2006.

[200] WC Lauerman, RC Platenberg, JE Cain, and VF Deeney. Age-Related Disk Degeneration: Preliminary Report of a Naturally Occurring Baboon Model. *Journal of Spinal Disorders*, 5:170–174, 1992.

[201] Cory J Laws, Dezba G Coughlin, Jeffrey C Lotz, Hassan a Serhan, and Serena S Hu. Direct Lateral Approach to Lumbar Fusion is a Biomechanically Equivalent Alternative to the Anterior Approach: An in vitro Study. *Spine*, 37(10):819–825, 2012.

[202] Tien V Le, Ali a. Baaj, Elias Dakwar, Clinton J Burkett, Gisela Murray, Donald a. Smith, and Juan S Uribe. Subsidence of Polyetheretherketone Intervertebral Cages in Minimally Invasive Lateral Retroperitoneal Transpsoas Lumbar Interbody Fusion. *Spine*, 37(14):1268–1273, 2012.

[203] Christine Lyn Le Maitre, Anthony J Freemont, and Judith Alison Hoyland. The role of interleukin-1 in the pathogenesis of human intervertebral disc degeneration. *Arthritis research & therapy*, 7(4):R732–R745, 2005.

[204] J. C. Leahy and D. W L Hukins. Viscoelastic properties of the nucleus pulposus of the intervertebral disk in compression. *Journal of Materials Science: Materials in Medicine*, 12(8):689–692, 2001.

[205] Steven K. Leckie, Bernard P. Bechara, Robert A. Hartman, Gwendolyn A. Sowa, Barrett I. Woods, Joao P. Coelho, William T. Witt, Qing D. Dong, Brent W. Bowman, Kevin M. Bell, Nam V. Vo, Bing Wang, and James D. Kang. Injection of AAV2-BMP2 and AAV2-TIMP1 into the nucleus pulposus slows the course of intervertebral disc degeneration in an in vivo rabbit model. *Spine Journal*, 12(1):7–20, 2012.

[206] KK Lee and EC Teo. Material sensitivity study on lumbar motion segment (L2-L3) under sagittal plane loadings using probabilistic method. *Journal of Spinal Disorders & Techniques*, 18(2):163–170, 2005.

[207] HS Lin, YK Liu, G Ray, and P Nikravesh. Systems identification for material properties of the intervertebral joint. *Journal of Biomechanics*, 11(1-2):1–14, 1978.

[208] S J Lipson and H Muir. Vertebral osteophyte formation in experimental disc degeneration. Morphologic and proteoglycan changes over time. *Arthritis and rheumatism*, 23(3):319–24, 1980.

[209] Xilin Liu, Jun Ma, Paul Park, Xiaodong Huang, Ning Xie, and Xiaojian Ye. Biomechanical comparison of multilevel lateral interbody fusion with and without supplementary instrumentation: a three-dimensional finite element study. *BMC Musculoskeletal Disorders*, 18(1):63, 2017.

[210] C. C. Lo, K. J. Tsai, Z. C. Zhong, Shih-Hao Chen, and C. Hung. Biomechanical differences of Coflex-F and pedicle screw fixation in stabilization of TLIF or ALIF condition - A finite element study. *Computer methods in biomechanics and biomedical engineering*, 14(11):947–956, 2011.

[211] JC. Lotz, OK. Colliou, JR. Chin, NA. Duncan, and E. Liebenberg. Volvo Award Winner in Biomechanical Studies. Compresssion-Induced Degeneration of the Intervertebral Disc: A in Vivo Mouse Model and Finite-Element Study. *Spine*, 23(23):2493–2506, 1998.

[212] J. Grafton Love. Protruded Intervertebral Disc (Fibrocartilage). *Proceedings of the Royal Society of Medicine*, 32(8):1697–1721, 1939.

[213] Thomas G Lowe, Shukor Hashim, Lucas a Wilson, Michael F O'Brien, David a B Smith, Molly J Diekmann, and Julie Trommeter. A biomechanical study of regional endplate strength and cage morphology as it relates to structural interbody support. *Spine*, 29(21):2389–2394, 2004.

[214] Y M Lu, W C Hutton, and V M Gharpuray. Can variations in intervertebral disc height affect the mechanical function of the disc? *Spine*, 21(19):2208–2217, 1996.

[215] K Lundon and K Bolton. Structure and function of the lumbar IVD in health, aging, and pathologic conditions. *Journal of orthopaedic & sports physical therapy*, 31(6):291–306, 2001.

[216] Tiruveedhula S. Madhu. Posterior and anterior lumbar interbody fusion. *Current Orthopaedics*, 22(6):406–413, 2008.

[217] Masoud Malakoutian, David Volkheimer, John Street, Marcel F.S. Dvorak, Hans-Joachim Wilke, and Thomas R. Oxland. Do in vivo kinematic studies provide insight into the degeneration of adjacent segments? âĂŞ a literature review. *Eur Spine J*, 24:1865–1881, 2015.

[218] Andrea Malandrino, J Noailly, and D Lacroix. Regional annulus fibre orientations used as a tool for the calibration of lumbar intervertebral disc finite element models. *Computer Methods in Biomechanics and Biomedical Engineering*, January:37–41, 2013.

[219] Andrea Malandrino, José M Pozo, Isaac Castro-Mateos, Alejandro F Frangi, Marc M van Rijsbergen, Keita Ito, Hans-Joachim Wilke, Tien Tuan Dao, Marie-Christine Ho Ba Tho, and Jérôme Noailly. On the relative relevance of subject-specific geometries and degeneration-specific mechanical properties for the study of cell death in human intervertebral disk models. *Frontiers in bioengineering and biotechnology*, 3(February):5, 2015.

[220] Nikolaos Maniadakis and Alastair Gray. The economic burden of back pain in the UK. *Pain*, 84(1):95–103, 2000.

[221] F Marchand and AM Ahmed. Investigation of the laminate structure of lumbar disc annulus fibrosus. *Spine (Phila Pa 1976)*, 15:102–410, 1990.

[222] Luis Marchi, Nitamar Abdala, Leonardo Oliveira, Rodrigo Amaral, Etevaldo Coutinho, and Luiz Pimenta. Stand-Alone Lateral Interbody Fusion for the Treatment of Low-Grade Degenerative Spondylolisthesis. *The Scientific World Journal*, 2012:1–7, 2012.

[223] Luis Marchi, Nitamar Abdala, Leonardo Oliveira, Rodrigo Amaral, Etevaldo Coutinho, and Luiz Pimenta. Radiographic and clinical evaluation of cage subsidence after stand-alone lateral interbody fusion. *Journal of neurosurgery. Spine*, 19:110–1188, 2013.

[224] Giacomo Marini and Stephen J. Ferguson. Modelling the influence of heterogeneous annulus material property distribution on intervertebral disk mechanics. *Annals of Biomedical Engineering*, 42(8):1760–1772, 2014.

[225] J.C. Maroon. Current concepts in minimally invasive discectomy. *Neurosurgery*, 51:S137–145, 2002.

[226] BI Martin, RA Deyo, SK Mirza, JA Turner, BA Comstock, W Hollingworth, and SD Sullivan. Expenditures and health status among adults with back and neck problems. *Journal of the American Medical Association*, 299(6):656–664, 2008.

[227] Marius Marusteri and Vladimir Bacarea. Comparing groups for statistical differences: how to choose the right statistical test? *Biochemia Medica*, 20(1):15–32, 2010.

[228] Christopher J Massey, Corrinus C van Donkelaar, Edward Vresilovic, Antonios Zavaliangos, and Michele Marcolongo. Effects of aging and degeneration on the human intervertebral disc during the diurnal cycle: a finite element study. *Journal of orthopaedic research*, 30(1):122–128, jan 2012.

[229] Muhammad Hazli Mazlan, Mitsugu Todo, Hiromitsu Takano, and Ikuho Yonezawa. Effect of Cage Insertion Orientation on Stress Profiles and Subsidence Phenomenon in Posterior Lumbar Interbody Fusion. *Journal of medical and bioengineering*, 5(2):93–97, 2016.

[230] Paul C McAfee, Bryan Cunningham, Gwen Holsapple, Karen Adams, Scott Blumenthal, Richard D Guyer, Anton Dmietriev, James H. Maxwell, John J Regan, and Jorge Isaza. A prospective, randomized, multicenter food and drug administration investigational device exemption study of lumbar total disc replacement with the Charité artificial disc versus lumbar fusion. Part II: Evaluation of radiographic outcomes and correlation. *Spine (Phila Pa 1976)*, 30(14):1576–1583, 2005.

[231] Matthew R McCann and Cheryle A Séguin. Notochord Cells in Intervertebral Disc Development and Degeneration. *Journal of developmental biology*, 4(1):1–18, 2016.

[232] Matthew J. McGirt, Sandro Eustacchio, Peter Varga, Milorad Vilendecic, Martin Trummer, Miro Gorensek, Darko Ledic, and Eugene J. Carragee. A Prospective Cohort Study of Close Interval Computed Tomography and Magnetic Res-

onance Imaging After Primary Lumbar Discectomy. *Spine*, 34(19):2044–2051, 2009.

[233] DS McNally and Michael A Adams. Internal intervertebral disc mechanics as revealed by stress profilometry. *Spine (Phila Pa 1976)*, 17:66–73, 1992.

[234] Gerdine J M Meijer, Jasper Homminga, Albert G Veldhuizen, and Gijsbertus J Verkerke. Influence of interpersonal geometrical variation on spinal motion segment stiffness: implications for patient-specific modeling. *Spine*, 36(14):E929–E935, 2011.

[235] C. Mercer, M. Y. He, R. Wang, and A. G. Evans. Mechanisms governing the inelastic deformation of cortical bone and application to trabecular bone. *Acta Biomaterialia*, 2(1):59–68, 2006.

[236] MA Meyers and KK Chawla. *Mechanical behavior of materials*. Cambridge University Press, 2009.

[237] M Mimura, MM Panjabi, TR Oxland, Joseph J. Crisco, I Yamamoto, and A Vasavada. Disc degeneration affects the multidirectional flexibility of the lumbar spine. *Spine (Phila Pa 1976)*, 19(12):1371–1380, 1994.

[238] Kei Miyamoto, Koichi Masuda, Jesse G. Kim, Nozomu Inoue, Koji Akeda, G. B J Andersson, and Howard S. An. Intradiscal injections of osteogenic protein-1 restore the viscoelastic properties of degenerated intervertebral discs. *Spine Journal*, 6(6):692–703, 2006.

[239] S Mizuno, S Watanabe, and T Takagi. Hydrostatic fluid pressures promotes cellularity and proliferation of human dermal fibroblast in a three-dimensional collagen gel/sponge. *Biochemical Engineering Journal*, 20:203–208, 2004.

[240] Seung Myung Moon, Aditya Ingalhalikar, Jason M. Highsmith, and Alexander R. Vaccaro. Biomechanical rigidity of an all-polyetheretherketone anterior thoracolumbar spinal reconstruction construct: an in vitro corpectomy model. *Spine Journal*, 9(4):330–335, 2009.

[241] V. Moramarco, A. Pérez del Palomar, C. Pappalettere, and M. Doblaré. An accurate validation of a computational model of a human lumbosacral segment. *Journal of Biomechanics*, 43(2):334–342, 2010.

[242] Pedro Moreo, José Manuel García-Aznar, and Manuel Doblaré. Bone ingrowth on the surface of endosseous implants. Part 1: Mathematical model. *Journal of Theoretical Biology*, 260(1):1–12, 2009.

[243] M. G. Mullender and R Huiskes. Proposal for the regulatory mechanism of Wolff's law. *Journal of orthopaedic research : official publication of the Orthopaedic Research Society*, 13(4):503–12, jul 1995.

[244] Praveen Mummaneni, Sanjay S Dhall, jason C Eck, Michael W Groff, Zoher Ghogawala, William C Watters iii, AnDreW Dailey, Daniel Resnick, Tanvir Choudhri, Alok Sharan, jeffrey C Wang, and Michael G Kaiser. Guideline update for the performance of fusion procedures for degenerative disease of the lumbar spine. Part 11: Interbody techniques for lumbar fusion. *J Neurosurg Spine J Neurosurg: Spine*, 21(21):67–74, 2014.

[245] A. Nachemson, T. Lewin, A. Maroudas, and MA. Freeman. In vitro diffusion of dye through the end-plates and annulus fibrosus of human lumbar intervertebral discs. *Acta Orthopaedica Scandinavica*, 41(6):589–607, 1970.

[246] T. Nakamura, T. Okada, M. Endo, T. Kadomatsu, T. Taniwaki, A. Sei, H. Odagiri, T. Masuda, T. Fujimoto, Y. Oike, and H. Mizuta. Angiopoietin-like protein 2 induced by mechanical stress accelerates degeneration and hypertrophy of the ligamentum flavum in lumbar spinal canal stenosis. *Plos one*, 9:e85542, 2014.

[247] R. Nasser, S. Yadla, M.G. Maltenfort, J.S. Harrop, D.G. Anderson, A.R. Vaccaro, A.D. Sharan, and J.K. Ratliff. Complications in spine surgery. *Journal of neurosurgery. Spine*, 13:144–157, 2010.

[248] R. N. Natarajan, J. R. Williams, S. A. Lavender, and G. B J Andersson. Poro-elastic finite element model to predict the failure progression in a lumbar disc due to cyclic loading. *Computers and Structures*, 85(11-14):1142–1151, 2007.

[249] Raghu N. Natarajan, Jamie R. Williams, and Gunnar B.J. Andersson. Modeling changes in intervertebral disc mechanics with degeneration. *Journal of Bone and Joint Surgery*, 88:36–40, 2006.

[250] RN Natarajan and Gunnar BJ Andersson. The influence of lumbar disc height and cross-sectional area on the mechanical response of the disc to physiologic loading. *Spine (Phila Pa 1976)*, 24(18):1873–1881, 1999.

[251] RN Natarajan, JR Williams, and GBJ Andersson. Recent advances in analytical modeling of lumbar disc degeneration. *Spine*, 29(23):2733–2741, 2004.

[252] Warren F Neely, Frank Fichtel, Diana Cardenas Del Monaco, and Jon E Block. Treatment of Symptomatic Lumbar Disc Degeneration with the VariLift-L Interbody Fusion System: Retrospective Review of 470 Cases. *International journal of spine surgery*, 10:7, 2016.

[253] Cornelia Neidlinger-Wilke, Fabio Galbusera, Harris Pratsinis, Eleni Mavrogonatou, Antje Mietsch, Dimitris Kletsas, and Hans Joachim Wilke. Mechanical loading of the intervertebral disc: From the macroscopic to the cellular level. *European Spine Journal*, 23(SUPPL. 3):S333–S343, 2014.

[254] Osamu Nemoto, Takashi Asazuma, Yoshiyuki Yato, Hideaki Imabayashi, Hiroki Yasuoka, and Akira Fujikawa. Comparison of fusion rates following transforaminal lumbar interbody fusion using polyetheretherketone cages or titanium cages with transpedicular instrumentation. *European Spine Journal*, 23(10):2150–2155, 2014.

[255] N Newell, JP Little, A Christou, MA Adams, CJ Adam, and SD Masouros. Biomechanics of the human intervertebral disc: a review of testing techniques and results. *Journal of the Mechanical Behavior of Biomedical Materials*, 2017.

[256] K Nibu, MM Panjabi, T Oxland, and J Cholewicki. Intervertebral disc distraction with a laparoscopic anterior spinal fusion system. *European Spine Journal*, 7(2):142–147, 1998.

[257] Glen L. Niebur, Michael J. Feldstein, Jonathan C. Yuen, Tony J. Chen, and Tony M. Keaveny. High-resolution finite element models with tissue strength asymmetry accurately predict failure of trabecular bone. *Journal of Biomechanics*, 33(12):1575–1583, 2000.

[258] Frank Niemeyer, Hans Joachim Wilke, and Hendrik Schmidt. Geometry strongly influences the response of numerical models of the lumbar spine-A probabilistic finite element analysis. *Journal of Biomechanics*, 45(8):1414–1423, 2012.

[259] Grace D O'Connell, Nathan T. Jacobs, Sounok Sen, Edward J. Vresilovic, and Dawn M. Elliott. Axial creep loading and unloaded recovery of the human intervertebral disc and the effect of degeneration. *Journal of mechanical behaviour of biomedical materials*, 4(7):933–942, 2011.

[260] D Oehme, T Goldschlager, P Ghosh, J V Rosenfeld, and G Jenkin. Cell-Based Therapies Used to Treat Lumbar Degenerative Disc Disease: A Systematic Review of Animal Studies and Human Clinical Trials. *Stem cells international*, 2015(Ivd):946031, 2015.

[261] J. M. Olsewski, M. J. Schendel, L. J. Wallace, J. W. Ogilvie, and C. R. Gundry. Magnetic resonance imaging and biological changes in injured intervertebral discs under normal and increased mechanical demands. *Spine*, 21(17):1945–1951, 1996.

[262] O L Osti, B Vernon-Roberts, and R D Fraser. 1990 Volvo Award in experimental studies. Anulus tears and intervertebral disc degeneration. An experimental study using an animal model. *Spine*, 15(8):762–767, 1990.

[263] P B O'Sullivan. Lumbar segmental 'instability': clinical presentation and specific stabilizing exercise management. *Manual therapy*, 5(1):2–12, 2000.

[264] TR Oxland and T Lund. Biomechanics of stand-alone cages and cages in combination with posterior fixation: a literature review. *European Spine Journal*, 9(1):S095–S101, 2000.

[265] David Paglia, Hardeep Singh, Teja Karukonda, Hicham Drissi, Isaac Moss, and MASc MD. PDGF-BB Delays Degeneration of the Intervertebral Discs in a Rabbit Preclinical Model. *Spine*, 41(8):E449–E458, 2016.

[266] Manohar M. Panjabi. Hybrid multidirectional test method to evaluate spinal adjacent-level effects. *Clinical Biomechanics*, 22(3):257–265, 2007.

[267] Manohar M. Panjabi, T R Oxland, I Yamamoto, and Joseph J. Crisco. Mechanical Behavior of the Human Lumbar and Lumbosacral Spine as Shown by Three-Dimensional Load-Displacement Curves. *The Journal of bone and joint surgery. American volume*, 76(3):413–24, 1994.

[268] Manohar M Panjabi, Thomas Oxland, Koichiro Takata, Vijay K Goel, Joanne Duranceau, and Martin Krag. Articular facets of the human spine. Quantitative three-dimensional anatomy. *Spine*, 18(10):1298–1310, 1993.

[269] MM Panjabi. Biomechanical evaluation of spinal fixation devices: I. A conceptual framework. *Spine (Phila Pa 1976)*, 13(10):1129–1134, 1988.

[270] MM Panjabi. The stabilizing system of the spine. Part II. Neutral zone and instability hypothesis. *Journal of Spinal Disorders*, 5(4):390–397, 1992.

[271] William C. Pannell, David D. Savin, Trevor P. Scott, Jeffrey C. Wang, and Michael D. Daubs. Trends in the surgical treatment of lumbar spine disease in the United States. *The Spine Journal*, 15(8):1719–1727, 2015.

[272] Paul Park, Hugh J Garton, Vishal C Gala, Julian T Hoff, and John E McGillicuddy. Adjacent segment disease after lumbar or lumbosacral fusion: review of the literature. *Spine*, 29(17):1938–1944, 2004.

[273] Won Man Park, Kyungsoo Kim, and Yoon Hyuk Kim. Effects of degenerated intervertebral discs on intersegmental rotations, intradiscal pressures, and facet joint forces of the whole lumbar spine. *Computers in Biology and Medicine*, 43(9):1234–1240, 2013.

[274] D.B. Pateder and E. Benzel. Noninstrumented facet fusion in patients undergoing lumbar laminectomy for degenerative spondylolisthesis. *Journal of surgical orthopaedic advances*, 19:153–158, 2010.

[275] John M. Peloquin, Jonathon H. Yoder, Nathan T. Jacobs, Sung M. Moon, Alexander C. Wright, Edward J. Vresilovic, and Dawn M. Elliott. Human L3L4 intervertebral disc mean 3D shape, modes of variation, and their relationship to degeneration. *Journal of Biomechanics*, 47(10):2452–2459, 2014.

[276] Luis Perez-Orribo, James Zucherman, Kenneth Hsu, Phillip Reyes, Nestor Rodriguez-Martinez, and Neil Crawford. Biomechanics of a Posterior Lumbar Motion Stabilizing Device: In Vitro Comparison to Intact and Fused Conditions. *Spine*, 41(2):E55–E63, 2016.

[277] CWA Pfirrmann, A Metzdorf, and M Zanetti. Magnetic resonance classification of lumbar intervertebral disc degeneration. *Spine*, 26(17):1873–1878, 2001.

[278] Andrew Phillips, Pankaj Pankaj, Fraser May, Kenneth Taylor, Colin Howie, and Asif Usmani. Constitutive models for impacted morsellised cortico-cancellous bone. *Biomaterials*, 27(9):2162–2170, 2006.

[279] F M Phillips, P J Slosar, J A Youssef, G Andersson, and F Papatheofanis. Lumbar Spine Fusion for Chronic Low Back Pain Due to Degenerative Disc Disease A Systematic Review. *Spine*, 38(7):E409–E422, 2013.

[280] RM Pilliar, HU Cameron, RP Welsh, and AG Binnington. Radiographic and morphologic studies of load-bearing porous-surfaced structured implants. *Clinical orthopaedics and related research*, 156:249–257, 1981.

[281] Luiz Pimenta, Alexander W L Turner, Zachary a Dooley, Rachit D Parikh, and Mark D Peterson. Biomechanics of lateral interbody spacers: going wider for going stiffer. *The Scientific World Journal*, 2012:6, 2012.

[282] FA Pintar, N Yoganandan, and T Myers. Biomechanical properties of human lumbar spine ligaments. *Journal of Biomechanics*, 25(11):1351–1356, 1992.

[283] Malcolm H Pope, Kheng Lim Goh, and Marianne L Magnusson. Spine ergonomics. *Annual review of biomedical engineering*, 4:49–68, 2002.

[284] F. Postacchini, S. Gumina, G. Cinotti, D. Perugia, and C. DeMartino. Ligamenta flava in lumbar disc herniation and spinal stenosis: light and electron microscopic morphology. *Spine (Phila Pa 1976)*, 19(8):917–922, 1994.

[285] F. Postacchini and R. Postacchini. Operative management of lumbar disc herniation : the evolution of knowledge and surgical techniques in the last century. *Acta Neurochirurgica*, Supplement:17–21, 2011.

[286] Sergio Postigo, Hendrik Schmidt, Antonius Rohlmann, Michael Putzier, Antonio Sim??n, Georg Duda, and Sara Checa. Investigation of different cage designs

and mechano-regulation algorithms in the lumbar interbody fusion process - A finite element analysis. *Journal of Biomechanics*, 47(6):1514–1519, 2014.

[287] S. Pourtaheri, C. Billings, M. Bogatch, K. Issa, C. Haraszti, D. Mangel, E. Lord, H. Park, R. Ajiboye, A. Ashana, and A. Emami. Outcomes of Instrumented and Noninstrumented Posterolateral Lumbar Fusion. *Orthopaedics*, 38:e1104–1109, 2015.

[288] Ben B Pradhan, John A Nassar, Rick B Delamarter, and Jeffrey C Wang. Single-Level Lumbar Spine Fusion : A Comparison of Anterior and Posterior Approaches. *Journal of Spinal Disorders & Techniques*, 15(5):355–361, 2002.

[289] H. Pratsinis and D. Kletsas. PDGF, bFGF and IGF-I stimulate the proliferation of intervertebral disc cells in vitro via the activation of the ERK and Akt signaling pathways. *European Spine Journal*, 16(11):1858–1866, 2007.

[290] P. J. Prendergast, R. Huiskes, and K. Søballe. Biophysical stimuli on cells during tissue differentiation at implant interfaces. *Journal of Biomechanics*, 30(6):539–548, 1997.

[291] M. Putzier, S.V. Schneider, J.F. Funk, S.W. Tohtz, and C. Perka. The surgical treatment of the lumbar disc prolapse: nucleotomy with additional transpedicular dynamic stabilization versus nucleotomy alone. *Spine (Phila Pa 1976)*, 30:E109–114, 2005.

[292] Muhammad Qasim, Raghu N. Natarajan, Howard S. An, and Gunnar B J Andersson. Damage accumulation location under cyclic loading in the lumbar disc shifts from inner annulus lamellae to peripheral annulus with increasing disc degeneration. *Journal of Biomechanics*, 47(1):24–31, 2014.

[293] Kristen E. Radcliff, Christopher K. Kepler, Andre Jakoi, Gursukhman S. Sidhu, Jeffrey Rihn, Alexander R. Vaccaro, Todd J. Albert, and Alan S. Hilibrand. Adjacent segment disease in the lumbar spine following different treatment interventions. *Spine Journal*, 13(10):1339–1349, 2013.

[294] P. Prithvi Raj. Intervertebral disc: Anatomy-physiology-pathophysiology-treatment. *Pain Practice*, 8(1):18–44, 2008.

[295] CD Ray. Threaded titanium cages for lumbar interbody fusions. *Spine (Phila Pa 1976)*, 15(22):667–79, 1997.

[296] Sandra Reitmaier, Ludwika Kreja, Katharina Gruchenberg, Britta Kanter, Joana Silva-Correia, Joaquim Miguel Oliveira, Rui Lu??s Reis, Valeria Perugini, Matteo Santin, Anita Ignatius, and Hans Joachim Wilke. In vivo biofunctional evaluation of hydrogels for disc regeneration. *European Spine Journal*, 23(1):19–26, 2014.

[297] Sandra Reitmaier, Julian Schuelke, Hendrik Schmidt, David Volkheimer, Anita Ignatius, and Hans Joachim Wilke. Spinal fusion without instrumentation âĂŞ Experimental animal study. *Clinical Biomechanics*, 46:6–14, 2017.

[298] Stephen M. Richardson, Gauthaman Kalamegam, Peter N. Pushparaj, Csaba Matta, Adnan Memic, Ali Khademhosseini, Reza Mobasheri, Fabian L. Poletti, Judith A. Hoyland, and Ali Mobasheri. Mesenchymal stem cells in regenerative medicine: Focus on articular cartilage and intervertebral disc regeneration. *Methods*, 99:69–80, 2016.

[299] Jeffrey A. Rihn, Sapan D. Gandhi, Patrick Sheehan, Alexander R. Vaccaro, Alan S. Hilibrand, Todd J. Albert, and David G. Anderson. Disc space preparation in transforaminal lumbar interbody fusion: A comparison of minimally invasive and open approaches. *Clinical Orthopaedics and Related Research*, 472(6):1800–1805, 2014.

[300] S Roberts, J Menage, and J. P G Urban. Biochemical and structural properties of the cartilage endplate and its relation to the intervertebral disc. *Spine (Phila Pa 1976)*, 14(2):166–174, 1989.

[301] S Roberts, J P Urban, H Evans, and S M Eisenstein. Transport properties of the human cartilage endplate in relation to its composition and calcification. *Spine*, 21(4):415–420, 1996.

[302] Daniel J. Robertson, Gregory A. Von Forell, Jeremy Alsup, and Anton E. Bowden. Thoracolumbar spinal ligaments exhibit negative and transverse prestrain. *Journal of the Mechanical Behavior of Biomedical Materials*, 23:44–52, 2013.

[303] A. Rohlmann, T. Zander, H. Schmidt, H.J. Wilke, and G. Bergmann. Analysis of the influence of disc degeneration on the mechanical behaviour of a lumbar motion segment using the finite element method. *Journal of Biomechanics*, 39(13):2484–2490, 2006.

[304] Antonius Rohlmann, Nagananda K. Burra, Thomas Zander, and Georg Bergmann. Comparison of the effects of bilateral posterior dynamic and rigid fixation devices on the loads in the lumbar spine: A finite element analysis. *European Spine Journal*, 16(8):1223–1231, 2007.

[305] Peter J. Roughley. Biology of Intervertebral Disc Aging and Degeneration. *Spine*, 29(23):2691–2699, 2004.

[306] Marc Antoine Rousseau, David S. Bradford, Rudi Bertagnoli, Serena S. Hu, and Jeffery C. Lotz. Disc arthroplasty design influences intervertebral kinematics and facet forces. *Spine Journal*, 6(3):258–266, 2006.

[307] Lissette M. Ruberté, Raghu N. Natarajan, and Gunnar BJ Andersson. Influence of single-level lumbar degenerative disc disease on the behavior of the adjacent segments-A finite element model study. *Journal of Biomechanics*, 42(3):341–348, 2009.

[308] Clinton T Rubin and Lance E Lanyon. Kappa Delta Award paper. Osteoregulatory nature of mechanical stimuli: function as a determinant for adaptive remodeling in bone. *Journal of orthopaedic research : official publication of the Orthopaedic Research Society*, 5(2):300–10, jan 1987.

[309] HS Sandhu, S Turner, JM Kabo, and LEA Kanim. Distractive properties of a threaded interbody fusion device: an in vivo model. *Spine*, 21(10):1201–1210, 1996.

[310] Christoph Schätz, Karsten Ritter-Lang, Lutz Gössel, and Nadine Dreßler. Comparison of Single-Level and Multiple-Level Outcomes of Total Disc Arthroplasty: 24-Month Results. *International Journal of Spine Surgery*, pages 1–11, 2015.

[311] R K Schenk. Histophysiology of bone remodelling and bone repair. In O C C Lin and E Y S Chao, editors, *Perspectives on Biomaterials*, pages 75–94. Elsevier, 1986.

[312] Hendrik Schmidt, Maxim Bashkuev, Fabio Galbusera, Hans-Joachim Wilke, and Aboulfazl Shirazi-Adl. Finite element study of human lumbar disc nucleus replacements. *Computer methods in biomechanics and biomedical engineering*, 17(16):1762–76, 2014.

[313] Hendrik Schmidt, Fabio Galbusera, A Rohlmann, and A Shirazi-Adl. What have we learned from finite element model studies of lumbar intervertebral discs in the past four decades? *Journal of Biomechanics*, 46(14):2342–2355, 2013.

[314] Hendrik Schmidt, Frank Heuer, Joerg Drumm, Zdenek Klezl, Lutz Claes, and Hans Joachim Wilke. Application of a calibration method provides more realistic results for a finite element model of a lumbar spinal segment. *Clinical Biomechanics*, 22(4):377–384, 2007.

[315] Hendrik Schmidt, Frank Heuer, Ulrich Simon, Annette Kettler, Antonius Rohlmann, Lutz Claes, and Hans Joachim Wilke. Application of a new calibration method for a three-dimensional finite element model of a human lumbar annulus fibrosus. *Clinical Biomechanics*, 21(4):337–344, 2006.

[316] Hendrik Schmidt, Stefan Midderhoff, Kyle Adkins, and Hans Joachim Wilke. The effect of different design concepts in lumbar total disc arthroplasty on the range of motion, facet joint forces and instantaneous center of rotation of a L4-5 segment. *European Spine Journal*, 18(11):1695–1705, 2009.

[317] Hendrik Schmidt and Sandra Reitmaier. Is the ovine intervertebral disc a small human one? A finite element model study. *Journal of the Mechanical Behavior of Biomedical Materials*, 17:229–241, 2012.

[318] Hendrik Schmidt, Aboulfazl Shirazi-Adl, Fabio Galbusera, and Hans Joachim Wilke. Response analysis of the lumbar spine during regular daily activities-A finite element analysis. *Journal of Biomechanics*, 43(10):1849–1856, 2010.

[319] Meredith L. Schollum, Richard C. Appleyard, Christopher B. Little, and James Melrose. A detailed microscopic examination of alterations in normal anular structure induced by mechanical destabilization in an ovine model of disc degeneration. *Spine*, 35(22):1965–1973, 2010.

[320] Y Schroeder and W Wilson. Osmoviscoelastic finite element model of the intervertebral disc. *European spine journal*, 15(3):361–371, 2006.

[321] AB Schultz, DN Warwick, MH Berkson, and AL Nachemson. Mechanical properties of human lumbar spine lotion segments âĂŤ Part I: Responses in flexion, extension, lateral bending , and torsion. *Journal of biomechanical engineering*, 101:46–52, 1979.

[322] William R. Sears, Ioannis G. Sergides, Noojan Kazemi, Mari Smith, Gavin J. White, and Barbara Osburg. Incidence and prevalence of surgery at segments adjacent to a previous posterior lumbar arthrodesis. *Spine Journal*, 11(1):11–20, 2011.

[323] Sandra J. Shefelbine, Peter Augat, Lutz Claes, and Ulrich Simon. Trabecular bone fracture healing simulation with finite element analysis and fuzzy logic. *Journal of Biomechanics*, 38(12):2440–2450, 2005.

[324] Shirazi-Adl, A.M. A., Ahmed, and S.C. Shrivastava. Mechanical response of a lumbar motion segment in axial torque alone and combined with compression. *Spine (Phila Pa 1976)*, 11(9):914–927, 1986.

[325] MJ Silva, C Wang, TM Keaveny, and Hayes WC. Direct and computed tomography thickness measurements of the human, lumbar vertebral shell and endplate. *Bone*, 15(4):409–414, 1994.

[326] Hong Bo Sim, Judith A. Murovic, Bo Young Cho, T. Jesse Lim, and Jon Park. Biomechanical comparison of single-level posterior versus transforaminal lumbar interbody fusions with bilateral pedicle screw fixation: Segmental stability and the effects on adjacent motion segments: Laboratory investigation. *Journal of neurosurgery. Spine*, 12(6):700–708, 2010.

[327] CA Simmons, S Matlis, AJ Thornton, S Chen, CY Wang, and DJ Mooney. Cyclic strain enhances matrix mineralization by adult human mesenchymal cells via the extracellular signal-regulated kinase (erk 1/2) signaling pathway. *Journal of Biomechanics*, 36:1087–1096, 2003.

[328] B R Simon, J S S Wu, M W Carlton, J H Evans, and L E Kazarian. Structural models for human spinal segments based on a poroelastic view of the invertertebral disk. *Journal of Biomedical Engineering*, 107:327–335, 1985.

[329] Kern Singh, Koichi Masuda, and Howard S An. Animal models for human disc degeneration. *The spine journal : official journal of the North American Spine Society*, 5(6 Suppl):267S–279S, 2005.

[330] Kern Singh, Koichi Masuda, Eugene J Thonar, Howard S. An, and Gabriella Cs-Szabo. Age-related changes in the extracellular matrix of nucleus pulposus and anulus fibrosus of human intervertebral disc. *Spine (Phila Pa 1976)*, 34(1):10–16, 2009.

[331] T.H. Smit. *The Mechanical Significance of the Trabecular Bone Architecture in a Human Vertebra [Ingenieur]*. Technische Universität Hamburg, Hamburg, 1996.

[332] Theo H Smit, Ralph Müller, Martijn van Dijk, and Paul I J M Wuisman. Changes in bone architecture during spinal fusion: three years follow-up and the role of cage stiffness. *Spine*, 28(16):1802–8; discussion 1809, 2003.

[333] Lachlan J Smith, Nandan L Nerurkar, Kyung-Suk Choi, Brian D Harfe, and Dawn M Elliott. Degeneration and regeneration of the intervertebral disc: lessons from development. *Disease models & mechanisms*, 4(1):31–41, 2011.

[334] S Sobajima, J S Kim, L G Gilbertson, and J D Kang. Gene therapy for degenerative disc disease. *Gene therapy*, 11(4):390–401, 2004.

[335] Satoshi Sobajima, John F Kompel, Joseph S Kim, Corey J Wallach, Douglas D Robertson, Molly T Vogt, James D Kang, and Lars G Gilbertson. A slowly progressive and reproducible animal model of intervertebral disc degeneration characterized by MRI, X-ray, and histology. *Spine*, 30(1):15–24, 2005.

[336] Moon-Jun Sohn, Mark M Kayanja, Cumhur Kilinçer, Lisa a Ferrara, and Edward C Benzel. Biomechanical evaluation of the ventral and lateral surface shear strain distributions in central compared with dorsolateral placement of cages for lumbar interbody fusion. *Journal of neurosurgery. Spine*, 4(3):219–224, 2006.

[337] J Soini. Lumbar disc space heights after external fixation and anterior interbody fusion: a prospective 2-year follow-up of clinical and radiographic results. *Journal of Spinal Disorders*, 7(6):487–494, 1994.

[338] M.D. Soukane, A. Shirazi-Adl, and J. P G Urban. Computation of coupled diffusion of oxygen, glucose and lactic acid in an intervertebral disc. *Journal of Biomechanics*, 40(12):2645–2654, 2007.

[339] I. A F Stokes and James C. Iatridis. Mechanical conditions that accelerate intervertebral disc degeneration: Overload versus immobilization. *Spine*, 29(23):2724–2732, 2004.

[340] Patrick Strube, Eike Hoff, Tony Hartwig, Carsten F. Perka, Christian Gross, and Michael Putzier. Stand-alone Anterior Versus Anteroposterior Lumbar Interbody Single-level Fusion After a Mean Follow-up of 41 Months. *Journal of Spinal Disorders & Techniques*, 25(7):362–369, 2012.

[341] Nobuhiro Tanaka, Howard S. An, Tae Hong Lim, Atsushi Fujiwara, Chang Hoon Jeon, and Victor M. Haughton. The relationship between disc degeneration and flexibility of the lumbar spine. *Spine Journal*, 1:47–56, 2001.

[342] Robert Tatsumi, Yu Po Lee, Kaveh Khajavi, William Taylor, Foster Chen, and Hyun Bae. In vitro comparison of endplate preparation between four mini-open interbody fusion approaches. *European Spine Journal*, 24:372–377, 2015.

[343] Fernando Techy, Prasath Mageswaran, Robb W Colbrunn, Tara F Bonner, and Robert F McLain. Properties of an interspinous fixation device (ISD) in lumbar fusion constructs: a biomechanical study. *The spine journal : official journal of the North American Spine Society*, 13(5):572–579, 2013.

[344] J P Thompson, R H Pearce, M T Schechter, M E Adams, I K Tsang, and P B Bishop. Preliminary evaluation of a scheme for grading the gross morphology of the human intervertebral disc. *Spine*, 15(5):411–415, 1990.

[345] K. Thomsen, F.B. Christensen, S.P. Eiskjaer, E.S. Hansen, S. Fruensgaard, and C.E. Bunger. 1997 Volvo Award winner in clinical studies. The effect of pedicle screw instrumentation on functional outcome and fusion rates in posterolateral lumbar spinal fusion: a prospective, randomized clinical study. *Spine (Phila Pa 1976)*, 22:2813–2822, 1997.

[346] Jeffrey M. Toth, Mei Wang, Bradley T. Estes, Jeffrey L. Scifert, Howard B. Seim, and A. Simon Turner. Polyetheretherketone as a biomaterial for spinal applications. *Biomaterials*, 27(3):324–334, 2006.

[347] J.M. Toth, K.T. Foley, M. Wang, H.B. Seim, and A.S. Turner. Is lumbar facet fusion biomechanically equivalent to lumbar posterolateral onlay fusion? *Journal of Neurosurgery: Spine*, 2017.

[348] Yang Hwei Tsuang, Yueh Feng Chiang, Chih Y. Hung, Hung W. Wei, Chang Hung Huang, and Cheng Kung Cheng. Comparison of cage application modality in posterior lumbar interbody fusion with posterior instrumentation-A finite element study. *Medical Engineering and Physics*, 31(5):565–570, 2009.

[349] C H Turner, I Owan, and Y Takano. Mechanotransduction in bone: role of strain rate. *The American journal of physiology*, 269(3 Pt 1):E438–E442, 1995.

[350] H K Uhthoff and B A Rahn. Healing patterns of metaphyseal fractures. *Clinical orthopaedics and related research*, (160):295–303, oct 1981.

[351] J P Urban, S Holm, A. Maroudas, and A Nachemson. Nutrition of the intervertebral disk. An in vivo study of solute transport. *Clinical orthopaedics and related research*, 129:101–114, 1977.

[352] Jill P G Urban and Sally Roberts. Degeneration of the intervertebral disc. *Arthritis research & therapy*, 5(3):120–130, 2003.

[353] J.P. Urban and J.F. McMullin. Swelling pressure of the lumbar intervertebral discs: influence of age, spinal level, composition, and degeneration. *Spine (Phila Pa 1976)*, 13(2):179–181, 1988.

[354] J.P.G. Urban. The effect of physical factors on disc cell metabolism. In J.A. Buckwalter, V.M. Goldberg, and SL-Y Woo, editors, *Musculoskeletal Soft Tissue Aging: Impact on Mobility.*, pages 391–412. American Academy of Orthopaedic Surgeons, Rosemont, IL, 1993.

[355] Martin R. Urban, Jeremy C.T. Fairbank, Philip J. Etherington, Lawrence Loh, C. Peter Winlove, and Jill P.G. Urban. Electrochemical measurement of transport into scoliotic intervertebral discs in vivo using nitrous oxide as a tracer. *Spine*, 26(8):984–990, 2001.

[356] Sasidhar Vadapalli, Koichi Sairyo, Vijay K Goel, Matt Robon, Ashok Biyani, Ashutosh Khandha, and Nabil a Ebraheim. Biomechanical rationale for using polyetheretherketone (PEEK) spacers for lumbar interbody fusion-A finite element study. *Spine*, 31(26):E992–E998, 2006.

[357] E. Van de Kelft, F. Costa, D. Van der Planken, and F. Schils. A Prospective Multicenter Registry on the Accuracy of Pedicle Screw Placement in the Thoracic, Lumbar and Sacral Level With the Use of the O-arm Imaging System and StealthStation Navigation. *Spine*, 37(25):1580–1587, 2012.

[358] Martijn van Dijk, Theo H Smit, S Sugihara, Elisabeth H Burger, and Paul I Wuisman. The effect of cage stiffness on the rate of lumbar interbody fusion: an in vivo model using poly(l-lactic Acid) and titanium cages. *Spine*, 27(7):682–688, 2002.

[359] M. M. van Rijsbergen, V. M P Barthelemy, A. C T Vrancken, S. P M Crijns, H. J. Wilke, W. Wilson, B. van Rietbergen, and K. Ito. Moderately degenerated lumbar motion segments: Are they truly unstable? *Biomechanics and Modeling in Mechanobiology*, pages 1–11, 2016.

[360] Alan T Villavicencio, Sigita Burneikiene, Ketan R Bulsara, and Jeffrey J Thramann. Perioperative Complications in Transforaminal Lumbar Interbody Fusion Versus Anterior âĂŞ Posterior Reconstruction for Lumbar Disc Degeneration and Instability. *Journal of Spinal Disorders & Techniques*, 19(2):92–97, 2006.

[361] Nam Vo, Laura J. Niedernhofer, Luigi Aurelio Nasto, Lloydine Jacobs, Paul D. Robbins, James Kang, and Christopher H. Evans. An overview of underlying causes and animal models for the study of age-related degenerative disorders of the spine and synovial joints. *Journal of Orthopaedic Research*, 31(6):831–837, 2013.

[362] David Volkheimer, Masoud Malakoutian, Thomas R Oxland, and Hans-Joachim Wilke. Limitations of current in vitro test protocols for investigation of instrumented adjacent segment biomechanics: critical analysis of the literature. *European spine journal : official publication of the European Spine Society, the European Spinal Deformity Society, and the European Section of the Cervical Spine Research Society*, 24(9):1882–92, 2015.

[363] Theo Vos, Abraham D. Flaxman, Mohsen Naghavi, Rafael Lozano, and et al. Years lived with disability (YLDs) for 1160 sequelae of 289 diseases and injuries 1990-2010: A systematic analysis for the Global Burden of Disease Study 2010. *The Lancet*, 380(9859):2163–2196, 2012.

[364] J.C. Wang, P.M. Arnold, J.T. Hermsmeyer, and D.C. Norvell. Do lumbar motion preserving devices reduce the risk of adjacent segment pathology compared with fusion surgery? A systematic review. *Spine (Phila Pa 1976)*, 37:S133–S143, 2012.

[365] J.Z. Wang, X.T. Fang, E. Lv, F. Yu, Z.W. Wang, and H.X. Song. TGF-beta1 related inflammation in the posterior longitudinal ligament of cervical spondylotic myelopathy patients. *International Journal of Clinical and Experimental Medicine*, 8:2233–2239, 2015.

[366] Kathryn T. Weber, Timothy D. Jacobsen, Robert Maidhof, Justin Virojanapa, Chris Overby, Ona Bloom, Shaheda Quraishi, Mitchell Levine, and Nadeen O. Chahine. Developments in intervertebral disc disease research: pathophysiology, mechanobiology, and therapeutics. *Current Reviews in Musculoskeletal Medicine*, 8(1):18–31, 2015.

[367] H Weinans, R Huiskes, and H J Grootenboer. The behavior of adaptive bone-remodeling simulation models. *Journal of biomechanics*, 25(12):1425–41, dec 1992.

[368] Bradley K Weiner and Rikin Patel. The accuracy of MRI in the detection of lumbar disc containment. *Journal of orthopaedic surgery and research*, 3:46, 2008.

[369] James N. Weinstein, Jon D. Lurie, Tor D. Tosteson, Brett Hanscom, Anna N.A. Tosteson, Emily A. Blood, Nancy J.O. Birkmeyer, Alan S. Hilibrand, Harry Herkowitz, Frank P. Gammisa, Todd J. Albert, Sanford E. Emery, Lawrence G. Lenke, William A. Abdu, Michael Longley, Thomas J. Errico, and Serena S. Hu. Surgical versus Nonsurgical Treatment for Lumbar Degenerative Spondylolisthesis. *The new england journal of medicine*, 356:2257–2270, 2007.

[370] Donna L. Wheeler, Douglas C. Fredericks, Randall F. Dryer, and Hyun W. Bae. Allogeneic mesenchymal precursor cells (MPCs) combined with an osteoconductive scaffold to promote lumbar interbody spine fusion in an ovine model. *Spine Journal*, 16(3):389–399, 2016.

[371] H Wilke, P Neef, B Hinz, H Seidel, and L Claes. Intradiscal pressure together with anthropometric data–a data set for the validation of models. *Clinical biomechanics (Bristol, Avon)*, 16 Suppl 1(1):S111–26, 2001.

[372] Jamie R. Williams, Raghu N. Natarajan, and Gunnar B J Andersson. Inclusion of regional poroelastic material properties better predicts biomechanical behavior of lumbar discs subjected to dynamic loading. *Journal of Biomechanics*, 40(9):1981–1987, 2007.

[373] Richard A. Wood and Ronald J. Favor. *Titanium Alloys Handbook*. Center, Airforce Materials Laboratory. Metals, Ceramics Information, 1972.

[374] Q-Q Wu and Q Chen. Mechanoregulation of chondrocyte proliferation, maturation, and hypertrophy: Ion-channel dependent transduction of matrix deformation signals. *Experimental Cell Research*, 256:383–391, 2000.

[375] Zhitao Xiao, Liya Wang, He Gong, Dong Zhu, and Xizheng Zhang. A nonlinear finite element model of human L4-L5 lumbar spinal segment with three-dimensional solid element ligaments. *Theoretical and Applied Mechanics Letters*, 1(6), 2011.

[376] Luzhong Yin and Dawn M. Elliott. A homogenization model of the annulus fibrosus. *Journal of Biomechanics*, 38(8):1674–1684, 2005.

[377] Mostyn R N O Yong, Siamak Saifzadeh, Geoffrey N. Askin, Robert D. Labrom, Dietmar W. Hutmacher, and Clayton J. Adam. Biological performance of

a polycaprolactone-based scaffold plus recombinant human morphogenetic protein-2 (rhBMP-2) in an ovine thoracic interbody fusion model. *European Spine Journal*, 23(3):650–657, 2014.

[378] Jae-Sung Yoo, Sang-Hyuk Min, and Sung-Hyun Yoon. Fusion rate according to mixture ratio and volumes of bone graft in minimally invasive transforaminal lumbar interbody fusion: minimum 2-year follow-up. *European Journal of Orthopaedic Surgery & Traumatology*, 25(1):183–189, 2014.

[379] J Yu. Elastic tissues of the intervertebral disc. *Biochemical Society Transactions*, 30(6):848–852, 2002.

[380] Thomas A Zdeblick and Frank M Phillips. Interbody cage devices. *Spine*, 28(15 Suppl):S2–7, 2003.

[381] Qing Hang Zhang and Ee Chon Teo. Finite element application in implant research for treatment of lumbar degenerative disc disease. *Medical Engineering and Physics*, 30(10):1246–1256, 2008.

[382] Z-J Zhang, J Huckle, CA Francomano, and RG Spencer. The effect of pulsed low-intensity ultrasound on chondrocyte viability, proliferation, gene expresion and matrix production. *Ultrasould Medicine Biology*, 29(11):1645–1651, 2003.

[383] Rong Ping Zhou, Zhong Min Zhang, Liang Wang, Min Jun Huang, Xiao Chen Zheng, Yun Neng Cui, Ming Yin, Xiao Kai Wang, Nv Zhao Yao, Tian Yu Chen, Jian Chen, Xiao Chun Bai, and Da Di Jin. Establishing a disc degeneration model using computed tomography-guided percutaneous puncture technique in the rabbit. *Journal of Surgical Research*, 181(2):e65–e74, 2013.

[384] Zhiyu Zhou, Manman Gao, Fuxin Wei, Jiabi Liang, Wenbin Deng, Xuejun Dai, Guangqian Zhou, and Xuenong Zou. Shock absorbing function study on denucleated intervertebral disc with or without hydrogel injection through static and dynamic biomechanical tests in vitro. *BioMed Research International*, 2014, 2014.